Zachodniopomorski Uniwersytet Technologiczny w Szczecinie

Wydział Technologii i Inżynierii Chemicznej

Katedra Technologii Chemicznej Nieorganicznej i Inżynierii Środowiska

Dziedzina nauk inżynieryjno-technicznych, dyscyplina: Inżynieria chemiczna

Preparatyka i charakterystyka fotokatalizatorów na bazie tlenku tytanu(IV) modyfikowanego aminosilanami do usuwania zanieczyszczeń organicznych z wody

Preparation and characterization of titanium dioxide-based photocatalysts modified with aminosilanes for the removal of organic pollutants from water

Agnieszka Emilia Sienkiewicz

Praca doktorska wykonana pod kierunkiem

dr hab. inż. Ewelina Kusiak-Nejman, prof. ZUT

Promotor pomocniczy: dr inż. Agnieszka Wanag

Szczecin 2023

Pracę dedykuję moim **Rodzicom**, dziękuję, że pozwoliliście mi rozwinąć skrzydła.

Za wyrozumiałość oraz nieocenioną pomoc przy realizacji tej pracy pragnę złożyć serdeczne podziękowania mojej **promotor** dr hab. inż. Ewelina Kusiak-Nejman, prof. ZUT.

Praca doktorska została wykonana w ramach realizacji projektu OPUS 14

„Hybrydowe nanomateriały ditlenek tytanu-krzem otrzymane przez kalcynację w atmosferze gazów inertnych do zastosowań w oczyszczaniu wody i powietrza”, grant nr 2017/27/B/ST8/02007 finansowany przez Narodowe Centrum Nauki.

Spis treści

Streszczenie

Głównym celem niniejszej pracy było otrzymanie fotokatalizatorów na bazie tlenku tytanu(IV) (Grupa Azoty Zakłady Chemiczne „Police" S.A.), wykorzystywanego do produkcji bieli tytanowej, który poddano modyfikacji krzemem, węglem oraz azotem. Jako prekursor Si, C oraz N wykorzystano związek z grupy aminosilanów: 3-trietoksysililopropan-1-amina (APTES). Fotokatalizatory APTES/TiO_2 otrzymano w wyniku modyfikacji solwotermalnej w autoklawie ciśnieniowym oraz kalcynacji w piecu rurowym w atmosferze gazu obojętnego (argonu). Otrzymane fotokatalizatory odznaczały się podwyższoną aktywnością w zakresie promieniowania UV oraz UV-Vis.

Kolejny etap badań obejmował charakterystykę strukturalno-morfologiczną uzyskanych nanomateriałów APTES/TiO_2 przy wykorzystaniu szeregu metod instrumentalnych w celu ustalenia wpływu przeprowadzonej modyfikacji na właściwości fizyko-chemiczne otrzymanych fotokatalizatorów. Określono również oddziaływanie modyfikatora na właściwości adsorpcyjne, aktywność fotokatalityczną oraz stabilność nowych materiałów. W celu oceny wydajności półprzewodników wykorzystano barwnik kationowy błękit metylenowy oraz barwnik anionowy Oranż II.

Na podstawie przeprowadzonych badań stwierdzono, że obecność krzemu oraz węgla w nanomateriałach na bazie tlenku tytanu(IV) modyfikowanego APTES przyczyniła się do wysoce efektywnego opóźnienia transformacji fazowej anatazu w rutyl oraz wpłynęła na ograniczenie wzrostu wielkości krystalitów anatazu i rutylu, jak również ograniczenia redukcji wielkości powierzchni właściwej podczas kalcynacji, co miało bezpośrednie przełożenie na poprawę efektywności procesu usuwania barwnych zanieczyszczeń organicznych z wody.

Odnotowano również, że dla uzyskanych nanomateriałów APTES/TiO_2 proces adsorpcji w istotny sposób wpływał na wydajność fotokatalitycznego rozkładu obu barwników. Ponadto otrzymane materiały odznaczały się wysokim stopniem usunięcia obu modelowych zanieczyszczeń organicznych wody. Proces kalcynacji w atmosferze argonu przyczynił się do poprawy żywotności modyfikowanych półprzewodników w odniesieniu do nanomateriałów niemodyfikowanych termicznie.

Słowa kluczowe: fotokataliza, tlenek tytanu(IV), TiO_2, 3-trietoksysililopropan-1-amina, APTES, oczyszczanie wody, aktywność fotokatalityczna, usuwanie zanieczyszczeń barwnych

Abstract

The main aim of presented PhD dissertation was to obtain photocatalysts based on titanium(IV) oxide (Grupa Azoty Zakłady Chemiczne „Police" S.A.) used in the production of titanium white, which was modified with silicon, carbon and nitrogen. 3-triethoxysilylpropan-1-amine (APTES) was used as a precursor of silicon, carbon, and nitrogen. APTES/TiO_2 photocatalysts were obtained by solvothermal modification in a pressure autoclave and calcination in a tube furnace under an inert gas atmosphere (argon). The obtained photocatalysts exhibited enhanced activity in the UV and UV-Vis range.

The next stage of the research involved the characterization of the obtained APTES/TiO_2 nanomaterials with the use of various instrumental methods in order to determine the influence of the modification on the physicochemical properties of the synthesized photocatalysts. The impact of the modifier on the adsorption properties, photocatalytic activity and reusability of the new materials was also determined. The cationic dye methylene blue and the anionic dye Orange II were used to evaluate the yield of the semiconductors.

Based on the conducted research, it was found that the presence of silicon and carbon in APTES-modified titanium(IV) oxide nanomaterials contributed to a highly effective delay in the anatase-to-rutile phase transformation and the growth of the crystallites size of both polymorphous forms of TiO_2, as well as a reduction in the size of the specific surface area during calcination, which had a direct impact on the improvement the effectiveness of the process of removing colored organic pollutants from water.

It was also reported that for the obtained APTES/TiO_2 nanomaterials, the adsorption process significantly affected the photocatalytic oxidation efficiency of both dyes. Moreover, the obtained materials exhibited a high removal degree of model water organic pollutants. The calcination process under argon atmosphere contributed to the improved reusability of the modified semiconductors compared to non-thermally modified nanomaterials.

Keywords: photocatalysis, titanium dioxide, TiO_2, 3-triethoxysilylpropan-1-amine, APTES, water treatment, photocatalytic activity, removal of dye contamination

1. Wykaz prac naukowych wchodzących w skład cyklu publikacji

[P1] Wanag Agnieszka, **Sienkiewicz Agnieszka**, Rokicka-Konieczna Paulina, Kusiak-Nejman Ewelina, Morawski Antoni W., Influence of modification of titanium dioxide by silane coupling agents on the photocatalytic activity and stability, Journal of Environmental Chemical Engineering 8 (2020) 103917, https://doi.org/10.1016/j.jece.2020.103917.

IF_{2020} = 5,909	IF_5 = 7,317	$MNiSW_{2020}$ = 100	LC_{WoS}^{*} = 18

LC_{WoS}^{*} - Liczba cytowań publikacji według bazy Web of Science (WoS) bez autocytowań na dzień 02/03/2023

Mój wkład w powstanie publikacji polegał na: otrzymaniu wszystkich badanych fotokatalizatorów, przeprowadzeniu testów aktywności fotokatalitycznej, określeniu właściwości fizyko-chemicznych: samodzielnie wykonałam i opracowałam wyniki analizy z wykorzystaniem spektroskopii w podczerwieni z transformacją Fouriera i techniką rozproszonego odbicia (DRS), samodzielnie opracowałam i omówiłam wyniki badań uzyskanych z wykorzystaniem metod dyfrakcji promieniowania rentgenowskiego (XRD), powierzchni właściwej wyznaczonej metodą BET, analizy zawartości węgla i azotu, skaningowej mikroskopii elektronowej (SEM) oraz spektroskopii rentgenowskiej z dyspersją energii (EDX). Ponadto mój wkład polegał na współprzygotowaniu pierwotnej wersji artykułu.

Mój udział w publikacji szacuję na: **30%**

[P2] Kusiak-Nejman Ewelina, **Sienkiewicz Agnieszka**, Wanag Agnieszka, Rokicka-Konieczna Paulina, Morawski Antoni W., The role of adsorption in the photocatalytic decomposition of dyes on APTES-modified TiO_2 nanomaterials, Catalysts 11 (2021) 172, https://doi.org/10.3390/catal11020172.

IF_{2021} = 4,501	IF_5 = 4,641	$MEiN_{2021}$ = 100	LC_{WoS} = 5

Mój wkład w powstanie publikacji polegał na: współopracowaniu koncepcji badań, otrzymaniu wszystkich badanych fotokatalizatorów, przeprowadzeniu badań mających na celu wyznaczenie pojemności adsorpcyjnej i aktywności fotokatalitycznej, określeniu właściwości fizyko-chemicznych: samodzielnie wykonałam analizy z wykorzystaniem spektrometrii DRIFT i UV-Vis/DRS, samodzielnie opracowałam i omówiłam wyniki badań uzyskanych z wykorzystaniem metod DRIFT, UV-Vis/DRS, XRD, pomiaru powierzchni właściwej metodą BET, analizy potencjału zeta, analizy zawartości węgla i azotu. Dodatkowo mój wkład

polegał na współprzygotowaniu pierwotnej wersji artykułu oraz odpowiedzi na uwagi recenzentów.

Mój udział w publikacji szacuję na: **35%**

[P3] **Sienkiewicz Agnieszka**, Wanag Agnieszka, Kusiak-Nejman Ewelina, Ekiert Ewa, Rokicka-Konieczna Paulina, Morawski Antoni W., Effect of calcination on the photocatalytic activity and stability of TiO_2 photocatalysts modified with APTES, Journal of Environmental Chemical Engineering 9 (2021) 104794, https://doi.org/10.1016/j.jece.2020.104794.

IF_{2021} = 7,968	IF_5 = 7,317	$MEiN_{2021}$ = 100	LC_{WoS} = 9

Mój wkład w powstanie publikacji polegał na: współopracowaniu koncepcji badań, otrzymaniu wszystkich badanych fotokatalizatorów, przeprowadzeniu testów aktywności fotokatalitycznej, określeniu właściwości fizyko-chemicznych: samodzielnie wykonałam analizy z wykorzystaniem spektrometrii DRIFT i UV-Vis/DRS, samodzielnie opracowałam i omówiłam wyniki badań uzyskanych z wykorzystaniem metod DRIFT, UV-Vis/DRS, XRD, pomiaru powierzchni właściwej metodą BET, analizy potencjału zeta, skaningowej mikroskopii elektronowej (SEM) oraz spektroskopii rentgenowskiej z dyspersją energii (EDX). Ponadto mój wkład polegał również na współprzygotowaniu pierwotnej i końcowej wersji artykułu.

Mój udział w publikacji szacuję na: **40%**

[P4] **Sienkiewicz Agnieszka**, Rokicka-Konieczna Paulina, Wanag Agnieszka, Kusiak-Nejman Ewelina, Morawski Antoni W., Artificial solar light-driven APTES/TiO_2 photocatalysts for methylene blue removal from water, Molecules 27 (2022) 947, https://doi.org/10.3390/molecules27030947.

IF_{2021} = 4,927	IF_5 = 5,110	$MEiN_{2022}$ = 140	LC_{WoS} = 4

Mój wkład w powstanie publikacji polegał na: współopracowaniu koncepcji badań, otrzymaniu wszystkich badanych fotokatalizatorów, przeprowadzeniu testów aktywności fotokatalitycznej, określeniu właściwości fizyko-chemicznych: samodzielnie wykonałam analizy z wykorzystaniem spektrometrii DRIFT i UV-Vis/DRS, samodzielnie opracowałam i omówiłam wyniki badań uzyskanych z wykorzystaniem metod DRIFT, UV-Vis/DRS, XRD, pomiaru powierzchni właściwej metodą BET, analizy potencjału zeta, analizy zawartości węgla i azotu, skaningowej mikroskopii elektronowej (SEM) oraz spektroskopii

rentgenowskiej z dyspersją energii (EDX). Ponadto mój wkład polegał również na współprzygotowaniu pierwotnej i końcowej wersji artykułu.

Mój udział w publikacji szacuję na: **40%**

[P5] **Sienkiewicz Agnieszka**, Rokicka-Konieczna Paulina, Wanag Agnieszka, Kusiak-Nejman Ewelina, Morawski Antoni W., Optimization of APTES/TiO_2 nanomaterials modification conditions for antibacterial properties and photocatalytic activity, Desalination and Water Treatment 256 (2022) 35–50, https://doi.org/10.5004/dwt.2022.28368.

IF_{2021} = 1,273	IF_5 = 1,452	$MEiN_{2022}$ = 100	LC_{WoS} = 0

Mój wkład w powstanie publikacji polegał na: współopracowaniu koncepcji badań, otrzymaniu wszystkich badanych fotokatalizatorów, przeprowadzeniu testów aktywności fotokatalitycznej, określeniu właściwości fizyko-chemicznych: samodzielnie wykonałam i opracowałam wyniki analizy z wykorzystaniem spektroskopii w podczerwieni z transformacją Fouriera i techniką rozproszonego odbicia (DRIFT). Samodzielnie opracowywałam i omówiłam wyniki badań uzyskanych z wykorzystaniem metod dyfrakcji promieniowania rentgenowskiego (XRD), pomiaru powierzchni właściwej metodą BET, analizy potencjału zeta, analizy zawartości węgla i azotu, skaningowej mikroskopii elektronowej (SEM) oraz spektroskopii rentgenowskiej z dyspersją energii (EDX). Ponadto mój wkład polegał również na współprzygotowaniu pierwotnej i końcowej wersji artykułu oraz odpowiedzi na uwagi recenzentów.

Mój udział w publikacji szacuję na: **40%**

Podsumowanie: Sumaryczny impact factor według listy Journal Citation Reports (JCR) pięcioletni (IF_5) oraz zgodny z rokiem opublikowania (IF_{RO}), sumaryczna wartość punktów zgodnie z wykazem czasopism określonym przez Ministra Nauki i Szkolnictwa Wyższego/Ministra Edukacji i Nauki ($MNiSW/MEiN_{2020\text{-}2022}$) oraz sumaryczna wartość liczby cytowań według bazy Web of Science (WoS) dla cyklu publikacji bez autocytowań (LC_{WoS}) na dzień 08/01/2023:

IF_{RO} = 24,578	IF_5 = 25,837	$MNiSW/MEiN_{2020\text{-}2022}$ = 540	LC_{WoS} = 36

2. Wykaz dodatkowych osiągnięć tematycznie związanych z realizowaną rozprawą doktorską

2.1. Publikacje naukowe

[1] Rokicka-Konieczna Paulina, Wanag Agnieszka, **Sienkiewicz Agnieszka**, Kusiak-Nejman Ewelina, Morawski Antoni W., Antibacterial effect of TiO_2 nanoparticles modified with APTES, Catalysis Communications 134 (2020) 105862, https://doi.org/10.1016/j.catcom.2019.105862.

IF_{2020} = 3,626	IF_5 = 3,501	$MNiSW_{2020}$ = 100	LC_{WoS} = 25

[2] Rokicka-Konieczna Paulina, Wanag Agnieszka, **Sienkiewicz Agnieszka**, Kusiak-Nejman Ewelina, Morawski Antoni W., Effect of APTES modified TiO_2 on antioxidant enzymes activity secreted by *Escherichia coli* and *Staphylococcus epidermidis*, Biochemical and Biophysical Research Communications 534 (2021) 1064–1068, https://doi.org/10.1016/j.bbrc.2020.10.034.

IF_{2021} = 3,322	IF_5 = 3,498	$MEiN_{2021}$ = 100	LC_{WoS} = 3

[3] **Sienkiewicz Agnieszka** Kusiak-Nejman Ewelina, Wanag Agnieszka, Aidinis Konstantinos, Piwowarska Danuta, Morawski Antoni W., Guskos Niko, High-temperature treated TiO_2 modified with 3-aminopropyltriethoxysilane as a photoactive nanomaterials, Reviews on Advanced Materials Science 61 (2022) 726–733, https://doi.org/10.1515/rams-2022-0264.

IF_{2021} = 5,028	IF_5 = 3,160	$MEiN_{2022}$ = 100	LC_{WoS} = 0

[4] Wanag Agnieszka, Kapica-Kozar Joanna, **Sienkiewicz Agnieszka**, Rokicka-Konieczna Paulina, Kusiak-Nejman Ewelina, Morawski Antoni W., Preliminary findings on CO_2 capture over APTES-modified TiO_2, Atmosphere 13 (2022) 1878, https://doi.org/10.3390/atmos13111878.

IF_{2021} = 3,110	IF_5 = 3,222	$MEiN_{2022}$ = 70	LC_{WoS} = 0

[5] Rokicka-Konieczna Paulina, Wanag Agnieszka, **Sienkiewicz Agnieszka**, Shun Izuma Dylan, Ekiert Ewa, Kusiak-Nejman Ewelina, Terashima Chiaki, Yasumori Atsuo, Fujishima Akira, Morawski Antoni W. Photocatalytic inactivation of co-culture of *E. coli* and *S. epidermidis* using APTES-modified TiO_2, Molecules 28 (2023) 1655, https://doi.org/10.3390/molecules28041655.

IF_{2021} = 4,927	IF_5 = 5,110	$MEiN_{2023}$ = 140	LC_{WoS} = 0

2.2. Udzielone patenty

[1] Morawski Antoni W. (20%), Wanag Agnieszka (20%), Kusiak-Nejman Ewelina (20%), **Sienkiewicz Agnieszka (20%)**, Rokicka-Konieczna Paulina (20%), Sposób ograniczania przejścia fazowego anatazu w rutyl, zgłoszenie patentowe nr P.436193 z dnia 02.12.2020 r., nr prawa wyłącznego 242341, data udzielenia prawa 15.11.2022 r., data publikacji WUP 13.02.2023 r.

2.3. Doniesienia konferencyjne

[1] **Sienkiewicz Agnieszka**, Wanag Agnieszka, Rokicka-Konieczna Paulina, Kusiak-Nejman Ewelina, Morawski Antoni W., Preparation and characterization of nano-titanium dioxide modified with organosilane, 11th Conference Wasteless Technologies and Waste Management in Industry and Agriculture, 11-14 czerwca 2019, Międzyzdroje, udział czynny, plakat naukowy w języku angielskim.

[2] **Sienkiewicz Agnieszka**, Wanag Agnieszka, Rokicka-Konieczna Paulina, Zgrzebnicki Michał, Kusiak-Nejman Ewelina, Morawski Antoni W., TiO_2/organosilane materials with enhanced photocatalytic properties, 62. Zjazd Naukowy Polskiego Towarzystwa Chemicznego, 2-6 września 2019, Warszawa, udział czynny, wystąpienie ustne w języku angielskim.

[3] **Sienkiewicz Agnieszka**, Wanag Agnieszka, Rokicka-Konieczna Paulina, Kusiak-Nejman Ewelina, Morawski Antoni W., TiO_2/APTES nanomaterials with enhanced photocatalytic properties, 9th Czech-Polish Catalytic Symposium, 7 lutego 2020, Ostrawa, Czechy, udział czynny, wystąpienie ustne w języku angielskim.

[4] **Sienkiewicz Agnieszka**, Wanag Agnieszka, Rokicka-Konieczna Paulina, Kusiak-Nejman Ewelina, Morawski Antoni W., Rola adsorpcji w fotokatalitycznym rozkładzie barwników w obecności nanomateriałów APTES/TiO_2, VI Szczecińskie Sympozjum Młodych Chemików, 10-14 maja 2021, Szczecin, konferencja w trybie zdalnym, wystąpienie ustne w języku polskim.

[5] **Sienkiewicz Agnieszka**, Wanag Agnieszka, Rokicka-Konieczna Paulina, Kusiak-Nejman Ewelina, Morawski Antoni W., APTES/TiO_2 Nanomaterials for Water Purification, GSCAEE-2021 Global Summit on Civil, Architectural and Environmental Engineering, 19-21 lipca 2021, Barcelona, Hiszpania, udział czynny, wystąpienie ustne w języku angielskim.

[6] **Sienkiewicz Agnieszka**, Wanag Agnieszka, Rokicka-Konieczna Paulina, Kusiak-Nejman Ewelina, Morawski Antoni W., Methylene blue decomposition in the presence of APTES-modified TiO_2 under artificial solar light irradiation, ogólnokrajowa konferencja naukowa

„OMINBUS CZ. XII Nauki Interdyscyplinarne”, 27 września 2021, Kraków, konferencja w trybie zdalnym, wystąpienie ustne w języku angielskim.

[7] **Sienkiewicz Agnieszka**, Wanag Agnieszka, Rokicka-Konieczna Paulina, Kusiak-Nejman Ewelina, Morawski Antoni W., Optimization of APTES/TiO_2 nanomaterials modification conditions for photocatalytic activity, ogólnokrajowa konferencja naukowa „OMINBUS CZ. XII Nauki Interdyscyplinarne”, 27 września 2021, Kraków, konferencja w trybie zdalnym, wystąpienie ustne w języku angielskim.

[8] **Sienkiewicz Agnieszka**, Wanag Agnieszka, Rokicka-Konieczna Paulina, Kusiak-Nejman Ewelina, Morawski Antoni W., APTES-modified TiO_2 nanomaterials: a brief overview on preparation methods and applications, Ogólnopolska Konferencja Interdyscyplinarna „ALFA I OMEGA CZ. V”, 16-17 grudnia 2021, Kraków, konferencja w trybie zdalnym, wystąpienie ustne w języku angielskim.

[9] **Sienkiewicz Agnieszka**, Wanag Agnieszka, Rokicka-Konieczna Paulina, Kusiak-Nejman Ewelina, Morawski Antoni W., APTES/TiO_2 photocatalysts for phenol removal, Ogólnopolska Konferencja Interdyscyplinarna „ALFA I OMEGA CZ. V”, 16-17 grudnia 2021, Kraków, konferencja w trybie zdalnym, wystąpienie ustne w języku angielskim.

2.4. Streszczenia konferencyjne

[1] **Sienkiewicz Agnieszka**, Wanag Agnieszka, Rokicka-Konieczna Paulina, Kusiak-Nejman Ewelina, Morawski Antoni W., Preparation and characterization of nano-titanium dioxide modified with organosilane, 11th Conference Wasteless Technologies and Waste Management in Industry and Agriculture, 11-14 czerwca 2019, s. 189–192, ISBN 978-83-7663-281-0, streszczenie w języku angielskim.

[2] **Sienkiewicz Agnieszka**, Wanag Agnieszka, Rokicka-Konieczna Paulina, Zgrzebnicki Michał, Kusiak-Nejman Ewelina, Morawski Antoni W., TiO_2/organosilane materials with enhanced photocatalytic properties, 62. Zjazd Naukowy Polskiego Towarzystwa Chemicznego, 2-6 września 2019, s. 29, ISBN 978-83-60988-29-9, streszczenie w języku angielskim.

[3] Morawski Antoni. W., Wanag Agnieszka, **Sienkiewicz Agnieszka**, Rokicka-Konieczna Paulina, Kusiak-Nejman Ewelina, Organosilane-functionalized TiO_2 nanomaterials for water purification, 7th International Conference on Semiconductor Photochemistry, 11-14 września 2019, s. 60, streszczenie w języku angielskim.

[4] **Sienkiewicz Agnieszka**, Wanag Agnieszka, Rokicka-Konieczna Paulina, Kusiak-Nejman Ewelina, Morawski Antoni W., Rola adsorpcji w fotokatalitycznym rozkładzie barwników w obecności nanomateriałów APTES/TiO_2, VI Szczecińskie Sympozjum Młodych

Chemików, Wydawnictwo Uczelniane Zachodniopomorskiego Uniwersytetu Technologicznego w Szczecinie, 10-14 maja 2021, s. 56–57, ISBN 978-83-7663-320-6, streszczenie w języku polskim.

[5] Morawski Antoni W., Wanag Agnieszka, **Sienkiewicz Agnieszka**, Rokicka-Konieczna Paulina, Babyszko Aleksandra, Kusiak-Nejman Ewelina, TiO_2/Silane Nanomaterials with Enhanced Photocatalytic Properties, The 5th International Conference on New Photocatalytic Materials for Environment, Energy and Sustainability/The 6th International Conference on Photocatalytic and Advanced Oxidation Technologies for the Treatment of Water, Air, Soil and Surfaces, 24-27 maja 2021, s. 11, ISBN 978-963-306-789-5, streszczenie w języku angielskim.

[6] **Sienkiewicz Agnieszka**, Wanag Agnieszka, Rokicka-Konieczna Paulina, Kusiak-Nejman Ewelina, Morawski Antoni W., APTES/TiO_2 Nanomaterials for Water Purification, GSCAEE-2021 Global Summit on Civil, Architectural and Environmental Engineering, 19-21 lipca 2021, s. 26–27, streszczenie w języku angielskim.

[7] Morawski Antoni W., Wanag Agnieszka, Rokicka-Konieczna Paulina, **Sienkiewicz Agnieszka**, Babyszko Aleksandra, Kusiak-Nejman Ewelina, TiO_2 modified with graphene or silicon as photocatalysts for environmental application, The 4th International Symposium on Energy and Environmental Photocatalytic Materials, 25-29 lipca 2021, s. 76–77, streszczenie w języku angielskim.

[8] **Sienkiewicz Agnieszka**, Wanag Agnieszka, Rokicka-Konieczna Paulina, Kusiak-Nejman Ewelina, Morawski Antoni W., Methylene blue decomposition in the presence of APTES-modified TiO_2 under artificial solar light irradiation, ogólnokrajowa konferencja naukowa „OMINBUS CZ. XII Nauki Interdyscyplinarne", 27 września 2021, s. 37, ISBN 978-83-63216-60-3, streszczenie w języku angielskim.

[9] **Sienkiewicz Agnieszka**, Wanag Agnieszka, Rokicka-Konieczna Paulina, Kusiak-Nejman Ewelina, Morawski Antoni W., Optimization of APTES/TiO_2 nanomaterials modification conditions for photocatalytic activity, ogólnokrajowa konferencja naukowa „OMINBUS CZ. XII Nauki Interdyscyplinarne", 27 września 2021, s. 36, ISBN 978-83-63216-60-3, streszczenie w języku angielskim.

[10] **Sienkiewicz Agnieszka**, Wanag Agnieszka, Rokicka-Konieczna Paulina, Kusiak-Nejman Ewelina, Morawski Antoni W., APTES-modified TiO_2 nanomaterials: A brief overview on preparation methods and applications, Ogólnopolska Konferencja Interdyscyplinarna „ALFA I OMEGA CZ. V", 16-17 grudnia 2021, s. 15–16, ISBN 978-83-63216-66-5, streszczenie w języku angielskim.

[11] **Sienkiewicz Agnieszka**, Wanag Agnieszka, Rokicka-Konieczna Paulina, Kusiak-Nejman Ewelina, Morawski Antoni W., APTES/TiO_2 photocatalysts for phenol removal, Ogólnopolska Konferencja Interdyscyplinarna „ALFA I OMEGA CZ. V", 16-17 grudnia 2021, s. 13–14, ISBN 978-83-63216-66-5, streszczenie w języku angielskim.

2.5. Wykaz pozostałego dorobku

[1] Uczestnictwo w projekcie badawczym:

11/2018 – 09/2021 realizacja projektu badawczego OPUS 14 finansowanego przez Narodowe Centrum Nauki pt. „Hybrydowe nanomateriały ditlenek tytanu-krzem otrzymane przez kalcynację w atmosferze gazów inertnych do zastosowań w oczyszczaniu wody i powietrza", grant nr 2017/27/B/ST8/02007.

[2] Publikacja naukowa:

Zielińska Edyta, Grzmil Barbara, **Sienkiewicz Agnieszka**, Regulski Paweł, Zienkiewicz Monika, Badania procesu kondensacji ekstrakcyjnego kwasu fosforowego, Przemysł Chemiczny 98/6 (2019) 958–961, DOI: 10.15199/62.2019.6.20.

IF_{2019} = 0,485	IF_5 = 0,370	$MNiSW_{2019}$ = 40	LC_{WoS} = 0

[3] Nagrody i wyróżnienia:

02/2020 Laureatka konkursu PROM-ZUT Narodowej Agencji Wymiany Akademickiej pn. „Międzynarodowa wymiana stypendialna doktorantów i kadry akademickiej", nr projektu POWR.03.03.00-IP.08-00-P13/18, realizowany w ramach Działania: 3.3 Umiędzynarodowienie polskiego szkolnictwa wyższego POWER.

3. Wykaz stosowanych skrótów/akronimów

APTES	- 3-trietoksysililopropan-1-amina
APTES/TiO_2	- tlenek tytanu(IV) modyfikowany 3-trietoksysililopropan-1-aminom
BM	- błękit metylenowy
EDX	- spektroskopia rentgenowska z dyspersją energii
FT-IR/DRS	- spektroskopia w podczerwieni z transformacją Fouriera i techniką rozproszonego odbicia (w publikacjach również DRIFT)
pH	- wykładnik stężenia jonów wodorowych
S_{BET}	- powierzchnia właściwa obliczona metodą Brunauera-Emmetta-Tellera
SEM	- skaningowa mikroskopia elektronowa
UV	- promieniowanie ultrafioletowe
UV-Vis/DRS	- spektroskopia UV-Vis z techniką rozproszonego odbicia
VIS	- promieniowanie widzialne
V_{meso}	- objętość mezoporów
V_{micro}	- objętość mikroporów
V_{total}	- całkowita objętość porów
XRD	- dyfrakcja promieniowania rentgenowskiego

Wstęp

Skażenie środowiska wodnego stanowi coraz poważniejszy problem. Często wpływ syntetycznych barwników organicznych na zanieczyszczenie środowiska uważany jest za niewielki. Zaliczane są do mikrozanieczyszczeń ze względu na niskie stężenie (ng/l do µg/l) w ekosystemach wodnych, jednakże są one wszechobecne ze względu na skalę ich produkcji oraz liczne obszary zastosowań [1-3]. Syntetyczne barwniki organiczne stanowią największą grupę wszystkich substancji barwiących i szacuje się, że na świecie komercyjnie dostępnych jest ponad 100 tys. syntetycznych barwników, których globalna wielkość produkcji wynosi ponad 1 mln ton rocznie [4, 5]. Ogromna ilość produkowanych barwników i ich szeroki obszar zastosowań generują duże ilości barwnych ścieków. Przemysł włókienniczy w znacznym stopniu przyczynia się do zanieczyszczania środowiska wodnego. Podczas różnych procesów barwienia straty barwników wynoszą co najmniej 5%, a mogą sięgać nawet 50%, w zależności od rodzaju tkaniny i barwnika, w wyniku czego rocznie powstaje prawie 200 mld litrów zanieczyszczonych ścieków [1, 6, 7]. Barwniki obecne w ściekach przemysłowych zmniejszają przenikalność światła, prowadząc do zwiększenia biochemicznego zapotrzebowania na tlen, tym samym obniżając aktywność fotosyntetyczną flory wodnej, co negatywnie wpływa na źródło pożywienia organizmów wodnych. Wyniki badań prowadzonych na przestrzeni lat, w których udowodniono, że uwalnianie barwników tekstylnych do zbiorników wodnych wywołuje efekty mutagenne, rakotwórcze i genotoksyczne oraz szkody estetyczne, wzbudziły duże zaniepokojenie wśród ekologów oraz przyczyniły się do sklasyfikowania barwników jako problematycznych i niebezpiecznych zanieczyszczeń wody [7, 8].

Rosnąca liczba publikacji naukowych, dotyczących skażenia wody wywołanego zanieczyszczeniem barwnikami, jest wskaźnikiem i dowodem globalnego problemu zanieczyszczenia środowiska. Obecnie w celu usunięcia zanieczyszczeń barwnych ze ścieków przemysłowych wykorzystuje się m. in. strącanie chemiczne, chlorowanie, ozonowanie, filtrację, adsorpcję na węglach aktywnych, techniki degradacji mikrobiologicznej i enzymatycznej oraz ciśnieniowe procesy membranowe [1, 9, 10]. Opracowując nowe technologie eliminacji zanieczyszczeń, szczególną uwagę zwraca się, aby proponowane rozwiązania były ekonomiczne, jak najbardziej wydajne, spełniały jak najwięcej zasad zielonej chemii oraz ograniczały prawdopodobieństwo generowania problematycznych do zagospodarowania zanieczyszczeń wtórnych. Fotokataliza heterogeniczna z wykorzystaniem tlenku tytanu(IV) stanowi jedno z takich rozwiązań. Główne zalety tego procesu to mineralizacja niebezpiecznych zanieczyszczeń organicznych do dwutlenku węgla, wody oraz prostych związków chemicznych o niskiej

toksyczności dla środowiska. Otrzymanie nowych materiałów na bazie TiO_2 o jak największej wydajności oraz stabilności pozwoli na stworzenie taniej, proekologicznej metody oczyszczania wody i ścieków, eliminującej problem przenoszenia zanieczyszczeń z jednej fazy do drugiej.

Wydajność fotokatalitycznego rozkładu barwników z wykorzystaniem tlenku tytanu(IV) jako fotokatalizatora zależy od jego właściwości fizyko-chemicznych takich jak: struktura krystaliczna, skład fazowy, wielkość krystalitów, powierzchnia właściwa czy ilość grup hydroksylowych. Niestety TiO_2 charakteryzuje szybka rekombinacja fotogenerowanych par elektron-dziura, co wpływa na obniżenie wydajności procesu oczyszczania. Wadę stanowi również wysoka wartość energii pasma wzbronionego (anataz 3,2 eV, rutyl 3,0 eV) i niemodyfikowany tlenek tytanu(IV) może być aktywowany głownie za pomocą promieniowania ultrafioletowego [11]. Dlatego jednym z ważniejszych celów badań naukowych z zakresu fotokatalizy jest opracowanie strategii modyfikacji TiO_2, która pozwoli na osiągnięcie jak najwyższej aktywności i stabilności, przy możliwie jak najniższych kosztach wytwarzania takich nanomateriałów.

Jednym z rozwiązań jest zastosowanie alkilosilanów, znanych z możliwości samoorganizacji na powierzchni materiałów tlenkowych, stosowanych jako środki sprzęgające do przyłączania organicznych cząsteczek lub nanocząsteczek do powierzchni tlenku. W tym zakresie, aminoalkilosilany, takie jak 3-trietoksysililopropan-1-amina (APTES), są coraz szerzej wykorzystywane w procesie modyfikacji tlenków [12]. Obecność zarówno krzemu, węgla, jak i azotu w cząsteczce APTES daje możliwość komodyfikacji TiO_2, wpływającej na poprawę aktywności fotokatalitycznej dzięki opóźnieniu transformacji fazowej anatazu w rutyl, czy zahamowania wzrostu wielkości krystalitów obu faz podczas procesu kalcynacji. Ponadto spadek wartości powierzchni właściwej i objętości porów nanomateriałów również wpływa na podwyższenie wydajności procesów usuwania zanieczyszczeń barwnych z wykorzystaniem tlenku tytanu(IV) modyfikowanego APTES.

4. Hipoteza i cel badań

Głównym celem prowadzonych badań było otrzymanie fotokatalizatorów na bazie tlenku tytanu(IV) modyfikowanego 3-trietoksysililopropan-1-aminą, stanowiącą źródło azotu, węgla i krzemu, które charakteryzowałyby się wysoką aktywnością fotokatalityczną w procesie usuwania barwnych zanieczyszczeń organicznych z wody w wyniku naświetlania zawiesiny reakcyjnej promieniowaniem o różnej długości fali. Uwzględniając aspekt ekonomiczny, bardzo ważnym założeniem pracy doktorskiej było wykorzystanie komercyjnie dostępnego półproduktu stosowanego w produkcji bieli tytanowej w Grupie Azoty Zakłady Chemiczne „Police" S.A., co pozwoliło na wyeliminowanie etapu preparatyki TiO_2, obejmującej wykorzystanie jego prekursorów. Synteza TiO_2 z prekursorów w dużej mierze uznawana jest za skomplikowaną, czasochłonną oraz mało efektywną w odniesieniu do wymaganych nakładów finansowych [13-15]. Dzięki wykorzystaniu zarówno krzemu, węgla jak i azotu, zaproponowana innowacyjna metoda preparatyki, opierająca się na komodyfikacji TiO_2, przyczyni się do zahamowania transformacji fazowej anatazu w rutyl w zakresie temperatur od 700 do 1000°C, opóźnienia wzrostu wielkości krystalitów obu faz podczas procesu kalcynacji, jak również przyczyni się do zahamowania spadku wielkości powierzchni właściwej (S_{BET}) oraz objętości porów otrzymanych nanomateriałów. Co więcej, uzyskane fotokatalizatory powinny charakteryzować się dobrą stabilnością w kilku kolejnych cyklach rozkładu nowych porcji barwników [16-21].

Założeniem pracy było określenie aktywności fotokatalitycznej otrzymanych nanomateriałów APTES/TiO_2 wyznaczonej na podstawie rozkładu modelowych zanieczyszczeń organicznych wody w postaci barwników (błękit metylenowy oraz Oranż II) w warunkach naświetlania zawiesiny reakcyjnej promieniowaniem z zakresu UV i UV-Vis. Badania obejmowały również określenie zależności pomiędzy fotoaktywnością a właściwościami fizyko-chemicznymi otrzymanych nanomateriałów, jak również wskazanie zależności pojemności adsorpcyjnej półprzewodników w stosunku do błękitu metylenowego i Oranżu II. Dodatkowo celem pracy było wyznaczenie stabilności nanomateriałów na bazie TiO_2 modyfikowanego APTES w czterech następujących po sobie cyklach fotokatalitycznego rozkładu obu barwników w obecności pierwotnie badanego materiału.

5. Materiały i metody badawcze

5.1. Charakterystyka stosowanych materiałów

5.1.1. TiO_2 (Grupa Azoty Zakłady Chemiczne „Police" S.A.)

Fotokatalizatory APTES/TiO_2 otrzymano na bazie tlenku tytanu(IV), stanowiącego półprodukt do produkcji bieli tytanowej metodą siarczanową, wytwarzanej przez Grupę Azoty Zakłady

Chemiczne „Police” S.A.. Uwodniony półprodukt składał się w 95%±1% z fazy anatazu oraz zarodków rutylu (5%±1%). Dodatkowo stwierdzono obecność zanieczyszczeń w postaci pozostałości kwasu siarkowego(VI), stanowiącego pozostałość etapu roztwarzania rudy tytanowej (średnio 2,1% mas. w przeliczeniu na siarkę) [22].

Przed modyfikacją, surowy półprodukt o pH wynoszącym ok. 2 poddano wstępnej obróbce w celu uzyskania materiału wyjściowego o pH zbliżonym do obojętnego. W pierwszej kolejności uwodniony TiO_2 przemywano 25% roztworem wody amoniakalnej w celu usunięcia łatwo rozpuszczalnego w wodzie siarczanu(VI) amonu. Następnie uzyskaną zawiesinę wielokrotnie przemywano wodą demineralizowaną w celu usunięcia pozostałych siarczanów oraz doprowadzenia zawiesiny do pH na poziomie ok. 7. Tak uzyskany materiał suszono w suszarce laboratoryjnej przez 24 h w temperaturze 105°C, aby usunąć wodę zaadsorbowaną powierzchniowo, a następnie poddano rozdrobnieniu. Przygotowany materiał oznaczono jako wyjściowy TiO_2.

5.1.2. 3-trietoksysililopropan-1-amina (APTES) jako prekursor krzemu, węgla i azotu

Rolę modyfikatora wyjściowego tlenku tytanu(IV) pełniła 3-trietoksysililopropan-1-amina (APTES). Jest to związek z grupy aminosilanów składający się z dwóch grup funkcyjnych: etoksy i aminopropylowej, przełączonych do centralnego atomu krzemu. Rysunek 1 przedstawia wzór strukturalny 3-trietoksysililopropan-1-aminy. Najważniejsze właściwości fizykochemiczne:

- wzór chemiczny: $C_9H_{23}NO_3Si$;
- masa molowa [g/mol]: 221,37;
- stan skupienia: ciecz;
- barwa: bezbarwny;
- gęstość w 25°C [g/dm^3]: 0,95;
- temperatura topnienia [°C]: -70;
- temperatura wrzenia w 1,013 hPa [°C]: 217;
- temperatura zapłonu [°C]: 93;
- temperatura samozapłonu [°C]: 270;
- rozpuszczalność w wodzie: tak ($7{,}6 \cdot 10^5$ mg/l w 25°C);
- rozpuszczalność w rozpuszczalnikach organicznych: rozpuszczalny w oktanolu;
- logarytm współczynnika podziału (oktanol/woda) = 1,7.

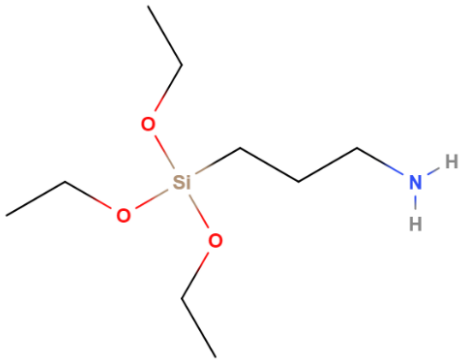

Rysunek 1. Wzór strukturalny 3-trietoksysililopropan-1-aminy (APTES) [23]

5.1.3. Barwniki organiczne jako modelowe zanieczyszczenia wody

Biorąc pod uwagę, że barwniki azowe stanowią najliczniejszą grupę barwników syntetycznych, a ich udział w przemyśle szacuje się aż na około 60-70%, jako modelowe zanieczyszczenia organiczne wody wybrano błękit metylenowy oraz Oranż II. Ta grupa środków barwiących charakteryzuje się obecnością co najmniej jednej grupy azowej (–N=N–). Barwniki azowe syntezowane są głównie w reakcjach diazowania i sprzęgania. Co więcej ze względu na swoją złożoną strukturę są one na ogół odporne na biodegradację [24, 25]. Oranż II zaliczany jest do barwników kwasowych (anionowych), dysocjujących w roztworze wodnym z wytworzeniem barwnych anionów. Odporny na degradację pod wpływem promieniowania słonecznego, stosowany głównie w przemyśle włókienniczym, spożywczym, farmaceutycznym [26]. Błękit metylenowy należy do grupy barwników zasadowych (kationowych), dysocjujących w roztworze wodnym z wytworzeniem barwnych kationów. Powszechnie stosowany w dużej ilości jako barwnik do papieru, wełny, jedwabiu i bawełny. Ponadto przemysł farmaceutyczny, kosmetyczny i spożywczy nie pozostaje w tyle, zużywając duże ilości BM do swoich potrzeb [27]. W Tabeli 1 zestawiono najważniejsze informacje o wykorzystanych związkach barwiących, a na Rysunku 2 przedstawiono wzory strukturalne obu barwników.

Tabela 1. Charakterystyka wykorzystanych modelowych zanieczyszczeń organicznych wody

Rodzaj barwnika / Właściwość	Oranż II (Orange II, Acid Orange 7)	Błękit metylenowy (Methylene Blue)
Charakter	anionowy	kationowy
Wzór sumaryczny	$C_{16}H_{11}N_2NaO_4S$	$C_{16}H_{18}ClN_3S$
Masa molowa [g/mol]	350,3	319,9
λ_{max} [nm]	486	664

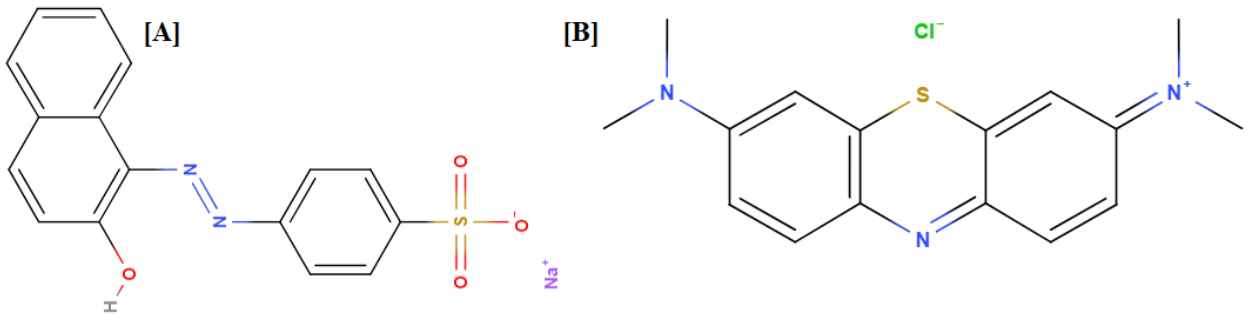

Rysunek 2. Wzór strukturalny Oranżu II [A] oraz błękitu metylenowego [B] [28, 29]

5.2. Charakterystyka stosowanych metod instrumentalnych

5.2.1. Spektroskopia w podczerwieni z transformacją Fouriera i techniką rozproszonego odbicia FT-IR/DRS

W celu identyfikacji grup funkcyjnych obecnych na powierzchni badanych nanomateriałów wykorzystano spektrometr FT-IR-4200 (JASCO International Co. Ltd., Tokio, Japonia), wyposażony w przystawkę odbiciową DiffuseIR (PIKE Technologies, Fitchburg, Wisconsin, USA). Widma zbierano w zakresie długości fali 4000-400 cm^{-1}. Przedmiotem badań spektroskopii w podczerwieni są widma rotacyjne oraz oscylacyjne rejestrowane w postaci pasm i linii. Podczas analizy próbka poddawana jest działaniu promieniowania podczerwonego, a zarejestrowane widmo stanowi obraz jego charakterystycznej absorpcji przez obecne w cząsteczce układy atomów, których energia oscylacyjno-rotacyjna uległa zwiększeniu. Połączenie spektroskopii w podczerwieni IR z transformacją Fouriera istotnie zwiększa czułość metody w porównaniu do tradycyjnej metody dyspersyjnej. W przypadku techniki opartej na odbiciu rozproszonym (DRS) istnieje możliwość prowadzenia bezpośrednich analiz materiałów proszkowych, na których adsorpcji ulegają określone cząsteczki reagenta [30, 31].

5.2.2. Spektroskopia UV-Vis i UV-Vis/DRS

Zmianę stężenia zanieczyszczeń organicznych podczas testów aktywności fotokatalitycznej określono na podstawie widm absorpcyjnych, do rejestracji których wykorzystano spektrofotometr UV-Vis V-630 (JASCO International Co., Tokio, Japonia). Pomiary przeprowadzono w świetle przechodzącym z wykorzystaniem kuwet kwarcowych o długości drogi optycznej 10 mm.

W celu określenia zdolności refleksji światła przez otrzymane fotokatalizatory użyto spektrofotometru UV-Vis V-650 (JASCO International Co., Tokio, Japonia), wyposażonego w przystawkę ze sferą integrującą PIV-756 do pomiaru widm DR (JASCO International Co., Tokio, Japonia). Aby określić wpływ modyfikacji APTES na wielkość przerwy energetycznej pomiędzy pasmem walencyjnym a pasem przewodnictwa, pomiary wykonano w świetle odbitym, natomiast jako materiał odniesienia zastosowano Spectralon® (Labsphere, Inc., North Sutton, USA). Energię pasma wzbronionego (E_g) obliczono wykorzystując przekształcenie Tauca (równanie 1) [32, 33]:

$$(\alpha h\vartheta)^{1/n} = A\left(h\vartheta - E_g\right) \tag{1}$$

gdzie: α – współczynnik linowy absorbcji,

h – stała Plancka [J·s],

υ – częstość padającej na materiał fali elektromagnetycznej [1/s],

E_g – wielkość przerwy wzbronionej [eV],

A – stała zwana parametrem ogonowania pasma,

n – liczba całkowita opisująca rodzaj przejścia elektronowego.

Wartość energii pasma wzbronionego wyznacza się wykreślając zależność $(\alpha h\upsilon)^{1/n}$ w funkcji $h\upsilon$, oraz ekstrapolując uzyskany wykres w zakresie zmienności liniowej. Wartość E_g jest miejscem zerowym uzyskanej w ten sposób zależności [34].

5.2.3. Dyfrakcja promieniowania rentgenowskiego XRD

Strukturę krystaliczną badanych fotokatalizatorów określono za pomocą analizy dyfrakcji proszkowej promieniowania rentgenowskiego (Malvern PANalytical Ltd., Almelo, Holandia) przy użyciu promieniowania Cu Kα (λ =1,54056 Å). Dyfraktogramy zbierano w zakresie 20-80° przy napięciu generatora 35 V oraz prądzie lampy 30 mA. Interpretacji dokonano poprzez porównanie dyfraktogramów analizowanych materiałów z kartami wzorców (JCPDS - Joint Committee for Powder Diffraction Studies, karta 04-002-8296 PDF4+ dla anatazu, karta 04-005-5923 PDF4+ dla rutylu). Do obliczenia średniej wielkości krystalitów wykorzystano równanie Scherrera (równanie 2) [35, 36].

$$D_{hkl} = \frac{K \cdot \lambda}{\beta_{hkl} \cdot cos\,\theta} \tag{2}$$

gdzie: D_{hkl} – średnia wielkość krystalitów [nm],

K – stała Scherrera, współczynnik wynoszący 0,94,

λ – długość fali promieniowania rentgenowskiego [nm],

β_{hkl} – szerokość w połowie wysokości analizowanego refleksu [rad],

θ – połowa kąta ugięcia [rad].

5.2.4. Niskotemperaturowa adsorpcja-desorpcja azotu

Niskotemperaturowe pomiary adsorpcji-desorpcji azotu (przeprowadzone w temperaturze 77 K), wykonane na analizatorze sorpcji gazów QUADRASORB evo™ (Anton Paar GmbH, Graz, Austria), wykorzystano do wyznaczenia powierzchni właściwej metodą Brunauer-Emmett-Teller (BET) i objętości porów. Wykorzystując pomiary niskotemperaturowej adsorpcji-desorpcji azotu całkowitą objętość porów (V_{total}) wyznaczono z jednego punktu izotermy adsorpcji N_2 odpowiadającego ciśnieniu względnemu p/p_0 równemu 0,99. Objętość mikroporów (V_{micro}) wyznaczono przy wykorzystaniu metody Dubinina-Radushkevicha (DR), a objętość mezoporów (V_{meso}) określono z różnicy V_{total} i V_{micro}. Przed wykonaniem pomiarów wszystkie próbki poddano wstępnemu oczyszczeniu poprzez odgazowanie (12 h, wysoka próżnia, 100°C), aby usunąć wszelkie pozostałości zanieczyszczeń obecnych na powierzchni i w porach badanych materiałów.

5.2.5. Skaningowa mikroskopia elektronowa z dyspersją energii promieniowania rentgenowskiego

Morfologię powierzchni otrzymanych fotokatalizatorów, zarówno przed, jak i po procesie modyfikacji, analizowano za pomocą skaningowego mikroskopu elektronowego Hitachi SU8020 o wysokiej rozdzielczości z emisją polową (Hitachi Ltd., Tokio, Japonia), sprzężonego z energetyczno-dyspersyjną spektroskopią rentgenowską EDS NSS 312 (Thermo Scientific, Waltham, Massachusetts, USA), umożliwiającą szybką identyfikację pierwiastków oraz uzyskanie informacji o przybliżonym składzie ilościowym. Skaningowa mikroskopia elektronowa (SEM) dostarcza szczegółowych obrazów próbki poprzez skanowanie powierzchni zogniskowaną wiązką elektronów i wykrywanie sygnału elektronów wtórnych lub wstecznie rozproszonych. Emitowane sygnały właściwe dla danego materiału rejestrowane są przez odpowiednie detektory i następnie konwertowane na obraz próbki [37, 38]. Zdjęcia SEM prezentowane w publikacjach zostały uzyskane na podstawie wtórnych elektronów przy napięciu 5 kV oraz 15 kV.

5.2.6. Metoda dynamicznego rozpraszania światła (pomiar potencjału zeta)

Pomiar potencjału zeta ζ, zwanego inaczej potencjałem elektrokinetycznym, jest jednym z ważniejszych parametrów w procesie fotokatalitycznego rozkładu barwnych zanieczyszczeń wody. Jest to potencjał obecny na powierzchni ciała stałego lub innych cząstek rozproszonych, które stykają się z roztworem elektrolitu. Powstaje w miejscu kontaktu jonów znajdujących się na powierzchni fazy stałej z jonami fazy płynnej, tak zwanej granicy poślizgu [39, 40]. Wartości potencjału zeta nanomateriałów określono za pomocą urządzenia ZetaSizer NanoSeries ZS (Malvern Panalytical Ltd., Malvern, Wielka Brytania), wykorzystując kuwetę DTS1070. Badane próbki były dyspergowane w wodzie, korekty pH dokonywano za pomocą mianowanych roztworów HCl i NaOH.

5.2.7. Analiza elementarna (pomiar zawartości węgla i azotu)

Do oznaczenia całkowitej zawartości węgla i azotu w badanych nanomateriałach wykorzystano analizator elementarny CN 628 (LECO Corporation, St. Joseph, Michigan, USA). Do sporządzenia krzywych kalibracyjnych zastosowano certyfikowany wzorzec EDTA (LECO Corporation, St. Joseph, Michigan, USA), zawierający 9,56±0,03% mas. azotu i 41,06±0,09% mas. węgla. Zakres błędu pomiaru wynosił maksymalnie ± 5%.

6. Omówienie wyników badań

Przed przystąpieniem do przeprowadzania testów aktywności fotokatalitycznej potwierdzono skuteczność modyfikacji wyjściowego TiO_2 za pomocą APTES, wykorzystując uzyskane widma

FT-IR/DRS, na podstawie których w otrzymanych próbkach potwierdzono obecność ugrupowań charakterystycznych dla APTES, takich jak drgania rozciągające $–CH_2$, drgania zginające pierwszorzędowych amin, rozciągające wiązań węgiel–azot, jak również drgania rozciągające Si–O–Si, Si–O–C oraz Ti–O–Si. Dodatkowo na podstawie wyników analizy zawartości węgla i azotu oraz SEM-EDX potwierdzono obecność krzemu, węgla oraz azotu. Co więcej odnotowano, że rozproszenie analizowanych pierwiastków na powierzchni było równomierne. Uzyskane wyniki opublikowane zostały w publikacjach P1-P5 zgodnie z podpunktem 1 [*Wykaz prac naukowych wchodzących w skład cyklu publikacji*].

Stężenie fotokatalizatora niezbędne do przeprowadzenia testów aktywności fotokatalitycznej zostało wyznaczone doświadczalnie [P5]. W tym celu przeprowadzono rozkład błękitu metylenowego (BM) w warunkach naświetlania promieniowaniem UV dla wyjściowego TiO_2 i wybranej serii fotokatalizatorów modyfikowanych w różnej temperaturze za pomocą 250 mM oraz 650 mM APTES. Testy aktywności fotokatalitycznej wykonano dla 5 wybranych stężeń fotokatalizatora, wynoszących 0,05; 0,1; 0,25; 0,5 oraz 0,75 g/l. Przed wyznaczeniem fotoaktywności, przeprowadzono testy mające na celu wyznaczenie czasu osiągnięcia równowagi adsorpcyjno-desorpcyjnej na granicy faz półprzewodnik-błękit metylenowy. Zaobserwowano, że stopień adsorpcji barwnika nie zależał ani od dawki fotokatalizatora, ani od temperatury modyfikacji, ani też od stężenia APTES użytego w procesie modyfikacji. Dla wszystkich badanych próbek równowaga adsorpcyjno-desorpcyjna ustaliła się po 60 minutach ciągłego mieszania. Zgodnie z wartościami potencjału zeta, wyjściowy TiO_2 oraz wszystkie nanomateriały APTES/TiO_2 charakteryzowały się dodatnio naładowaną powierzchnią, a wiadomo, że dodatnio naładowana powierzchnia półprzewodnika ma niski potencjał kontaktu z dodatnio naładowanymi cząsteczkami kationowego barwnika, jakim jest błękit metylenowy [41-43]. Dlatego też adsorpcja BM była znikoma i wynosiła maksymalnie 4%. W przypadku wszystkich badanych fotokatalizatorów, po ustaleniu się równowagi adsorpcyjno-desorpcyjnej nie odnotowano desorpcji barwnika z powierzchni nanomateriału. Na podstawie przeprowadzonych testów określenia aktywności fotokatalitycznej ustalono, że skuteczność usuwania BM wzrastała wraz ze wzrostem stężenia fotokatalizatora. Pomimo, iż największy stopień rozkładu barwnika odnotowano w większości przypadków dla stężenia 0,75 g/l, to biorąc pod uwagę aspekt ekonomiczny, zgodnie z którym im mniej fotokatalizatora zużyjemy tym niższe koszty procesu oczyszczania, oraz niewielką różnicę w wydajności procesu rozkładu BM jaką uzyskano dla dwóch najwyższych stężeń fotokatalizatora, to stężenie 0,5 g/l zostało uznane za optymalne i aktywność wszystkich pozostałych próbek wyznaczona była dla tego stężenia badanych fotokatalizatorów.

W oparciu o rozkład błękitu metylenowego w warunkach naświetlania promieniowaniem UV dokonano także optymalizacji temperaturowej. Optymalizację przeprowadzono poniżej temperatury wrzenia APTES, wynoszącej 217°C [45] oraz w zakresie mieszczącym się w granicach możliwości zastosowanego autoklawu ciśnieniowego. Stąd też optymalizacji dokonano od 120 do 180°C (dla $\Delta t = 20°C$) dla czterech wybranych stężeń APTES, wynoszących 50, 250, 450 oraz 650 mM. Na podstawie uzyskanych wyników odnotowano, że przy stałej ilości modyfikatora temperatura prowadzenia modyfikacji poniżej 180°C włącznie nie miała znaczącego wpływu na zmianę wydajności otrzymanych materiałów [P5].

Następnie określono wpływ stężenia modyfikatora w zakresie od 50 do 650 mM ($\Delta c = 200$ mM) dla stałej temperatury modyfikacji równiej 140°C [P5] oraz 10, 100, 1000, 2000, 3000 i 4000 mM dla nanomateriałów modyfikowanych w 120°C [P1] na aktywność fotokatalityczną przygotowanych nanomateriałów. W obu przypadkach stwierdzono, że wszystkie niekalcynowane próbki APTES/TiO_2 charakteryzowały się lepszą wydajnością w porównaniu do wyjściowego TiO_2. Co więcej stopień rozkładu błękitu metylenowego wzrastał wraz ze wzrostem ilości użytego APTES do stężenia 2000 mM. Powyżej tej wartości fotoaktywność nanomateriałów malała. Na podstawie wyników zawartości krzemu, jak również węgla i azotu, można wnioskować, że poprawa wydajności związana była ze wzrostem zawartości analizowanych pierwiastków w badanych nanomateriałach. Wzrost zawartości Si, C oraz N w otrzymanych półprzewodnikach ułatwia wzbudzenie elektronów z pasma walencyjnego do pasma przewodnictwa oraz przyczynia się do zmniejszenia energii pasma wzbronionego TiO_2, co przekłada się na zwiększenie aktywności fotokatalitycznej. Powyżej stężenia 2000 mM miało miejsce wysycenie powierzchni TiO_2 cząsteczkami APTES, spadek zawartości krzemu oraz powierzchni właściwej w nanomateriałach APTES/TiO_2, dodatkowo spadek zawartości C i N powyżej 3000 mM, co przyczyniło się do zmniejszenia wydajności fotokatalitycznej półprzewodników [46-50].

W przypadku nanomateriałów niekalcynowanych modyfikowanych APTES, podczas rozkładu Oranżu II po 60 minutach naświetlania promieniowaniem UV odnotowano znaczny stopień desorpcji barwnika z powierzchni fotokatalizatora (32%), co związane było z desorpcją grup węglowych APTES słabo związanych z powierzchnią TiO_2, na których zaadsorbowały się cząsteczki Oranżu II [P2]. Znaczący wzrost ilości uwolnionych cząsteczek barwnika zaburzył proces fotokatalitycznego utleniania poprzez tzw. efekt ekranowania, który polega na pochłanianiu przez cząsteczki zanieczyszczenia znacznej ilości promieniowania, w wyniku czego do powierzchni TiO_2 dociera mniejsza liczba fotonów, przez co generowanych jest mniej rodników hydroksylowych biorących udział w procesie fotokatalitycznego rozkładu [51, 52].

W celu poprawy aktywności i stabilności otrzymanych fotokatalizatorów w procesach usuwania zanieczyszczeń barwnych pod wpływem naświetlania promieniowaniem UV, przeprowadzono proces kalcynacji wybranej serii nanomateriałów w atmosferze argonu (przepływ gazu 180 ml/min) w czasie 4 h. Kalcynacji poddano próbki modyfikowane w autoklawie ciśnieniowym w 120°C za pomocą 500 mM APTES [P2] oraz 2000 mM w 180°C [P3], w zakresie temperatur 300-900°C (Δt = 200°C). W przypadku TiO_2 modyfikowanego APTES proces obróbki cieplnej powyżej temperatury 300°C przyczynił się do poprawy właściwości adsorpcyjnych, a ujemnie naładowana powierzchnia nanomateriału charakteryzowała się wyższą zdolnością do kontaktu z dodatnio naładowanymi cząsteczkami, jak błękit metylenowy [41-44, 43]. Ujemna wartość potencjału zeta, oznaczona dla badanej grupy półprzewodników, wpłynęła na poprawę właściwości adsorpcyjnych nanomateriałów APTES/TiO_2. Natomiast dla próbek o dodatnio naładowanej powierzchni odnotowano niski stopień adsorpcji barwnika kationowego BM [41, 54]. Jednakże nanomateriały kalcynowane w temperaturze 900°C, pomimo że wykazywały zbliżone do siebie wartości potencjału zeta, odznaczały się odmiennym stopniem adsorpcji BM. Dla materiału odniesienia TiO_2-Ar-900°C stopień adsorpcji wynosił zaledwie 5%, natomiast dla próbek TiO_2-4h-180°C-2000mM-Ar-900°C i TiO_2-4h-120°C-500mM-Ar-900°C wynosił odpowiednio 32 i 30%. Ogólnie przyjmuje się, że właściwości adsorpcyjne przypisuje się większym wartościom powierzchni właściwej. W tym przypadku powierzchnia właściwa próbki referencyjnej (TiO_2-Ar-900°C) wynosiła zaledwie 3 m^2/g, a dla materiałów modyfikowanych APTES odpowiednio 45 i 50 m^2/g. Zatem zwiększenie właściwości adsorpcyjnych dla próbki kalcynowanej w 900°C było związane z zahamowaniem przemiany fazowej anatazu w rutyl oraz spiekania krystalitów w zakresie wysokich temperatur procesu kalcynacji.

Aby lepiej zrozumieć proces adsorpcji, przeprowadzono dodatkowe badania w celu określenia pojemności adsorpcyjnej badanych nanomateriałów. Na podstawie uzyskanych współczynników korelacji dla adsorpcji BM wykazano, że najlepsze dopasowanie danych doświadczalnych do modelu izotermy Langmuira-Freundlicha uzyskano dla wyjściowego TiO_2, materiałów referencyjnych oraz próbek TiO_2 modyfikowanych APTES i dodatkowo kalcynowanych w temperaturze 300-900°C (Δt = 200°C). Dopasowanie danych doświadczalnych do modelu izotermy Temkina uzyskano dla nanomateriału TiO_2-4h-120°C-500mM. Dla fotokatalizatorów, które wykazały najlepsze dopasowanie do modelu izotermy Langmuira-Freundlicha, można przyjąć, że powierzchnie półprzewodników są heterogeniczne, energetycznie niejednorodne [55]. Ponadto zauważono, że wartości maksymalnej pojemności adsorpcyjnej wzrosły z 0,19 do 8,35 mg/g BM próbki. Wzrost pojemności adsorpcyjnej dla błękitu metylenowego można tłumaczyć wpływem modyfikacji, która obejmowała zarówno wzrost powierzchni właściwej, jaki i zmianę

ładunku powierzchniowego z dodatniego na ujemny, oraz mezoporowatą strukturą nanomateriałów APTES/TiO_2 [56, 57].

Po modyfikacji termicznej w temperaturze 300 i 500°C odnotowano niewielką zmianę aktywności fotokatalitycznej wyjściowego TiO_2. Istotną poprawę wydajności (z 31 do 88%) zaobserwowano jedynie dla próbki kalcynowanej w 700°C, zawierającej 88% anatazu i 12% rutylu, o wartości energii pasma wzbronionego wynoszącej 3,07 eV i powierzchni właściwej równej 16 m^2/g [P3]. Odnotowane zależności były zgodne z wynikami uzyskanymi przez Luís i in. [58] oraz Ohno i in. [59], według których współistnienie różnych form polimorficznych TiO_2 jest jednym z najważniejszych parametrów warunkujących fotoaktywność TiO_2. Zaobserwowali oni, że najbardziej efektywne wyniki podczas rozkładu błękitu metylenowego uzyskano dla materiałów o obniżonej energii przerwy energetycznej, będących mieszaniną anatazu i rutylu. Materiały te nie charakteryzowały się wcale największą powierzchną właściwą spośród wszystkich badanych próbek [58, 59]. W przypadku próbek modyfikowanych APTES, po procesie kalcynacji praktycznie wszystkie modyfikowane fotokatalizatory TiO_2 charakteryzowały się lepszym stopniem rozkładu błękitu metylenowego w porównaniu z próbkami referencyjnymi, wygrzewanymi w tej samej temperaturze. Jedynie próbka TiO_2-4h-120°C-500mM-Ar-700°C wykazała nieznaczny (7%) spadek efektywności w porównaniu do próbki TiO_2-Ar-700°C. Modyfikacja krzemem oraz węglem przyczyniła się do efektywnego zahamowanie przemiany fazowej anatazu w rutyl (próbka TiO_2-Ar-900°C składała się w 100% z rutylu, zaś TiO_2-4h-120°C-500mM-Ar-900°C stanowiła mieszaninę 95% anatazu i 5% rutylu), a także wzrostu wielkości krystalitów (52 nm anataz oraz >100 nm rutyl w przypadku próbki TiO_2-Ar-700°C, zaś 17 nm anataz oraz 45 nm rutyl dla próbki TiO_2-4h-120°C-500mM-Ar-700°C) [P2]. Redukcja defektów sieciowych oraz opóźnienie wzrostu wielkości krystalitów fazy anatazu po kalcynacji zwiększyły szybkość dyfuzji elektronów do powierzchni poprzez zahamowanie rekombinacji par elektron-dziura. Dodatkowo wysoka porowatość ułatwiała transfer masy reagentów, takich jak półprodukty reakcji i tlen, przyczyniając się do wzrostu aktywności fotokatalitycznej otrzymanych kalcynowanych nanomateriałów APTES/TiO_2 [60-62]. Fotokatalizatory modyfikowane APTES, kalcynowane w 700°C, charakteryzowały się nie tylko najwyższą aktywnością fotokatalityczną, ale również najwyższym stopniem adsorpcji błękitu metylenowego, a wiadomo, że właściwości adsorpcyjne odgrywają istotną rolę podczas reakcji fotokatalitycznej degradacji [62, 64].

W celu lepszego opisu procesu fotokatalitycznego rozkładu BM wyznaczono również pozorne stałe szybkości reakcji dla serii nanomateriałów modyfikowanych w 180°C za pomocą 2000 mM APTES i wygrzewanych w atmosferze argonu w zakresie temperatur 300°C-900°C (Δt = 200°C) [P3]. W przypadku wyjściowego TiO_2, TiO_2-Ar-300°C, TiO_2-Ar-500°C, TiO_2-Ar-700°C oraz

TiO_2-4h-180°C-2000mM rozkład błękitu metylenowego przebiegał zgodnie z modelem pseudo-pierwszego rzędu Langmuira-Hinshelwooda, a dla TiO_2-Ar-900°C i wszystkich kalcynowanych nanomateriałów APTES/TiO_2 rozkład BM przebiegał zgodnie modelem pseudo-drugiego rzędu. Zaobserwowano więc, że kinetyka reakcji rozkładu barwnika uległa zmianie po modyfikacji APTES w połączeniu z kalcynacją na skutek zmiany charakteru powierzchni otrzymanych fotokatalizatorów APTES/TiO_2.

W przypadku usuwania Oranżu II, po kalcynacji w 300 i 500°C, odnotowano niewielki spadek aktywności fotokatalitycznej (odpowiednio o ok. 10 i 5%) w porównaniu z wyjściowym TiO_2 [P3]. Znaczne obniżenie stopnia rozkładu barwnika (ok. 95%) zaobserwowano dla materiału referencyjnego TiO_2-Ar-900°C, co związane było z całkowitą transformacją fazową anatazu w rutyl oraz wzrostem agregacji cząstek, wpływającej na zmniejszenie powierzchni właściwej S_{BET} [65, 66]. W przypadku fotokatalizatorów TiO_2 modyfikowanych APTES wygrzewanych w 300 i 500°C potwierdzono, że odznaczały się one znacznie niższym stopniem rozkładu Oranżu II niż materiały referencyjne, otrzymane w tej samej temperaturze. Próbki TiO_2-Ar-300°C i TiO_2-Ar-500°C wykazywały wyraźnie wyższy stopień adsorpcji Oranżu II niż nanomateriały TiO_2-4h-120°C-500mM-Ar-300°C i TiO_2-4h-120°C-500mM-Ar-500°C. Próbki referencyjne kalcynowane w 300 i 500°C posiadały niemal identyczny skład fazowy oraz charakteryzowały się mniejszą powierzchnią właściwą niż odpowiadające im nanomateriały APTES/TiO_2, a uzyskane wyniki sugerują, że proces adsorpcji miał silny wpływ na degradację barwnika, co jest zgodne z doniesieniami innych badaczy [56, 63, 64]. Po 240 minutach ekspozycji na promieniowanie UV jedynie próbka TiO_2-4h-120°C-500mM-Ar-900°C wykazała 92% wzrost fotoaktywności w porównaniu do materiału referencyjnego TiO_2-Ar-900°C. Podobnie jak w przypadku rozkładu błękitu metylenowego, ponieważ oba materiały wykazywały prawie takie same wartości potencjału zeta, odnotowany wzrost wydajności związany był ze skutecznym zahamowaniem transformacji fazowej anatazu w rutyl oraz nadal stosunkowo dużą powierzchnią właściwą próbki modyfikowanej APTES (50 m^2/g) w porównaniu z materiałem referencyjnym (3 m^2/g) [61, 65, 66]. Również w przypadku Oranżu II w celu lepszego opisu procesu fotokatalitycznego rozkładu barwnika wyznaczono pozorne stałe szybkości reakcji. Degradacja Oranżu II z wykorzystaniem fotokatalizatorów TiO_2-4h-120°C-500mM, TiO_2-Ar-500°C oraz TiO_2-4h-120°C-500mM-Ar-300°C przebiegała zgodnie z modelem zerowego rzędu, natomiast dla TiO_2-Ar-900°C zgodnie z modelem pseudo-drugiego rzędu. Dla wszystkich pozostałych nanomateriałów rozkład przebiegał zgodnie z modelem pseudo-pierwszego rzędu.

Aby lepiej zrozumieć proces adsorpcji, przeprowadzono również dodatkowe badania, mające na celu określenie pojemności adsorpcyjnej wybranych materiałów [P3]. Zgodnie z uzyskanymi

współczynnikami korelacji, eksperymentalne dane równowagi dla adsorpcji Oranżu II dla próbek wyjściowy TiO_2, TiO_2-Ar-300°C, TiO_2-Ar-500°C i TiO_2-Ar-700°C wykazywały największe dopasowanie do izotermy Freundlicha. Dla próbek TiO_2-4h-120°C-500mM-Ar-900°C i TiO_2-Ar-900°C najlepsze dopasowanie uzyskano dla modelu izotermy Redlicha-Petersona. Natomiast dla TiO_2-4h-120°C-500mM oraz TiO_2 modyfikowanego APTES kalcynowanego w 300, 500 i 700°C najlepszą symulację danych eksperymentalnych zapewnił model izotermy Langmuira-Freundlicha. Dla materiałów, które wykazały najlepsze dopasowanie do modelu izotermy Freundlicha i Langmuira-Freundlicha, można stwierdzić, że powierzchnie półprzewodników są heterogeniczne [55, 56]. Odnotowany wzrost wartości pojemności adsorpcyjnej z 197 do 638 mg/g związany był ze zmianą ładunku powierzchniowego z ujemnego na dodatni, uzyskanego w wyniku modyfikacji TiO_2.

Kolejny etap badań obejmował określenie stabilności wybranej serii nanomateriałów w warunkach naświetlania promieniowaniem UV w czterech następujących po sobie cyklach fotokatalitycznego rozkładu barwników. W przypadku błękitu metylenowego wybrano w tym celu fotokatalizatory TiO_2-4h-120°C-2000mM [P1], modyfikowane w autoklawie ciśnieniowym w 120°C za pomocą 500 mM APTES [P2], oraz 2000 mM w 180°C [P3] kalcynowane w zakresie temperatur 300-900°C (Δt = 200°C). Odnotowano, że nanomateriały niekalcynowane odznaczały się brakiem stabilności fotokatalitycznej (po pierwszym cyklu stopień rozkładu BM zmalał o około 30%). Na podstawie widm FT-IR/DRS zaobserwowano, brak ugrupowań pochodzących od $–CH_2$ oraz Si–O–C na powierzchni badanych nanomateriałów. Destrukcji nie uległy jedynie wiązania pomiędzy Si oraz Ti. Meroni i in. [67] również odnotowali, że światło powoduje utlenienie łańcucha alkilowego i odłączenie grup aminowych APTES. Zaobserwowali również, że naświetlanie nie niszczy wiązań pomiędzy krzemem i tytanem. W celu wyjaśnienia powyższych obserwacji przeprowadzono dodatkowe testy obejmujące pomiar zawartości węgla i azotu w próbce po każdym cyklu fotokatalitycznym. Doświadczenia przeprowadzono w roztworze wodnym w ciemności oraz w warunkach naświetlania promieniowaniem UV [P1]. Analiza elementarna oraz test stabilności przeprowadzony w wodzie potwierdziły, że cząsteczki APTES nie były w sposób trwały związane z powierzchnią TiO_2. Odnotowano, że łańcuch alkilowy APTES ulegał destrukcji pod wpływem promieniowania UV, co więcej węgiel oraz azot były usuwane podczas mieszania, co przyczyniło się do zaobserwowanego spadku fotoaktywności już w drugim cyklu fotokatalitycznego rozkładu barwnika. Stąd też najwyższa wydajność rozkładu BM w pierwszym cyklu skorelowana była z obecnością C i N w próbce. Podobne wnioski odnotowali również Zamiri i Giahi [68], którzy wykorzystali mocznik jako źródło węgla i azotu do modyfikacji TiO_2. Po kalcynacji w temperaturze 300°C [P3] oraz 500 i 700°C [P2, P3] na

skutek zwiększenia powierzchni właściwej oraz objętości porów w porównaniu do próbek niekalcynowanych, odnotowano poprawę stabilności badanych nanomateriałów. Dodatkowo na podstawie widm FT-IR/DRS oraz analizy zawartości węgla i azotu odnotowano brak C i N, wymywanie których przyczyniło się do spadku stabilności fotokatalizatorów niewygrzewanych. Aby wytłumaczyć spadek wydajności nanomateriałów kalcynowanych w kolejnych cyklach fotokatalitycznych zmierzono widma FT-IR/DRS próbek po ostatnim 4 cyklu. Odnotowany znaczny wzrost intensywności pasma zlokalizowanego pomiędzy 1200 a 1600 cm^{-1} wskazuje na to, że w kolejnych cyklach depozyty węglowe pochodzące od BM pojawiają się na powierzchni TiO_2, powodując spadek wydajności nanomateriałów APTES/TiO_2 [69].

W przypadku nanomateriałów TiO_2-4h-120°C-500mM oraz TiO_2-4h-120°C-500mM-Ar-300°C odnotowano wyraźny wzrost wydajności w kolejnych cyklach fotokatalitycznego rozkładu Oranżu II [P2]. W porównaniu do 1 cyklu stopień rozkładu zwiększył się z 38% do 100% już po 2 cyklu i pozostał na tym poziomie aż do ostatniego 4 cyklu. Dla próbki kalcynowanej w 300°C zaobserwowano wyraźny stopniowy wzrost w miarę upływu kolejnych cykli fotokatalitycznych. Nanomateriały kalcynowane w 500 oraz 900°C charakteryzowały się dobrą stabilnością. Jedynie próbka TiO_2-4h-120°C-500mM-Ar-700°C wykazywała niewielki spadek wydajności po 4 cyklach z 100 do 80% w porównaniu do pierwszego cyklu. Wzrost wydajności w kolejnych następujących po sobie cyklach fotokatalitycznego rozkładu Oranżu II związany był z pojawieniem się na powierzchni nanomateriałów grup $–SO_3^-$ pochodzących od barwnika, które odnotowano na widmach FT-IR/DRS przy długości fali 1175 cm^{-1}. Obecność grup $–SO_3^-$ przyczyniła się do poprawy fotoaktywności badanych nanomateriałów [56, 70]. Wzrost intensywności pasma zlokalizowanego pomiędzy 1200 a 1600 cm^{-1} wskazuje na pojawiające się półprodukty rozkładu Oranżu II w kolejnych cyklach procesu, co przyczyniło się do spadku wydajności nanomateriału kalcynowanego w 700°C. Poza potwierdzonym znaczącym wpływem składu fazowego na aktywność fotokatalityczną uzyskane widma FT-IR/DRS wykazały, że proces rozkładu barwników był silnie zależny od procesu adsorpcji. Ujemnie naładowana powierzchnia fotokatalizatorów APTES/TiO_2 wpływa na sorpcję produktów rozkładu BM w każdym kolejnym cyklu, zmniejszając tym samym fotoaktywność. Z drugiej strony obecność ujemnie naładowanych grup na powierzchni badanych półprzewodników (tj. grup $–SiO_3^-$) hamuje sorpcję półproduktów degradacji Oranżu II. Dlatego proces adsorpcji odgrywa również istotną rolę w fotokatalitycznym rozkładzie zanieczyszczeń [56, 63, 69, 70].

Ostatni etap prac obejmował określenie aktywności fotokatalitycznej wybranej serii nanomateriałów w warunkach sztucznego promieniowania słonecznego (natężenie promieniowania 837 W/m^2 dla zakresu 300-2800 nm i 0,3 W/m^2 dla zakresu 280-400 nm).

W tym celu wykorzystano TiO_2 modyfikowany za pomocą 100, 500 oraz 1000 mM APTES kalcynowany przez 4 h w zakresie temperatur 800-1000°C (Δt = 100°C) [P4]. Wydajność półprzewodników wyznaczono na podstawie rozkładu BM. Degradacja barwnika w warunkach braku fotokatalizatora była znikoma i wynosiła jedynie 2%, z tego względu można pominąć efekt fotosensybilizacji. W przypadku nanomateriałów na bazie TiO_2 modyfikowanych APTES, proces kalcynacji przyczynił się do poprawy aktywności fotokatalitycznej. Obecność Si oraz C w próbkach APTES/TiO_2 przyczyniła się do efektywnego opóźnienia transformacji fazowej anatazu w rutyl oraz spiekania krystalitów podczas kalcynacji [73-75]. W porównaniu z próbkami referencyjnymi wygrzewanymi w tej samej temperaturze, kalcynowane fotokatalizatory APTES/TiO_2 wykazywały wyższe wartości powierzchni właściwej i objętości porów, a także większą zawartość bardziej aktywnej fazy anatazu, co przyczyniło się do wyższego stopnia rozkładu błękitu metylenowego [74, 75]. Dla wszystkich trzech przebadanych stężeń APTES najlepszy stopień rozkładu BM zaobserwowano dla próbek APTES/TiO_2 wygrzewanych w 900°C. Aby wyjaśnić najwyższą wydajność nanomateriałów wykonano widma FT-IR/DRS wybranych próbek po procesie ustalenia się równowagi adsorpcyjno-desorpcyjnej na granicy faz fotokatalizator-barwnik. Wzrost intensywności pasma zlokalizowanego pomiędzy 1200-1600 cm^{-1} wskazuje na to, że depozyty węglowe pochodzące od barwnika pojawiły się na powierzchni nanomateriałów po procesie adsorpcji, ograniczając wydajność fotokatalityczną [69, 76]. Pomimo że próbki APTES/TiO_2 kalcynowane w 800°C charakteryzowały się największą wartością powierzchni właściwej i objętością porów wykazywały również największy stopień adsorpcji BM. W wyniki czego największa liczba miejsc aktywnych na powierzchni TiO_2 była blokowana przez cząsteczki barwnika, co prowadziło do spadku aktywności [52]. Fotokatalizatory wygrzewane w 1000°C odznaczały się bardzo małą powierzchnią właściwą oraz objętością porów, składały się również w większym stopniu z mniej aktywnej fazy rutylu (94% dla próbki modyfikowanej za pomocą 100 mM APTES, oraz odpowiednio 88 i 84% dla stężenia modyfikatora równego 500 i 1000 mM) [77]. Dlatego nanomateriały na bazie TiO_2 modyfikowanego APTES kalcynowane w 900°C wykazywały najwyższy stopień rozkładu BM. Dla stałej temperatury wygrzewania równej 900°C fotokatalizator TiO_2-4h-180°C-500mM-Ar-900°C odznaczał się najwyższą wydajnością w procesie fotokatalitycznego rozkładu BM. Nanomateriały modyfikowane za pomocą 100 oraz 1000 mM APTES wykazywały wyższy stopień adsorpcji barwnika w porównaniu do próbki TiO_2-4h-180°C-500mM-Ar-900°C, przez co większa liczba miejsc aktywnych była blokowana przez zaadsorbowane cząsteczki barwnika na powierzchni półprzewodnika, co przyczyniło się do spadku wydajności fotokatalitycznej.

7. Wnioski

1) Otrzymano serię nowych nanokrystalicznych fotokatalizatorów w wyniku modyfikacji wyjściowego TiO_2, stanowiącego półprodukt do produkcji bieli tytanowej, wytwarzanej przez Grupę Azoty Zakłady Chemiczne „Police" S.A., za pomocą 3-trietoksysililopropan-1-aminy. Uzyskane nanomateriały charakteryzowały się wyższą aktywnością fotokatalityczną w zakresie promieniowania UV oraz sztucznego promieniowania słonecznego w odniesieniu do wyjściowego TiO_2.
2) Zawartość azotu, krzemu i węgla rosła wraz ze wzrostem stężenia APTES użytego do modyfikacji. Przy stałym stężeniu modyfikatora zawartość C i N malała wraz ze wzrostem temperatury kalcynacji. Ze względu na śladowe ilości C i N w zakresie wysokich temperatur wygrzewania nie miały one istotnego wpływu na właściwości fotokatalizatorów.
3) Wraz ze wzrostem stężenia użytego modyfikatora, a tym samym wzrostem zawartości Si, C i N w próbkach APTES/TiO_2, wydajność fotokatalitycznego rozkładu błękitu metylenowego rosła.
4) Temperatura modyfikacji w warunkach podwyższonego ciśnienia w zakresie 120-180°C (Δt = 20°C) nie miała istotnego wpływu na aktywność fotokatalityczną.
5) Powierzchnia właściwa oraz całkowita objętość porów niekalcynowanych nanomateriałów APTES/TiO_2 malała w wyniku obecności cząsteczek aminy zarówno na powierzchni i porach TiO_2.
6) Niekalcynowane fotokatalizatory APTES/TiO_2 odznaczały się brakiem stabilności podczas kolejnych cykli rozkładu błękitu metylenowego ze względu na destrukcję łańcucha cząsteczki APTES pod wpływem promieniowania UV oraz usuwania C i N z powierzchni fotokatalizatorów podczas mieszania wodnej zawiesiny.
7) Modyfikacja za pomocą APTES przyczyniła się do wyraźnego opóźnienia transformacji fazowej anatazu w rutyl oraz spowolnienia wzrostu wielkości krystalitów podczas kalcynacji (w porównaniu do materiałów referencyjnych).
8) Dla nanomateriałów APTES/TiO_2 spadek wielkości powierzchni właściwej i objętości porów po wygrzewaniu był znacznie niższy niż dla kalcynowanych materiałów odniesienia, ze względu na opóźnienie transformacji fazowej oraz spowolnienie wzrostu wielkości krystalitów obu faz.
9) Proces kalcynacji zmienił charakter powierzchni fotokatalizatorów TiO_2 modyfikowanych APTES (wartość potencjału zeta zmieniła się z dodatniego na ujemny).

10) Kalcynacja wpłynęła na zmniejszenie energii pasma wzbronionego (E_g) TiO_2 w przypadku kalcynowanych próbek referencyjnych (3,01 eV dla TiO_2-Ar-1000°C) w porównaniu do wyjściowego TiO_2 (3,29 eV). Dla nanomateriałów APTES/TiO_2 w zakresie niskich stężeń modyfikatora spadek wartości E_g do poziomu próbek odniesienia odnotowano dla materiałów wygrzewanych powyżej 800°C, natomiast dla wysokich stężeń modyfikatora jedynie dla próbek kalcynowanych w 1000°C (przewaga fazowy rutylowej).
11) Odnotowane zmiany pojemności adsorpcyjnej względem błękitu metylenowego oraz Oranżu II związane były ze zmianą ładunku powierzchniowego oraz wartością S_{BET} fotokatalizatorów APTES/TiO_2.
12) Kalcynacja w temperaturze 500 i 700°C przyczyniła się do poprawy stabilności nanomateriałów w kolejnych cyklach rozkładu błękitu metylenowego w porównaniu do próbki niekalcynowanej.
13) W przypadku Oranżu II wszystkie badane półprzewodniki odznaczały się wysoką stabilnością podczas testów ponownego użycia.
14) Biorąc pod uwagę wszystkie przebadane stężenia APTES, za optymalne uznane zostało stężenie 500 mM ze względu na wysoką aktywność fotokatalityczną zarówno w warunkach promieniowania UV oraz UV-Vis.

Literatura

1. Tkaczyk A., Mitrowska K., Posyniak A., Sci. Total Environ. 717 (2020) 137222. https://doi.org/10.1016/j.scitotenv.2020.137222
2. Kümmerer K., Annu. Rev. Environ. Resour. 35(1) (2010) 57–75. https://doi.org/10.1146/annurev-environ-052809-161223
3. Pereira L., Alves M., Dyes-Environmental Impact and Remediation, Environmental Protection Strategies for Sustainable Development. Strategies for Sustainability. Springer (2012) 111–162. https://doi.org/10.1007/978-94-007-1591-2_4
4. Ali H., Water Air Soil Pollut. 213 (2010) 251–273. https://doi.org/10.1007/s11270-010-0382-4
5. Arora S., J. Bioremed. Biodeg. 5(3) (2014) 146. https://doi.org/10.4172/2155- 6199.1000e146
6. Kant R., Nat. Sci. 4(1) (2012) 22–26. https://doi.org/10.4236/ns.2012.41004
7. Zaharia C., Suteu D., Organic Pollutants Ten Years After the Stockholm Convention-Environmental and Analytical Update. InTech (2012) 55–86. https://doi.org/10.5772/32373
8. Chequer F.M.D., de Oliveira G.A.R., Ferraz E.R.A., Cardoso J.C., Zanoni M.V.B., de Oliveira D.P., Eco-friendly Textile Dyeing and Finishing. IntechOpen (2013) 150–176. https://doi.org/10.5772/53659
9. Moradihamedani P., Polym. Bull. 79 (2022) 2603–2631. https://doi.org/10.1007/s00289-021-03603-2
10. Fetimi A., Merouani S., Khan M.S., Asghar M.N., Yadav K.K., Jeon B.-H., Hamachi M., Kebiche-Senhadji O., Benguerba Y., ACS Omega 7 (2022) 13818−13825. https://doi.org/10.1021/acsomega.2c00074

11. Zhang D., Dong S., Prog. Nat. Sci.: Mater. Int. 29 (2019) 277–284. https://doi.org/10.1016/j.pnsc.2019.03.012

12. Sakeye M., Smått J.-H., Langmuir 28 (2012) 16941−16950. https://doi.org/10.1021/la303925x

13. Dong F., Wang H., Wu Z., J. Phys. Chem. C 113 (2009) 16717–16723. https://doi.org/10.1021/jp9049654

14. Dong F., Guo S., Wang H., Li X., Wu Z., J. Phys. Chem. C 115 (2011) 13285–13292. https://doi.org/10.1021/jp111916q

15. Gupta S., Tripathi M., Cent. Eur. J. Chem. 10(2) (2012) 279–294. https://doi.org/10.2478/s11532-011-0155-y

16. Viet P.V., Huy T.H., You S.-J., Hieu L.V., Thic C.M., Superlattices Microstruct. 123 (2018) 447–455. https://doi.org/10.1016/j.spmi.2018.09.035

17. Piątkowska A., Janus M., Szymański K., Mozia S., Catalysts 11 (2021) 144. https://doi.org/10.3390/catal11010144

18. Daghrir R., Drogui P., Robert D., Ind. Eng. Chem. Res. 52 (2013) 3581–3599. https://doi.org/10.1021/ie303468t

19. Khan T.T., Bari G.A.K.M.R., Kang H.-J., Lee T.-G., Park J.-W., Hwang H.J., Hossain S.M., Mun J.S., Suzuki N., Fujishima A., Kim J.-H., Shon H.K., Jun Y.-S., Catalysts 11(1) (2021) 109. https://doi.org/10.3390/catal11010109

20. Alkorbi A.S., Javed H.M.A., Hussain S., Latif S., Mahr M.S., Mustafa M.S., Alsaiari R., Alhemiary N.A., Opt. Mater. 127 (2022) 112259. https://doi.org/10.1016/j.optmat.2022.112259

21. Zhao J., Milanova M., Warmoeskerken M.M.C.G., Dutschk V., Colloids Surf. A Physicochem. Eng. Asp. 413 (2012) 273–279. https://doi.org/10.1016/j.colsurfa.2011.11.033

22. Kusiak-Nejman E., Wanag A., Kapica-Kozar J., Morawski A.W., Int. J. Mater. Prod. Technol. 52 (2016) 286–297. https://doi.org/10.1504/ IJMPT.2016.075501

23. https://molview.org/?cid=13521

24. Chung K.-T., J. Environ. Sci. Health C: Toxicol. 34(4) (2016) 233–261, https://doi.org/10.1080/10590501.2016.1236602

25. Ohashi T., Jara A.M.T., Batista A.C.L., Franco L.O., Lima M.A.B., Benachour M., Alves da Silva C.A., Campos-Takaki G.M., Molecules 17 (2012) 14219–14229. https://doi:10.3390/molecules171214219

26. Riaz N., Chong F.K., Man Z.B., Khan M.S., Dutta B.K., Ind. Eng. Chem. Res. 52(12) (2013) 4491–4503. https://doi.org/10.1021/ie303255v

27. Oladoye P.O., Ajiboye T.O., Omotola E.O., Oyewola O.J., Results Eng. 16 (2022) 100678. https://doi.org/10.1016/j.rineng.2022.100678

28. https://molview.org/?cid=135442941

29. https://molview.org/?q=Methylene%20blue

30. Sarbak Z., Wiadomości chemiczne 65 (2011) 5–6.

31. Santos C., Fraga M.E., Kozakiewicz Z., Lima N., Res. Microbiol. 161 (2010) 168–175. https://doi.org/10.1016/j.resmic.2009.12.007

32. Hassanien S.A., Akl A.A., Superlattices Microstruct. 89 (2016) 153–169. https://doi.org/10.1016/j.spmi.2015.10.044

33. Förster H., Mol. Sieves 4 (2004) 337–426. https://doi.org/10.1007/b94239

34. Chen D., Zou L., Li S., Zheng F., Sci. Rep. 6 (2016) 20335. https://doi.org/10.1038/srep20335

35. Canchanya-Huaman Y., Mayta-Armas A.F., Pomalaya-Velasco J., Bendezú-Roca Y., Guerra J.A., Ramos-Guivar J.A., Nanomaterials 11(9) 2021 2311. https://doi.org/10.3390/nano11092311

36. Nwaokafor P., Okeoma K.B., Echendu O.K., Ohajianya A.C., Egbo K.O., Metallogr. Microstruct. Anal. 10 (2021) 727–735. https://doi.org/10.1007/s13632-021-00792-0

37. Vernon-Parry K.D., III-Vs Review 13 (2000) 40–44. https://doi.org/10.1016/S0961-1290(00)80006-X

38. Bazin D., Bouderlique E., Daudon E., Frochot V., Haymann J.-P., Letavernier E., Tielens F., Weil R., C. R. Chim. 25 (2022) 37–60. https://doi.org/10.5802/crchim.101

39. Lunardi C.N., Gomes A.J., Rocha F.S., Tommaso J.D., Patience G.S, Can. J. Chem. Eng. 99 (2021) 627–639. https://doi.org/10.1002/cjce.23914

40. Dembek M., Bocian S., Buszewski B., Molecules 27(3) 2022 968. https://doi.org/10.3390/molecules27030968

41. Bubacz K., Tryba B., Morawski A.W., Mater. Res. Bull. 47 (2012) 3697−3703. https://doi.org/10.1016/j. materresbull.2012.06.038

42. Al-Ghouti M.A., Al-Absi R.S., Sci. Rep. 10 (2020) 15928. https://doi.org/10.1038/s41598-020-72996-3

43. Saxena V., Aswal D.K., Semicond. Sci. Technol. 30 (2015) 064005. https://doi.org/10.1088/0268-1242/30/6/064005

44. Shenoy M.R., Ayyasamy S., Reddy M.V.V., Kadarkarai G., Suryakanth J., Tamilarasan S., Thangavelu S., Jeyaramane A.Ch., J. Mater. Sci: Mater. Electron. 31 (2020) 17703−17717. https://doi.org/10.1007/s10854-020-04325-3

45. Buckingham J., Dictionary of Organic Compounds, wydanie 5, Chapman and Hall, Nowy Jork 1982.

46. Kassir M., Roques-Carmes T., Assaker K., Hamieh T., Razafitianamaharavo A., Toufaily J., Villiéras F., Phys. Procedia 55 (2014) 403–408. https://doi.org/10.1016/j.phpro.2014.07.058

47. Bui D.-N., Kang S.-Z., Li X., J. Mu, Catal. Commun. 13 (2011) 14–17. https://doi.org/10.1016/j.catcom.2011.06.016

48. Van Viet P., Huy T.H., You S.J., Hieu L.V., Thi C.M., Superlattice. Micro. 123 (2018) 447–455. https://doi.org/10.1016/j.spmi.2018.09.035

49. Zamiri M., Giahi M., Russ. J. Phys. Chem. 90 (2016) 2668–2674. https://doi.org/10.1134/S0036024416130240

50. Yu W., Zhang J., Peng T., Appl. Catal. B Environ. 181 (2016) 220–227. https://doi.org/10.1016/j.apcatb.2015.07.031

51. Rauf M.A., Salman Ashraf S., Chem. Eng. J. 151 (2009) 10–18. https://doi.org/10.1016/j.cej.2009.02.026

52. Konstantinou I.K., Albanis T.A., Appl. Catal. B Environ. 49 (2004) 1–14. https://doi.org/10.1016/j.apcatb.2003.11.010

53. Wang S., Zhu Z.H., Coomes A., Haghseresht F., Lu G.Q., J. Colloid Interface Sci. 284 (2005) 440–446. https://doi.org/10.1016/j.jcis.2004.10.050

54. Beegam M.Sh., Ullattil S.G., Periyat P., Sol. Energy 160 (2018) 10–17. https://doi.org/10.1016/j.solener.2017.11.065

55. Ayawei N., Ebelegi A.N., Wankasi D., J. Chem. 2017 (2017) 3039817. https://doi.org/10.1155/2017/3039817

56. Jafari S., Tryba B., Kusiak-Nejman E., Kapica-Kozar J., Morawski A.W., Sillanpää M., J. Mol. Liq. 220 (2016) 504–512. https://doi.org/10.1016/j.molliq.2016.02.014

57. Konicki W., Aleksandrzak M., Moszyński D., Mijowska E., J. Colloid Interface Sci. 496 (2017) 188–200. https://doi.org/10.1016/j.jcis.2017.02.031

58. Luís A.M., Neves M.C., Mendonça M.H., Monteiro O.C., Mater. Chem. Phys. 125 (2011) 20–25. https://doi.org/10.1016/j.matchemphys.2010.08.019

59. Ohno T., Tokieda K., Higashida S., Matsumura M., Appl. Catal. A: Gen. 244 (2003) 383–391. https://doi.org/10.1016/S0926-860X(02)00610-5

60. Su Y., Wu J., Quan X., Chen Sh., Desalination 252 (2010) 143–148. https://doi.org/10.1016/j.desal.2009.10.011

61. Zhang R.-B., J. Non-Cryst. Solids 351 (2005) 2129–2132. https://doi.org/10.1016/j.jnoncrysol.2005.04.048

62. Fu G., Zhou P., Zhao M., Zhu W., Yan S., Yu T., Zou T., Dalton Trans. 44 (2015) 12812–12817. https://doi.org/10.1039/C5DT01204J

63. Cheng Y., Luo F., Jiang Y., Li F., Wei C., Colloids Surf. A 554 (2018) 81–85. https://doi.org/10.1016/j.colsurfa.2018.06.032

64. Wang Q., Chen Ch., Zhao D., Ma W., J. Zhao, Langmuir 24 (2008) 7338–7345. https://doi.org/10.1021/la800313s

65. Bao N., Wu G., Niu J., Zhang Q., He S., Wang J., J. Alloys Compd. 599 (2014) 40–48. https://doi.org/10.1016/j.jallcom.2014.02.072

66. Yu H.-F., J. Phys. Chem. Solids 68 (2007) 600–607. https://doi.org/10.1016/j.jpcs.2007.01.050

67. Meroni D., Lo Presti L., Di Liberto G., Ceotto M., Acres R.G., Prince K.C., Bellani R., Soliveri G., Ardizzone S., J. Phys. Chem. C 121 (2017) 430–440. https://doi.org/10.1021/acs.jpcc.6b10720

68. Zamiri M., Giahi M., Russ. J. Phys. Chem. A 90 (2016) 2668–2674. https://doi.org/10.1134/S0036024416130240

69. Bartošová A., Blinová L., Sirotiak M., Michalíková M., Res. Pap. Fac. Mater. Sci. Technol. Slovak Univ. Technol. 25 (2017) 103–111. https://doi.org/10.1515/rput-2017-0012

70. Yahyaei B., Azizian S., Chem. Eng. J. 209 (2012) 589–596. https://doi.org/10.1016/j.cej.2012.08.055

71. Tobaldi D.M., Tucci A., Skapin A.S., Esposito L., J. Eur. Ceram. Soc. 30 (2010) 2481–2490. https://doi.org/10.1016/j.jeurceramsoc.2010.05.014

72. Okada K., Yamamoto N., Kameshima Y., Yasumori A., MacKenzie K.J.D., Ceram. Soc. 84 (2001) 1591–1596. https://doi.org/10.1111/j.1151-2916.2001.tb00882.x

73. Morawski A.W., Janus M., Tryba B., Toyoda M., Tsumura T., Inagaki M., Pol. J. Chem. Technol. 11 (2009) 46–50. https://doi.org/10.2478/v10026-009-0023-0

74. Klaysri R., Tubchareon T., Praserthdam P., J. Ind. Eng. Chem. 45 (2017) 229–236. https://doi.org/10.1016/j.jiec.2016.09.027

75. Li Z., Hou B., Xu Y., Wu D., Sun Y., J. Colloid Interface Sci. 288 (2005) 149–154. https://doi.org/10.1016/j.jcis.2005.02.082

76. Ovchinnikov O.V., Evtukhova A.V., Kondratenko T.S., Smirnov M.S., Khokhlov V.Y., Erina O.V., Vib. Spectrosc. 86 (2016) 181–189. https://doi.org/10.1016/j.vibspec.2016.06.016

77. Cai J., Xin W., Liu G., Lin D., Zhu D., Mater. Res. 19 (2016) 401–407. https://doi.org/10.1590/1980-5373-MR-2015-0381

Journal of Environmental Chemical Engineering 8 (2020) 103917

Contents lists available at ScienceDirect

Journal of Environmental Chemical Engineering

journal homepage: www.elsevier.com/locate/jece

Influence of modification of titanium dioxide by silane coupling agents on the photocatalytic activity and stability

Agnieszka Wanag*, Agnieszka Sienkiewicz, Paulina Rokicka-Konieczna, Ewelina Kusiak-Nejman, Antoni W. Morawski

West Pomeranian University of Technology in Szczecin, Faculty of Chemical Technology and Engineering, Department of Inorganic Chemical Technology and Environment Engineering, Pułaskiego 10, 70-322, Szczecin, Poland

ARTICLE INFO

Editor: G.L. Dotto

Keywords:
Photocatalysis
Titanium dioxide
3-aminopropyltriethoxysilane
Methylene blue decomposition

ABSTRACT

In this paper, titanium dioxide modification with 3-aminopropyltriethoxysilane as a silicon source is presented. The TiO_2/APTES photocatalysts were obtained utilizing a solvothermal method. Different concentrations of APTES dissolved in ethanol were used for materials preparation (10 − 3000 mM). The samples were characterized by different analytical methods such as FT-IR/DRS, UV–vis/DRS, XRD, SEM. The carbon and nitrogen content to confirm, as well as the BET specific surface area, were also measured. The analysis confirmed the presence of silicon, carbon and nitrogen in the TiO_2 structure, suggesting that modification was carried out successfully. The carbon and nitrogen were also indications in the sample after the reusability test in water. The photocatalytic activity of the nanomaterials was investigated on the basis of methylene blue decomposition under UV light irradiation. Photocatalytic activity increases with the increase of APTES concentration used for modification. The novelty of research was to check the possibility of photocatalysts reuse. In this case, the sample with the highest decomposition degree was subjected to the reusability test. It it was found that the samples after this type of modification are not stable due to destruction of the APTES alkyl chains and detachment the amine groups during UV irradiation.

1. Introduction

A serious problem facing modern societies, threatening the life and health of future generations is water pollutions. Every day industrial, civil and militaries activities create an enormous amount of organic pollutants that end up in our lakes, rivers and [1]. Thus, scientists are interested in searching for new alternative methods for removing environmental contaminants [2]. The researches on photocatalysis show that it is a promising method for the decomposition of pollutants without producing any harmful by-products [3,4].

One of the most often used photocatalysts is titanium dioxide (TiO_2), large bandgap semiconductor that exhibits photocatalytic activity primarily in the UV region [5]. TiO_2 due to its non-toxicity, high oxidation efficiency and photostability, chemical inertness and low cost remains one of the most promising materials. Currently, many researchers tried to add various additives to TiO_2 in order to improve its photocatalytic activity and physicochemical properties. Much attention has been focused on the doping of pure TiO_2 with either cations (i.e. Al, Ag, Pt, Co, Fe or Si) or anions (i.e. N, C, I or S) [6–8].

Currently, one of the very promising approaches involves using silicon for TiO_2 surface modification. Xu et al. [9] and Tobaldi et al. [10] reported that the incorporation of silicon into the TiO_2 would enhance the specific surface area, decrease particles size, and repress the phase transformation from anatase to rutile. The most recent way involves using as precursors of silicon, organosilane coupling agents for titanium dioxide surface modification. The general formula of organosilanes is $R_nSiX_{(4-n)}$, where X is a hydrolyzable group, i.e. ethoxy or methoxy group, and R is a nonhydrolyzable organic functional group [11]. While the surface modification, hydrolysis of silanes to silanols takes place at first, and then there is a condensation reaction between OH groups on the substrate surface and the silanols. The formation of covalent bonds or non-covalent hydrogen bonds between OH groups and different molecular groups of silanes is the pivotal chemical process of surface modification. But, when the organic functional groups derived from the silane interact with the particle surface in a different way than the interaction between surface OH groups and silanols. The chemical image of particle surface modified by organosilanes is still unclear [12]. 3-aminopropyltriethoxysilane (APTES) is an aminosilane which consists of one aminopropyl and three ethoxy functional groups, attached to the central silicon atom, which is frequently used as a silane

* Corresponding author.
E-mail address: awanag@zut.edu.pl (A. Wanag).

https://doi.org/10.1016/j.jece.2020.103917
Received 10 February 2020; Received in revised form 28 March 2020; Accepted 29 March 2020
Available online 04 April 2020

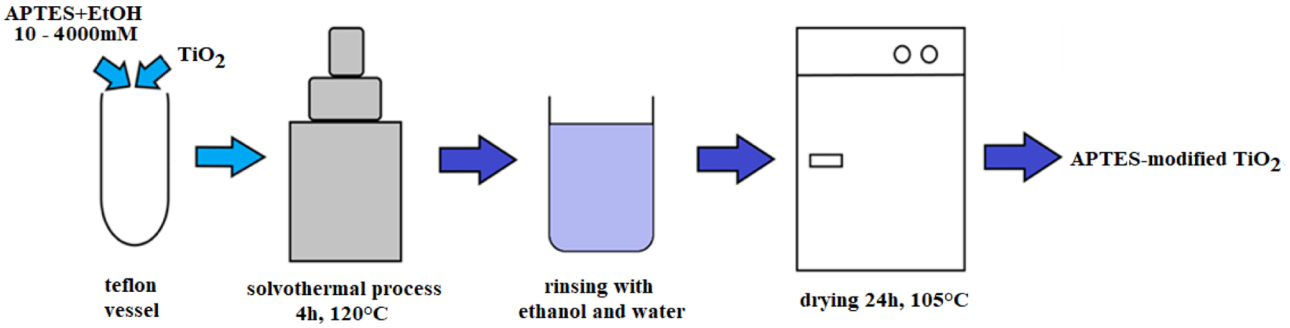

Fig. 1. Schematic illustration of the photocatalysts synthesis.

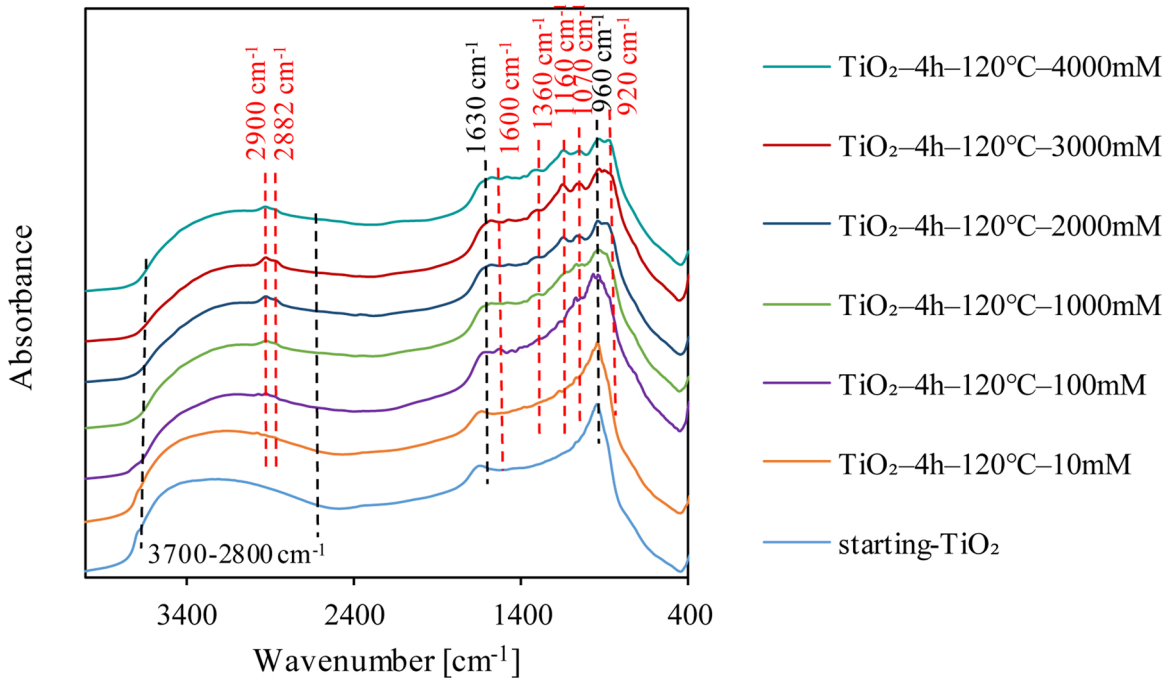

Fig. 2. FT-IR/DR spectra of starting-TiO_2 and APTES-modified TiO_2.

coupling agent [13]. APTES-functionalized TiO_2 nanomaterials can be used in a different area. For example, Andrzejewska et al. [14] studied a result of modifications that were executed to received pigments by adsorption of organic dyes on a modified surface of a TiO_2 pigment system. In this research, organosilanes were used as a TiO_2 surface modification agent. Shakeri et al. [15] studied the self-cleaning capability of the surface of ceramic tiles covered by APTES-functionalized TiO_2 nanoparticles. They have shown that the obtained coating was stable, and the surface was able to degrade the dye, which was used as an organic pollutant. López-Zamora et al. [16] studied the improvement of the colloidal stability of TiO_2 particles in water through organosilane coupling agents. They proved that APTES-modified TiO_2 exhibit higher colloidal stability in water than unmodified titanium dioxide. Klaysri et al. [17] proposed a one-step synthesis method of APTES-functionalized TiO_2 surface. They showed that obtained nanomaterials are capable of photocatalytic decolorization of methylene blue. Despite the enlarging interest in APTES-modified TiO_2 photocatalysts, no possible general mechanism of the formation of a covalent linkage between anchoring group of APTES and oxide metal surface has been proposed. One of the possible mechanisms says that OH groups on the titanium dioxide surface reacted with the ethoxy groups of aminosilane to form the primary Ti—O—Si [17]. In general, APTES-functionalized TiO_2 surface is linked as Si—N co-doped titanium dioxide [18]. The partial monolayer of N- and Si-doped TiO_2 can additionally increase the adsorption and degradation of methylene blue under UV light irradiation [17].

The primary purpose of the present paper was a preparation method of titanium dioxide nanomaterials modified with 3-aminopropyltriethoxysilane. APTES-modified TiO_2 photocatalysts were obtained by a solvothermal process using ethanol as a solvent. The photocatalytic activity of gained samples was measured based on methylene blue decomposition under UV irradiation. The relation between APTES content and the photocatalytic activity of new nanomaterials is discussed. To the best of our knowledge, this is the first paper presenting the results on multicycle photostability measurements of APTES-modified TiO_2 photocatalysts. The recoverability, hence the reusability of utilizing photocatalysts is one of the most crucial key factors due to the reduction of the costs of the photocatalytic process.

2. Experimental

2.1. Materials and reagents

The new photocatalysts were obtained by modification of raw TiO_2 slurry gained by sulphate technology, provided by chemical plant Grupa Azoty Zakłady Chemiczne “Police” S.A. (Poland). Before modification, a crude TiO_2 containing residual sulphur from post-production sulphuric acid was rinsed with an aqueous solution of NH_4OH (25

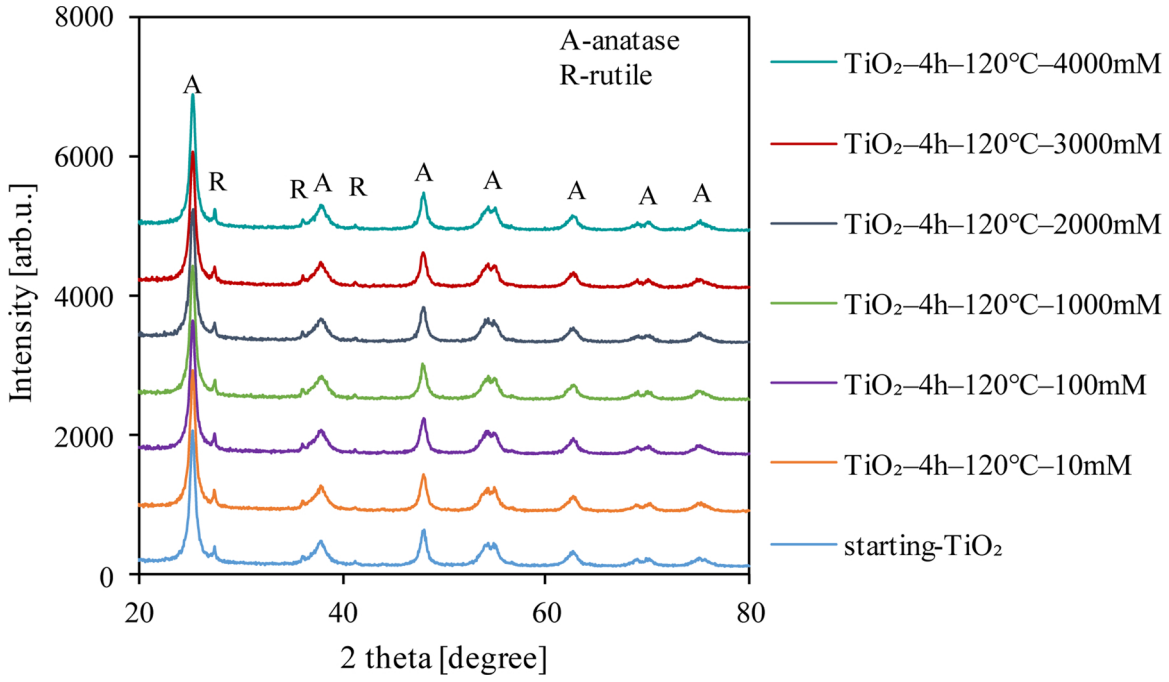

Fig. 3. XRD patterns of starting-TiO_2 and APTES-modified TiO_2.

% pure p.a., Firma Chempur®, Poland) to remove the residues of sulphuric compounds through the formation of $(NH_4)_2SO_4$ as a well-dissolved salt in water, and then was rinsed with distilled water to pH = 6.8. The received material was dried for 24 h at 105 °C in a muffle furnace to remove water molecules adsorbed on the surface TiO_2. The obtained material was named as starting-TiO_2. Ethanol (96 % from P.P.H. "STANLAB" Sp.J., Poland) was used as an APTES solvent, and Sigma-Aldrich® APTES (Merck KGaA, Germany) was used as a modifier. As an organic dye in photocatalytic tests methylene blue (Firma Chempur®, Poland) was used.

2.2. Surface modification of titanium dioxide

In this research, different amount of APTES was used to titanium dioxide surface modification, and the concentrations of 3-aminopropyltriethoxysilane in ethanol were 10, 100, 1000, 2000, 3000 and 4000 mM. First, 5 g of starting-TiO_2 powder was dispersed in 25 mL of APTES solution and then modified in a pressure autoclave for 4 h at 120 °C with continuous stirring at 500 rpm. The obtained slurry was rinsed with ethanol and distilled water to remove residual chemicals. Finally, the received material was dried at 105 °C for 24 h in a muffle furnace. Schematic illustration of the photocatalysts synthesis is presented in Fig. 1.

2.3. Characterization

FT-IR/DRS spectrophotometer FT-IR 4200 (Jasco International Co. Ltd., Japan) provided with a diffuse reflectance accessory (PIKE Technologies, USA) was used to identify the surface functional groups of the APTES-modified TiO_2. The FT-IR bands were examined in the range of $400-4000\ cm^{-1}$. The morphology of the surface of obtained photocatalysts was examined via scanning electron microscopy (SEM). For this purpose, Hitachi SU8020 Ultra-High Resolution Field Emission Scanning Electron Microscope (Hitachi Ltd., Japan) was utilized. The crystalline phase of received nanomaterials was identified by means of XRD analysis (PANalytical Empyrean X-ray diffractometer, USA) using Cu Kα radiation (λ = 0.154056 nm). The XRD diffractograms were collected in the range 2 − 80° of 2θ scale. For specification of the phase composition, the PDF-4 + 2014 International Centre for Diffraction Data database (04-002-8296 PDF4 + card for anatase and 04-005-5923 PDF4 + card for rutile identification) was used. To calculate the average anatase crystallite size the Scherrer's equation was used. According to a simple peak intensity-based method, the anatase percentage content was calculated. The percentage of anatase in the crystalline phase [%A] was calculated, as shown in Eq. (1), where I_A and I_R are the diffraction intensities of the anatase peak at 25.4° and rutile peak at 27.5°, respectively:

$$\%A = \frac{I_A}{I_A + I_R} \cdot 100\% \quad (1)$$

The Brunauer-Emmett-Teller (BET) surface area and pore volume distribution of the tested photocatalysts were carried out by nitrogen adsorption-desorption measurements at 77 K conducted by QUADRASORB evoTM Gas Sorption analyzer (Anton Paar GmbH, Austria), previously Quantachrome Instruments, USA) device. Prior to measurements, all samples were degassed for 12 h at 100 °C under high vacuum to pre-clean the surface of tested sample. Total nitrogen and carbon content in studied materials were determined using CN 628 elemental analyzer (LECO Corporation, USA). The certified EDTAstandard (LECO Corporation, USA) containing 41.06 ± 0.09 wt.% of carbon and 9.56 ± 0.03 wt.% of nitrogen was used for the preparation of a calibration curve. The error range for measurements was ± 0.1 %.

2.4. Photocatalytic activity test

The degradation process of methylene blue under UV–vis light with high UV intensity was used to determine the photocatalytic activity of APTES-modified TiO_2 photocatalysts. The light was provided by 6 lamps with the power of 20 W each with the radiation intensity of about $110\ W/m^2$ for UV (measured in the range of 280 − 400 nm) and $5\ W/m^2$ for the range of 300 − 2800 nm. The utilized type of irradiation source was named as UV light, in view of the low intensity of Vis irradiation. All photocatalytic experiments were carried out in a glass beakers containing 0.5 L of methylene blue solution with the initial concentration of 15 mg/L, and 0.5 g/L of the appropriate photocatalyst. Before the photocatalytic experiment, the suspension was stirred in a magnetic stirrer in the darkness for 60 min to provide the establishment of the adsorption-desorption equilibrium between methylene blue molecules

Table 1
XRD phase composition, crystallites size, specific surface area, carbon and nitrogen content of starting-TiO_2 and APTES-modified photocatalysts.

Sample name	Anatase in crystallite phase [%]	Anatase crystallite size [nm]	S_{BET} [m^2/g]	V_{total} [a] [cm^3/g]	V_{micro} [b] [cm^3/g]	V_{meso} [c] [cm^3/g]	Carbon content (wt.%)	Nitrogen content (wt.%)
starting-TiO_2	95 ± 1	14 ± 0.4	207 ± 10	0.36 ± 0.02	0.07 ± 0.00	0.32 ± 0.02	–	0.18 ± 0.01
TiO_2-4h-120°C-10mM	95 ± 1	15 ± 0.4	202 ± 10	0.37 ± 0.02	0.07 ± 0.00	0.33 ± 0.02	1.35 ± 0.01	0.19 ± 0.01
TiO_2-4h-120°C-100mM	96 ± 1	15 ± 0.4	178 ± 9	0.31 ± 0.02	0.06 ± 0.00	0.25 ± 0.02	1.89 ± 0.01	0.77 ± 0.01
TiO_2-4h-120°C-1000mM	96 ± 1	14 ± 0.4	106 ± 5	0.25 ± 0.01	0.04 ± 0.00	0.21 ± 0.01	4.27 ± 0.00	1.61 ± 0.07
TiO_2-4h-120°C-2000 mM	95 ± 1	14 ± 0.4	65 ± 3	0.18 ± 0.01	0.02 ± 0.00	0.16 ± 0.01	5.48 ± 0.26	2.08 ± 0.09
TiO_2-4h-120°C-3000mM	95 ± 1	14 ± 0.4	40 ± 2	0.16 ± 0.01	0.01 ± 0.00	0.15 ± 0.01	6.43 ± 0.13	2.43 ± 0.02
TiO_2-4h-120°C-4000mM	95 ± 1	15 ± 0.4	52 ± 3	0.16 ± 0.01	0.02 ± 0.00	0.14 ± 0.01	6.09 ± 0.17	2.30 ± 0.06

[a] Total pore volume determined by the single point from the nitrogen adsorption isotherms at relative pressure $p/p_0 = 0.99$.
[b] Micropore volume estimated using the Dubinin–Radushkevich method.
[c] Mesopore volume determined as the difference between V_{total} and V_{micro}.

and TiO_2 surface. Next, the solution was exposed to UV light irradiation. After 240 min, 10 mL of suspension solution was taken and centrifuged to separate the TiO_2 nanoparticles from the methylene blue solution. V-630 UV–vis spectrometer (Jasco International Co., Japan) was used to measure the methylene blue absorbance, which value was then used to calculate the dye concentration. The reusability test of the selected sample was investigated based on the degradation of methylene blue under UV light during 240 min of irradiation. After each cycle, the photocatalyst was separated by filtration and dried at 100 °C and then added to a new portion of the methylene blue solution.

3. Results and discussion

3.1. Characterization of the photocatalysts

Fig. 2 shows the FT-IR/DRS spectra of starting and organosilane-modified TiO_2. The comparison among the spectra of unmodified and modified TiO_2 shows some new characteristics peaks derived from APTES. This indicates that APTES was successfully coupled to TiO_2 surface. The peaks around 2900 and 2882 cm^{-1} can be assigned the asymmetric and symmetric stretches of $-CH_2$ groups on the alkyl chain [19,20]. It can be observed that the intensity of the mentioned peaks grows with the increasing amount of APTES used for modification. The N—H bending vibrations of primary amine are observed at around 1600 cm^{-1} [21,22]. Another slight peak located around 1360 cm^{-1} confirms the presence of C—N bands [19]. Moreover, the peak at around 920 cm^{-1} indicates that the reaction of condensation between hydroxyl groups on TiO_2 surface and silanol groups occurred [23]. According to Li et al. [24] band presented at 960–910 cm^{-1} is assigned to the stretching vibrations of Ti—O—Si bonds. The peak at around 1160 cm^{-1} corresponds to the asymmetric stretching vibrations of Si—O—Si, which indicates the reaction of condensation between silanol groups [19,24]. In addition, the Si—O—C stretching modes are also present at around 1070 cm^{-1} [19]. As can be seen in Fig. 2, the intensity of the upper-mentioned bands increases with the increase of APTES amount used for TiO_2 modification. All of the presented spectra also exhibit some bands typical for TiO_2-based nanomaterials. A broad band at 3700–2600 cm^{-1} is assigned to O—H stretching vibrations [25,26]. Peak located around 1630 cm^{-1} corresponds to the molecular water bending mode [27]. In turn, the intensive band at 960 cm^{-1} is attributed to the O—Ti—O stretching modes [28].

The XRD patterns of the starting and APTES-modified TiO_2 are shown in Fig. 3. The percentage and crystallite size of anatase in tested samples are listed in Table 1. After APTES modification tested samples show similar patterns to starting-TiO_2. As can be observed, all tested samples exhibit reflections characteristic for anatase phase: (101), (004), (200), (105), (211), (204), (116), (220), (215) located at 25.3, 37.6, 47.8, 53.7, 54.8, 62.6, 68.7, 70.2 and 75.0°, respectively (JCPDS 01-070-7348) and one small reflection located at 27.1° characteristic for rutile (110) phase (JCPDS 01-076-0318). It can be noted that prepared photocatalysts contain mainly of anatase phase (95–96 %) with a small amount of rutile. The presence of rutile in the materials is associated with the titania white production process via sulphate technology. From Table 1 can be seen that the APTES modification did not contribute to phase transformation, what is typical matter because anatase-to-rutile transformation takes place above 600 °C [29]. No significant changes in the crystalline structure of TiO_2 are observed. The crystallite size of anatase is similar for all tested nanomaterials and equals 14 – 15 nm.

In Fig. 4 the adsorption-desorption isotherms of all tested nanomaterials are shown. It can be observed that photocatalysts show two kinds of isotherm type. Starting-TiO_2, as well as samples modified with APTES concentration between 10 and 1000 mM, present a type IV isotherm (according to IUPAC classification) characteristic for mesoporous materials [30]. These materials also exhibit the same H3 type of hysteresis loops which characterise by slit-shaped pores (they do not

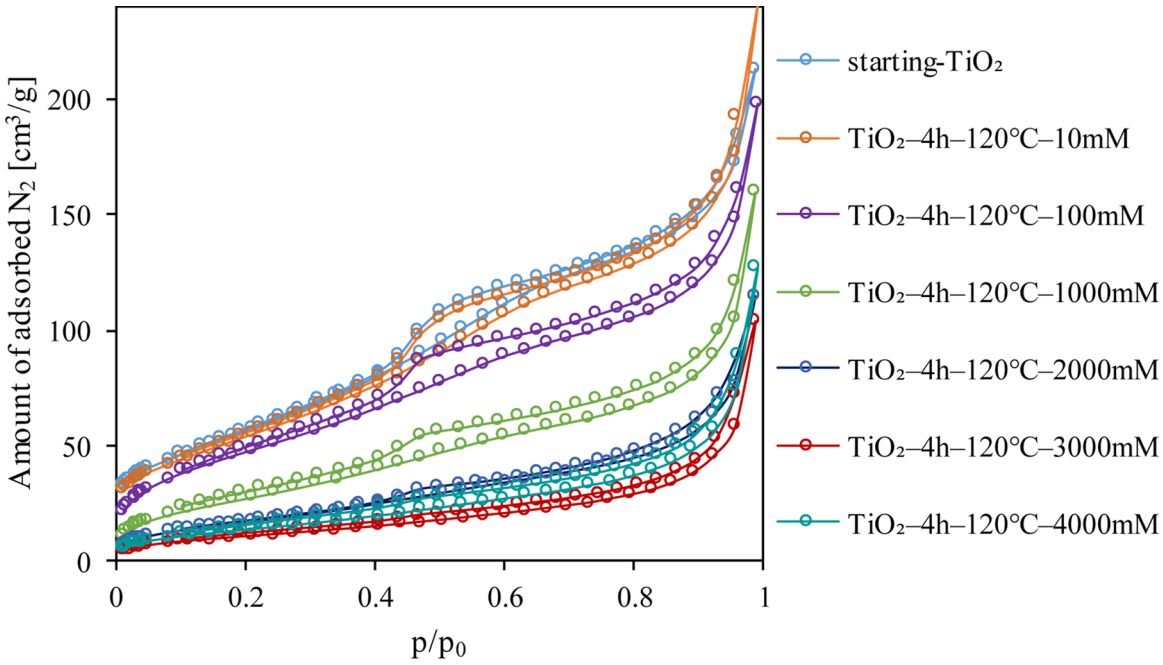

Fig. 4. Adsorption-desorption isotherms of starting-TiO_2 and APTES-modified TiO_2.

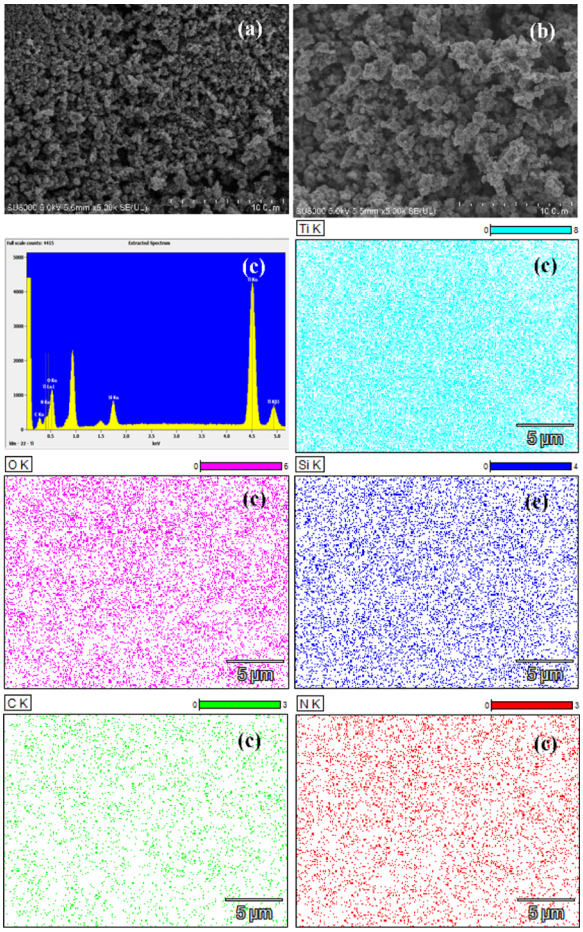

Fig. 5. The SEM image of (a) starting-TiO_2, (b) TiO_2–4h – 120°C–2000 mM, and EDX spectrum and EDX mappings of (c) TiO_2–4h – 120°C–2000 mM.

show any limiting adsorption at high p/p_0) [31,32]. As the APTES concentration increases above 1000 mM, the samples demonstrate II type isotherm typical for non-porous materials [32]. In this case, the hysteresis loop is not observed. It should be noted that the presence of different types of isotherms is related to pore volume changes (see Table 1). The decrease of total pore volume from 0.36 to 0.16 cm^3/g after a modification indicates that APTES molecules are located in TiO_2 external surface as well as captured in pores. Our observations comply with results obtained by Zhuang et al. [21] and Ukaji et al. [22]. Table 1 summarizes the structural properties of BET specific surface area (S_{BET}), total pore volume (V_{total}), micro (V_{micro}) and mesopores volume (V_{meso}), as well as including nitrogen and carbon content in all obtained nanomaterials. The specific surface area for starting-TiO_2 equals 207 m^2/g, while for APTES-modified TiO_2 is in a range from 202 to 40 m^2/g. It can also be observed that carbon and nitrogen contents increase with the increase of APTES concentration used to modification. Furthermore, the correlation between specific surface area, total pore volume and APTES concentration is observed. Thus, the increase of APTES concentrations causes a significant reduction of the specific surface area and pore size volume of tested nanomaterials.

Representative SEM images of starting-TiO_2 and TiO_2-4h-120°C–2000 mM photocatalysts are presented in Fig. 5a and b. Starting-TiO_2 consists of particles aggregated to a larger size. The morphology of this sample is quite homogenous, but the grains form aggregates. The particles of the photocatalysts after APTES modification are also characterized by not regular and undefined shape, but it can be observed that modification causes the increase of aggregates size. The elemental composition of obtained samples was confirmed by EDX mapping analysis, which results are shown in Fig. 5c, including the element stratification and the distribution diagram of an appropriate tested element. The images show that the obtained sample contains Ti, O, Si, C and N elements. It can also be observed that all elements are homogeneously dispersed throughout the surface. In Fig. 6, the intensity of the Si peak for each obtained samples is shown. On the basis of the ratio of the peaks, it can be noted that silicon content increases with the increase of APTES concentration used during modification. Thus, the highest silicon content is noted for TiO_2-4h-120°C-2000 mM photocatalyst. This result also suggests that 2000 mM of APTES concentration was found to be an optimal value for modification. The APTES concentration of 3000 and 4000 mM is too high, and probably some amount of the component could separate during rinsing with ethanol and water.

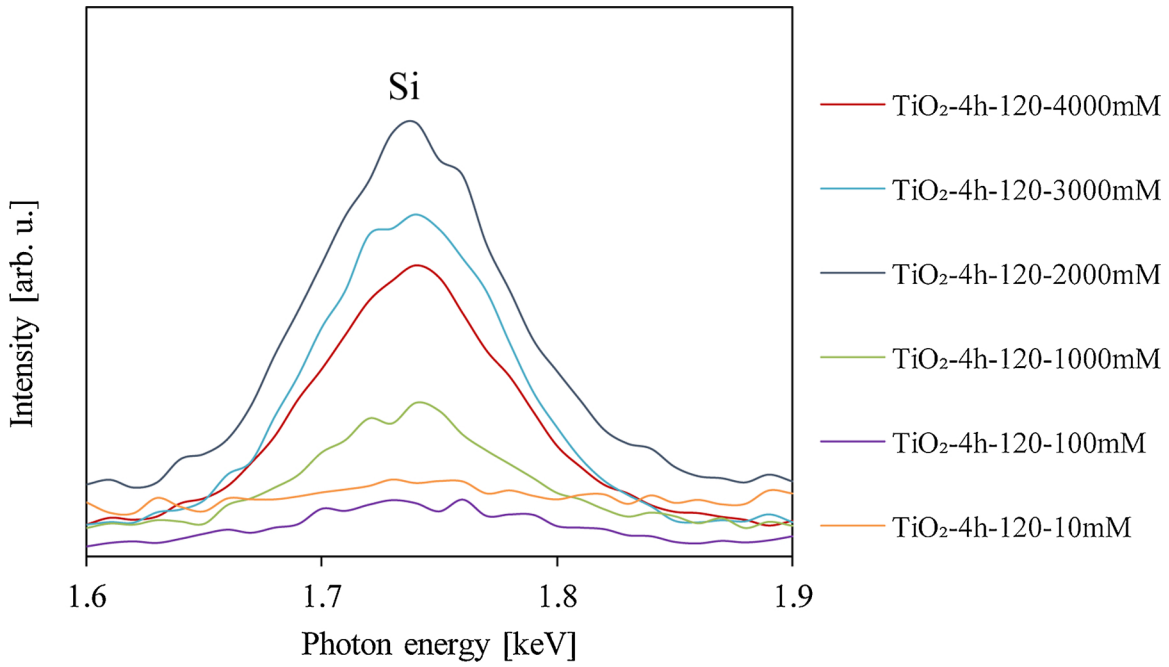

Fig. 6. Silicon EDX spectra of modified TiO_2.

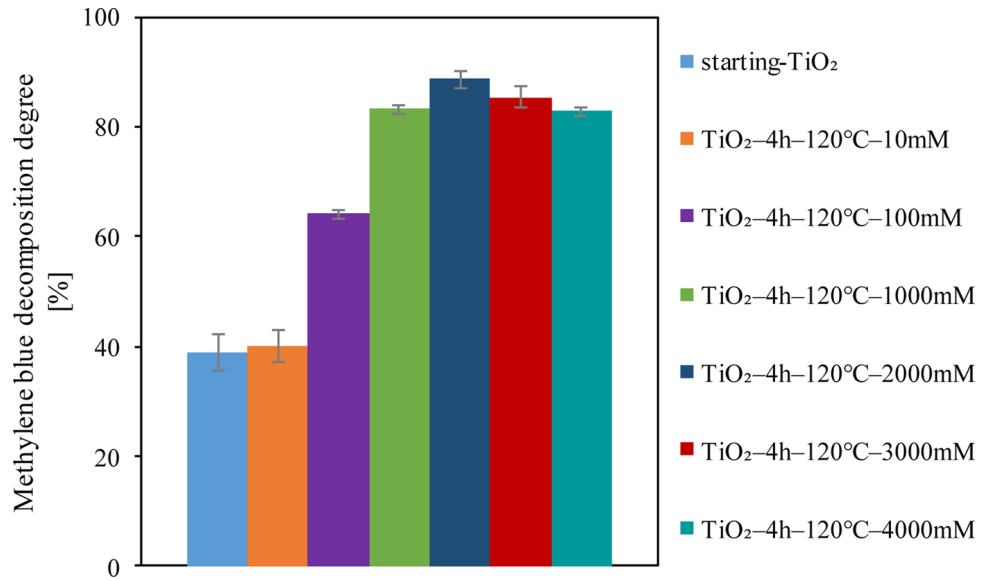

Fig. 7. Methylene blue decomposition degree after 240 min of irradiation. (For interpretation of the references to colour in this figure legend, the reader is referred to the web version of this article).

3.2. Photocatalytic degradation of methylene blue

The photocatalytic activity of the starting-TiO_2 and new APTES-modified titania nanomaterials was tested during decomposition of methylene blue under UV irradiation. The results of the photocatalytic test are shown in Fig. 7. It can be seen that the decomposition degree increases with the increase of the APTES concentration up to 2000 mM. Furthermore, all modified photocatalysts show higher decomposition degree than the starting-TiO_2. The highest photoactivity is observed for TiO_2-4h-120°C–2000 mM sample. It should also be mentioned that photoefficiency for photocatalysts with modified with 1000, 2000, 3000 and 4000 mM of APTES is similar, and the value is between 83.1–88.5 %, which differences are negligible.

From the application point of view, the photocatalytic stability of semiconductors during subsequent photocatalytic cycles is a significant factor. The long-term efficiency of TiO_2-4h-120°C–2000 mM sample was conducted for four consecutive photocatalytic cycles (the experiment in detail is described in the experimental section). After the first cycle (see Fig. 8), the activity decreased about 30 % and after the fourth about 55 %. In order to explain this phenomenon, before and after each cycle, the FT-IR/DRS spectra were measured (Fig. 9). It is noted that the shape of spectra after cycles is slightly different than it is shown in Fig. 2. Thus, the photocatalyst structure was changed during the photocatalytic reaction. After the first cycle, the peaks around 2900 and 2882 cm^{-1} attributed to the $-CH_2$ groups, as well as located around 1070 cm^{-1} (and assigned to the Si—O—C stretching modes) have not already been observed. It can be suggested that APTES molecules were disintegrated and only bond between Si and Ti was not destroyed what is possible to observe on the FT-IR/DRS spectra. These conclusions are consistent with the results obtained by Meroni et al. [19]. They found

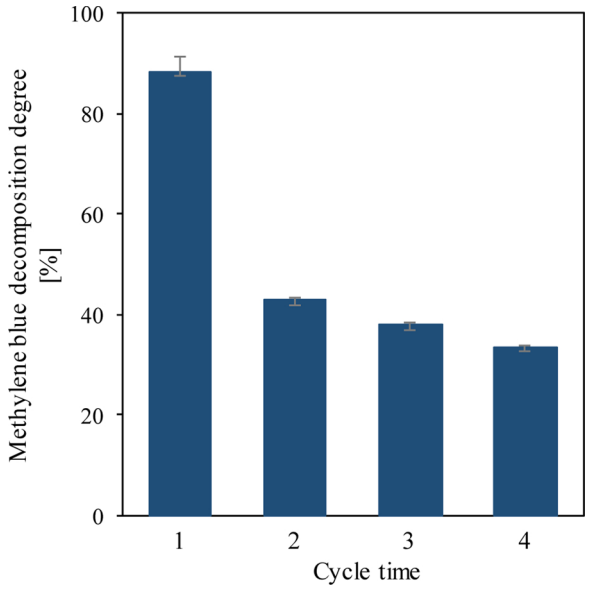

Fig. 8. Cycling photodegradation runs of methylene blue with TiO_2–4h – 120°C–2000 mM sample. (For interpretation of the references to colour in this figure legend, the reader is referred to the web version of this article).

that solar light causes oxidation of the alkyl chains in APTES and detachment of the amine groups. Moreover, they noted that irradiation does not destroy the bond between Ti and Si.

In order to verify the above observations, the test of the composition stability of studied material was carried out. The test involved the measurements of carbon and nitrogen content in the sample after each irradiation cycle (experiment similar to photostability tests). The experiment was performed in an aqueous suspension without methylene blue compound. Additionally, to confirm the role of UV irradiation in APTES particles disintegration, the same experiment was also conducted without light. Based on results shown in Fig. 10, a significant decrease in carbon and nitrogen content after the first cycle, carried out both in darkness and under UV irradiation, can be observed. This indicates the leaching of these elements from the surface of the sample. It should be stressed that higher amount of carbon and nitrogen was removed during a test conducted under UV irradiation. During the next cycles of the test of composition stability, the lower decrease in carbon and nitrogen was noted in comparison with results from the first cycle. It is worth mentioning that after the fourth cycle, the sample did not contain any carbon, while nitrogen was present in negligible amount. Based on the obtained results, it was confirmed that APTES molecules are not sustainably bonded with TiO_2 surface. On the one hand, it is caused by leaching of compounds during stirring (results from the test without UV irradiation). On the other hand, it was confirmed that UV radiation destroys the APTES molecules, what is related to the rapid decrease in photocatalytic efficiency already observed in the second cycle. The high photoefficiency observed in the first cycle of methylene blue decomposition is correlated with the presence of carbon and nitrogen in the sample. The similar conclusions were drawn by Zamiri and Giahi [33], which used urea as a carbon and nitrogen source in TiO_2 modification.

4. Conclusions

The APTES-modified TiO_2 photocatalysts were obtained by solvothermal process at 120 °C with different APTES concentration. The presence of APTES was confirmed by the analysis of carbon and nitrogen content and the FT-IR/DRS analysis. It was found that APTES inserts in both TiO_2 external surface and pores, causing a decrease of S_{BET} values and total pore volume. It was generally found that the APTES modification of TiO_2 caused the improvement of photocatalytic activity. It was observed that nanomaterials modified with at least 100 mM of APTES exhibit higher activity in comparison with starting-TiO_2. Furthermore, photocatalytic activity increases with the increase of APTES concentration. The highest decomposition degree of methylene blue was noted for the sample containing 2000 mM of APTES. The high efficiency in the first cycle was related to carbon and nitrogen presence in the sample. However, the tested sample was not chemically stable. After the first cycle, the decomposition degree decreased by about 30 % what was caused by destabilization of APTES molecule. The FT-IR/DRS spectrum of TiO_2-4h-120°C–2000 mM sample after the first cycle of irradiation confirmed changes in the photocatalyst structure. The reusability test in water and elemental analysis confirmed that APTES molecules are not sustainably bonded with TiO_2 surface. It was found that the chain of APTES molecule was destroyed under UV irradiation and then carbon and nitrogen were removed during stirring of an aqueous suspension.

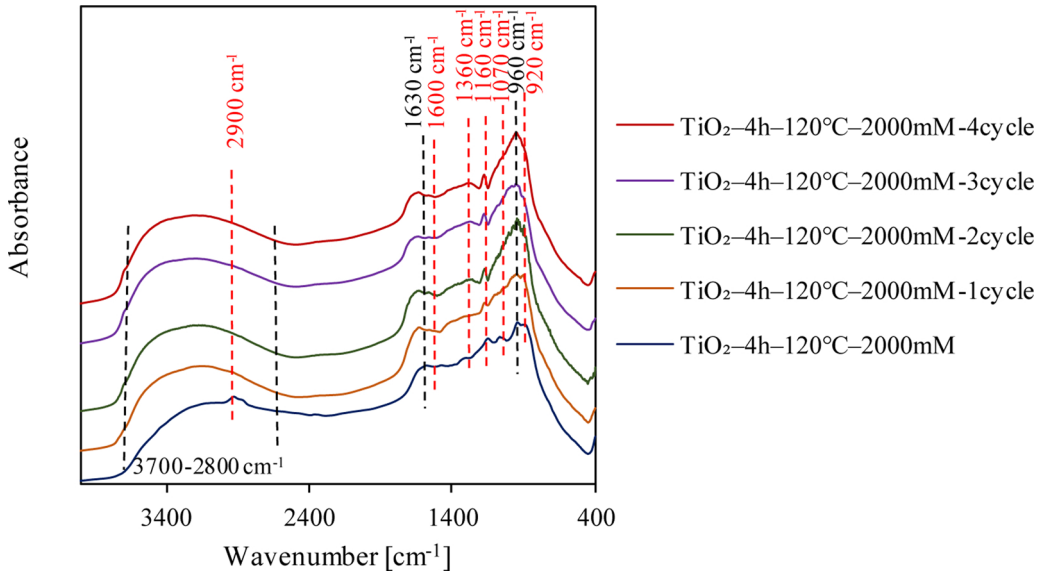

Fig. 9. FT-IR/DR spectra of TiO_2–4h – 120°C–2000 mM sample before and after each cycle.

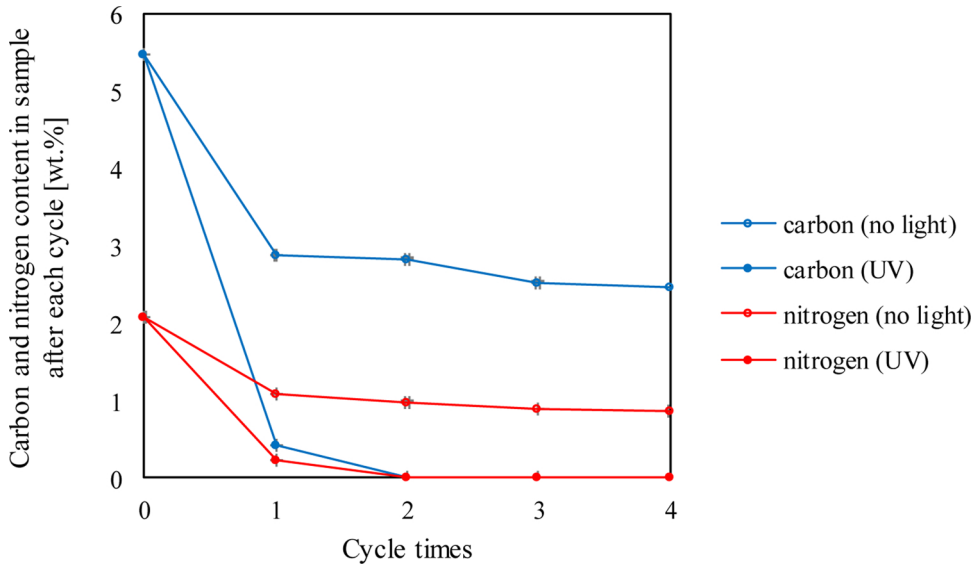

Fig. 10. Carbon and nitrogen content in TiO_2–4h – 120°C–2000 mM sample after each cycle with water.

CRediT authorship contribution statement

Agnieszka Wanag: Conceptualization, Methodology, Investigation, Data curation, Writing - original draft, Project administration. **Agnieszka Sienkiewicz:** Investigation, Writing - original draft. **Paulina Rokicka-Konieczna:** Writing - review & editing. **Ewelina Kusiak-Nejman:** Methodology, Data curation, Writing - review & editing. **Antoni W. Morawski:** Writing - review & editing, Supervision, Project administration.

Declaration of Competing Interest

The authors declare that they have no known competing financial interests or personal relationships that could have appeared to influence the work reported in this paper.

Acknowledgement

This work was supported by grant 2017/27/B/ST8/02007 from the National Science Centre, Poland.

References

[1] A.J. Haider, R.H. AL-Anbari, G.R. Kadhim, Ch. T. Salame, Exploring potential environmental applications of TiO2 nanoparticles, Energy Procedia 119 (2017) 332–345, https://doi.org/10.1016/j.egypro.2017.07.117.
[2] Z. Lu, G. Zhou, M. Song, X. Liu, H. Tang, H. Dong, P. Huo, F. Yan, P. Du, G. Xing, Development of magnetic imprinted PEDOT/CdS heterojunction photocatalytic nanoreactors: 3-Dimensional specific recognition for selectively photocatalyzing danofloxacin mesylate, Appl. Catal. B: Environ. 268 (2020) 118433, , https://doi.org/10.1016/j.apcatb.2019.118433.
[3] H.Y. Chun, S.S. Park, S.H. You, G.H. Kang, W.T. Bae, K.W. Kim, J.E. Park, A. Öztürk, D.W. Shin, Preparation of a transparent hydrophilic TiO2 thin film photocatalyst, J. Ceram. Process. Res. 10 (2019) 219–223, https://doi.org/10.1021/la400191x.
[4] Z. Lu, J. Peng, M. Song, Y. Liu, X. Liu, P. Hou, H. Dong, S. Uuan, Z. Ma, S. Han, Improved recyclability and selectivity of environment-friendly MFA-based heterojunction imprinted photocatalyst for secondary pollution free tetracycline orientation degradation, Chem. Eng. J. 260 (2019) 1262–1276, https://doi.org/10.1016/j.cej.2018.10.200.
[5] L.H. Lin, H.J. Liu, J.J. Hwang, K.M. Chen, J.Ch. Chao, Photocatalytic effects and surface morphologies of modified silicone–TiO2 polymer composites, Mater. Chem. Phys. 127 (2011) 248–252, https://doi.org/10.1016/j.matchemphys.2011.01.069.
[6] R. Daghrir, P. Drogui, D. Robert, Modified TiO2 for environmental photocatalytic applications: a review, Ind. Eng. Chem. Res. 52 (2013) 3581–3599, https://doi.org/10.1021/ie303468t.
[7] Z. Lu, G. Zhou, M. Song, D. Wang, P. Huo, W. Fan, H. Dong, H. Tang, F. Yan, G. Xing, Magnetic functional heterojunction reactors with 3D specific recognition for selective photocatalysis and synergistic photodegradation in binary antibiotic solutions, J. Mater. Chem. 7 (2019) 13986–14000, https://doi.org/10.1039/c9ta01863h.
[8] Z. Lu, F. Chen, M. He, M. Song, Z. Ma, W. Shi, Y. Yan, J. Lan, F. Li, P. Xiao, Microwave synthesis of a novel magnetic imprinted TiO2 photocatalyst with excellent transparency for selective photodegradation of enrofloxacin hydrochloride residues solution, Chem. Eng. J. 249 (2014) 15–26, https://doi.org/10.1016/j.cej.2014.03.077.
[9] G.Q. Xu, Z.X. Zheng, Y.C. Wu, N. Feng, Effect of silica on the microstructure and photocatalytic properties of titania, Ceramics 35 (2009) 1–5, https://doi.org/10.1016/j.ceramint.2007.09.008.
[10] D.M. Tobaldi, A. Tucci, A.S. Skapin, L. Esposito, Effects of SiO2 addition on TiO2 crystal structure and photocatalytic activity, J. Eur. Ceram. Soc. 30 (2010) 2481–2490, https://doi.org/10.1016/j.jeurceramsoc.2010.05.014.
[11] K. Byrappa, M. Yoshimura, Hydrothermal technology for nanotechnology – a technology for processing of advanced materials, Handbook of Hydrothermal Technology, (2013), pp. 615–762, https://doi.org/10.1016/j.pcrysgrow.2007.04.001.
[12] Q. Chen, N.L. Yakovlev, Adsorption and interaction of organosilanes on TiO2 nanoparticles, Appl. Surf. Sci. 257 (2010) 1395–1400, https://doi.org/10.1016/j.apsusc.2010.08.036.
[13] F. Cheng, S.M. Sajedina, S.M. Kelly, A.F. Leeb, A. Kornherr, UV-stable paper coated with APTES-modified P25 TiO2 nanoparticles, Carbohydrate 114 (2014) 246–252, https://doi.org/10.1016/j.carbpol.2014.07.076.
[14] A. Andrzejewska, A. Krysztafkiewicz, T. Jesionowski, Adsorption of organic dyes on the aminosilane modified TiO2 surface, Dyes Pigm. 62 (2004) 121–130, https://doi.org/10.1016/j.dyepig.2003.11.014.
[15] A. Shakeri, D. Yip, M. Badv, S.M. Imani, M. Sanjari, T.F. Didar, Self-cleaning ceramic tiles produced via stable coating of TiO2 nanoparticles, Materials 11 (2018) 1003, https://doi.org/10.3390/ma11061003.
[16] L. López-Zamoraa, H.N. Martínez-Martínezа, J.A. González-Calderón, Improvement of the colloidal stability of titanium dioxide particles in water through silicon based coupling agent, Mater. Chem. Phys. 217 (2018) 285–290, https://doi.org/10.1016/j.matchemphys.2018.06.063.
[17] R. Klaysri, T. Tubchareon, P. Praserthdam, One-step synthesis of amine-functionalized TiO2 surface for photocatalytic decolorization under visible light irradiation, J. Ind. Eng. Chem. 45 (2017) 229–236, https://doi.org/10.1016/j.jiec.2016.09.027.
[18] N. Bao, G. Wu, J. Niu, Q. Zhang, S. He, J. Wang, Wide spectral response and enhanced photocatalytic activity of TiO2 continuous fibers modified with aminosilane coupling agents, J. Alloys. Compd. 599 (2014) 40–48, https://doi.org/10.1016/j.jallcom.2014.02.072.
[19] D. Meroni, L. Lo Presti, G. Di Liberto, M. Ceotto, R.G. Acres, K.C. Prince, R. Bellani, G. Soliveri, S. Ardizzone, A close look at the structure of the TiO2 APTES interface in hybrid nanomaterials and its degradation pathway: an experimental and theoretical study, J. Phys. Chem. C 121 (2017) 430–440, https://doi.org/10.1021/acs.jpcc.6b10720.
[20] A. Razmjou, A. Resosudarmo, R.L. Holmes, H. Li, J. Mansouri, V. Chen, The effect of modified TiO2 nanoparticles on the polyethersulfone ultrafiltration hollow fiber membranes, Desalination 287 (2012) 271–280, https://doi.org/10.1016/j.desal.2011.11.025.
[21] W. Zhuang, Y. Zhang, L. He, R. An, B. Li, H. Ying, J. Wu, Y. Chen, J. Zhou, X. Lu, Facile synthesis of amino-functionalized mesoporous TiO2 microparticles for adenosine deaminase immobilization, Microporous Mesoporous Mater. 239 (2017) 158–166, https://doi.org/10.1016/j.micromeso.2016.09.006.
[22] E. Ukaji, T. Furusawa, M. Sato, M. Suzuki, The effect of surface modification with silane coupling agent on suppressing the photo-catalytic activity of fine TiO2 particles as inorganic UV filter, Appl. Surf. Sci. 254 (2007) 563569, , https://doi.org/

10.1016/j.colsurfa.2011.11.033.
[23] A. Razmjou, J. Mansouri, V. Chen, The effects of mechanical and chemical modification of TiO2 nanoparticles on the surface chemistry, structure and fouling performance of PES ultrafiltration membranes, J. Membr. Sci. 378 (2011) 73–84, https://doi.org/10.1016/j.memsci.2010.10.019.
[24] Z. Li, B. Hou, Y. Xu, D. Wu, Y. Sun, W. Hu, F. Deng, Comparative study of sol–gel-hydrothermal and sol-gel synthesis of titania–silica composite nanoparticles, J. Solid. State Chem. 178 (2005) 1395–1405, https://doi.org/10.1016/j.jssc.2004.12.034.
[25] P. Rokicka-Konieczna, A. Markowska-Szczupak, E. Kusiak-Nejman, A.W. Morawski, Photocatalytic water disinfection under the artificial solar light by fructose modified TiO2, Chem. Eng. J. 372 (2019) 203–215, https://doi.org/10.1016/j.cej.2019.04.113.
[26] M. Winter, D. Hamal, X. Yang, H. Kwen, D. Jones, Sh. Rajagopalan, K.J. Klabunde, Defining reactivity of solid sorbents: what is the most appropriate metric? Chem. Mater. 21 (2009) 2367–2374, https://doi.org/10.1021/cm8032884.
[27] A.J. Maria, J.M. Coronado, V. Augugliaro, K.L. Yeung, J.C. Conesa, J. Soria, Fourier transform infrared study of the performance of nanostructured TiO2 particles for the photocatalytic oxidation of gaseous toluene, J. Catal. 202 (2001) 413–420, https://doi.org/10.1006/jcat.2001.3301.
[28] M.E. Azim Araghi, N. Shaban, M. Bahar, Synthesis and characterization of nanocrystalline barium strontium titanate powder by a modified sol-gel processing, Mater. Sci. Poland 34 (2016) 63–68, https://doi.org/10.1515/msp-2016-0020.
[29] M. Pelaez, T.N. Nolan, S.C. Pillai, M.K. Seery, A.G. Kontos, P.S.M. Dunlop, J.W.J. Hamilton, J.A. Byrne, K. O'Shea, M.M. Entezari, D.D. Dionysiou, A review on the visible light active titanium dioxide photocatalysts for environmental applications, Appl. Catal. B: Environ. 125 (2012) 331–349, https://doi.org/10.1016/j.apcatb.2012.05.036.
[30] K.S.W. Sing, Reporting physisorption data for gas/solid systems with special reference to the determination of surface area and porosity, Pure Appl. Chem. 54 (1982) 2201–2218, https://doi.org/10.1515/iupac.57.0007.
[31] G. Leofant, M. Padovan, G. Tozzola, B. Venturelli, Surface area and pore texture of catalysts, Catal. Today 41 (1998) 207–219, https://doi.org/10.1016/S0920-5861(98)00050-9.
[32] Z. Al-Othman, A review: fundamental aspects of silicate mesoporous materials, Materials 5 (2012) 2874–2902, https://doi.org/10.3390/ma5122874.
[33] M. Zamiri, M. Giahi, Photochemical degradation of an anionic surfactant by TiO2 nanoparticle doped with C, N in aqueous solution, Russ. J. Phys. Chem. A 90 (2016) 2668–2674, https://doi.org/10.1134/S0036024416130240.

catalysts

MDPI

Article

The Role of Adsorption in the Photocatalytic Decomposition of Dyes on APTES-Modified TiO_2 Nanomaterials

Ewelina Kusiak-Nejman *, Agnieszka Sienkiewicz, Agnieszka Wanag, Paulina Rokicka-Konieczna and Antoni W. Morawski

Department of Inorganic Chemical Technology and Environment Engineering, Faculty of Chemical Technology and Engineering, West Pomeranian University of Technology in Szczecin, Pułaskiego 10, 70-322 Szczecin, Poland; Agnieszka.Sienkiewicz@zut.edu.pl (A.S.); awanag@zut.edu.pl (A.W.); prokicka@zut.edu.pl (P.R.-K.); amor@zut.edu.pl (A.W.M.)

* Correspondence: ekusiak@zut.edu.pl; Tel: +48-91-449-42-44

Abstract: This work investigated for the first time the role of adsorption in the photocatalytic degradation of methylene blue and Orange II dyes in the presence of 3-aminopropyltriethoxysilane (APTES)-modified TiO_2 nanomaterials. It has been demonstrated that the decrease in adsorption has a detrimental effect on photocatalytic activity. APTES/TiO_2 photocatalysts were successfully prepared by solvothermal modification of TiO_2 in a pressure autoclave, followed by heat treatment in an inert gas atmosphere at the temperature range from 300 °C to 900 °C. It was observed that functionalization of TiO_2 via APTES effectively suppressed the anatase-to-rutile phase transformation, as well as the growth of crystallites size during calcination, and reduction of specific surface area (APTES modification inhibits sintering of crystallites). The noted alterations in the adsorption properties, observed after the calcination, were generally related to changes in the surface characteristics, mainly surface charges expressed by the zeta potential. Positively charged surface enhances adsorption of anionic dye (Orange II), while negatively charged surface was better for adsorption of cationic dye (methylene blue). The adsorption process substantially affects the efficiency of the photocatalytic oxidation of both dyes. The methylene blue decomposition proceeded according to the pseudo-first and pseudo-second-order kinetic models, while the degradation of Orange II followed the zero, pseudo-first, and pseudo-second order kinetic models.

Keywords: titanium dioxide; 3-aminopropyltriethoxysilane; calcination; dyes photodegradation; adsorption capacity

Citation: Kusiak-Nejman, E.; Sienkiewicz, A.; Wanag, A.; Rokicka-Konieczna, P.; Morawski, A.W. The Role of Adsorption in the Photocatalytic Decomposition of Dyes on APTES-Modified TiO_2 Nanomaterials. **2021**, *11*, 172. https://doi.org/10.3390/catal11020172

Received: 15 December 2020
Accepted: 21 January 2021
Published: 27 January 2021

1. Introduction

In addition to consuming large amounts of water, the textile industry also uses a wide range of synthetic dyes, as a result of which it contributes to the discharge of a large quantity of wastewater. In the states of Gujarat and Maharashtra, India, the annual production of synthetic dyes for textiles and other industries is about 130,000 tons, and due to the high toxicity, solubility, mutagenicity and lack of biodegradability, these colourants are one of the most problematic and hazardous water pollutants [1]. Therefore, many researchers are trying to develop the best method to remove different types of dye from water.

Currently, the elimination of this organic contaminant is carried out using various techniques such as flocculation and coagulation [2,3], biological oxidation [4,5], adsorption [6,7], and membrane filtration [5,8]. Recent studies also focus on using advanced oxidation processes (AOPs) to decompose synthetic dyes present in water. Among AOPs, for example, H_2O_2/ultraviolet (UV) processes [9] or Fenton and photo-Fenton catalytic reactions [10,11], heterogeneous photocatalysis using titanium dioxide as a photocatalyst appear to be one of the most influential technologies [12,13]. The main

advantages are that photocatalysis could be carried out under ambient conditions, does not involve mass transfer, and can also lead to total transformation of organic carbon to CO_2 [14]. Additionally, TiO_2 is widely used due to its low cost, chemical and biological stability, low toxicity, and high photoactivity [15].

It is commonly known that photocatalytic reactions occur primarily on the surface of the semiconductor. Therefore, the adsorption of contaminants on the surface of the material plays a crucial role in affecting the photodegradation efficiency [16]. Many experiments measured the adsorption and the kinetics of photodecomposition of various dyes on TiO_2, for instance, Reactive Black [17], Rhodamine B [18,19], Orange II [20], methylene blue [17,21], Direct Green 99 [22] and thionine [19]. In all presented research, organic compounds are adsorbed on the surface of the semiconductor, until the adsorption-desorption equilibrium between the dye molecules and the TiO_2 surface is reached. After that, the lamps are turned on, and the photooxidation is carried out [22]. Moreover, Zhu et al. [23] noted that the high adsorption capacity of polythiophene/TiO_2 photocatalyst could potentially increase the rate of photocatalytic decomposition of methyl orange. Wang et al. [24] also reported that the enhancement of the degradation kinetics of dyes after fluorination of TiO_2 was due to increased adsorption and decreased flat band potential.

Additionally, TiO_2 surface properties are also crucial for the effectiveness of photooxidation. Therefore, photocatalytic studies' significant field concentrates on modifying TiO_2 to improve its physicochemical properties and photocatalytic activity [21]. In recent years, organosilanes such as 3-aminopropyltriethoxysilane (APTES), as surface modifiers, have received increasing research interest, since most applications of modified nanomaterials require them to be chemically and thermally stable, well dispersed in the media and characterized by a large specific surface area [25,26]. For example, APTES-modified TiO_2 nanoparticles have been used to induce the self-cleaning capability of ceramic tiles [27] or-enhance the decomposition degree of Reactive Brilliant Red X-3B [28]. Moreover, the adsorption properties of organic dyes (Acid Orange 7 and Reactive Blue 19) on the APTES-functionalized TiO_2 pigment surface was also investigated [29]. In this case, the modified rutile titanium oxide was used as an adsorbent, and due to the weak photoactivity of this polymorphous form of TiO_2 no photocatalytic degradation of tested dyes was performed.

In the present study, the APTES-modified TiO_2 nanomaterials were obtained by a solvothermal process, and then calcination in an inert gas atmosphere. This combined method has been proposed for the first time by our research group [30]. Other preparation methods described in the literature, where APTES-modified TiO_2 were utilized in the removal process of dyes by adsorption or photooxidation, involve the sol-gel method [28] and simple mixing of TiO_2 slurry with aminosilane coupling agents [29]. Here, two commercial textile dyes: cationic methylene blue and anionic Orange II, were removed from aqueous solution. To the best of our knowledge, this is the first paper presenting the results of research on the role of adsorption in the photocatalytic degradation of methylene blue and Orange II in the presence of APTES-modified TiO_2 photocatalysts. The novelty of the presented studies was also to establish the impact of modifying the efficiency and potential reuse of the prepared photocatalysts during subsequent dye decomposition cycles.

2. Results and Discussion

2.1. Characterization of Materials

X-ray diffraction (XRD) patterns of APTES/TiO_2 nanomaterials are presented in Figure 1. The structural characteristics of the starting-TiO_2 and calcined reference samples were discussed in detail in our previously published work [30]. Except for the sample calcined at 900 °C, all tested nanomaterials showed reflections characteristic of the anatase phase located at 25.3, 37.8, 48.1, 53.9, 55.1, 62.7, 68.9, 70.3 and 75.1°, which cor-

respond to (101), (004), (200), (105), (211), (204), (116), (220), (215) indexed by JCPDS 01-070-7348, and certain reflections characteristic of the rutile phase located in 27.4, 36.0 and 41.2°, corresponding to (110), (101) and (111) indexed by JCPDS 01-076-0318. While the TiO_2-Ar-900°C sample demonstrated only reflections characteristic for the rutile phase located at 27.4, 36.0, 39.1, 41.2, 44.0, 54.3, 56.6, 62.7, 64.0, 69.0 and 69.7°, which correspond to (110), (101), (200), (111), (210), (211), (220), (002), (310), (301) and (112), respectively. The presence of rutile in the starting-TiO_2 resulted from the addition of rutile nuclei during the production process of TiO_2 pulp via sulphate technology. For starting-TiO_2, the anatase-to-rutile phase transformation typically occurs between 600 °C and 700 °C [31,32]. In our case, the phase transformation started above 500 °C, and starting TiO_2 was fully transformed into rutile at 900 °C [30]. According to the XRD phase composition and the crystallites size data shown in Table 1, the amount of anatase in APTES-modified TiO_2 samples was constant, and its content was about 96%. Moreover, it is important to note that after calcination at 900 °C, the TiO_2-4h–120°C–500mM-Ar–900°C sample still contained 95% of anatase phase. Silicon present in the APTES contributed to the effective suppression of anatase-to-rutile phase transformation during thermal modification [33–35]. For all tested photocatalysts, the crystallites size enhanced with the increase of the modification temperature. For starting-TiO_2 and calcined reference samples, the crystallites size of anatase was in the range of 14–52 nm [30], and 14–30 nm for APTES/TiO_2 nanomaterials. Whereas, the crystallites size of rutile for starting-TiO_2 and reference samples was from 21 nm to >100 nm, and from 46 nm to 79 nm for APTES/TiO_2 nanomaterials. Nevertheless, comparing the crystallites size of photocatalysts calcined at the same temperature with and without APTES, the crystallites size of both polymorphous forms of TiO_2 was significantly smaller for APTES-modified samples than for the reference materials. For example, the anatase crystallite size for TiO_2-4h–120°C–500mM-Ar–700°C sample equalled only 17 nm, while for TiO_2-Ar–700°C it was 52 nm [30]. According to Dalod et al. [33], the use of such stabilizers as APTES can lead to the formation of an amorphous SiO_2 layer on the surface, derived from the organosilane coupling agent, and leading to TiO_2-SiO_2 core-shell nanostructures, so that, during the thermal modification both the growth of the crystallites size and phase transformation can be successfully inhibited. Furthermore, the results presented by Lu et al. [35] and Xu et al. [36] also showed that silicon could effectively suppress the growth of titania grains over the calcination process.

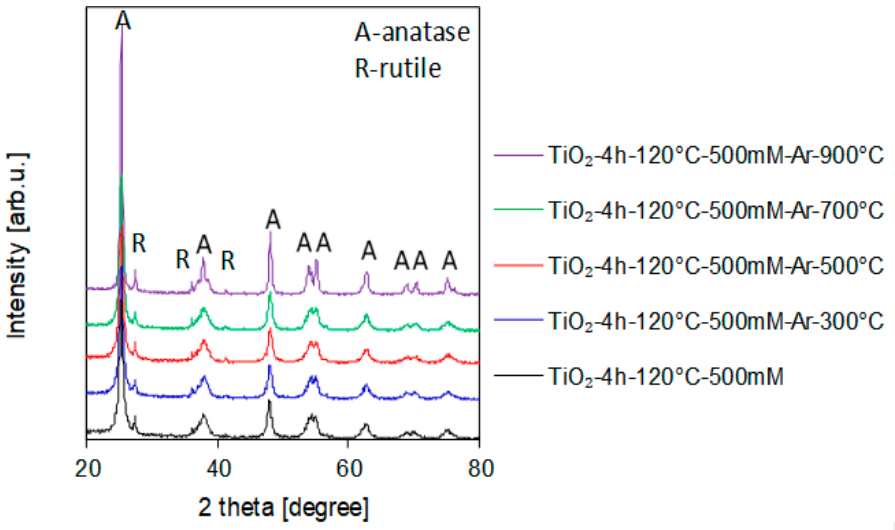

Figure 1. X-ray diffraction (XRD) patterns of 3-aminopropyltriethoxysilane (APTES)-modified TiO_2 before and after the calcination process.

Table 1. Structural parameters of starting TiO_2 and APTES-modified photocatalysts prior and after the calcination process.

Sample Name	Anatase in Crystallite Phase (%)	Anatase Crystallite Size (nm)	Rutile in Crystallite Phase (%)	Rutile Crystallite Size (nm)	S_{BET} (m^2/g)	V_{total} (cm^3/g)	V_{micro} (cm^3/g)	V_{meso} (cm^3/g)
starting TiO_2	95	14	5	21	207	0.370	0.070	0.300
TiO_2–4h–120°C–500mM	96	14	4	46	140	0.272	0.053	0.219
TiO_2–4h–120°C–500mM -Ar-300°C	95	14	5	36	158	0.242	0.058	0.184
TiO_2–4h–120°C–500mM -Ar-500 °C	96	15	4	51	170	0.272	0.062	0.210
TiO_2–4h–120°C–500mM -Ar–700°C	96	17	4	45	140	0.267	0.053	0.214
TiO_2–4h–120°C–500mM -Ar-900°C	95	30	5	79	50	0.150	0.019	0.131

In Figure 2 the adsorption-desorption isotherms of the obtained photocatalysts were shown. Most of them presented a type IV isotherm in IUPAC classification, characteristic for mesoporous materials [37]. Other nanomaterials presented the H3 type of the hysteresis loops. The H3 loops have characteristic desorption shoulders, lower closure points, and no plateau in the high p/p_0 value [38,39]. The pore size distribution was presented in Figure S1 (in the Supplementary Materials section).

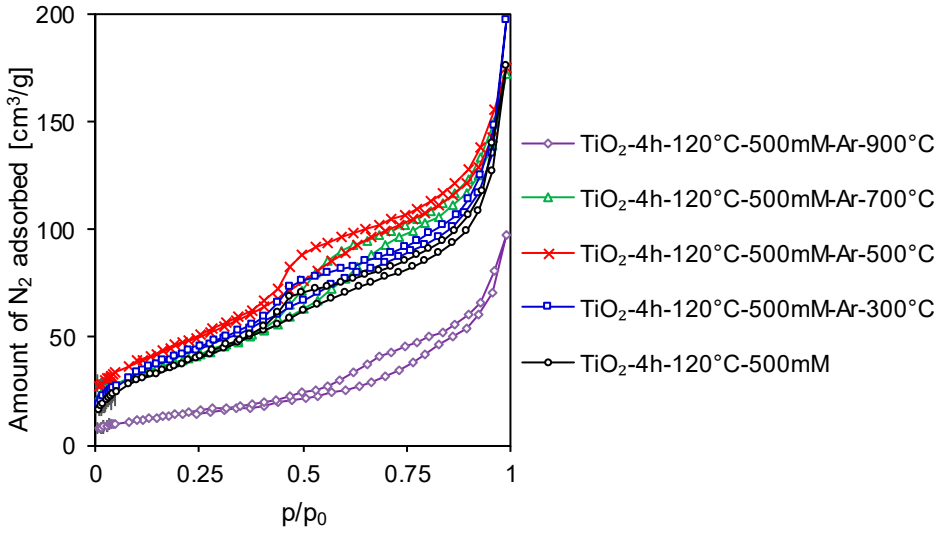

Figure 2. Adsorption/desorption isotherms of APTES-modified TiO_2 prior and after calcination process.

Furthermore, according to the data exhibited in Table 1, most of the tested semiconductors were mesoporous materials with a small number of micropores (except for the TiO_2-Ar–900°C sample that was a non-porous material, as presented in our previous paper [30]). In starting TiO_2, after modification with 500 mM of APTES, a significant decrease of the specific surface area and total pore volume was noted. Compared to the starting-TiO_2, the S_{BET} of TiO_2-4h–120°C–500mM reduced by 67 m^2/g and V_{total} by 0.098 cm^3/g. Dalod et al. [33] observed that TiO_2 surface functionalization using different silane coupling agents such as 3-aminopropyltriethoxysilane, 3-(2-aminoethylamino)propyldimethoxy-methylsilane and *n*-decyltriethoxysilane decreased the specific surface area, from 195 m^2/g for unmodified TiO_2 to 178 m^2/g, 149 m^2/g and 114 m^2/g, respectively. Siwińska-Stefańska et al. [40] also noted that modification via different alkoxysilanes compounds such as vinyltrimethoxysilane, n-2-(aminoethyl)-3-aminopropyltrimethoxysilane and 3-methacryloxypropyltrimethoxysilane, caused a decrease of the S_{BET} and V_{total} of obtained nanomaterials. This was most likely because the modifier particles blocked

the active centers on the TiO_2-SiO_2 surface. Zhuang et al. [41] also found that the specific surface area and the pore volume were smaller for the nanocomposites than for the unmodified TiO_2 because APTES also penetrated inside the pores, rather than only dispersing on the external surface.

After calcination, the S_{BET} of APTES-modified TiO_2 increased from 140 m^2/g for TiO_2–4 h–120 °C–500mM through 158 m^2/g for the sample calcined at 300 °C to 170 m^2/g for heated at 500 °C. Diminishing and eventually disappearing APTES-characteristic peaks with the increase of the modification temperature, observed on diffuse reflectance Fourier-transform infrared spectra (DRIFTS), presented in Figure 3, as well as the observed significant decrease in carbon and nitrogen content (see Table 2) indicated the unblocking of the surface of the nanomaterials. Therefore, the increase in the specific surface area was related to the decomposition of APTES molecules during the calcination process. The increase of V_{total} value from 0.242 cm^3/g (for sample calcined at 300 °C) to 0.272 cm^3/g after thermal modification at 500 °C, also pointed out that the modifier molecules unblocked both the external surface of TiO_2 and the pores. As shown in Table 1, a further increase in the modification temperature above 500 °C caused a decrease in the specific surface area and pore volume of the tested photocatalysts, which resulted in the increase of the anatase and rutile crystallites size and sintering of photocatalysts particles [42].

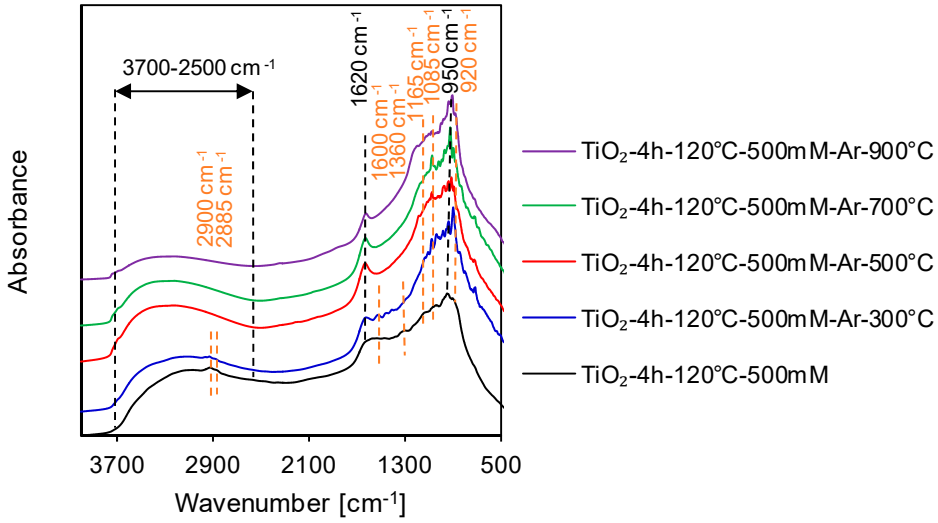

Figure 3. Diffuse refletrance Fourier transform infrared spectra (DRIFTS) of and APTES-modified TiO_2 before and after calcination process.

The DRIFTS measurements were utilized to determine the surface characteristics of the prepared photocatalysts. All spectra presented in Figure 3 showed a narrow band at 1620 cm^{-1}, as well as a wide band from 3700 cm^{-1} to 2500 cm^{-1}, associated with the molecular water and stretching vibrations of surface hydroxyl groups [28,43,44]. An increase of the modification temperature of APTES/TiO_2 samples resulted in a decrease of the intensity of these bands, due to the changes in the amount of surface −OH groups [45,46]. All materials exhibited the intensive band at around 950 cm^{-1} assigned to the self-absorption of titania [46,47]. Some new characteristic bands of APTES were observed in the spectra, shown in Figure 3, which indicates that the modified photocatalysts were prepared successfully. The bands detected at 2900 cm^{-1} and 2885 cm^{-1}, which belongs to the bending and stretching contributions of the alkyl groups [(CH_n)] [48–50]. The asymmetric $-NH_3^+$ deformation modes were observed near 1600 cm^{-1} [49,51,52]. Another low-intensity band at 1360 cm^{-1}, indicating the existence of C–N bonds [51,53]. Bands noted 960–910 cm^{-1} ascribe the stretching vibrations of Ti–O–Si chemical interactions

[54,55]. Additionally, the band localized at 920 cm^{-1} indicated the condensation reaction between silanol and −OH groups on the surface of the semiconductor [54]. Above 300 °C, bands characteristic for APTES assigned to alkyl groups, $-NH_3^+$, C−N and Ti–O–Si bonds were no longer observed. Furthermore, the band at around 1165 cm^{-1} corresponds to the Si–O–Si stretching vibrations, created by the condensation reaction between silanol groups [43,51]. The presence of Si–O–C stretching mode was noted at around 1085 cm^{-1} [51,53].

From the ultraviolet–visible diffuse reflectance spectra (UV–Vis/DRS) of all APTES-modified TiO_2, shown in Figure 4, it was noted that TiO_2–4h–120°C–500mM exhibited the characteristic absorption in the UV region due to the intrinsic band gap absorption of Ti [56,57]. Moreover, for all APTES/TiO_2 photocatalysts calcined in an inert gas conditions, the f reflectance in the visible range decreased as the heating temperature increased, due to the change of colour from white for TiO_2-4h–120°C–500mM through greyish for TiO_2-4h–120°C–500mM-Ar–500°C, to dark grey for TiO_2-4h–120°C–500mM-Ar–900°C material [58,59]. Interestingly, the bang gap energy values determined for all calcined APTES-modified TiO_2 samples did not change in comparison to starting titania sample, including nanomaterials calcined at 700 and 900 °C. These results also provide the evidence of the inhibition of phase transition.

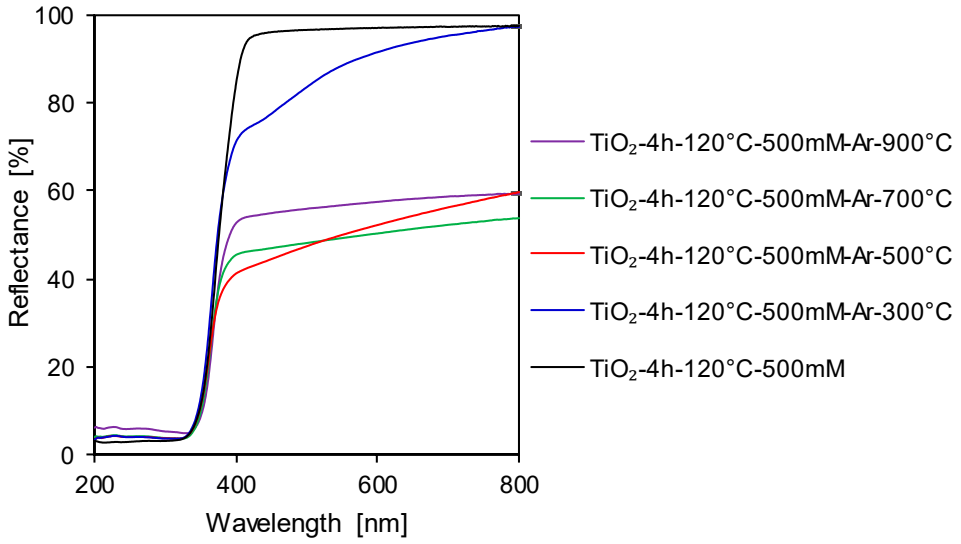

Figure 4. Ultraviolet–visible diffuse reflectance spectra (UV–Vis/DRS) of and APTES-modified TiO_2 prior and after calcination process.

Table 2. The carbon and nitrogen content, and zeta potential values of starting TiO_2, reference samples and APTES-modified photocatalysts prior to and after the calcination process.

Sample Name	Zeta Potential δ (mV)	Carbon Content (wt.%)	Nitrogen Content (wt.%)
starting TiO_2	+11.00	-	0.18
TiO_2-Ar–300°C	+12.34	-	-
TiO_2-Ar–500°C	+12.43	-	-
TiO_2-Ar–700°C	+24.77	-	-
TiO_2-Ar–900°C	−29.67	-	-
TiO_2–4h–120°C–500mM	+4.43	3.34	1.24
TiO_2-4h–120°C-500mM-Ar-300°C	+19.43	2.33	0.66
TiO_2-4h–120°C–500mM-Ar–500°C	−25.63	0.50	0.14
TiO_2–4h–120°C–500mM-Ar–700°C	−25.57	0.30	0.11
TiO_2–4h–120°C–500mM-Ar-900°C	−36.13	0.16	0.07

Following the data presented in Table 2, the occurrence of carbon (3.34 wt.%) and nitrogen (1.24 wt.%) in TiO_2-4h–120°C–500mM sample, confirmed the presence of APTES

in the material obtained after TiO_2 modification. Additionally, it was found that the content of the analyzed elements decreased with the increase of calcination temperature, most probably as a result of nitrogen and carbon decomposition from the solid phase [46,60]. The data obtained from DRIFT spectra (see Figure 3) agreed with the analysis of carbon and nitrogen content, which showed a continued decrease of carbon and nitrogen in APTES-modified TiO_2 samples as the calcination temperature increases. The preparation procedure can explain the presence of nitrogen in the starting-TiO_2 (preliminary rinsing with NH_4OH), used to eliminate the residual sulfuric acid from the raw slurry of TiO_2 obtained by sulphate technology [61].

Based on the data shown in Table 2, the zeta potential values of APTES/TiO_2 photocatalysts changed from +4.43 mV for TiO_2–4h–120°C–500mM to −36.13 mV for TiO_2-4h–120°C–500mM-Ar–900°C. Goscianska et al. [62], Ukaji et al. [54] and Talavera-Pech et al. [63] found that the amine groups of APTES tend to gain protons, and thus, NH_3^+ species can be formed. The NH_3^+ can easily be attached to the TiO_2 surface, which results in a positive surface charge of the semiconductor. The FT-IR/DR spectra presented in Figure 3, as well as the noted significant decrease of the nitrogen content (see Table 2), showed that the positively charged amino groups were not observed on the TiO_2 surface when the calcination temperature exceeded 300 °C. Above this temperature, mostly silicon groups were found on the TiO_2 surface. Wilhelm et al. [64] and Ferreira-Neto et al. [65] noted that silica-modified TiO_2 exhibited negative zeta potential values. The zeta potential of APTES/TiO_2 nanomaterials prepared via calcination at temperature above 300 °C, changed from positive to negative.

2.2. Adsorption Experiments

Before the photocatalytic activity test, studies on determination of the adsorption-desorption equilibrium were performed. The adsorption degree of methylene blue was shown in Figure 5 while the adsorption degree of Orange II was presented in Figure 6A,B. For methylene blue the adsorption-desorption equilibrium was established after 60 min for starting TiO_2 and TiO_2–4 h–120 °C–500mM samples, whereas after 180 min for calcined reference materials and APTES-modified TiO_2 nanomaterials received after the calcination. Different adsorption-desorption equilibrium time is associated with the surface characteristics of semiconductors (see Table 2). For starting TiO_2, all calcined reference materials [30], TiO_2–4 h–120 °C–500mM and TiO_2–4 h–120 °C–500mM-Ar-300°C, the adsorption degree of methylene blue reached c.a. 5%. For other APTES/TiO_2 nanomaterials, an increase of the calcination temperature above 300 °C resulted in the notable improvement of adsorption properties. Based on zeta potential values (shown in Table 2), for materials with positively charged surface, the low adsorption of a cationic dye was observed. While, photocatalysts with the negatively charged surface exhibited a good adsorption efficiency, due to the higher potential of contact with the positively charged methylene blue molecules. The highest adsorption degree of methylene blue equalled 30%, was found for the TiO_2-4h–120°C–500mM-Ar–900°C sample with the most negative zeta potential value of −36.13 mV and the lowest value for specific surface area. Therefore, the change in TiO_2 surface charge after calcination from positive to negative was found to be the main factor that enhances the adsorption properties of the APTES-modified TiO_2 [66–68]. It can be additionally noted that both photocatalysts calcined at 900 °C exhibited a different dye adsorption degree, although almost the same zeta potential value characterized them (for TiO_2-Ar-900°C was only 5%). For this reason, the noted enhancement of the adsorption properties at the highest temperature of modification was mainly associated with the values of specific surface area (50 m^2/g for TiO_2-4h–120°C–500mM-Ar-900°C and 3 m^2/g for TiO_2-Ar-900°C [30]). It was confirmed that APTES modification successfully prevents the anatase-to-rutile transformation and sintering of the crystallites at a higher temperature of calcination process.

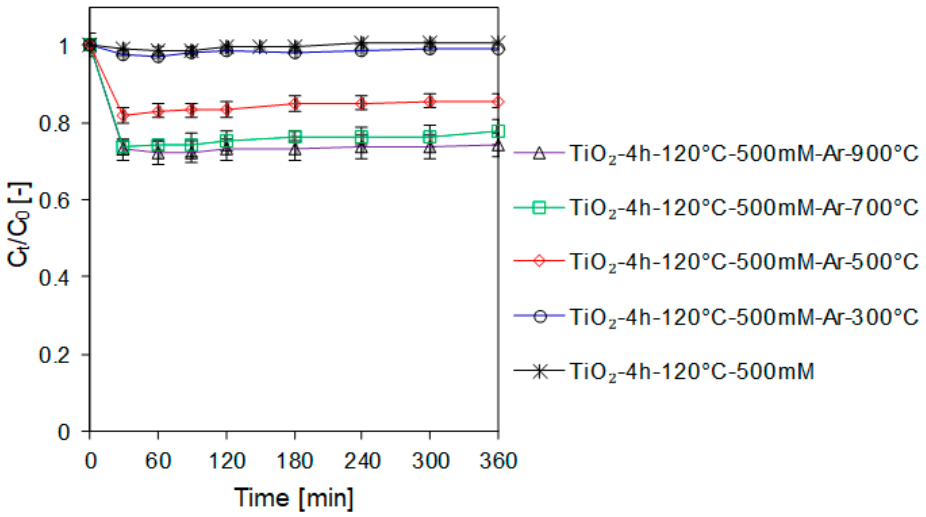

Figure 5. Adsorption degree of methylene blue dye on the surface of APTES-modified TiO_2 before and after calcination.

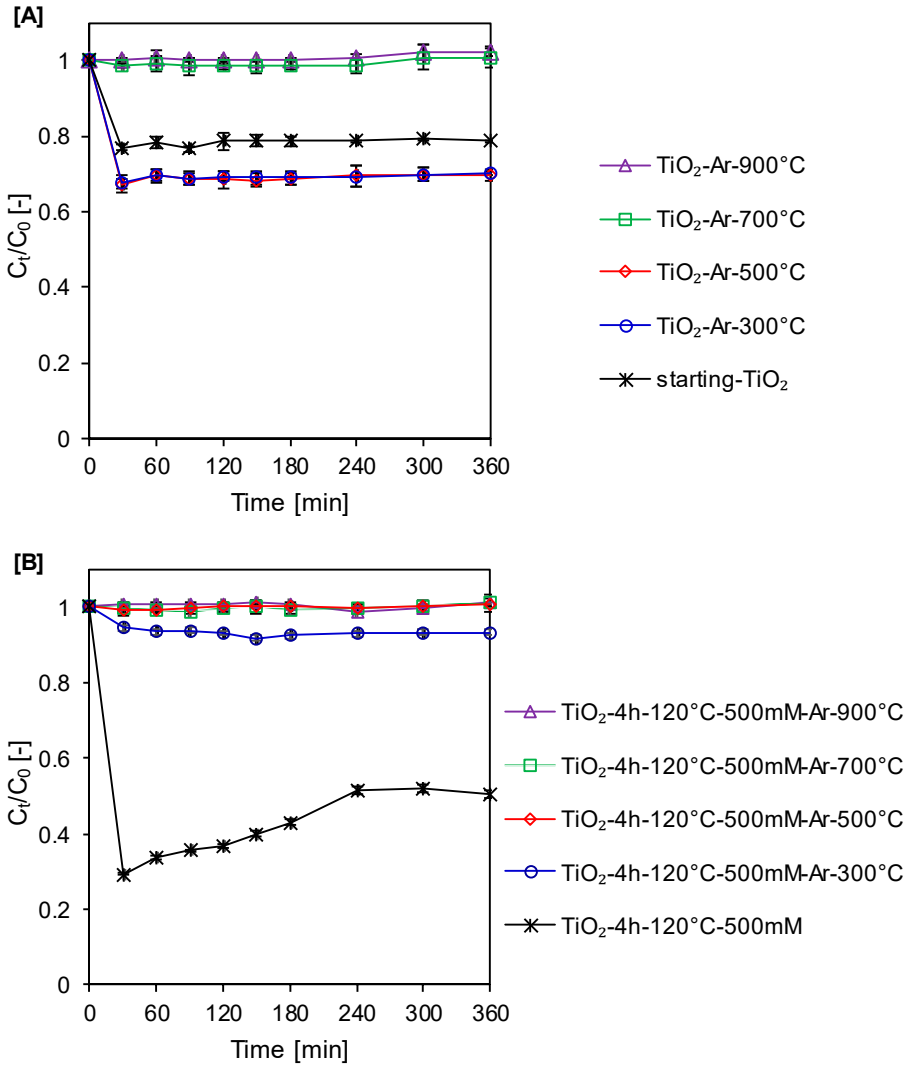

Figure 6. Adsorption degree of Orange II dye on the surface of starting TiO_2 and calcined reference samples (**A**), and APTES-modified TiO_2 before and after calcination process (**B**).

For Orange II, the adsorption-desorption equilibrium was established after 90 min for all calcined reference materials, whereas after 60 min for starting and calcined APTES-modified TiO_2 photocatalysts. In case of TiO_2-4h–120°C–500mM sample, significant Orange II desorption (approximately 23%) was observed prior to the adsorption-desorption equilibrium established after 240 min. For APTES/TiO_2 photocatalysts, the increase of the calcination temperature resulted in a decrease of adsorption properties related to the change of the TiO_2 surface charge from positive to negative (see Table 2). The positively charged surface of the semiconductor has a higher potential of contact with the negatively charged dye molecules like Orange II. Therefore, for nanomaterials with a negatively charged surface, the low adsorption efficiency of anionic dye was noted [20,66–69].

Adsorption Capacity

To better understand the adsorption process, additional tests were conducted to determine the adsorption capacity of examined materials. The values of constants and correlation coefficients for Freundlich, Langmuir, Langmuir–Freundlich, and Temkin isotherm models are listed in Table S1 for methylene blue and in Table S2 for Orange II dye.

Based on the correlation coefficients obtained for methylene blue adsorption, it was revealed that the Langmuir and Langmuir–Freundlich isotherm models gave similar and the best simulation of the experimental data with the highest R^2 for all APTES-modified TiO_2 samples. The Langmuir–Freundlich isotherm model describes most accurately the adsorption properties of starting-TiO_2 and all calcined reference photocatalysts, while for TiO_2-4h–120°C–500mM the best simulation of the experimental data provided the Temkin isotherm. For photocatalysts that have shown the best fit to the Langmuir–Freundlich isotherm model, it can be assumed that the surface of the semiconductors is heterogeneous [70]. The increase of the adsorption capacity for methylene blue can be explained as the effects of modification, including an increase of the specific surface area (see Table 1), a change in surface charge (see Table 2), and mesoporous structure of APTES/TiO_2 nanomaterials [20,71].

Following the calculated correlation coefficients, the experimental equilibrium data for the adsorption of Orange II for starting TiO_2 and reference samples calcined at 300–700 °C were most closely fitted to the Freundlich isotherm. TiO_2-Ar–900°C and TiO2–4 h–120°C–500mM-Ar-900°C samples were found to be the weakest adsorbents of Orange II dye due to the negative character of the surface (see Table 2), and characterized by negligible adsorption of anionic dye (see Figure 6A,B), which effectively made it very difficult to match the appropriate model of adsorption isotherm. For TiO_2–4h–120°C–500mM and APTES-modified TiO_2 calcined at 300–700 °C, the best simulation of the experimental data was provided by the Freundlich or Langmuir–Freundlich isotherm model. It can be concluded that the surfaces of APTES-modified semiconductors are heterogeneous [20,71]. The noted increase of the n and q_m values was related to the change of surface charge from negative to positive due to TiO_2 modification (see Table 2) [20,71,72].

2.3. Photocatalytic Activity Test

The photocatalytic activity of the examined nanomaterials was calculated based on the degradation of methylene blue and Orange II dyes under UV light irradiation. Tests performed in the absence of the photocatalyst (see Figures 7A and 8A) revealed that, for both methylene blue and Orange II, the decomposition due to the photolysis process was insignificant compared to the photocatalysis process. After 360 min of exposure under the same conditions as in the photocatalytic activity tests, about 2.5% decomposition of dyes was recorded.

For methylene blue, a significant improvement of the photoactivity from 39% to 95% for starting TiO_2 was noted only for the nanomaterial calcined at 700 °C, consisting of

88% of anatase and 12% of rutile phase, and the band gap energy value of 3.07 eV [30]. Ohno et al. [73] observed that TiO_2, being an optimal mixture of anatase and rutile phases, exhibited higher photocatalytic activity than TiO_2 composed of only one phase. Moreover, the co-existence of various-forms of TiO_2 is essential for determining the TiO_2 photoactivity, and the most effective performance during methylene blue degradation was achieved for photocatalysts with slightly reduced E_g (3.04 eV) and a mixture of both phases. Additionally, these samples did not have the largest S_{BET} among all examined materials. After 240 min of exposure to UV light, the methylene blue removal degree determined in the presence of TiO_2-4h–120°C–500mM sample compared to starting TiO_2, enhanced from 39% to 82% (see Figure 9). After modification of TiO_2 via APTES, the increase of the efficiency was essentially associated with the presence of nitrogen and carbon in the materials obtained (see Table 2) [74]. After thermal modification, almost all APTES/TiO_2 photocatalysts showed an improved methylene blue decomposition degree in comparison to reference materials heat treated at the same temperature. Only TiO_2-4h–120°C–500mM-Ar–700°C sample showed a slight 7% decrease in efficiency compared to TiO_2-Ar-700°C. The reported increase in the activity was related to the fact that the modification with APTES, which is a good source of silicon, effectively suppressed the anatase-to-rutile phase transformation, as well as the growth of crystallites size (see Table 1). The growth of the anatase phase crystallinity and the decrease of the bulk defects after thermal modification resulted in an increase of the electron diffusion rate to the surface of the semiconductor by inhibiting electron-hole recombination.

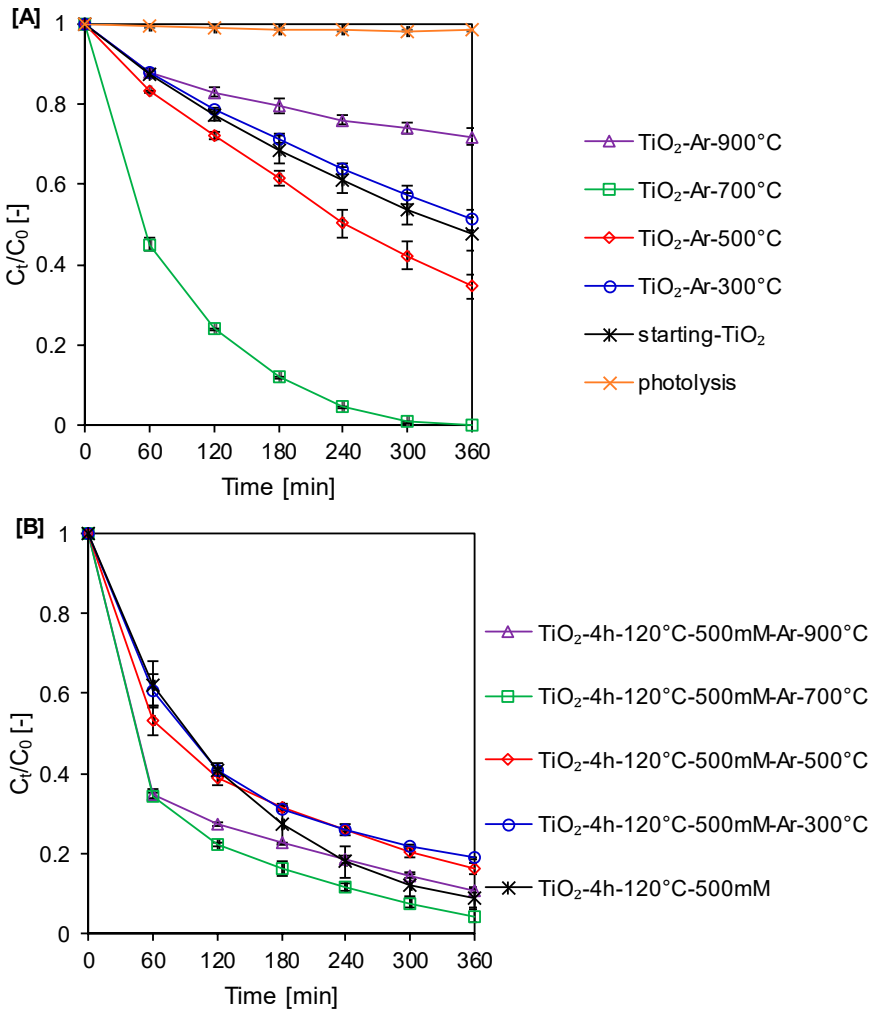

Figure 7. Methylene blue decomposition under UV irradiation for starting TiO_2 and calcined reference samples (**A**), and APTES-modified TiO_2 before and after calcination (**B**).

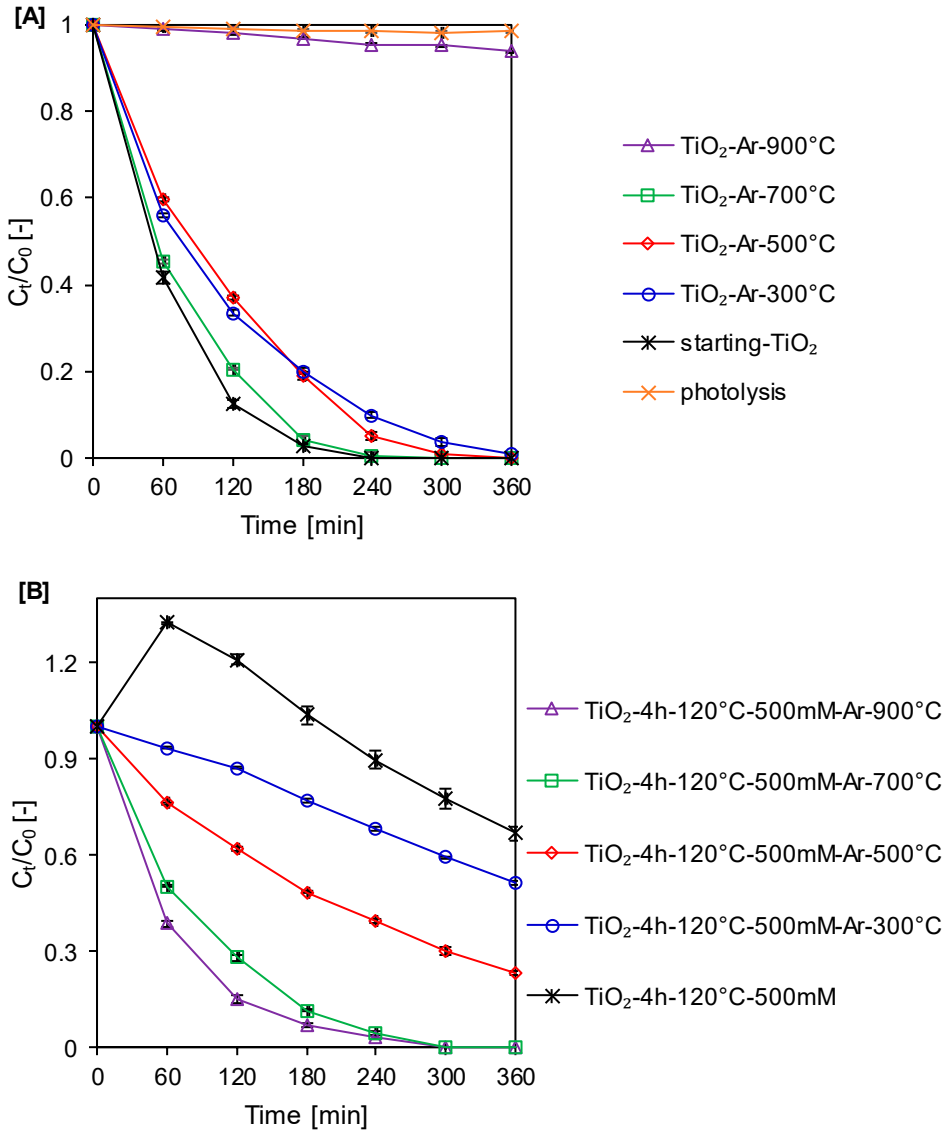

Figure 8. Orange II decomposition under UV irradiation for starting TiO_2 and calcined reference samples (**A**), and APTES-modified TiO_2 before and after calcination (**B**).

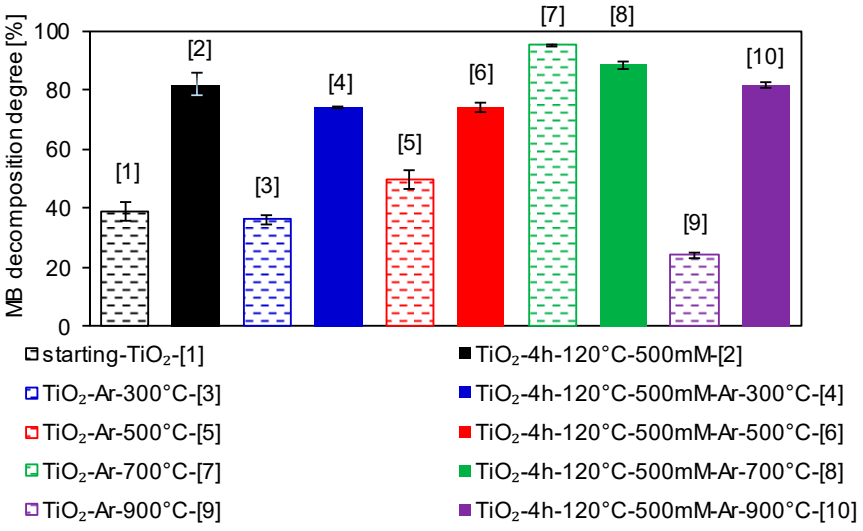

Figure 9. Methylene blue decomposition degree after 240 min of UV light irradiation for starting TiO_2, calcined reference samples, and APTES-modified TiO_2 prior to and after process.

Furthermore, the high porosity facilitated the mass transfer of reagents such as reaction by-products or oxygen, contributing to enhancing the photoactivity of the tested calcined APTES-functionalized TiO_2 photocatalysts [75,76]. Moreover, it was found that APTES-modified TiO_2 samples calcined at 500–900 °C were characterized not only by a high dye decomposition degree (see Figure 9), but also by excellent adsorption properties (see Figure 5). These observations were consistent with the reports indicating that the adsorption process strongly influences the photocatalytic degradation reaction [20,24,77]. Furthermore, it was noted that APTES/TiO_2 nanomaterial calcined at 900 °C showed the highest efficiency enhancement concerning the reference material. Methylene blue decomposition degree of TiO_2-4h–120°C–500mM-Ar–900°C increased by 58% compared to TiO_2-Ar-900°C. Since both photocatalysts showed similar zeta potential values (see Table 2), the noticed gain of activity was mostly related to the suppression of anatase-to-rutile phase transformation, thus the higher value of the S_{BET} of the modified samples (see Table 1).

In the case of Orange II, after calcination at 300 °C and 500 °C, a slight decrease (approximately 10% and 5%, respectively) in the photocatalytic activity was noted in comparison to starting TiO_2. Significant reduction of the decomposition degree (approximately 95%) was observed for TiO_2-Ar–900°C, which was associated with the complete formation of the rutile phase and an increase in the aggregation of molecules, which reduced the specific surface area [30]. After TiO_2 modification with APTES, the photocatalytic activity of TiO_2-4h–120°C-500mM decreased by 90% after 240 min of irradiation compared to the starting TiO_2. For TiO_2–4h–120°C–500mM sample, after 60 min of UV light irradiation, significant desorption of dye molecules from the surface of the photocatalyst was noted (see Figure 8B), which may be related to the increase of the temperature of the reaction suspension, caused by the heat generated by the 6 lamps used in the experiments. The significant amount of the Orange II molecules released effectively disrupted the photocatalytic decomposition, causing a decrease in the activity. It was noted that APTES-modified TiO_2 calcined at 300 °C and 500 °C exhibited a significantly lower decomposition degree of Orange II than the reference materials prepared at the same temperature. The TiO_2-Ar–300 °C and TiO_2-Ar–500 °C samples (see Figure 6A) exhibited a higher adsorption degree of Orange II than TiO_2-4h–120°C–500mM-Ar–300°C and TiO_2-4h–120°C–500mM-Ar–500°C materials (see Figure 6B). The reference samples calcined at 300 °C and 500 °C showed almost identical phase composition and were characterized by a smaller specific surface area than the corresponding APTES-modified TiO_2 nanomaterials (see Table 1), the obtained results imply that the adsorption process had a strong influence on the Orange II degradation. Our observations were consistent with the reports indicating that the adsorption process has a substantial impact on the photocatalytic oxidation process and may improve the efficiency of the studied materials [20,24,77]. As the modification temperature increased, the difference between the dye decomposition degree achieved by the reference materials and those modified with APTES decreased. For photocatalysts calcined at 300 °C, the difference in yield was 58%, and at 500 °C it equaled 34%, while at 700 °C the difference in efficiency was only 4%. Only for TiO_2-4h–120°C–500mM-Ar–900°C did the sample show a 92% increase in photoactivity after 240 min of exposure to UV light compared to the TiO_2-Ar–900 °C (see Figure 10). Similar to the methylene blue decomposition, because both materials exhibited almost the same zeta potential values, the noted increase in the photoactivity was connected with the effective suppression of anatase-to-rutile phase transformation (see Table 1) and still the relatively high specific surface area of TiO_2–4h–120°C–500mM-Ar–900°C sample (50 m^2/g) in comparison to TiO_2-Ar–900°C (3 m^2/g) [30,75].

The apparent reaction rate constants were established to better understand the photocatalytic decomposition process of both methylene blue and Orange II. The zero-order, pseudo-first order, and pseudo-second order linear transformations are presented for methylene blue in Figures S2A,B, and for Orange II in Figures S3A-C, respectively.

The reaction rate constants were determined after 240 min of exposure to UV light, due to the fact that when the irradiation time was extended to 360 min, after 240 min the points in the graph start to deviate from the typical linear course of the curve (see Figures S2B and S3C). The reported reduction in the reaction rate was related to the formation of intermediates during the decomposition of dyes and the adsorption of these carbon deposits on the surface of the semiconductor. To avoid impairing the visibility of all graphs, the kinetics of the decomposition after 360 min of irradiation were presented only for the pseudo-second order reactions.

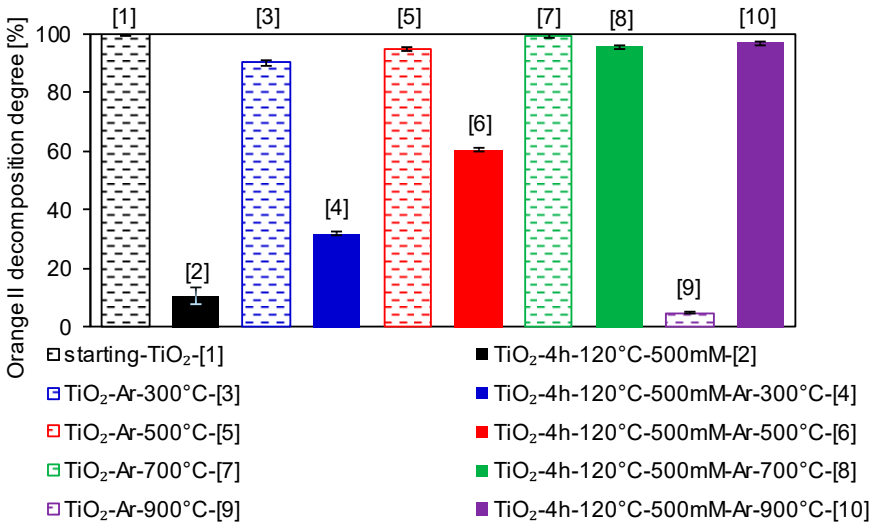

Figure 10. Orange II decomposition degree after 240 min of UV light irradiation for starting TiO_2, calcined reference samples, and APTES-modified TiO_2 before and after calcination.

It was found that the degradation of methylene blue in the case of starting-TiO_2, the reference materials calcined at 300–700 °C [30] and TiO_2–4h–120°C–500mM followed the Langmuir–Hinshelwood pseudo-first order model. According to the pseudo-second-order model for TiO_2-Ar–900°C and all APTES/TiO_2 nanomaterials after calcination proceeds. It was noted that after TiO_2 functionalization via APTES combined with thermal modification, the kinetics of the methylene blue decomposition changed from pseudo-first to the pseudo-second order. The calculated reaction rate constants were listed in Table S3.

The degradation of Orange II in the case of TiO_2–4h–120°C–500mM, TiO_2-Ar-500°C and TiO_2-4h–120°C–500mM-Ar–300°C followed the zero-order model, while for TiO_2-Ar–900°C proceeds according to the pseudo-second-order model. For all other photocatalysts, the decomposition was in accordance with the pseudo-first order model. Based on the data shown in Table S4, the obtained values of k_0 were 0.0171 mg/(L·min) for TiO_2-4h–120°C–500mM sample, 0.0337 mg/(L·min) for the reference material and 0.0175 mg/(L·min) for TiO_2-modified APTES calcined at 300 °C. The noted values of k_1 were between 0.0019 L/min and 0.0143 L/min. For TiO_2-Ar–900°C sample, k_2 equalled 0.0001 L/(min·mg).

The Reusability Tests

Determining the stability of photocatalysts in subsequent cycles of pollutants decomposition plays a crucial role in assessing the possibility of their industrial use. The performance of the studied nanomaterials was tested for four subsequent photocatalytic cycles. For methylene blue decomposition, the results obtained were shown in Figure 11A–E, and for Orange II in Figure 12A–E. In the case of methylene blue, the modification in the Ar atmosphere at 500 °C (TiO_2–4h–120°C–500mM-Ar–500°C) and 700 °C (TiO_2-4h–120°C–500mM-Ar–700°C) contributed to an improvement in the stability com-

pared to TiO_2–4h–120°C–500mM sample. After the first cycle, the decomposition degree of TiO_2-4h–120°C–500mM reduced by about 31%, whereas after calcination the photocatalytic activity decreased by about 21% and 26%, respectively. The increase in S_{BET} and V_{total} after calcination (see Table 1) improved the performance of subsequent dye decomposition cycles. Moreover, DRIFT spectra presented in Figure 3, as well as the results of the C and N content shown in Table 2, confirmed the absence of carbon and nitrogen in the materials obtained after the calcination process, the leaching of which reduced the effectiveness of TiO_2-4h–120°C–500mM sample [74].

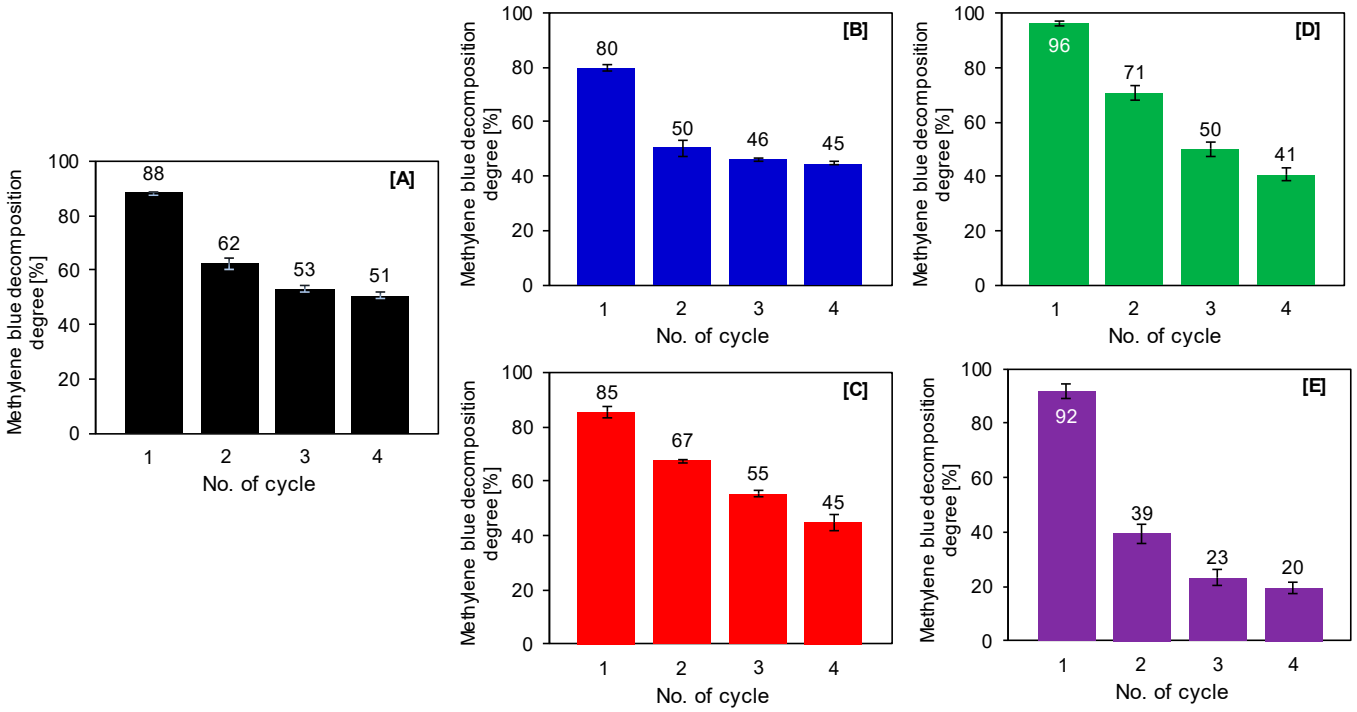

Figure 11. Photocatalytic activity in subsequent cycles of methylene blue degradation of TiO_2–4h–120°C–500mM (**A**), TiO_2–4h–120°C–500mM-Ar-300°C (**B**), TiO_2–4h–120°C–500mM-Ar-500°C (**C**), TiO_2–4h–120°C–500mM-Ar–700°C (**D**), and TiO_2–4h–120°C-500mM-Ar-900°C (**E**) materials.

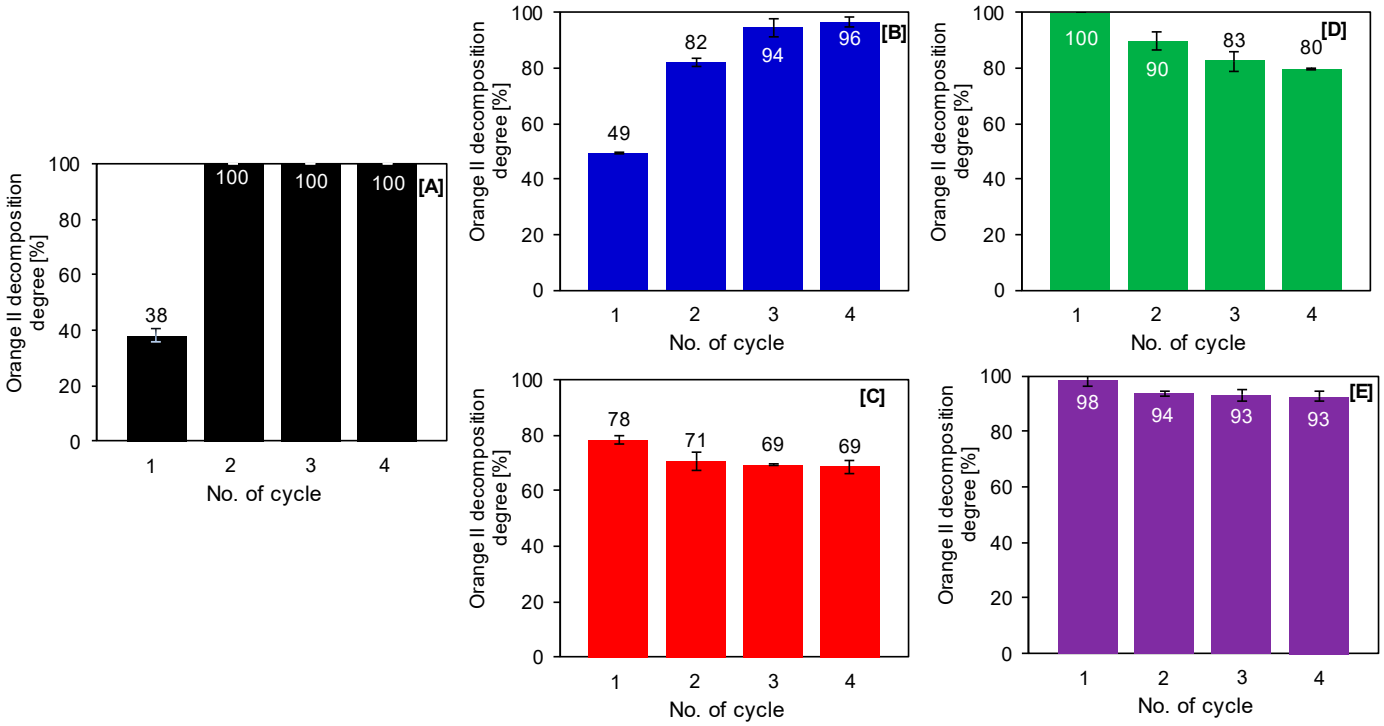

Figure 12. Photocatalytic activity in subsequent cycles of Orange II degradation of TiO_2-4h–120°C–500mM (**A**), TiO_2–4h–120°C–500mM-Ar-300°C (**B**), TiO_2–4h-120°C–500mM-Ar-500°C (**C**), TiO_2–4h–120°C–500mM-Ar–700°C (**D**), and TiO_2-4h–120°C–500mM-Ar-900°C (**E**) nanomaterials.

Additionally, to explain the decrease in the efficiency of calcined materials, after the last fourth cycle of methylene blue decomposition, DRIFT spectra of selected photocatalysts were measured and shown in Figure 13A in combination with the spectra of samples before the exposure process. The observed change in the shape of the spectra after four cycles indicates that the structure of the semiconductor has changed during the photocatalytic reaction. An apparent increase in the intensity of the band located from 1200 cm^{-1} to 1600 cm^{-1} suggested that in subsequent cycles carbon deposits originating from methylene blue appeared, which caused a decrease in the photocatalytic activity [78].

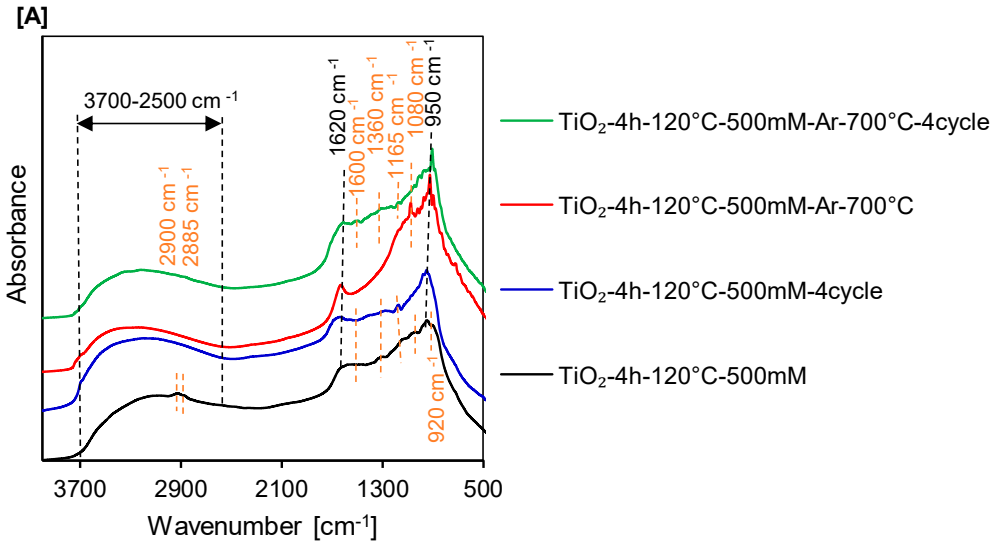

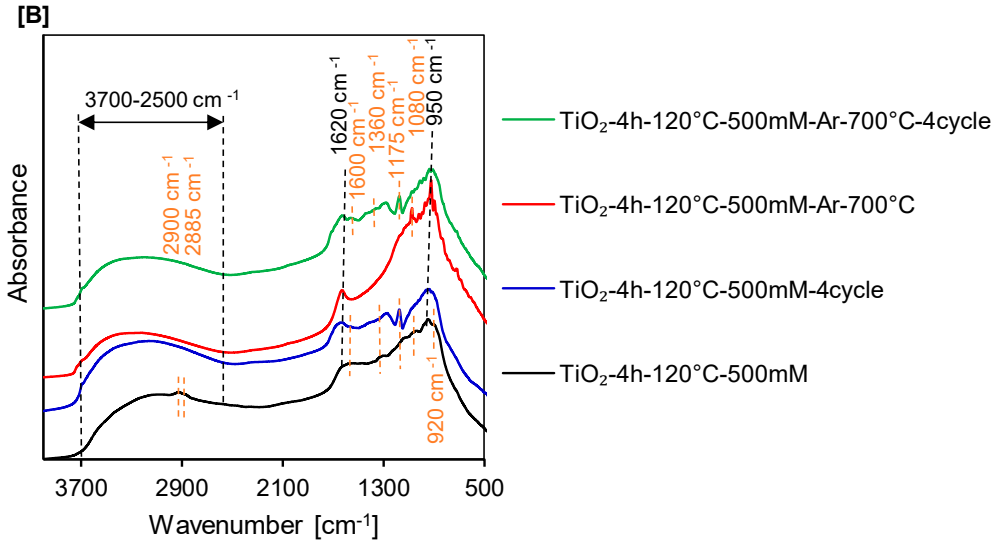

Figure 13. DRIFT spectra of TiO_2–4h–120°C–50 mM and TiO_2–4h–120°C–500mM-Ar–700°C photocatalysts before the first cycle and after the fourth cycle for methylene blue (**A**), and Orange II (**B**) decomposition.

For TiO_2-4h–120°C–500mM and TiO_2-4h–120°C–500mM-Ar–300°C samples, a significant enhancement in yield was noted in the subsequent cycles of Orange II decomposition (see Figure 12A,B). Compared to the first cycle, the decomposition degree of TiO_2–4h–120°C–500mM increased from 38% to 100% after the second cycle and remained at this level even after the last cycle. For TiO_2–4h–120°C–500mM-Ar–300°C there was a gradual increase in activity from 49% after the first cycle, through 82% after the second to 96% after the fourth cycle. The materials calcined at 500 °C and 900 °C had relatively high stability, because after four cycles only a slight decrease in the activity of 9% and 5%, respectively, was recorded. Only a TiO_2–4h–120°C–500mM-Ar–700°C sample exhibited a slight reduction in the activity during the reusability test, for which the decomposition degree decreased from 100% after the first cycle to 80% after the fourth cycle. The increase in the activity and high stability of photocatalysts in the subsequent cycles of Orange II decomposition resulted from the appearance of $-SiO_3^-$ groups on the TiO_2 surface, which were observed on DRIFT spectra at 1175 cm^{-1} (see Figure 13B) [78]. According to the literature [17], the presence of the $-SO_3^-$ group could be assumed to improve the removal efficiency. An increase in the intensity of the band located from 1200 cm^{-1} to 1600 cm^{-1} indicated that in subsequent cycles semiproducts originating from Orange II decomposition appeared, which contributed to a slight decrease in the efficiency of the sample calcined at 700 °C. Apart from the confirmed significant influence of the phase composition on the photocatalytic efficiency, the obtained FT-IR/DR spectra demonstrated that the reduction of the dye decomposition degree was strongly influenced by the adsorption of methylene blue on the surface of the tested nanomaterials. A negatively charged surface of APTES-modified photocatalysts impacts the sorption of degradation co-products of methylene blue in each next cycle, thus decreasing the photoactivity. On the other hand, the presence of the negative-loaded groups on the surface of tested materials (i.e. SiO_3^- groups) inhibits sorption of Orange II degradation semiproducts. Therefore, the adsorption process also plays an essential role in the photocatalytic decomposition of pollutants [17,79,80].

3. Materials and Methods

3.1. Materials and Reagents

Crude TiO_2 pulp, purchased from the chemical plant Grupa Azoty Zakłady Chemiczne "Police" S.A. (Police, Poland), was used as a TiO_2 source. Before modification,

the raw pulp was pre-prepared to reach pH equal to 6.8 due to the presence of post-production sulphuric acid remains. This stage was described in detail in our previous article [61]. The received material was named as starting TiO_2. 3-aminopropyltriethoxysilane (APTES, $C_9H_{23}NO_3Si$, ≥98%) from Merck KGaA (Darmstadt, Germany) was used as a modifier of the TiO_2. Ethyl alcohol (purity 96%, pure p.a.) purchased from P.P.H. "STANLAB" Sp.J. (Lublin, Poland) was used as a solvent of APTES. During photocatalytic decomposition tests, Orange II ($C_{16}H_{11}N_2NaO_4S$, ≥85%, Firma Chempur®, Piekary Śląskie, Poland) and methylene blue ($C_{16}H_{18}ClN_3S$, ≥82%, Firma Chempur®, Piekary Śląskie, Poland) were used as model organic water pollution.

3.2. Synthesis of 3-Aminopropyltriethoxysilane (APTES)-Modified TiO_2

The APTES/TiO_2 nanomaterials were obtained by the solvothermal process and calcination. In the beginning, 5 g of starting TiO_2 was dispersed in 25 mL of APTES solution. The concentration of the modifier in ethanol was 500 mM. Next, the prepared mixture was modified in a pressure autoclave for 4 h at 120 °C, ensuring continuous stirring at 500 rpm. Then, the suspension obtained was rinsed with ethanol and distilled water to eliminate all residual chemicals. The sample was dried at 105 °C for 24 h in a lab dryer. The material obtained was denoted as TiO_2–4h–120°C–500mM. Finally, the prepared material was heated in argon atmosphere (purity 5.0, Messer Polska Sp. z o.o., Chorzów, Poland). The quartz crucible containing the obtained photocatalyst was placed inside a quartz tube in the middle of the GHC 12/900 horizontal furnace (Carbolite Gero, Ltd., Sheffield, UK). Calcination was conducted in the range of 300–900 °C (Δt = 200 °C). Prior to the heating step, the argon was passed through the quartz tube for 30 min to remove the air present in the quartz pipe. After that, the furnace was heated up to the set temperature in the argon flow of 180 mL/min. The calcination time was 4 h. After the set time, the furnace was slowly cooled down to room temperature. Nanomaterials received after the thermal modification of starting TiO_2 in the Ar atmosphere were named as reference samples denoted as TiO_2-Ar-t, while APTES/TiO_2 materials obtained after heat treatment were marked as TiO_2–4h–120°C–500mM-Ar-t, where *t* is the calcination temperature.

3.3. Characterization Methods

The low-temperature nitrogen adsorption-desorption measurements (conducted at 77 K) carried out on the QUADRASORB evo™ Gas Sorption analyzer (Anton Paar GmbH, Graz, Austria) were used to calculate the Brunauer–Emmett–Teller (BET) specific surface area and pore volume. Before the measurements, all samples were degassed for 12 h at 100 °C under high vacuum to remove any residual contaminants present on the surface of tested materials. The single-point value determined the total pore volume from the nitrogen adsorption isotherms at relative pressure $p/p_0 = 0.99$. Micropore volume was estimated using the Dubinin–Radushkevich method, while mesopore volume was determined as the difference between V_{total} and V_{micro}. The zeta potential values were determined with the ZetaSizer NanoSeries ZS (Malvern PANalytical Ltd., Malvern, UK). The crystalline structure of the tested photocatalysts was identified by the X-ray powder diffraction analysis (Malvern PANalytical B.V., Almelo, Netherlands) using Cu Kα radiation (λ =1.54056 Å). Scherrer's equation was used to calculate the mean crystallites size. To identify the phase composition, the PDF-4+ 2014 International Centre for Diffraction Data database (for anatase: 04-002-8296 PDF4+ card, and for rutile: 04-005-5923 PDF4+ card) was applied. The FT-IR-4200 spectrometer (number of scans 100, resolution 4.0 cm^{-1}, JASCO International Co. Ltd., Tokyo, Japan) equipped with DiffuseIR accessory (PIKE Technologies, Fitchburg, WI, USA) was utilized to determine the surface functional groups and to notice the surface changes during the reusability test. The V-650 UV-Vis spectrophotometer (JASCO International Co., Tokyo, Japan) equipped with a PIV-756 integrating sphere accessory for measuring DR spectra (JASCO International Co., Tokyo, Japan) was used to examine the light reflectance abilities of the new APT-

ES/TiO_2 samples. Spectralon® Diffuse Reflectance Material (Labsphere, New Hampshire, NE, USA) was applied as the reference material. The optical bandgap energy (E_g) of the samples was calculated by plotting $[F(R)h\upsilon]^{1/2}$ as a function of photon energy and next extrapolating the linear parts to $[F(R)h\upsilon]^{1/2} = 0$ [81]. The CN 628 elemental analyzer (LECO Corporation, St. Joseph, MI, USA) was used to determine the total carbon and nitrogen content in the studied nanomaterials. The certified ethylenediaminetetraacetic acid (EDTA) standard (LECO Corporation, St. Joseph, MI, USA) containing 9.56 ± 0.03 wt.% of nitrogen and 41.06 ± 0.09 wt.% of carbon was utilized to prepare the calibration curve for preparing calibration curves. The error range for measurements was maximally ±0.1%.

3.4. Adsorption Capacity

To determine the adsorption capacity, the adsorption experiments were carried out in Erlenmeyer flask with starting-TiO_2, reference samples and APTES-modified TiO_2 nanomaterials, by stirring at 150 rpm 0.125 g of the photocatalyst in 0.25 L of methylene blue and Orange II aqueous solutions with concentrations of 1, 2, 4, 6, 8, 10, 12 and 15 mg/L, under light-free conditions in a thermostatic chamber at 20 °C (Pol-Eko-Aparatura sp.j., Włodzisław Śląski, Poland). This process continued for 240 min to establish the adsorption-desorption equilibrium between the dye and photocatalysts surface. Ultrapure water (Merck Millipore Sp. z o.o., Warszawa, Poland) was used to prepare all solutions. After 240 min, 10 mL of the withdrawn suspension was centrifuged to separate all suspended nanoparticles. The concentration of methylene blue and Orange II was analyzed by the V-630 UV-Vis spectrometer (JASCO International Co., Tokyo, Japan). The experimental equilibrium adsorption data were analyzed using Freundlich [82], Langmuir [72], Langmuir–Freundlich [70], and Temkin [71] isotherm models. The Statistica software (version 13.1) was used to plot the adsorption isotherms.

3.5. Photocatalytic Activity Test

Methylene blue and Orange II were selected for the photocatalytic activity and reusability tests. Photocatalytic decomposition was carried out under UV-Vis light with the radiation intensity of 65 W/m^2 for 300–2800 nm and 36 W/m^2 for the 280–400 nm region, supplied by a series of 6 lamps of 20 W each (Philips, Amsterdam, Netherlands). Because of the low intensity of visible (Vis) irradiation used, this type of light was named as UV light. The experiments were performed in a 0.6 L glass beaker using 0.5 L of dye solution, with an initial concentration of 15 mg/L and the concentration of photocatalyst equalled 0.5 g/L. The experimental procedure consisted of two steps. Firstly, before the irradiation stage, the prepared suspension was magnetically stirred under dark conditions to establish the adsorption-desorption equilibrium between the TiO_2 surface and dye molecules. The time necessary to achieve the adsorption-desorption equilibrium was determined based on research on the sorption properties of the photocatalysts. Secondly, the suspension was exposed to UV light irradiation. The total exposure time was 360 min. The dye concentration was measured every 60 min with the V-630 UV-Vis spectrometer (JASCO International Co., Tokyo, Japan). Prior to each measurement, 10 mL of the withdrawn suspension was centrifuged to remove all suspended photocatalyst nanoparticles. Additionally, the reusability test was determined based on the decomposition of dyes under UV light after 360 min of irradiation. After each cycle, the material was separated by filtration and dried for 12 h at 105 °C and then added to a new dose of the dye solution with appropriate initial concentration. Based on the results obtained, the reaction rates of model organic pollutants decomposition were determined by adjusting the appropriate order of the reaction. The zero reaction rate constant was established according to the zero-order model [47].

The pseudo-first reaction rate constant was calculated using the Langmuir– Hinshelwood pseudo-first order model and the pseudo-second reaction rate constant was determined following the pseudo-second order model [83].

4. Conclusions

The APTES/TiO_2 nanomaterials were obtained by a solvothermal process at 120 °C, and subsequent calcination in Ar atmosphere in the range of 300 °C–900 °C. In the present article, for the first time, the role of adsorption in the photocatalytic decomposition of dyes on APTES-modified TiO_2 nanomaterials, as well as the influence of calcination in the inert gas atmosphere on the adsorption capacity and stability of APTES/TiO_2 samples were determined. The presence of the modifier on the TiO_2 surface was confirmed by DRIFTS measurements and carbon and nitrogen content analysis. It was found that the Langmuir and Langmuir–Freundlich isotherm models, due to their highest fit, best describe the adsorption of methylene blue on the surface of the examined APTES-modified photocatalysts, while for the Orange II adsorption process, the best fit was found for Freundlich and Langmuir–Freundlich isotherm models. The recorded alterations in the adsorption capacity were related to the changes in the surface charge and the S_{BET} of the APTES-modified TiO_2. It was also observed that the adsorption process had a significant impact on the photooxidation of dyes. The APTES/TiO_2 photocatalysts calcined at 900 °C, showed a markedly higher methylene blue and Orange II degradation degree in comparison to calcined reference materials, which was related to the fact that functionalization via APTES, which is a good source of silicon, effectively suppressed anatase-to-rutile phase transition, as well as the growth of crystallites size. Furthermore, in the case of methylene blue, thermal modification at 500 °C and 700 °C contributed to an improvement in the stability compared to TiO_2–4h–120°C–500mM sample for Orange II, all photocatalysts showed high efficiency during the reusability test.

Supplementary Materials: The following are available online at www.mdpi.com/2073-4344/11/2/172/s1, Figure S1: Pore size distribution plots of starting-TiO_2, calcined reference samples (A), and APTES-modified TiO_2 photocatalysts (B)., Figure S2: The pseudo-first-order plot (A), and the pseudo-second-order plot (B) of methylene blue decomposition., Figure S3: The zero-order plot (A), the pseudo-first-order plot (B), and the pseudo-second-order plot (C) of Orange II decomposition., Table S1: Isotherm constants for the adsorption process of methylene blue on starting TiO_2, calcined reference samples and APTES-modified photocatalysts., Table S2: Isotherm constants for the adsorption process of Orange II on starting TiO_2, calcined reference samples and APTES-modified photocatalysts., Table S3: The fitting parameters, the pseudo-first and pseudo-second reaction rate constants for methylene blue photoremoval (after 240 min of UV radiation)., Table S4: The fitting parameters, zero, pseudo-first, and pseudo-second reaction rate constants for Orange II photoremoval (after 240 min of UV radiation).

Author Contributions: Conceptualization, A.S., A.W. and A.W.M.; Formal analysis, E.K.-N.; Funding acquisition, A.W.M.; Investigation, A.S., A.W. and P.R.-K.; Methodology, A.S. and A.W.; Software, A.S. and E.K.-N.; Supervision, E.K.-N., A.W. and A.W.M.; Writing—original draft, A.S. and E.K.-N.; Writing—review and editing, E.K.-N., A.W., A.S., A.W.M. All authors have read and agreed to the published version of the manuscript.

Funding: This research was funded by the National Science Centre, Poland, grant no. 2017/27/B/ST8/02007.

Conflicts of Interest: On behalf of all authors, the corresponding author states no conflict of interest.

References

1. Rathour, R.; Patel, D.; Shaikh, S.; Desai, C. Eco-electrogenic treatment of dyestuff wastewater using constructed wetland-microbial fuel cell system with an evaluation of electrode-enriched microbial community structures. *Bioresour. Technol.* **2019**, *285*, 121349.
2. Lau, Y.-Y.; Wong, Y.-S.; Teng, T.-T.; Morad, N.; Rafatullah, M.; Ong, S.-A. Coagulation—Flocculation of azo dye Acid Orange 7 with green refined laterite soil. *Chem. Eng. J.* **2014**, *246*, 383–390.
3. Karthik, V.; Saravanan, K.; Bharathi, P.; Dharanya, V.; Meiaraj, C. An overview of treatments for the removal of textile dyes. *J. Chem. Pharm. Sci.* **2014**, *7*, 301–307.
4. Kuppusamy, S.; Sethurajan, M.; Kadarkarai, M.; Aruliah, R. Biodecolourization of textile dyes by novel, indigenous *Pseudomonas stutzeri* MN1 and *Acinetobacter baumannii* MN3. *J. Environ. Chem. Eng.* **2017**, *5*, 716–724.

5. Mokif, L.A. Removal methods of synthetic dyes from industrial wastewater: A review. *Mesop. Environ. J.* **2019**, *5*, 23–40.
6. Venkata Mohan, S.; Karthikeyan, J. Adsorptive removal of reactive azo dye from an aqueous phase onto charfines and activated carbon. *Clean Technol. Environ. Policy* **2004**, *6*, 196–200.
7. Forgacs, E.; Cserháti, T.; Oros, G. Removal of synthetic dyes from wastewaters: A review. *Environ. Inter.* **2004**, *30*, 953–971.
8. Kim, T.-H.; Park, C.; Kim, S. Water recycling from desalination and purification process of reactive dye manufacturing industry by combined membrane filtration. *J. Clean. Prod.* **2005**, *13*, 779–786.
9. Arslan, I.; Akmehmet Balcioglu, I.; Tuhkanen, T. Advanced Oxidation of Synthetic Dyehouse Effluent by O_3, H_2O_2/O_3 and H_2O_2/UV Processes. *Environ. Technol.* **1999**, *20*, 921–931.
10. Balanosky, E.; Fernandez, J.; Kiwi, J.; Lopez, A. Degradation of membrane concentrates of the textile industry by Fenton like reactions in iron-free solutions at biocompatible pH values (pH ≈ 7–8). *Water Sci. Technol.* **1999**, *40*, 417–424.
11. Kang, S.-F.; Liao, C.-H.; Po, S.-T. Decolorization of textile wastewater by photo-fenton oxidation technology. *Chemosphere* **2000**, *41*, 1287–1294.
12. Piaskowski, K.; Świderska-Dąbrowska, R.; Zarzycki, P.K. Dye Removal from Water and Wastewater Using Various Physical, Chemical, and Biological Processes. *J. AOAC Int.* **2018**, *101*, 1371–1384.
13. Da Silva, C.G.; Faria, J.L.S. Photochemical and photocatalytic degradation of an azodye in aqueous solution by UV irradiation. *J. Photochem. Photobiol. A* **2003**, *155*, 133–143.
14. Konstantinou, I.K.; Albanis, T.A. TiO_2-assisted photocatalytic degradation of azo dyes in aqueous solution: Kinetic and mechanistic investigations: A review. *Appl. Catal. B* **2004**, *49*, 1–14.
15. Ratova, M.; Sawtell, D.; Kelly, P.J. Micro-Patterning of Magnetron Sputtered Titanium Dioxide Coatings and Their Efficiency for Photocatalytic Applications. *Coatings* **2020**, *10*, 68.
16. Xue, G.; Liu, H.; Chen, Q.; Hills, C.; Tyrer, M.; Innocent, F. Synergy between surface adsorption and photocatalysis during degradation of humic acid on TiO_2/activated carbon composites. *J. Hazard. Mater.* **2011**, *186*, 765–772.
17. Tryba, B.; Morawski, A.W.; Tsumura, T.; Toyoda, M.; Inagaki, M. Hybridization of adsorptivity with photocatalytic activity-carbon-coated anatase. *J. Photochem. Photobiol. A* **2004**, *167*, 127–135.
18. Ariyanti, D.; Maillot, M.; Gao, W. TiO_2 used as photocatalyst for rhodamine B degradation under solar radiation. *Int. J. Mod. Phys. B* **2017**, *31*, 1744095.
19. Chatterjee, D.; Ruj, B.; Mahata, A. Adsorption and photocatalysis of colour removal from wastewater using flash and sunlight. *Catal. Commun.* **2001**, *2*, 113–117.
20. Jafari, S.; Tryba, B.; Kusiak-Nejman, E.; Kapica-Kozar, J.; Morawski, A.W.; Sillanpää, M. The role of adsorption in the photocatalytic decomposition of Orange II on carbon-modified TiO_2. *J. Mol. Liq.* **2016**, *220*, 504–512.
21. Kusiak-Nejman, E.; Wanag, A.; Kapica-Kozar, J.; Kowalczyk, Ł.; Zgrzebnicki, M.; Tryba, B.; Przepiórski, J.; Morawski, A.W. Methylene blue decomposition on TiO_2/reduced graphene oxide hybrid photocatalysts obtained by a two-step hydrothermal and calcination synthesis. *Catal. Today* **2020**, *357*, 630–637.
22. Janus, M.; Kusiak-Nejman, E.; Morawski, A.W. Determination of the photocatalytic activity of TiO_2 with high adsorption capacity. *React. Kinet. Mech. Catal.* **2011**, *103*, 279–288.
23. Zhu, Y.; Xu, S.; Yi, D. Photocatalytic degradation of methyl orange using polythiophene/titanium dioxide composites. *React. Funct. Polym.* **2010**, *70*, 282–287.
24. Wang, Q.; Chen, C.; Zhao, D.; Ma, W.; Zhao, J. Change of adsorption modes of dyes on fluorinated TiO_2 and its effect on photocatalytic degradation of dyes under visible irradiation. *Langmuir* **2008**, *24*, 7338–7345.
25. Chen, Q.; Yakovlev, N.L. Adsorption and interaction of organosilanes on TiO_2 nanoparticles. *Appl. Surf. Sci.* **2010**, *257*, 1395–1400.
26. Kim, J.; Cho, J.; Seidler, P.; Kurland, N.; Yadavalli, V. Investigations of Chemical Modifications of Amino-Terminated Organic Films on Silicon Substrates and Controlled Protein Immobilization. *Langmuir* **2010**, *26*, 2599–2608.
27. Shakeri, A.; Yip, D.; Badv, M.; Imani, S.M.; Sanjari, M.; Didar, T.F. Self-cleaning ceramic tiles produced via stable coating of TiO_2 nanoparticles. *Materials* **2018**, *11*, 1003.
28. Bao, N.; Wu, G.; Niu, J.; Zhang, Q.; He, S.; Wang, J. Wide spectral response and enhanced photocatalytic activity of TiO_2 continuous fibers modified with aminosilane coupling agents. *J. Alloys Compd.* **2014**, *599*, 40–48.
29. Andrzejewska, A.; Krysztafkiewicz, A.; Jesionowski, T. Adsorption of organic dyes on the aminosilane modified TiO_2 surface. *Dyes Pigm.* **2004**, *62*, 121–130.
30. Sienkiewicz, A.; Wanag, A.; Kusiak-Nejman, E.; Ekiert, E.; Rokicka-Konieczna, P.; Morawski, A.W. Effect of calcination on the photocatalytic activity and stability of TiO_2 photocatalysts modified with APTES. *J. Environ. Chem. Eng.* **2021**, *9*, 104794.
31. Wetchakun, N.; Incessungvorn, B.; Wetchakun, K.; Phanichphant, S. Influence of calcination temperature on anatase to rutile phase transformation in TiO_2 nanoparticles synthesized by the modified sol-gel method. *Mater. Lett.* **2012**, *82*, 195–198.
32. Byrne, C.; Fagan, R.; Hinder, S.; McCormack, D.E.; Pillai, S.C. New approach of modifying the anatase to rutile transition temperature in TiO_2 photocatalysts. *RSC Adv.* **2016**, *6*, 95232–95238.
33. Dalod, A.R.M.; Henriksen, L.; Grande, T.; Einarsrud, M.-A. Functionalized TiO_2 nanoparticles by single-step hydrothermal synthesis: The role of the silane coupling agents. *Beilstein J. Nanotechnol.* **2017**, *8*, 304–312.
34. Tobaldi, D.M.; Tucci, A.; Škapin, A.S.; Esposito, L. Effects of SiO_2 addition on TiO_2 crystal structure and photocatalytic activity. *J. Eur. Ceram. Soc.* **2010**, *30*, 2481–2490.

35. Lu, Z.; Jiang, X.; Zhou, B.; Wu, X.; Lu, L. Study of effect annealing temperature on the structure, morphology and photocatalytic activity of Si doped TiO_2 thin films deposited by electron beam evaporation. *Appl. Surf. Sci.* **2011**, *257*, 10715–10720.
36. Xu, G.; Zheng, Z.; Wu, Y.; Feng, N. Effect of silica on the microstructure and photocatalytic properties of titania. *Ceram. Int.* **2009**, *35*, 1–5.
37. Schneider, P. Adsorption isotherms of microporous-mesoporous solids revisited. *Appl. Catal. A Gen.* **1995**, *129*, 157–165.
38. Sing, K.S.W.; William, R.T. Physisorption hysteresis loops and the characterization of nanoporous materials. *Adsorp. Sci. Technol*. **2004**, *22*, 773–782.
39. Sun, Q.; Hu, X.; Zheng, S.; Sun, Z.; Liu, S.; Li, H. Influence of calcination temperature on the structural, adsorption and photocatalytic properties of TiO_2 nanoparticles supported on natural zeolite. *Powder Technol.* **2015**, *274*, 88–97.
40. Siwińska-Stefańska, K.; Ciesielczyk, F.; Nowacka, M.; Jesionowski, T. Influence of selected alkoxysilanes on dispersive properties and surface chemistry of titanium dioxide and TiO_2-SiO_2 composite material. *J. Nanomater.* **2012**, *2012*, 1–19.
41. Zhuang, W.; Zhang, Y.; He, L.; An, R.; Li, B.; Ying, H.; Wu, J.; Chen, Y.J.; Zhou, J.; Lu, X. Facile synthesis of amino-functionalized mesoporous TiO_2 microparticles for adenosine deaminase immobilization. *Micropor. Mesopor. Mat.* **2017**, *239*, 158–166.
42. Górska, P.; Zaleska, A.; Kowalska, E.; Klimczuk, T.; Sobczak, J.W.; Skwarek, E.; Janusz, W.; Hupka, J. TiO_2 photoactivity in vis and UV light: The influence of calcination temperature and surface properties. *Appl. Catal. B Environ.* **2008**, *84*, 440–447.
43. Cheng, F.; Sajedin, S.M.; Kelly, S.M.; Lee, A.F.; Kornherr, A. UV-stable paper coated with APTES-modified P25 TiO_2 nanoparticles. *Carbohydr. Polym.* **2016**, *114*, 246–252.
44. Rokicka-Konieczna, P.; Markowska-Szczupak, A.; Kusiak-Nejman, E.; Morawski, A.W. Photocatalytic water disinfection under the artificial solar light by fructose modified TiO_2. *Chem. Eng. J.* **2019**, *372*, 203–215.
45. Kuroda, Y.; Mori, T.; Yagi, K.; Makihata, N.; Kawahara, Y.; Nagao, M.; Kittaka, S. Preparation of visible-light-responsive $TiO_{2-x}N_x$ photocatalyst by a sol-gel method: Analysis of the active center on TiO_2 that reacts with NH_3. *Langmuir* **2005**, *21*, 8026–8034.
46. Kusiak-Nejman, E.; Wanag, A.; Kapica-Kozar, J.; Morawski, A.W. Preparation and characterisation of TiO_2 thermally modified with cyclohexane vapours. *Int. J. Mater. Prod. Technol*. **2016**, *52*, 286–297.
47. Abdullah, S.M.A.; Chong, F.K. Dual-effects of adsorption and photodegradation of methylene blue by tungsten-loaded titanium dioxide. *Chem. Eng. J.* **2010**, *158*, 418–425.
48. Saliba, P.A.; Mansur, A.A.P.; Mansur, H.S. Advanced Nanocomposite Coatings of Fusion Bonded Epoxy Reinforced with Amino-Functionalized Nanoparticles for Applications in Underwater Oil Pipelines. *J. Nanomater.* **2016**, *2016*, 1–16.
49. Razmjou, A.; Resosudarmo, A.; Holmes, R.L.; Li, H.; Mansouri, J.; Chen, V. The effect of modified TiO_2 nanoparticles on the polyethersulfone ultrafiltration hollow fiber membranes. *Desalination* **2012**, *287*, 271–280.
50. De Melo Pinheiro, A.F.; Nijmeijer, A.; Prasad Sripathi, V.G.; Winnubst, L. Chemical modification/grafting of mesoporous alumina with polydimethylsiloxane (PDMS). *Eur. J. Chem.* **2015**, *6*, 287–295.
51. Meroni, D.; Lo Presti, L.; Di Liberto, G.; Ceotto, M.; Acres, R.G.; Prince, K.C.; Bellani, R.; Soliveri, G.; Ardizzone, S. A Close Look at the Structure of the TiO_2-APTES Interface in Hybrid Nanomaterials and Its Degradation Pathway: An Experimental and Theoretical Study. *J. Phys. Chem. C* **2017**, *121*, 430–440.
52. Vandenberg, E.T.; Bertilsson, L.; Liedberg, B.; Uvdal, K.; Erlandsson, R.; Elwing, H.; Lundström, I. Structure of 3-aminopropyl triethoxy silane on silicon oxide. *J. Colloid Interface Sci.* **1991**, *147*, 103–118.
53. Milanesi, F.; Cappelletti, G.; Annunziata, R.; Bianchi, C.L.; Meroni, D.; Ardizzone, S. Siloxane-TiO_2 Hybrid Nanocomposites. The Structure of the Hydrophobic Layer. *J. Phys. Chem. C* **2010**, *114*, 8287–8293.
54. Ukaji, E.; Furusawa, T.; Sato, M.; Suzuki, M. The effect of surface modification with silane coupling agent on suppressing the photocatalytic activity of fine TiO_2 particles as inorganic UV filter. *Appl. Surf. Sci.* **2007**, *254*, 563−569.
55. Razmjou, A.; Mansouri, J.; Chen, V. The effects of mechanical and chemical modification of TiO_2 nanoparticles on the surface chemistry, structure and fouling performance of PES ultrafiltration membranes. *J. Membr. Sci.* **2011**, *378*, 73–84.
56. Zhang, W.; Guo, H.; Sun, H.; Zeng, R.-C. Hydrothermal synthesis and photoelectrochemical performance enhancement of TiO_2 graphene composite in photo-generated cathodic protection. *Appl. Surf. Sci.* **2016**, *382*, 128–134.
57. Chen, Y.; Wang, Y.; Li, W.; Yang, Q.; Hou, Q.; Wei, L.; Liu, L.; Huang, F.; Ju, M. Enhancement of photocatalytic performance with the use of noble-metal-decorated TiO_2 nanocrystals as highly active catalysts for aerobic oxidation under visible-light irradiation. *Appl. Catal. B* **2017**, *210*, 352–367.
58. Yuan, L.; Weng, X.; Zhou, M.; Zhang, Q.; Deng, L. Structural and Visible-Near Infrared Optical Properties of Cr-Doped TiO_2 for Colored Cool Pigments. *Nanoscale Res. Lett*. **2017**, *12*, 597.
59. Kusiak-Nejman, E.; Janus, M.; Grzmil, B.; Morawski, A.W. Methylene blue decomposition under visible light irradiation in the presence of carbon-modified TiO_2 photocatalysts. *J. Photochem. Photobiol. A Chem.* **2011**, *226*, 68–72.
60. Suwannaruang, T.; Kamonsuangkasem, K.; Kidkhunthod, P.; Chirawatkul, P.; Saiyasombat, C.; Chanlek, N.; Wantala, K. Influence of nitrogen content levels on structural properties and photocatalytic activities of nanorice-like N-doped TiO_2 with various calcination temperatures. *Mater. Res. Bull.* **2018**, *105*, 265–276.
61. Janus, M.; Bubacz, K.; Zatorska, J.; Kusiak-Nejman, E.; Czyżewski, A.; Morawski, A.W. Preliminary studies of photocatalytic activity of gypsum plasters containing TiO_2 co-modified with nitrogen and carbon. *Pol. J. Chem. Technol.* **2015**, *17*, 96–102.
62. Goscianska, J.; Olejnik, A.; Nowak, I. APTES-functionalized mesoporous silica as a vehicle for antipyrine-adsorption and release studies. *Colloids Surf. A* **2017**, *533*, 187–196.

63. Talavera-Pech, W.A.; Esparza-Ruiz, A.; Quintana-Owen, P.; Vilchis-Nestor, A.F.; Carrera-Figueiras, C.; Ávila-Ortega, A. Effects of different amounts of APTES on physicochemical and structural properties of amino-functionalized MCM-41-MSNs. *J. Sol-Gel Sci. Technol.* **2016**, *80*, 697–708.
64. Wilhelm, P.; Stephan, D. Photodegradation of rhodamine B in aqueous solution via SiO_2@TiO_2 nano-spheres. *J. Photochem. Photobiol. A* **2007**, *185*, 19–25.
65. Ferreira-Neto, E.P.; Ullah, S.; Simões, M.B.; Perissinotto, A.P.; Vicente, F.S.; Noeske, P.-L.M.; Ribeiro, S.J.L.; Rodrigues-Filho, U.P. Solvent-controlled deposition of titania on silica spheres for the preparation of SiO_2@TiO_2 core@shell nanoparticles with enhanced photocatalytic activity. *Colloids Surf. A* **2019**, *570*, 293–305.
66. Medeiros Borsagli, F.G.L. A green 3D scaffolds based on chitosan with thiol group as a model for adsorption of hazardous organic dye pollutants. *Desalination Water Treat.* **2019**, *169*, 395–411.
67. Wang, S.; Zhu, Z.H.; Coomes, A.; Haghseresht, F.; Lu, G.Q. The physical and surface chemical characteristics of activated carbons and the adsorption of methylene blue from wastewater. *J. Colloid Interface Sci.* **2005**, *284*, 440–446.
68. Beegam, M.S.; Ullattil, S.G.; Periyat, P. Selective Solar Photocatalysis by High Temperature Stable Anatase TiO_2. *Sol. Energy* **2018**, *160*, 10–17.
69. Bubacz, K.; Tryba, B.; Morawski, A.W. The role of adsorption in decomposition of dyes on TiO_2 and N-modified TiO_2 photocatalysts under UV and visible light irradiations. *Mater. Res. Bull.* **2012**, *47*, 3697–3703.
70. Ayawei, N.; Ebelegi, A.N.; Wankasi, D. Modelling and Interpretation of Adsorption Isotherms. *J. Chem.* **2017**, *2017*, 3039817.
71. Konicki, W.; Aleksandrzak, M.; Moszyński, D.; Mijowska, E. Adsorption of anionic azo-dyes from aqueous solutions onto graphene oxide: Equilibrium, kinetic and thermodynamic studies. *J. Colloid Interface Sci.* **2017**, *496*, 188–200.
72. Jafari, S.; Yahyaei, B.; Kusiak-Nejman, E.; Sillanpää, M. The influence of carbonization temperature on the modification of TiO_2 in the removal of methyl orange from aqueous solution by adsorption. *Desalination Water Treat.* **2016**, *57*, 18825–18835.
73. Ohno, T.; Tokieda, K.; Higashida, S.; Matsumura, M. Synergism between rutile and anatase TiO_2 particles in photocatalytic oxidation of naphthalene. *Appl. Catal. A Gen.* **2003**, *244*, 383–391.
74. Wanag, A.; Sienkiewicz, A.; Rokicka-Konieczna, P.; Kusiak-Nejman, E.; Morawski, A.W. Influence of modification of titanium dioxide by silane coupling agents on the photocatalytic activity and stability. *J. Environ. Chem. Eng.* **2020**, *8*, 103917.
75. Zhang, R.-B. Photodegradation of toluene using silica-embedded titania. *J. Non-Cryst. Solids* **2005**, *351*, 2129–2132.
76. Su, Y.; Wu, J.; Quan, X.; Chen, S. Electrochemically assisted photocatalytic degradation of phenol using silicon-doped TiO_2 nanofilm electrode. *Desalination* **2010**, *252*, 143–148.
77. Cheng, Y.; Luo, F.; Jiang, Y.; Li, F.; Wei, C. The effect of calcination temperature on the structure and activity of TiO_2/SiO_2 composite catalysts derived from titanium sulfate and fly ash acid sludge. *Colloids Surf. A* **2018**, *554*, 81–85.
78. Bartošová, A.; Blinová, L.; Sirotiak, M.; Michalíková, M. Usage of FTIR-ATR as Non-Destructive Analysis of Selected Toxic Dyes. *Res. Pap. Fac. Mater. Sci. Technol. Slovak Univ. Technol.* **2017**, *25*, 103–111.
79. Wang, H.; Huang, Y. Prussian-blue-modified iron oxide magnetic nanoparticles as effective peroxidase-like catalysts to degrade methylene blue with H_2O_2. *J. Hazard. Mater.* **2011**, *191*, 163–169.
80. Abbas, M.; Parvatheeswara, R.B.; Reddy, V.; Kim, C. Fe_3O_4/TiO_2 core/shell nanocubes: Single-batch surfactant less synthesis, characterization and efficient catalysts for methylene blue degradation. *Ceram. Int.* **2014**, *40*, 11177–11186.
81. Chen, D.; Zou, L.; Li, S.; Zheng, F. Nanospherical like reduced graphene oxide decorated TiO_2 nanoparticles: An advanced catalyst for the hydrogen evolution reaction. *Sci. Rep.* **2016**, *6*, 20335.
82. Inyinbor, A.A.; Adekola, F.A.; Olatunji, G.A. Kinetics, isotherms and thermodynamic modeling of liquid phase adsorption of Rhodamine B dye onto Raphia hookerie fruit epicarp. *Water Resour. Ind.* **2016**, *15*, 14–27.
83. Wu, F.; Liu, W.; Qiu, J.; Li, J.; Zhou, W.; Fang, Y.; Zhang, S.; Li, X. Enhanced photocatalytic degradation and adsorption of methylene blue via TiO_2 nanocrystals supported on graphene-like bamboo charcoal, *Appl. Surf. Sci.* **2015**, *358*, 425–435.

catalysts

Supplementary Materials: The Role of Adsorption in the Photocatalytic Decomposition of Dyes on APTES-Modified TiO_2 Nanomaterials

Ewelina Kusiak-Nejman*, Agnieszka Sienkiewicz, Agnieszka Wanag, Paulina Rokicka-Konieczna and Antoni W. Morawski

Department of Inorganic Chemical Technology and Environment Engineering, Faculty of Chemical Technology and Engineering, West Pomeranian University of Technology in Szczecin, Pułaskiego 10, 70-322 Szczecin, Poland; Agnieszka.Sienkiewicz@zut.edu.pl (A.S.); awanag@zut.edu.pl (A.W.); prokicka@zut.edu.pl (P.R.-K.); amor@zut.edu.pl (A.W.M.)

* Correspondence: ekusiak@zut.edu.pl; Tel: +48 91 449 42 44

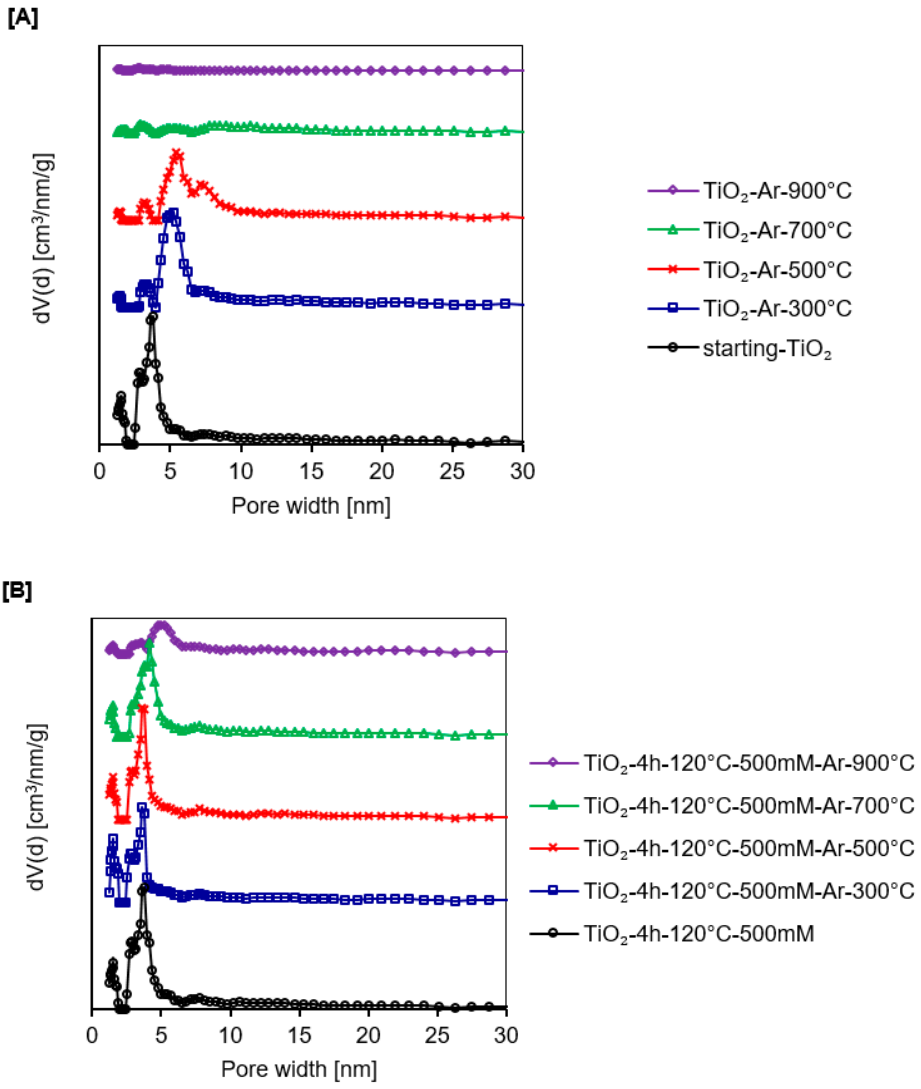

Figure S1. Pore size distribution plots of starting-TiO_2, calcined reference samples (**A**), and APTES-modified TiO_2 photocatalysts (**B**).

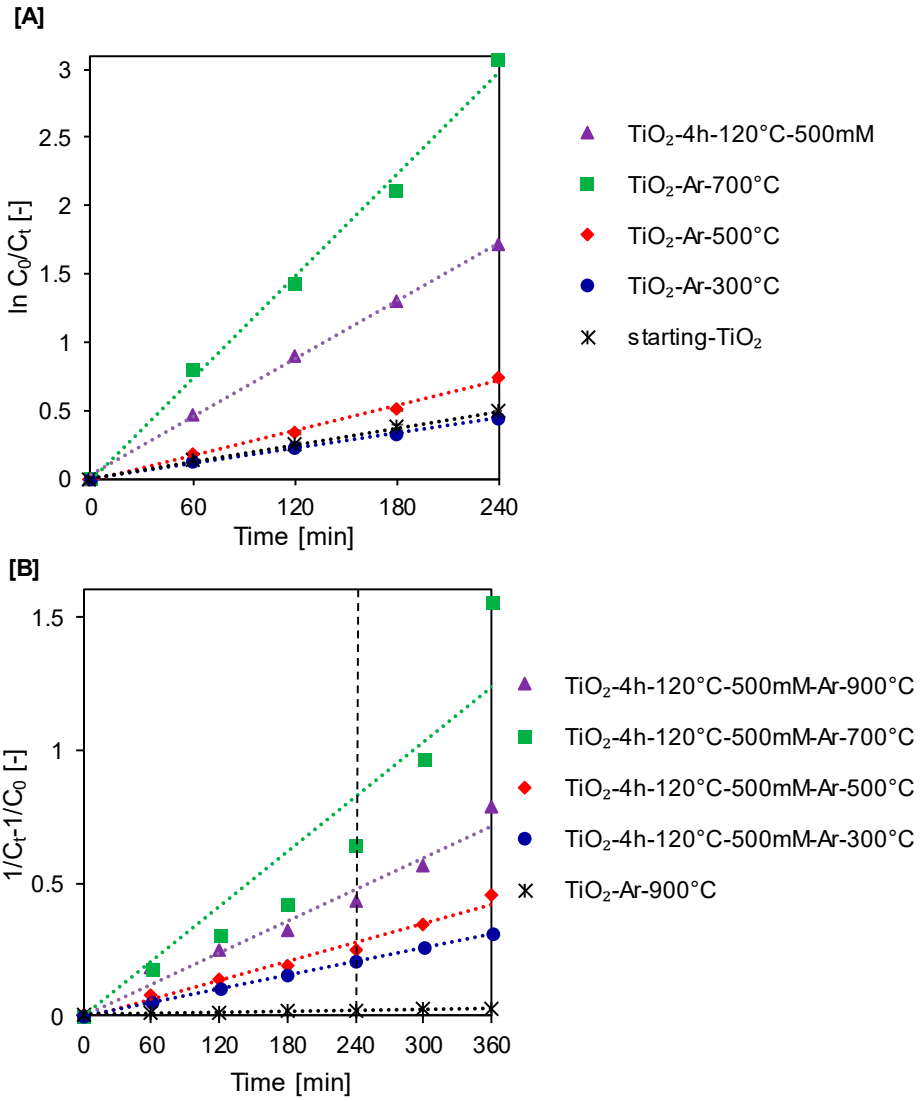

Figure S2. The pseudo-first-order plot (**A**), and the pseudo-second-order plot (**B**) of methylene blue decomposition.

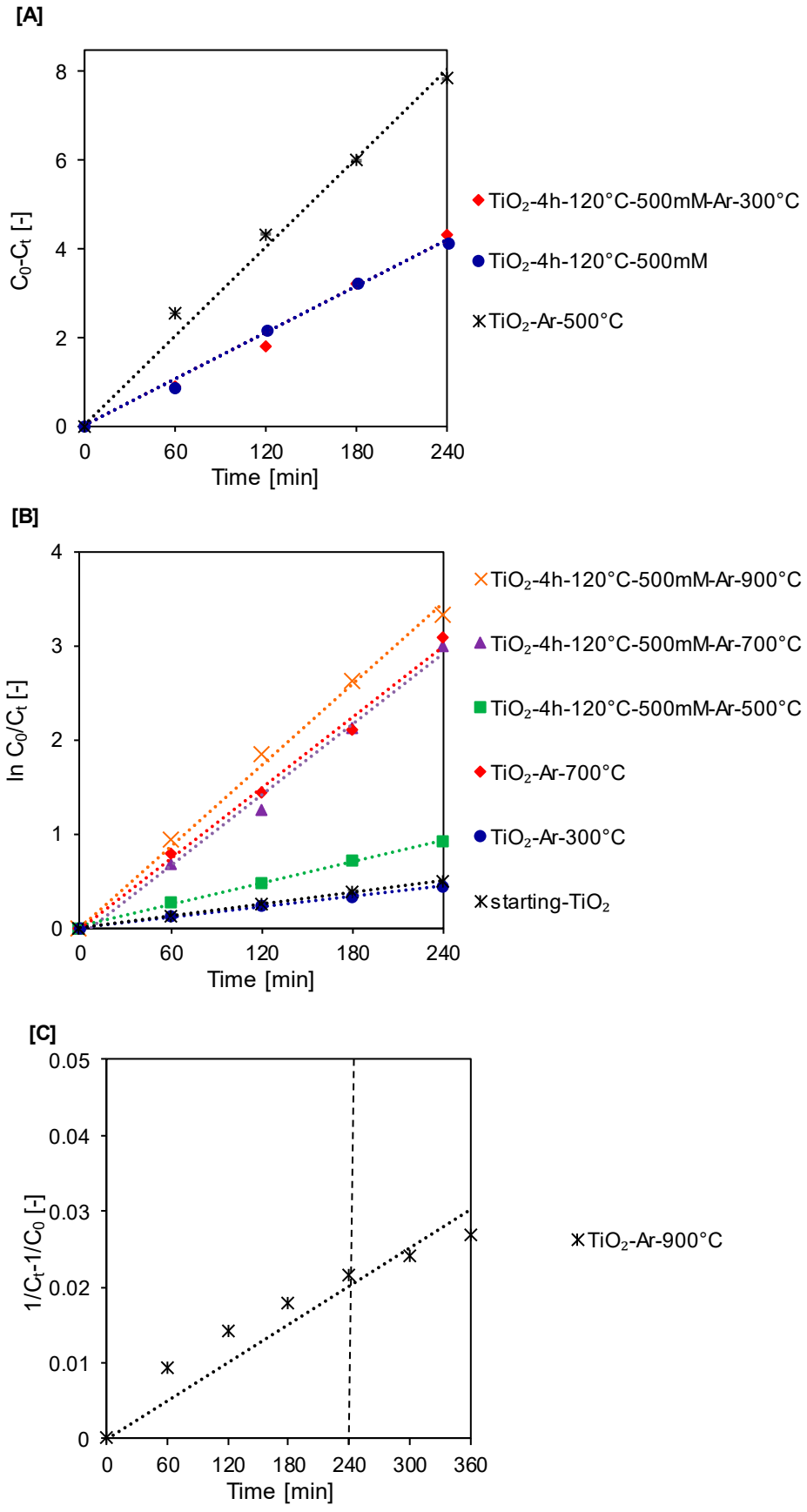

Figure S3. The zero-order plot (**A**), the pseudo-first-order plot (**B**), and the pseudo-second-order plot (**C**) of Orange II decomposition.

Table S1. Isotherm constants for the adsorption process of methylene blue on starting TiO_2, calcined reference samples and APTES-modified photocatalysts.

Sample name	Isotherm models												
	Freundlich			Langmuir			Langmuir-Freundlich				Temkin		
	K_F ((mg/g)·(L/mg)$^{1/n}$)	n	R^2	K_L (L/mg)	q_m (mg/g)	R^2	K_{LF} (L/mg)	q_m (mg/g)	n	R^2	K_T (L/mg)	B	R^2
starting TiO_2	0.12	2.52	0.71	0.42	0.35	0.69	0.00	1.87	0.45	0.71	0.10	0.08	0.71
TiO_2-Ar-300°C	0.13	4.99	0.30	0.93	0.23	0.35	0.93	0.23	1.12	0.35	0.12	0.04	0.32
TiO_2-Ar-500°C	0.12	7.12	0.09	3.93	0.13	0.02	0.10	0.22	4.54	0.76	0.28	0.08	0.50
TiO_2-Ar-700°C	0.33	3.27	0.81	0.64	0.75	0.73	0.001	3.77	0.35	0.81	0.32	0.15	0.79
TiO_2-Ar-900°C	0.67	4.54	0.58	1.00	1.22	0.70	0.87	1.25	1.88	0.88	0.64	0.29	0.78
TiO_2-4h-120°C-500mM	0.29	16.44	0.24	4.33	0.34	0.29	1.48	0.37	2.28	0.24	0.28	0.01	0.73
TiO_2-4h-120°C-500mM-Ar-300°C	0.53	3.67	0.93	0.78	1.10	0.98	0.88	1.01	1.43	0.99	0.50	0.21	0.96
TiO_2-4h-120°C-500mM-Ar-500°C	2.98	3.64	0.91	1.50	5.21	0.99	1.49	5.22	1.00	0.99	3.05	0.93	0.91
TiO_2-4h-120°C-500mM-Ar-700°C	5.17	4.25	0.92	3.56	7.64	0.99	3.11	8.02	0.81	1.00	5.25	1.16	0.97
TiO_2-4h-120°C-500mM-Ar-900°C	6.43	7.04	0.82	19.29	7.92	0.93	24.19	7.61	0.78	0.91	6.70	0.89	0.89

Table S2. Isotherm constants for the adsorption process of Orange II onstarting TiO_2, calcined reference samples and APTES-modified photocatalysts.

Sample name	Isotherm models												
	Freundlich			Langmuir			Langmuir-Freundlich				Temkin		
	K_F ((mg/g)·(L/mg)$^{1/n}$)	n	R^2	K_L (L/mg)	q_m (mg/g)	R^2	K_{LF} (L/mg)	q_m (mg/g)	n	R^2	K_T (L/mg)	B	R^2
starting-TiO_2	0.003	0.31	1.00	0.0002	18.47	0.75	0.027	3.65	3.31	1.00	0.85	1.84	0.70
TiO_2-Ar-300°C	0.08	0.51	0.98	0.0004	18.69	0.95	0.004	19.49	1.97	0.98	0.68	1.86	0.77
TiO_2-Ar-500°C	0.02	0.39	1.00	0.0002	23.70	0.85	0.061	42.87	2.91	1.00	3.67	3.86	0.79
TiO_2-Ar-700°C	0.0006	0.01	0.95	0.0006	9.30	0.01	0.194	0.02	177	0.38	0.01	0.004	0.05
TiO_2-Ar-900°C	0.18	3.85	0.23	1.19	0.34	0.12	0.001	2.62	0.36	0.52	0.19	0.06	0.19
TiO_2-4h-120°C-500mM	0.25	0.66	0.98	0.0006	10.78	0.96	0.003	13.58	1.52	0.98	0.98	1.93	0.83
TiO_2-4h-120°C-500mM-Ar-300°C	1.07	2.38	0.98	0.04	11.85	0.95	0.001	51.13	0.58	0.94	1.16	0.67	0.94
TiO_2-4h-120°C-500mM-Ar-500°C	0.84	3.72	0.99	0.94	1.70	0.90	0.001	7.75	0.32	0.99	0.85	0.31	0.97
TiO_2-4h-120°C-500mM-Ar-700°C	0.67	7.79	0.82	3.32	0.90	0.57	0.001	2.86	0.18	0.81	0.67	0.10	0.79
TiO_2-4h-120°C-500mM-Ar-900°C	0.18	3.85	0.23	1.19	0.34	0.12	0.001	2.62	0.36	0.52	0.19	0.06	0.19

Table S3. The fitting parameters, the pseudo-first and pseudo-second reaction rate constants for methylene blue photoremoval (after 240 min of UV radiation).

Sample name	k_1 (L/min)	R^2	Sample name	k_2 (L/(min·mg))	R^2
TiO_2-Ar-300°C	0.0019	0.99	TiO_2-Ar-900°C	0.0001	0.92
starting TiO_2	0.0021	0.99	TiO_2-4h-120°C-500mM-Ar-300°C	0.0009	0.99
TiO_2-Ar-500°C	0.0030	0.99	TiO_2-4h-120°C-500mM-Ar-500°C	0.0011	0.99
TiO_2-4h-120°C-500mM	0.0072	0.99	TiO_2-4h-120°C-500mM-Ar-900°C	0.0019	0.94
TiO_2-Ar-700°C	0.0124	0.99	TiO_2-4h-120°C-500mM-Ar-700°C	0.0025	0.99

Table S4. The fitting parameters, zero, pseudo-first, and pseudo-second reaction rate constants for Orange II photoremoval (after 240 min of UV radiation).

Sample name	k_0 (mg/(L·min))	R^2	Sample name	k_1 (1/min)	R^2	Sample name	k_2 (L/(min·mg))	R^2
TiO_2-4h-120 °C-500mM	0.0171	0.99	TiO_2-Ar-300 °C	0.0019	0.99	TiO_2-Ar-900 °C	0.0001	0.92
TiO_2-4h-120 °C-500mM-Ar-300 °C	0.0175	0.99	starting-TiO_2	0.0021	0.99			
TiO_2-Ar-500 °C	0.0337	0.99	TiO_2-4h-120 °C-500mM-Ar-500 °C	0.0039	0.99			
			TiO_2-4h-120 °C-500mM-Ar-700 °C	0.0114	0.99			
			TiO_2-Ar-700 °C	0.0124	0.99			
			TiO_2-4h-120 °C-500mM-Ar-900 °C	0.0143	0.99			

catalysts

MDPI

Journal of Environmental Chemical Engineering 9 (2021) 104794

Contents lists available at ScienceDirect

Journal of Environmental Chemical Engineering

journal homepage: www.elsevier.com/locate/jece

Effect of calcination on the photocatalytic activity and stability of TiO_2 photocatalysts modified with APTES

Agnieszka Sienkiewicz, Agnieszka Wanag *, Ewelina Kusiak-Nejman, Ewa Ekiert, Paulina Rokicka-Konieczna, Antoni W. Morawski

West Pomeranian University of Technology in Szczecin, Faculty of Chemical Technology and Engineering, Department of Inorganic Chemical Technology and Environment Engineering, Pułaskiego 10, 70-322 Szczecin, Poland

ARTICLE INFO

Editor: Zhang Xiwang

Keywords:
Titanium dioxide
3-Aminopropyltriethoxysilane
Methylene blue decomposition
Reusability test

ABSTRACT

In this article, the influence of calcination temperature on the photocatalytic properties and stability of titanium dioxide modified with 3-aminopropyltriethoxysilane (APTES) was presented. The new APTES-functionalized TiO_2 nanomaterials were obtained by solvothermal process and thermal modification in the argon atmosphere. The obtained photocatalysts were characterized via various techniques including diffuse reflectance spectroscopy (UV–vis/DRS), X-ray diffraction (XRD), Fourier transform infrared (FT-IR/DRS), SEM, BET surface area measurement and zeta potential analyses. Modification with APTES suppressed phase transformation and the growth of crystallite size of anatase and rutile during heating. The crystallites size of anatase was in the range of 14–52 nm for heat-treated starting-TiO_2 and 14–31 nm for APTES-modified TiO_2. Calcination process influenced the surface characteristics i.e. zeta potential of APTES-modified TiO_2 nanomaterials. The photocatalytic activity of obtained samples was investigated during the decomposition of methylene blue using as a model water contaminant under UV light irradiation. Thermal modification in the argon atmosphere significantly enhanced adsorption properties and photocatalytic activity of obtained nanomaterials. Furthermore, calcination up to 700 °C improved photocatalytic stability of the examined photocatalysts. It is also worth mentioning that APTES modification significantly improved photocatalytic performance of nanomaterials calcined at 900 °C. In this case the decomposition degree of TiO_2-4h-180 °C-2000 mM-Ar-900 °C in comparison to TiO_2-Ar-900 °C increased by 50 %.

1. Introduction

Over the past few decades, economic and social development has been accelerating significantly. The increasing demand leads to the faster expansion of industry and the creation of more factories. Wastewaters from different industries, laboratories and factories, are harmful to the general well-being of people and the environmental condition. The effluents containing different dyes are toxic not only to microorganisms but also for human and aquatic life. Nowadays, this harmful influence of chemicals on earth ecosystems is the cause of serious concerns [1]. For that reason, the degradation of dyes in industrial wastewaters has received increasing attention. Traditional physical methods, e.g. adsorption, coagulation, reverse osmosis and ultrafiltration, have been used for the removal of dye pollutants [1,2]. Unfortunately, most of these methods generate a lot of sludge constituting a major problem with their utilization. The solution would be to use photocatalysis in the removal of dyes from wastewaters, due to the capability of this process to mineralize the target pollutants completely [1]. Titanium dioxide is the most widely used photocatalyst due to its low toxicity, chemical stability, relatively high oxidation efficiency and low cost [3]. Unfortunately, TiO_2 also has some disadvantages, for instance, the presence of a large band gap (3.2 eV) and substantial recombination of photogenerated hole-electron pairs reduces general photocatalytic efficiency of the semiconductor [4]. Therefore, to improve its photocatalytic activity and physicochemical properties, many solutions have been intensively studied such as non-metal or metal ions doping, dye sensitization or semiconductor coupling. Lately, much attention has been paid to TiO_2 co-doping [5–7]. One of the new approaches involves using organic silane coupling agents for modifying TiO_2 surface. For this purpose, alkoxysilane compounds, such as 3-aminopropyltriethoxysilane (APTES) are used. APTES consists of two functional groups ethoxy and aminopropyl that are attached to the central silicon atom.

* Corresponding author.
E-mail addresses: awanag@zut.edu.pl, agnieszka.wanag@zut.edu.pl (A. Wanag).

https://doi.org/10.1016/j.jece.2020.104794
Received 19 August 2020; Received in revised form 16 October 2020; Accepted 16 November 2020
Available online 26 November 2020

Alkylsilanes such as APTES are well known from self-organization at the surface of oxide materials [8–11]. Despite the growing interest in APTES-modified TiO_2 nanomaterials, no general agreement exists on the possible mechanism of the formation of a covalent linkage between the anchoring group of APTES and TiO_2 surface. Meroni et al. [9] suggested that chemisorption of APTES on TiO_2 surface mostly implies one or two Si-O-Ti bonds involving the silicon headgroup. The tripod configurations, due to the high strained seems infeasible. Different interactions, for instance, physisorption via terminal amino groups are expected to be significantly more unstable. Nevertheless, dimerization of the silane at the surface via Si-O-Si bonds is feasible. However, further polymerization appears to be not so much possible. Generally, APTES-modified TiO_2 surface liked as Si-N co-doped TiO_2. Thus, the advantage of using APTES is that it is possible to create a partial monolayer of N- and Si doped titanium dioxide which can increase the adsorption and degradation of methylene blue during the photocatalysis process [12].

In order to improve the photocatalytic activity and physicochemical properties of TiO_2-based nanomaterials bestides doping, the calcination process is also commonly used. The literature on the study of the effect of the calcination process on photocatalytic and physicochemical properties of APTES-functionalized TiO_2 nanomaterials is very limited. Dalod et al. [13] proposed a new method of in situ aqueous hydrothermal synthesis of TiO_2 materials using different silane coupling agents such as APTES, DTES and AEAPS as a modifiers, where photocatalysts were calcined at 700 °C in synthetic air. They noted that, due to the formation of an amorphous SiO_2 layer, the increase in the crystallites size and the effect of inhibition of the phase transformation during the calcination.

The novelty of the presented research was to determine the influence of the calcination temperature on photocatalytic properties and stability of APTES-modified TiO_2 nanomaterials obtained in the argon atmosphere. To the best of our knowledge, this is the first paper presenting the results of the influence of calcination temperature on photocatalytic and physicochemical properties of APTES-functionalized TiO_2 nanomaterials prepared in an inert gas atmosphere

2. Experimental

2.1. Materials and reagents

Raw TiO_2 slurry containing post-production residues of sulphuric acid, produced with the use of the sulphate technology by chemical plant Grupa Azoty Zakłady Chemiczne "Police" S.A. (Poland), was used as a TiO_2 source. Prior to modification, a crude TiO_2 pulp was rinsed with an aqueous solution of ammonia water (25 % pure p.a., Firma Chempur®, Poland), in order to remove the residues of sulphuric compounds by creating $(NH_4)_2SO_4$ easily dissolved in water. The suspension was then rinsed with distilled water to pH = 6.8 [14]. The obtained material was named as starting-TiO_2. 3-aminopropyltriethoxysilane (APTES) ($C_9H_{23}NO_3Si$, purity ≥98 %, 221.37 g/mol, Merck KGaA, Germany) was used as a modifier. Ethanol (purity 96 % from P.P.H. "STANLAB" Sp.J., Poland) was used as a solvent of APTES. Methylene blue ($C_{16}H_{18}ClN_3S$, purity min 82 %, 319.86 g/mol, Firma Chempur®, Poland) was used as an organic dye during photocatalytic decomposition tests.

2.2. Surface modification of titanium dioxide

In these studies, the new nanomaterials were obtained from TiO_2 and APTES by the solvothermal process and calcination. Firstly, 5 g of starting-TiO_2 powder was dispersed in 25 mL of APTES solution, the concentration of APTES in ethanol was 2000 mM and then modified in a pressure autoclave for 4 h at 180 °C ensuring continuous stirring at 500 rpm. Next, to remove any remaining chemicals, the received slurry was rinsed with ethanol and distilled water. After that, the material was dried for 24 h at 105 °C in a muffle furnace. Finally, the sample was subjected to thermal modification in an argon atmosphere (purity 5.0, Messer Polska Sp. z o.o., Poland). The obtained photocatalyst placed in a quartz crucible was put inside a quartz tube in a middle part of the GHC 12/900 horizontal furnace (Carbolite Gero, Ltd., UK). The calcination of nanomaterials was carried out in the range of 300 °C–900 °C (Δt = 200 °C). First, the argon was passed through the quartz tube for 30 min to remove all present air. Secondly, the furnace was heated up to the programmed temperature in the argon flow of 180 mL/min. Then, the nanomaterial was calcined at a set temperature in argon flow for 4 h. After all of that, the furnace was slowly cooled to the room temperature in the argon atmosphere. Photocatalysts obtained after the calcination of starting-TiO_2 in the argon atmosphere were named as a reference sample.

2.3. Characterization

The XRD analysis (Malvern PANalytical Ltd., Netherlands) using Cu Kα radiation (λ = 1.54056 Å) was used for identifying the crystalline structure of received nanomaterials. The PDF-4 + 2014 International Centre for Diffraction Data database (04-002-8296 PDF4+ card for anatase and 04-005-5923 PDF4+ card for rutile) was used for identification of the phase composition. The mean crystallite sizes of the photocatalysts were calculated according to Scherrer's equation. The light abilities of the new nanomaterials were examined on a V-650 UV–vis spectrophotometer (JASCO International Co., Japan) equipped with a PIV-756 integrating sphere accessory for examining DR spectra (JASCO International Co., Japan). Spectralon (Spectralon® Diffuse Reflectance Material) was used as the standard sample. The band gap energy was calculated by plotting $[F(R)h\upsilon]^{1/2}$ as a function of photon energy (hυ), taking into account the linear portion of the basic absorption edge of the UV–vis spectra and then extrapolating the straight parts of these relations to $[F(R)h\upsilon]^{1/2} = 0$ [15]. The Brunauer-Emmett-Teller (BET) surface area and pore volume of photocatalysts were calculated from the nitrogen adsorption-desorption measurements at 77 K carried out in QUADRASORB evo™ Gas Sorption analyzer (Anton Paar GmbH, Austria). Before the measurements, in order to pre-clean the surface of tested samples all materials were degassed at 100 °C for 12 h under high vacuum. To identify the surface functional groups of the APTES-functionalized TiO_2 and to observe the surface changes during reusability test, the FT-IR/DRS analysis was recorded on FT-IR-4200 spectrometer (JASCO International Co. Ltd., Japan) equipped with DiffuseIR accessory (PIKE Technologies, USA). The FT-IR spectra were collected in the range of 4000–400 cm^{-1} with a resolution of 4.0 cm^{-1}, by averaging 100 scans. ZetaSizer NanoSeries ZS (Malvern Panalytical Ltd., UK) was used to determine the zeta potential values. The surface morphology of the obtained photocatalysts was analyzed using a Hitachi SU8020 Ultra-High Resolution Field Emission Scanning Electron Microscope (Hitachi Ltd., Japan). The pseudo-first reaction rate constant was determined based on the Langmuir-Hinshelwood pseudo-first order model, described by [16,17]:

$$\ln\left(C_0/C_t\right) = kKt = k_1 t \tag{1}$$

While the pseudo-second reaction rate constant was established based on the pseudo-second order model, described by [18,19]:

$$1/C_t - C/C_0 = k_2 t \tag{2}$$

where C_0 is the initial concentration of dye (mg/L), C_t is the concentration of the methylene blue at time t (mg/L), k_1 and k_2 are the pseudo-first and the pseudo-second reaction rate constants [1/min, L/(min mg)], t is the time of illumination (min) and K is the adsorption coefficient of the reactant (L/mg).

2.4. Measurement of photocatalytic activity

2.4.1. Photocatalytic activity test

In order to determine the photocatalytic properties of APTES-modified TiO_2 nanomaterials, the degradation process of the

methylene blue under the UV–vis light, provided by a set of 6 lamps with the power of 20 W each (Philips, Netherlands) with the radiation intensity of 110 W/m^2 UV and 5 W/m^2 Vis, was carried out. Due to the low Vis irradiation intensity used type of radiation was named as UV light. The experiments were carried out in a 0.6 L glass beaker containing 0.5 L of methylene blue solution. The concentration of photocatalyst was 0.5 g/L and the initial concentration of dye was 15 mg/L. Before irradiation, the prepared suspension was stirred on a magnetic stirrer under light-free conditions for 30, 60, 90 or 180 min, to ensure the establishment of the adsorption-desorption equilibrium between the dye and semiconductor surface. Then, the suspension was exposed to UV light irradiation. During the photocatalytic activity test, the concentration of the methylene blue was measured every 60 min by means of the V-630 UV–vis spectrometer (Jasco International Co., Japan). 10 mL of withdrawn suspension was centrifuged in order to remove suspended TiO_2 nanoparticles before each measurement. The degradation degree of MB was calculated as follows:

$$\eta = (C_0 - C_t)/C_0 \times 100\ \% \quad (3)$$

where η is the depcgradation degree of MB, C_0 is the initial concentration of the non-degraded MB solution, and C_t is the concentration of the MB solution after illumination for t min.

2.4.2. Reusability test

The reusability test of the selected photocatalyst was examined based on the decomposition of methylene blue under UV light after 360 min of irradiation. After each cycle, the sample was separated by filtration and dried at 100 °C for 12 h and next added to a new portion of the dye solution.

3. Results and discussion

3.1. Characterization of the photocatalysts

3.1.1. FT-IR/DRS measurements

The FT-IR/DR spectra of starting-TiO_2, reference samples and APTES-modified TiO_2 were presented in Fig. 1A and B, respectively. All spectra showed some peaks typical for TiO_2-based nanomaterials. A wide band in the region of 3700–2500 cm^{-1} is assigned to —OH stretching vibrations [20] and the narrow band at around 1620 cm^{-1} is associated with the molecular water bending mode [21]. The increase of the calcination temperature of APTES-modified TiO_2 samples (see Fig. 1B) causes the reduction of the intensity of these two above mentioned bands, due to the changes in the content of hydroxyl groups on the semiconductor surface [22,23]. A strong band at 950 cm^{-1} attributed to the self-absorption of titania also characterizes all samples [18,19]. The starting-TiO_2 calcined from 500 °C showed the weak band at 3690 cm^{-1} characteristic for stretching mode of different types of free hydroxyl groups, which generated by condensation of water and silanol groups present in the APTES molecule [24–26]. The comparison of starting-TiO_2 and TiO_2-4h-180 °C-2000 mM spectra showed some new characteristic bands coming from APTES, which indicated that the modification of TiO_2 surface was carried out successfully. According to Razmjou et al. [27] bands around 2900 cm^{-1} and 2882 cm^{-1} are ascribed to the alkyl groups [$(CH_2)_n$]. The low-intensity band around 1600 cm^{-1} is assigned to the –NH bending vibrations of primary amine [27,28]. One more slight-intensity band, located at 1360 cm^{-1}, indicated the presence of C—N bonds [9,29]. The bands showed in the region of 960–910 cm^{-1} are assigned to the stretching vibrations of Ti-O-Si bonds [28]. Furthermore, the band located at 920 cm^{-1} indicated that the reaction of condensation between silanol and —OH groups on TiO_2 surface took place [28]. All five latest mentioned band characteristic for APTES were not observed above the temperature 300 °C. The stretching mode of Si-O-Si bonds was noted at around 1160 cm^{-1}. These bands are related to the reaction of condensation between silanol groups [9,30]. Besides,

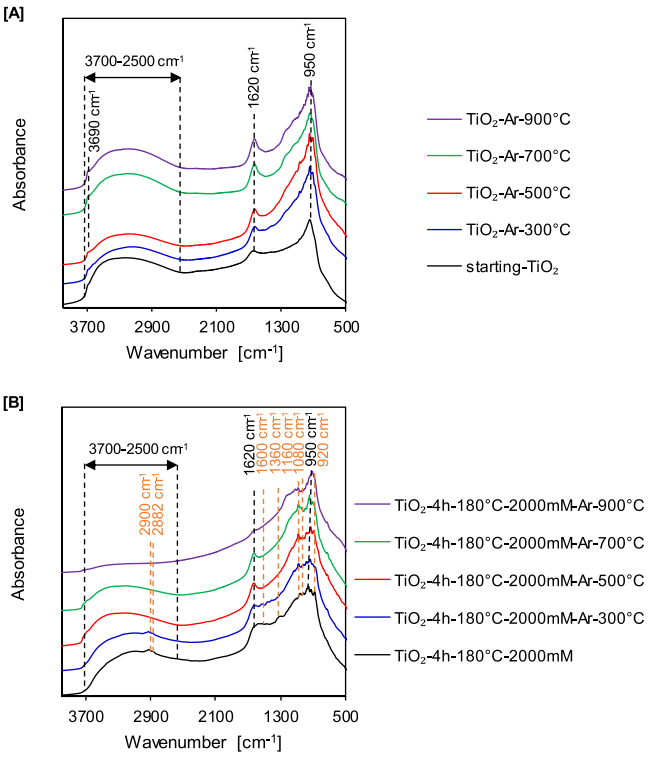

Fig. 1. FT-IR/DR spectra of starting-TiO_2 and reference samples [A] and APTES-modified TiO_2 prior and after heat treatment [B].

the Si-O-C stretching modes were also observed at around 1080 cm^{-1} [9].

3.1.2. X-ray diffraction analysis

In Fig. 2A and B, XRD diffraction patterns of the starting-TiO_2, reference samples calcined in an argon atmosphere and APTES-functionalized TiO_2 were presented. According to the data presented in Table 1, almost all analyzed samples showed reflections characteristic for anatase phase located at 25.3, 37.8, 48.1, 53.9, 55.1, 62.7, 68.9, 70.3 and 75.1°, which correspond to (101), (004), (200), (105), (211), (204), (116), (220), (215) (JCPDS 01-070-7348) and some characteristic reflections for rutile phase located at 27.4, 36.0 and 41.2°, corresponding to (110), (101) and (111) respectively. Merely one tested TiO_2-Ar-900 °C sample had reflections characteristic for rutile phase (JCPDS 01-076-0318): (110), (101), (200), (111), (210), (211), (220), (002), (310), (301), (112) located at 27.4, 36.0, 39.1, 41.2, 44.0, 54.3, 56.6, 62.7, 64.0, 69.0 and 69.7°, respectively. The anatase phase starts transforming into the rutile phase when the temperature is above 600 °C [31]. In this case, the starting-TiO_2 was completely transformed into rutile at 900 °C. Based on the phase composition and the crystallites size data presented in Table 2, it is remarkable to note that after calcination at 900 °C the TiO_2-4h-180 °C-2000 mM-Ar-900 °C sample still contained 93 % of anatase. The amount of anatase phase in APTES/TiO_2 nanomaterials was quite constant, and its share is about 96 % at 300 °C. Modification via APTES, which is the source of silicon, caused that the transformation of anatase to rutile phase during the thermal modification was effectively suppressed [32,33]. The crystallites size of anatase was in the range of 14–52 nm for heat-treated starting-TiO_2 and 14–31 nm for APTES-modified TiO_2. The crystallites size of rutile was from 21 to >100 nm for heat-treated starting-TiO_2 and 33–68 nm for APTES-functionalized TiO_2. For all examined nanomaterials, the crystallites size increased with the increase of the modification temperature. However, comparing the crystallites size of samples with and without APTES modification, the crystallite size of the anatase and rutile was smaller for APTES-modified samples than that of materials without

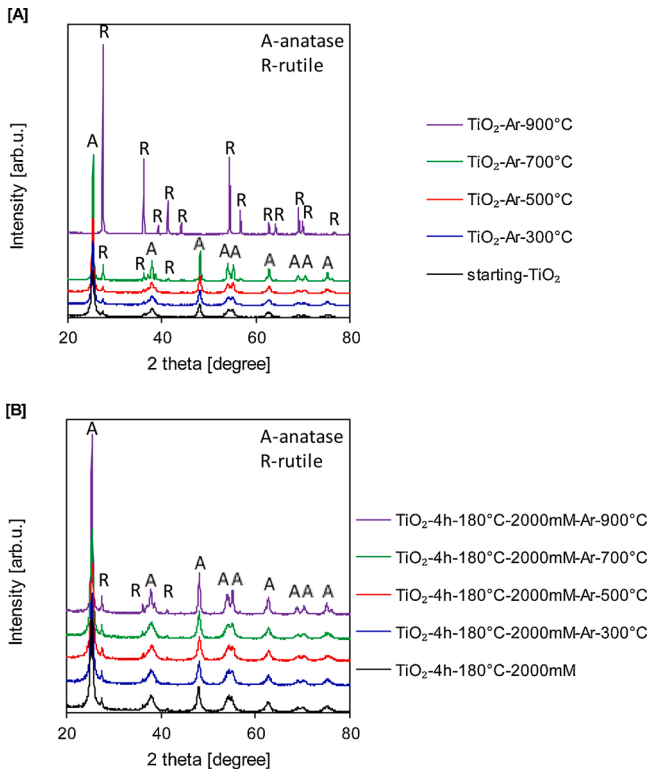

Fig. 2. XRD patterns of starting-TiO_2 and reference samples [A] and APTES-modified TiO_2 prior and after heat treatment [B].

Table 1
Position of the diffraction peaks on the XRD patterns and Miller indices of the anatase and rutile phase.

Anatase phase		Rutile phase	
2 theta [degree]	Miller indices	2 theta [degree]	Miller indices
25.3	(101)	27.4	(110)
37.8	(004)	36.0	(101)
48.1	(200)	39.1	(200)
53.9	(105)	41.2	(111)
55.1	(211)	44.0	(210)
62.7	(204)	54.3	(211)
68.9	(116)	56.6	(220)
70.3	(220)	62.7	(002)
75.1	(215)	64.0	(310)
		69.0	(301)
		69.7	(112)

APTES. For example, the anatase crystallite size for TiO_2-Ar-700 °C equalled 52 nm, while for TiO_2-4h-180 °C-2000 mM-Ar-700 °C sample was only 16 nm. According to Xu et al. [34] silicon can effectively prevent the growth of titania grains over thermal modification. Moreover, based on the results presented by Dalod et al. [13], the use of such stabilizers as APTES for TiO_2 modification can result in the formation of an amorphous SiO_2 layer on the surface, originating from the silane-coupling agents, and leading to TiO_2-SiO_2 core-shell nanoparticles. Thus, during the calcination process both the increase in the crystallites size and phase transformation can be effectively inhibited.

3.1.3. BET analysis

Based on the adsorption-desorption isotherms of starting-TiO_2 and reference samples (Fig. 3A) and APTES-modified TiO_2 (Fig. 3B), two types of isotherms can be observed. According to IUPAC classification, most of the photocatalysts demonstrated a type IV of isotherm, characteristic for mesoporous materials [35]. Only TiO_2-Ar-900 °C sample demonstrated type II of isotherm characteristic for non-porous materials. Except for this sample, all nanomaterials also showed the same H3 type of the hysteresis loops, which is characterized by the presence of typical desorption shoulders and lower closure points, also does not have a plateau at high p/p_0 range [36,37]. The isotherm of TiO_2-Ar-700 °C sample exhibited the narrow and limited type H4 of hysteresis loop, which indicated the existence of a small slit mesopores in the material [38]. For TiO_2-Ar-900 °C material the hysteresis loop has not appeared. It is worth noting that the size of the hysteresis loops, exhibited in Fig. 3A, decreased with the increasing temperature of modification, which was associated with the decreasing amount of mesopores in the material [39].

Based on the data presented in the Table 2, most of the examined photocatalysts were mesoporous materials with the small amount of the micropores. Only TiO_2-Ar-900 °C sample turned out to be non-porous material. The specific surface area and total pore volume (see Table 2) of starting-TiO_2 photocatalyst significantly decreased after TiO_2 modification with 2000 mM of APTES. For starting-TiO_2 the S_{BET} was 207 m^2/g, and V_{total} equalled 0.37 cm^3/g, while for TiO_2-4h-180 °C-2000 mM was 125 m^2/g, and V_{total} equalled 0.174 cm^3/g. Other researcher also obtained similar results. Siwińska-Stefańska et al. [40] observed that the specific surface area and total pore volume decreased after TiO_2 modification via different alkoxysilanes compounds. They noted that, modification with 3-methacryloxypropyltrimethoxysilane, vinyltrimethoxysilane and n-2-(aminoethyl)-3-aminopropyltrimethoxysilane, caused decrease of the S_{BET} of the unmodified sample from 10 m^2/g to 7.1 m^2/g, 7.4 m^2/g and 4.9 m^2/g, respectively. Whereas, V_{total} reduced from 0.020 cm^3/g for untreated TiO_2 to 0.005 cm^3/g and 0.004 cm^3/g, respectively. Most probably this was due to the active centers on the surface of TiO_2 and TiO_2-SiO_2 were blocked by modifier particles. Zhuang et al. [41] also noted that APTES molecules could penetrate the TiO_2 pores causing the decrease of both the S_{BET} and V_{total}. After heat treating of APTES-modified TiO_2 photocatalysts, the S_{BET} increased from 125 m^2/g to 170 m^2/g at 500 °C, and decreased with increasing temperature to 140 m^2/g at 700 °C and subsequent to 45 m^2/g at 900 °C. The increase of the specific surface area at low modification temperatures was associated with the decomposition of APTES molecules. Decreasing and ultimately-disappearing peaks with the increasing temperature of modification characteristic for APTES on the FT-IR/DR spectra, shown in Fig. 1B, indicate that the surface of nanomaterials was unblocked. The total pore volume also increased from 0.174 cm^3/g to 0.306 cm^3/g after heat treatment at 300 °C, which indicates that APTES molecules unblock not only external surface of TiO_2 but also pores. The decrease of the specific surface area and total pore volume above 500 °C was associated with an increase of the crystallites size of the anatase and rutile (see Table 2). The specific surface area and total pore volume of the reference samples decreased with the increasing calcination temperature. The S_{BET} and V_{total} were found to change from 112 m^2/g and 0.288 cm^3/g for TiO_2-Ar-300 °C to 3 m^2/g and 0.008 cm^3/g for TiO_2-Ar-900 °C, which can be explained by the higher amount of rutile and the increase of crystallite size of anatase and rutile enhancing the degree of crystallites agglomeration during the calcination [42–44].

3.1.4. UV–vis diffuse absorbance spectroscopy

The UV–vis/DR spectra of starting-TiO_2, reference samples and APTES-modified TiO_2 were presented in Fig. 4A and B, respectively. It was observed that the starting-TiO_2 did not show absorption in the visible region but show the characteristic absorption in the ultraviolet region, due to intrinsic band gap absorption of titania [45]. The negligible effect of calcination on the absorption abilities was found for most reference samples. Significant changes in band gap energy were observed only for reference samples calcined at 700 °C and 900 °C. The band gap energy for these photocatalysts was 3.07 eV and 3.03 eV, respectively. The decrease in band gap energy was mostly attributed to the partial transformation of the anatase to rutile at 700 °C and the complete formation of the rutile phase at 900 °C [46]. It was also found that for all APTES-modified TiO_2

Table 2
XRD phase composition, average crystallites size, specific surface area, pore volume distribution of starting-TiO_2, reference samples and APTES-modified photocatalysts prior and after heat treatment.

Sample name	Anatase in crystallite phase [%]	Anatase crystallite size [nm]	Rutile in crystallite phase [%]	Rutile crystallite size [nm]	S_{BET} [m^2/g]	V_{total} [a] [cm^3/g]	V_{micro} [b] [cm^3/g]	V_{meso} [c] [cm^3/g]
starting-TiO_2	95	14	5	21	207	0.370	0.070	0.300
TiO_2-Ar-300 °C	96	18	4	51	112	0.288	0.041	0.247
TiO_2-Ar-500 °C	95	22	5	41	75	0.223	0.030	0.193
TiO_2-Ar-700 °C	88	52	12	>100	16	0.089	0.007	0.082
TiO_2-Ar-900 °C	–	–	100	>100	3	0.008	0.002	0.006
TiO_2-4h-180 °C-2000 mM	95	14	5	38	125	0.174	0.049	0.125
TiO_2-4h-180 °C -2000 mM-Ar-300 °C	96	15	4	39	154	0.306	0.060	0.246
TiO_2-4h-180 °C -2000 mM-Ar-500 °C	96	15	4	38	170	0.275	0.066	0.209
TiO_2-4h-180 °C -2000 mM-Ar-700 °C	96	16	4	89	140	0.234	0.054	0.180
TiO_2-4h-180 °C -2000 mM-Ar-900 °C	93	31	7	68	45	0.124	0.018	0.106

[a] Total pore volume determined by the single point from the nitrogen adsorption isotherms at relative pressure $p/p_0 = 0.99$.
[b] Micropore volume estimated using the Dubinin–Radushkevich method.
[c] Mesopore volume determined as the difference between V_{total} and V_{micro}.

after thermal modification in the argon atmosphere the intensity of reflectance in the visible region decreased with the increase of heat treatment temperature. These results were feasible to observe due to the color changes from white for TiO_2-4h-180 °C-2000 mM through greyish for TiO_2-4h-180 °C-2000 mM-Ar-500 °C, to dark grey for TiO_2-4h-180 °C-2000 mM-Ar-900 °C samples [47].

3.1.5. Zeta potential analysis

According to data presented in Table 3, the zeta potential of APTES-modified TiO_2 nanomaterials changed from +17.88 mV for TiO_2-4h-180 °C-2000 mM to -36.25 mV for TiO_2-4h-180 °C-2000 mM-Ar-900 °C. Rokicka-Konieczna et al. [48] and Ukaji et al. [27] found that the cationic amino groups from APTES can easily link to TiO_2 surface, whereby, the surface charge of the materials become positive. After calcination above 300 °C, the positively charged amino groups were not observed on the TiO_2 surface, which was confirmed by FT-IR/DRS measurements (see Fig. 1B). Mainly the silicon groups were observed on the surface of the examined samples. Ferreira-Neto et al. [49] and Huang et al. [50] proved that the silica-modified TiO_2 photocatalysts exhibit negative values of zeta potential. Therefore, the zeta potential of the APTES-modified TiO_2 obtained after calcination process changed from positive to negative.

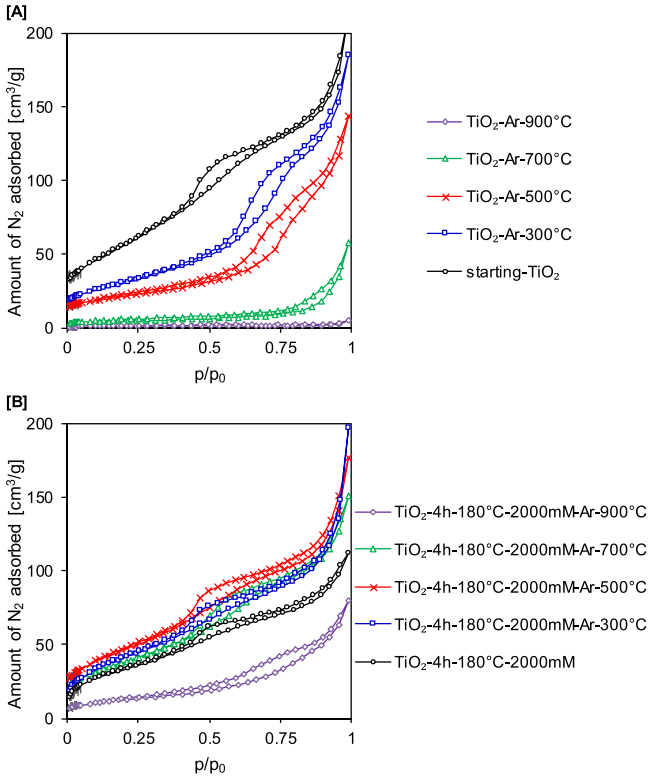

Fig. 3. Adsorption-desorption isotherms of starting-TiO_2 and reference samples [A] and APTES-modified TiO_2 prior and after heat treatment [B].

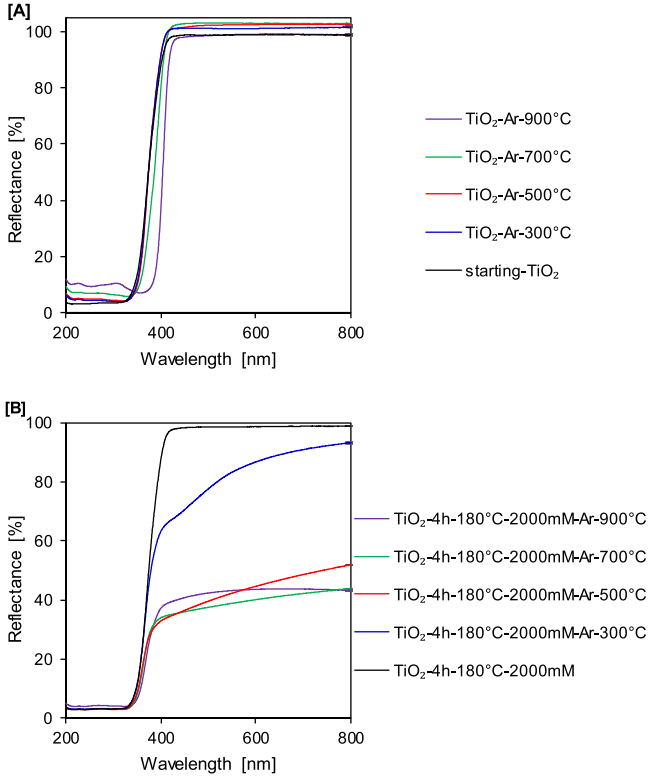

Fig. 4. UV–vis/DR spectra of starting-TiO_2 and reference samples [A] and APTES-modified TiO_2 prior and after heat treatment [B].

Table 3
The band gap energy and zeta potential values of starting-TiO_2, reference samples and APTES-modified photocatalysts prior and after heat treatment.

Sample name	E_g [eV]	pH	Zeta potential δ [mV]
starting-TiO_2	3.29	4.3	+12.80
TiO_2-Ar-300 °C	3.29	4.1	+14.08
TiO_2-Ar-500 °C	3.29	4.4	+15.01
TiO_2-Ar-700 °C	3.07	4.6	+16.50
TiO_2-Ar-900 °C	3.03	4.9	−30.25
TiO_2-4h-180 °C-2000 mM	3.31	7.4	+17.88
TiO_2-4h-180 °C-2000 mM-Ar-300 °C	3.32	5.5	+19.92
TiO_2-4h-180 °C-2000 mM-Ar-500 °C	3.29	4.7	−12.40
TiO_2-4h-180 °C-2000 mM-Ar-700 °C	3.27	4.1	−22.58
TiO_2-4h-180 °C-2000 mM-Ar-900 °C	3.22	4.3	−36.25

3.1.6. SEM images-analysis

The SEM images of starting-TiO_2, TiO_2-4h-180 °C-2000 mM and TiO_2-4h-180 °C-2000 mM-Ar-500 °C samples were presented in Fig. 5A, B and C, respectively. It was observed that the morphology of the starting-TiO_2 photocatalyst was homogeneous. However, with formed aggregates. After APTES modification (see Fig. 5B) and calcination in the Ar atmosphere (see Fig. 5C), the particles of photocatalysts were also characterized by unspecified and irregular shape. However, it was noted that after modification, the size of the aggregates of TiO_2-4h-180 °C-2000 mM and TiO_2-4h-180 °C-2000 mM-Ar-500 °C materials increased. In Fig. 6, the elemental composition of the TiO_2-4h-180 °C-2000 mM-Ar-500 °C photocatalyst, confirmed by EDX mapping analysis with the element stratification and distribution diagram of examined appropriate element, was presented. The images exhibited that the tested sample contained Ti, O and Si elements. Furthermore, all elements were homogeneously dispersed throughout the examined surface.

3.2. Adsorption test

Prior the photocatalytic activity test, studies were carried out to determine the adsorption-desorption equilibrium at the interface between semiconductor and colorful contaminant. The adsorption degree of methylene blue in the darkness for different nanomaterials were showed in Fig. 7A and B. The adsorption-desorption equilibrium established after 60 min for starting-TiO_2 and after 180 min for reference samples. For APTES-modified samples, the equilibrium was generally reached after 30 min. In the case of TiO_2-4h-180 °C-2000 mM-Ar-700 °C sample, a slight MB desorption (approx. 5%) was noted, before the adsorption-desorption equilibrium established after 150 min. Different adsorption-desorption equilibrium time is related to surface characteristics of individual photocatalyst (see Table 3). For starting-TiO_2, all reference samples, TiO_2-4h-180 °C-2000 mM and TiO_2-4h-180 °C-2000 mM-Ar-300 °C the adsorption of the methylene blue reached 5 %. In the case of APTES-modified TiO_2 the heat treatment process above the temperature of 300 °C resulted in the improvement of adsorption properties. It is commonly known that the negatively charged surface of the nanomaterial has a higher potential of contact with the positively charged molecules such as methylene blue [51–53]. Therefore, according to the zeta potential values presented in Table 3, the change in TiO_2 surface charge after thermal modification improved the adsorption properties of the APTES-functionalized TiO_2. While, for samples with a positively charged surface, low adsorption capacity of cationic dye was noted [54,55]. Nanomaterials calcined at 900 °C showed different adsorption degree of the methylene blue, even though they exhibited nearly the same zeta potential values (see Table 3). For TiO_2-Ar-900 °C sample the adsorption degree equaled only 5 %, whereas for TiO_2-4h-180 °C-2000 mM-Ar-900 °C reached 32 %. It is widely known that adsorption properties are attributed to higher S_{BET} values and porous structure of the sample. In this case S_{BET} area for TiO_2-4h-180 °C -2000 mM-Ar-900 °C is 45 m^2/g and for TiO_2-Ar-900 °C is 3 m^2/g.

3.3. Photocatalytic activity test

3.3.1. Photoactivity test

The photocatalytic activity of the starting-TiO_2 and new APTES-modified TiO_2 nanomaterials was determined based on decomposition of methylene blue under UV light irradiation. Experiments carried out in the absence of a photocatalyst (see Fig. 8) showed that methylene blue decomposition as a result of photolysis process was negligible in relation to the corresponding photocatalysis process, which resulted in about 2.5 % dye decomposition after 360 min of irradiation, using the same lamps as during the photocatalytic activity tests. The results of dye decomposition degree after 180 min of UV light irradiation for starting-TiO_2, reference samples and APTES-modified TiO_2 prior and after heat treatment were presented in Fig. 9. After thermal modification at 300 °C and 500 °C a slight change of the photocatalytic activity of starting-TiO_2 was noted. The major improvement in the activity from 31 % to 88 % was only observed for sample calcined at 700 °C, containing 88 % of anatase and 12 % of rutile phase with 3.07 eV of band gap energy. Our observations were consistent with the results obtained by Luís et al. [43], according to which the co-existence of different polymorphous forms of TiO_2 is one of the most important parameters to conditioning the TiO_2 photoactivity. They observed that the most efficient results during methylene blue decomposition were obtained for materials with reduced band gap energy (3.04 eV) and being a mixture of anatase and rutile. What is more, these materials did not have the largest specific surface area among all tested samples. After APTES modification the photocatalytic activity of TiO_2-4h-180 °C-2000 mM sample in comparison to starting-TiO_2 increased by 44 % after 180 min of irradiation. Basically, the enhancement of the efficiency was related to the nitrogen and carbon presence in tested material, but the influence of modification via APTES on TiO_2 photocatalytic activity was described in detail in our previous work [56]. After calcination, all APTES-functionalized TiO_2 photocatalysts were characterized by improved methylene blue decomposition degree in comparison to reference samples prepared at the same temperature. Modification with silicon suppressed both anatase-to-rutile the phase transformation of TiO_2, and the growth of crystallites. The enhancement of the crystallinity of anatase phase after calcination resulted in the high rate of electron diffusion to the surface through inhibition the

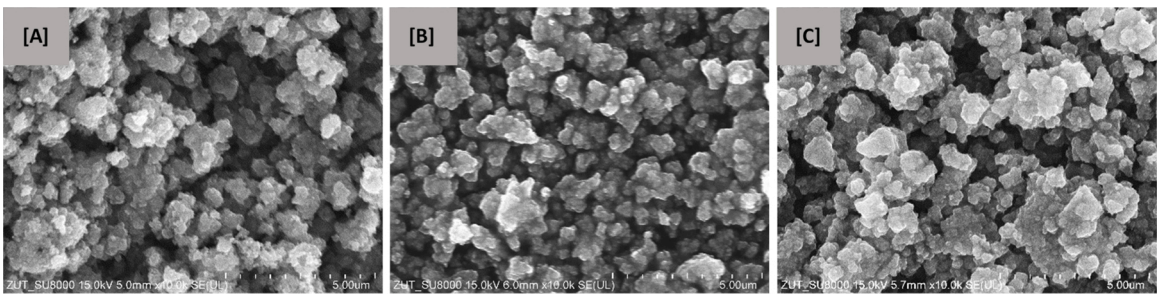

Fig. 5. The SEM image of [A] starting-TiO_2, [B] TiO_2-4h-180 °C-2000 mM, [C] TiO_2-4h-180 °C-2000 mM-Ar-500 °C.

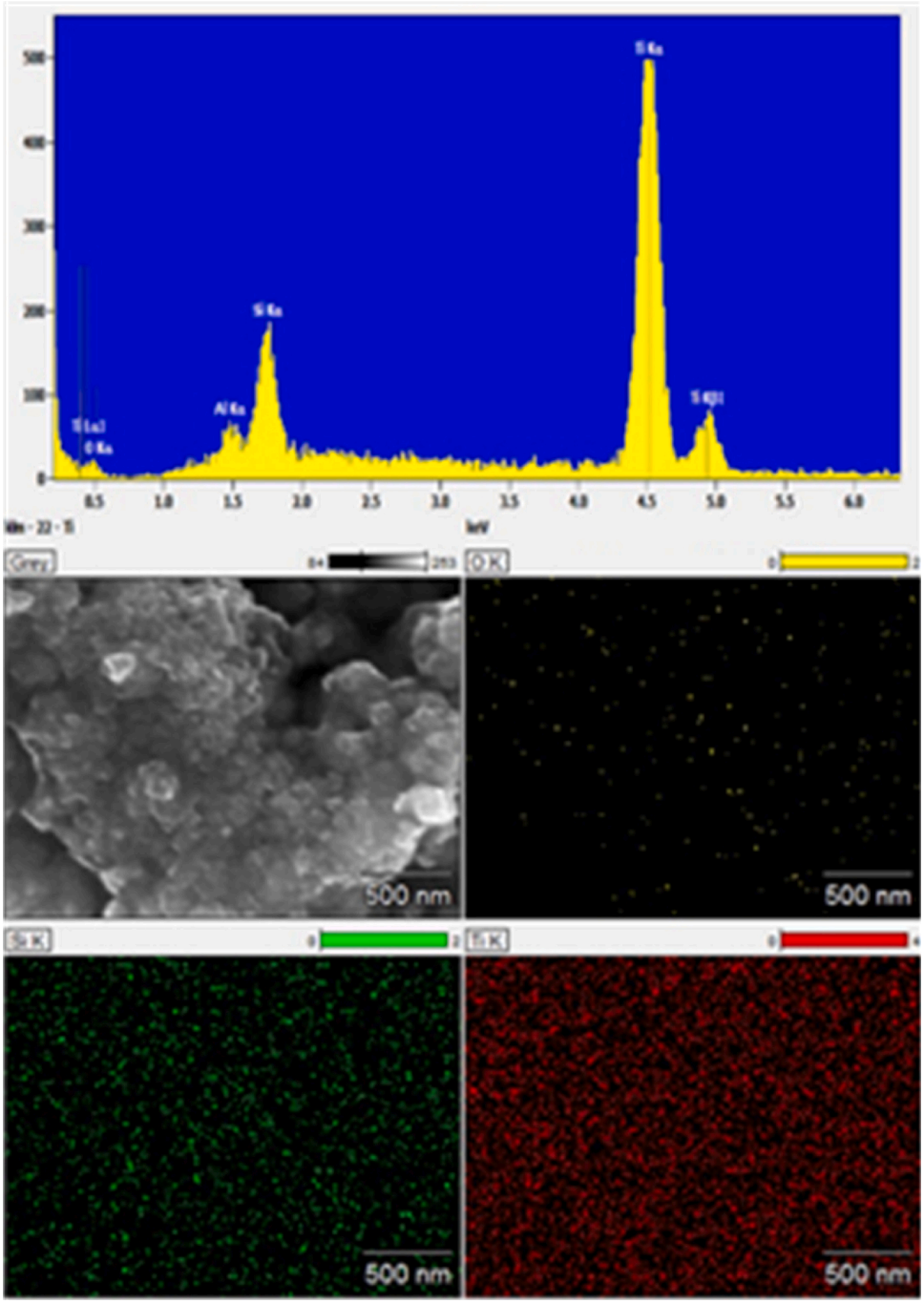

Fig. 6. The EDX spectrum and EDX mappings of [C] TiO_2-4h-180 °C-2000 mM-Ar-500 °C.

electron-hole recombination. Additionally, the high porosity simplified the mass transfer of reactants, like reaction intermediates or oxygen, and contributed to the increase of the photocatalytic activity of obtained calcined APTES/TiO_2 nanomaterials [57,58]. Moreover, it was observed that TiO_2-4h-180 °C-2000 mM-Ar-700 °C sample characterized only by not the highest photocatalytic activity, but also the highest adsorption degree of methylene blue (equaled 41 %). It is commonly known that the adsorption properties play significant role in the photocatalytic degradation reaction [59,60]. It is also worth mentioning that APTES modification significantly improved photocatalytic performance of nanomaterials calcined at 900 °C, notably extending the possibilities of their use. Methylene blue decomposition degree of TiO_2-4h-180 °C-2000 mM-Ar-900 °C in comparison to TiO_2-Ar-900 °C increased by 50 %. Both samples calcined at 900 °C were characterized by almost the same zeta potential values (see Table 3), therefore the observed improvement of the photoactivity was associated with the suppression of the phase transformation of anatase to rutile. It is commonly known that rutile is less active phase of TiO_2 than anatase due to less number of active sites and hydroxyl groups on the surface [61].

3.3.2. *Reaction rate*

In order to better understand the photocatalytic dye decomposition process, the apparent reaction rate constants were determined. It was noted that methylene blue degradation in the case of starting-TiO_2, TiO_2-Ar-300 °C, TiO_2-Ar-500 °C, TiO_2-Ar-700 °C and TiO_2-4h-180 °C-2000 mM proceeds according to the Langmuir-Hinshelwood pseudo-first order model. While for TiO_2-Ar-700 °C and all APTES-modified TiO_2 after thermal modification methylene blue decomposition follows

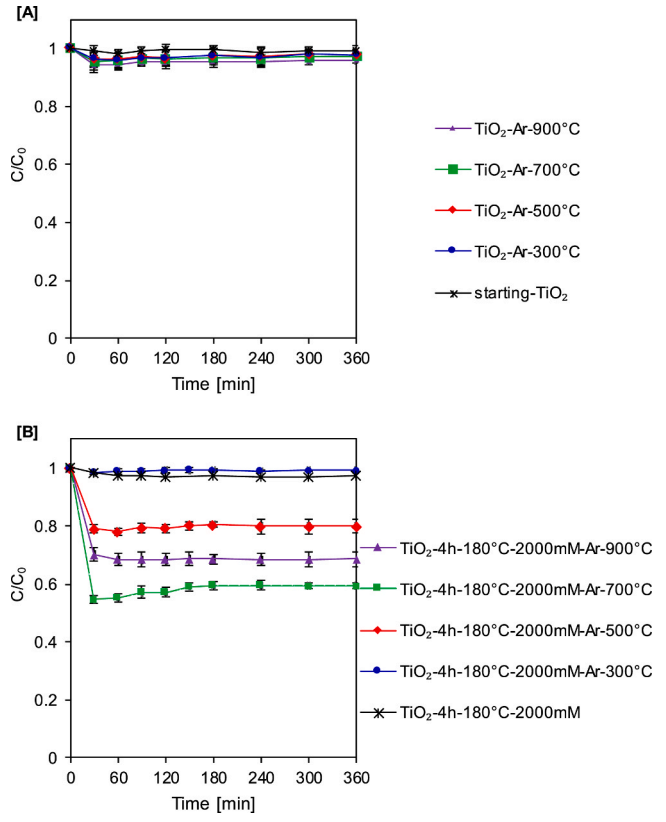

Fig. 7. Adsorption of methylene blue on the surface of starting-TiO_2 and reference samples [A] and APTES-modified TiO_2 prior and after heat treatment [B].

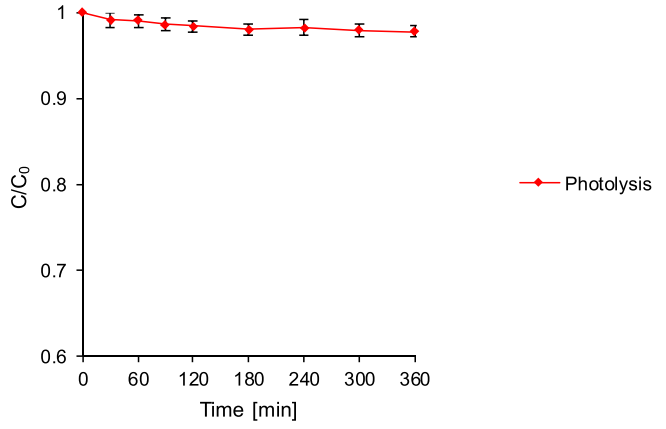

Fig. 8. Methylene blue photolysis curve after 360 min of UV light irradiation (C_0 = 15 mg/L).

the pseudo-second order model. The pseudo-first order and the pseudo-second order linear transforms are presented in Fig. 10A and B, respectively. Based on the data presented in Table 4, the obtained values of the k_1 for methylene blue decomposition for APTES/TiO_2 nanomaterials were between 0.0019 1/min and 0.0119 1/min, whereas the noted values of k_2 were between 0.0001 L/(min mg) and 0.0047 L/(min mg). It was also observed that the kinetics of the dye decomposition reaction changed after modification with APTES in combination with calcination from the pseudo-first to the pseudo-second order what is related to changes of the surface characteristics i.e. zeta potential values. When extending the irradiation time to 360 min, it was possible to observe that after 180 min, the points in the graph start diverging

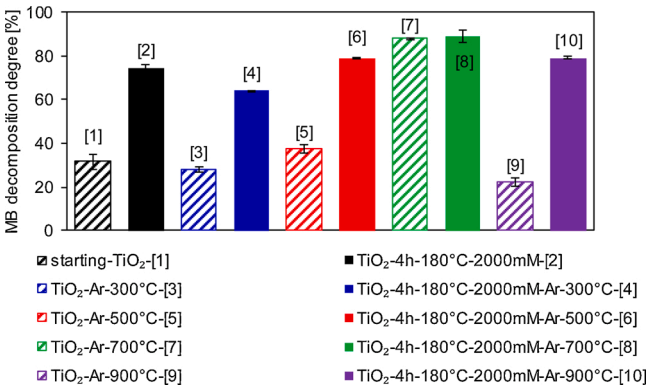

Fig. 9. Methylene blue decomposition degree after 180 min of UV light irradiation for starting-TiO_2, reference samples and APTES-modified TiO_2 prior and after heat treatment.

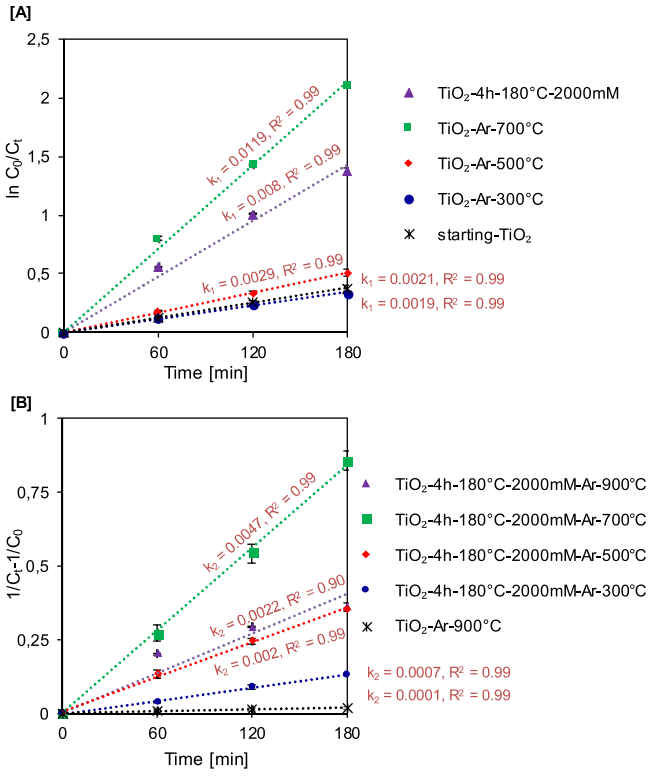

Fig. 10. The pseudo-first order plot [A] and the pseudo-second order plot [B] of methylene blue decomposition.

Table 4
The fitting parameters, the pseudo-first and the pseudo-second reaction rate constants for methylene blue decomposition.

Sample name	k_1 [1/min]	R^2	Sample name	k_2 [L/(min mg)]	R^2
starting-TiO_2	0.0021	0.99	TiO_2-Ar-900 °C	0.0001	0.99
TiO_2-Ar-300 °C	0.0019	0.99	TiO_2-4h-180 °C-2000 mM-Ar-300 °C	0.0007	0.99
TiO_2-Ar-500 °C	0.0029	0.99	TiO_2-4h-180 °C-2000 mM-Ar-500 °C	0.0020	0.99
TiO_2-Ar-700 °C	0.0119	0.99	TiO_2-4h-180 °C-2000 mM-Ar-700 °C	0.0047	0.99
TiO_2-4h-180 °C-2000 mM	0.0080	0.93	TiO_2-4h-180 °C-2000 mM-Ar-900 °C	0.0022	0.90

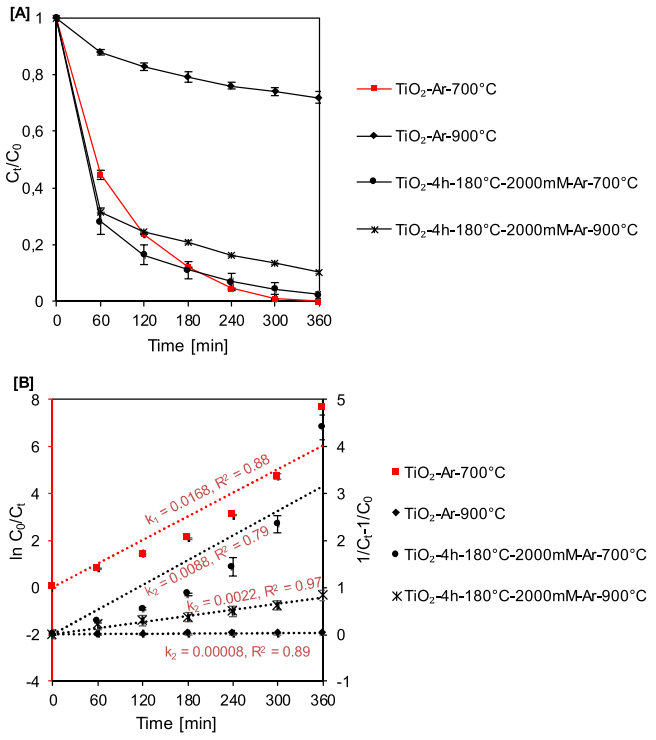

Fig. 11. Methylene blue decomposition under UV irradiation [A] and the pseudo-first order plot and the pseudo-second order plot of MB decomposition [B].

from the normal linear course of the curve (see Fig. 11B). The observed decrease in the reaction rate was associated with the creation of intermediate products during the decomposition of methylene blue and sorption of these carbon deposits on the surface of TiO_2.

3.3.3. Photocatalytic stability test

The photocatalytic stability of materials is very important parameter from the application point of view. In our previous paper [56] we presented that before thermal modification APTES-modified TiO_2 photocatalysts were not stable due to the destruction of the alkyl chains and detachment of the amine groups during UV irradiation. Therefore, to improve the efficiency and stability in following dye decomposition cycles, the calcination process of the obtained nanomaterials was carried out. The efficiency of examined photocatalysts was conducted for four subsequent photocatalytic cycles. The obtained results were presented in Fig. from 12 A–E. Modification in the argon atmosphere at 300 °C, 500 °C and 700 °C resulted in improved stability of the tested samples in comparison to solvothermally prepared TiO_2-4h-180 °C-2000 mM sample. After the first cycle, the activity of TiO_2-4h-180 °C-2000 mM decreased about 41 %, while for calcined samples the activity reduced only for approx. 22 %. The increase of the specific surface area and total pore volume after calcination (see Table 2) influenced the increase in the efficiency of obtained nanomaterials. The FT-IR/DR spectra, presented in Fig. 1B, confirmed that APTES-modified TiO_2 photocatalysts obtained via calcination were characterized by the absence of carbon and nitrogen, whose leaching caused a decrease in stability in the next cycles of methylene blue decomposition, in the case of not calcined TiO_2-4h-180 °C-2000 mM sample. However, in order to explain the decrease in the photoactivity of calcined materials, before the first cycle and after the last fourth cycle, the FT-IR/DR spectra of selected samples were measured and presented in Fig. 13. It was observed that the shape of spectra after four cycles was little different than it was shown in Fig. 1B. Thus, the structure of photocatalyst was changed throughout the photocatalytic reaction. Significant increase of the intensity of the band located at 1360 cm^{-1} (noted for the TiO_2-4h-180 °C-2000 mM-Ar-500 °C sample after fourth cycle) indicated that during subsequent cycles, carbon deposits, derived from methylene blue, occurred on the surface of the semiconductor, which resulted in the decrease of the photocatalytic activity. These FT-IR/DRS results showed that the reduction in the degree of dye decomposition were strongly affected by adsorption of the methylene blue on the surface of the modified titanium dioxide [62,63]. In addition to the confirmed significant influence of phase composition on photocatalytic activity of the obtained nanomaterials, the adsorption process also played a crucial role.

3.3.4. Photocatalytic reaction mechanism

A photocatalytic activity enhanced mechanism has been proposed in Fig. 14. When a photocatalyst absorbs a photon of energy, the valance

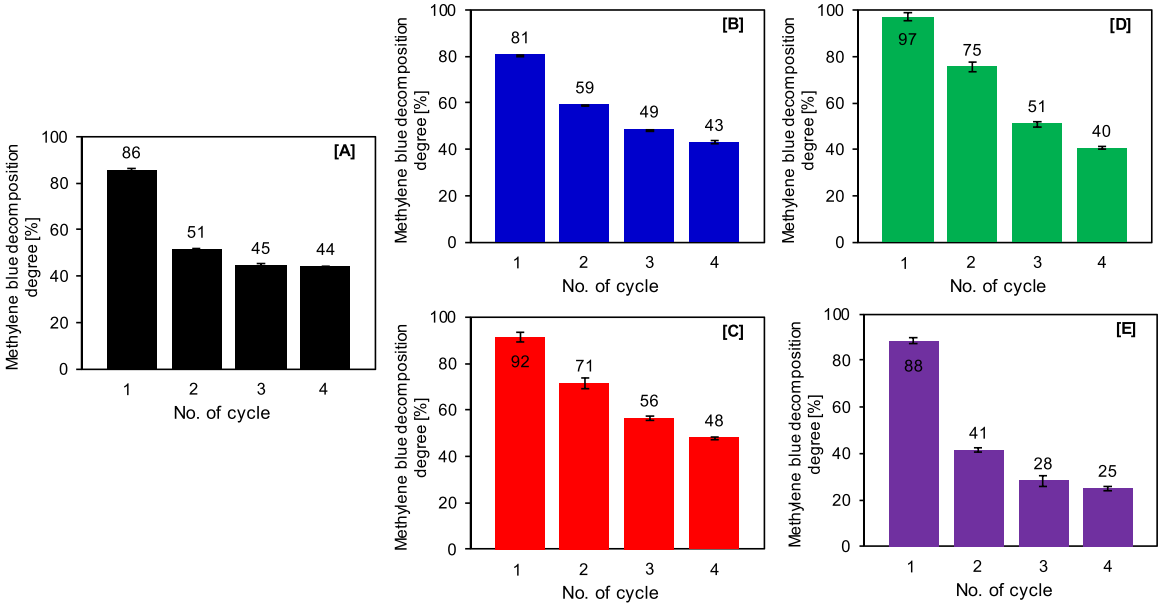

Fig. 12. Photocatalytic activity in subsequent cycles of methylene blue decomposition of [A] TiO_2-4h-180 °C-2000 mM, [B] TiO_2-4h-180 °C-2000 mM-Ar-300 °C, [C] TiO_2-4h-180 °C-2000 mM-Ar-500 °C, [D] TiO_2-4h-180 °C-2000 mM-Ar-700 °C and [E] TiO_2-4h-180 °C-2000 mM-Ar-900 °C samples.

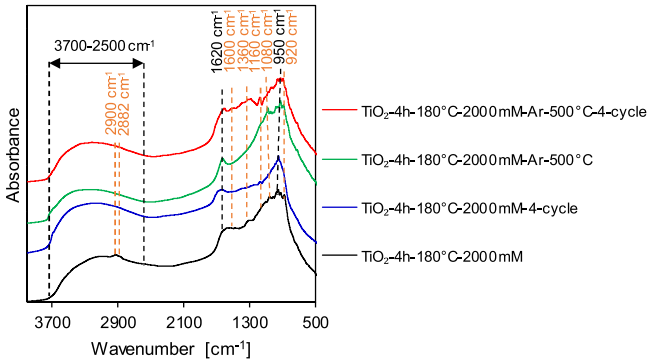

Fig. 13. FT-IR/DR spectra of TiO_2-4h-180 °C-2000 mM and TiO_2-4h-180 °C-2000 mM-Ar-500 °C samples before the first cycle and after the last fourth cycle.

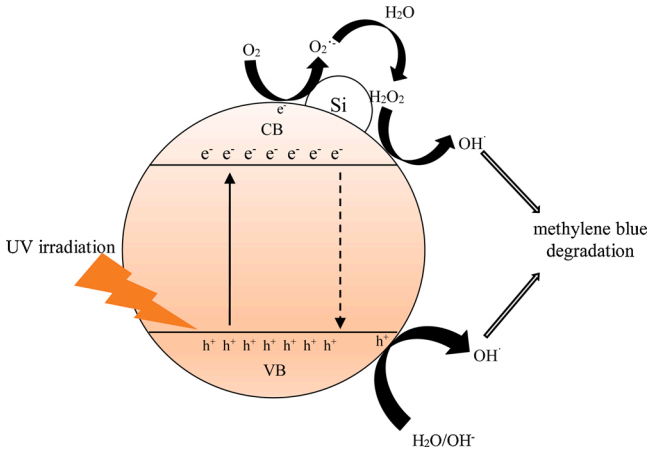

Fig. 14. Scheme of mechanism of TiO_2 photocatalysis with modifications by APTES.

band electrons migrate to the conduction band causing the electron-hole generation. Generally, the electron-hole pairs recombine very fast. However, after TiO_2 modification with silicon, it was noted that electron-hole recombination was successfully supressed. According to the Su et al. [64] suppression of recombination is related to increase of the rate of electron diffusion related to the enhancement of the anatase crystallinity and decrease of bulk defected caused by high-temperature calcination. Summarizing, the enhanced photocatalytic activity of APTES-modified TiO_2 is correlated to phase content, character of the modified TiO_2 surface, specific surface area as well as suppression of electron-hole recombination rate.

4. Conclusions

In summary, this paper presents the physicochemical characterization and photocatalytic properties of TiO_2 nanomaterials modified with 3-aminopropyltriethoxysilane (APTES). The photocatalysts were obtained by solvothermal process at 180 °C with the concentration of APTES equal 2000 mM and calcination in the range form 300 °C–900 °C in the argon atmosphere. Application of the calcination step in the argon atmosphere as well as describe influence the influence of the temperature on the photocatalytic properties and stability are a novelty of the presented research. The silanol groups after APTES modification were confirmed by the FT-IR/DRS analysis. The influence of crystallite size, changes of the phase content, and specific surface area as well as zeta potential for photoactivity was determined. It was found that modification via APTES suppressed phase transformation and the growth of crystallite size of anatase and rutile during thermal modification. Calcination process changed the surface characteristics i.e. zeta potential of APTES-modified TiO_2 photocatalysts. Additionally, thermal modification up to a maximum of 500 °C resulted in partial unblocking of pores and the TiO_2 surface by releasing some of the APTES particles from the surface of the tested nanomaterials. The adsorption effect after thermal modification was also noted. The samples showed enhanced adsorption properties, which was related to the change in the character of the TiO_2 surface. The obtained photocatalysts were tested under UV irradiation during methylene blue decomposition. It was found that calcination above 300 °C increased photocatalytic properties of APTES-modified TiO_2 photocatalysts. Furthermore, the calcination up to 700 °C improved stability of the examined photocatalysts. Taking into account improved photocatalytic stability in subsequent cycles of dye decomposition and the increased removal of methylene blue after calcination by 40 % compared with TiO_2-4h-180 °C-2000 mM sample, the TiO_2-4h-180 °C-2000 mM-Ar-500 °C photocatalyst was considered the most promising sample.

CRediT authorship contribution statement

Agnieszka Sienkiewicz: Conceptualization, Investigation, Writing - original draft. **Agnieszka Wanag:** Conceptualization, Investigation, Data curation, Writing - review & editing. **Ewelina Kusiak-Nejman:** Conceptualization, Methodology, Data curation, Writing - review & editing. **Ewa Ekiert:** . **Paulina Rokicka-Konieczna:** Writing - review & editing. **Antoni W. Morawski:** Writing - review & editing, Supervision.

Declaration of Competing Interest

The authors report no declarations of interest.

Acknowledgement

This work was supported by grant 2017/27/B/ST8/02007 from the National Science Centre, Poland.

References

[1] U.G. Akpan, B.H. Hameed, Parameters affecting the photocatalytic degradation of dyes using TiO_2-based photocatalysts: a review, J. Hazard. Mater. 170 (2009) 520–529, https://doi.org/10.1016/j.jhazmat.2009.05.039.
[2] M. Al-Amin, S. Chandra Dey, T.Ur. Rashid, Md. Ashaduzzaman, S.Md. Shamsuddin, Solar assisted photocatalytic degradation of reactive azo dyes in presence of anatase titanium dioxide, Int. J. Latest Res. Eng. Technol. 2 (3) (2016) 14–21.
[3] P.V.L. Reddy, B. Kavitha, P.A.K. Reddy, K.H. Kim, TiO_2-based photocatalytic disinfection of microbes in aqueous media: a review, Environ. Res. 154 (2017) 296–303, https://doi.org/10.1016/j.envres.2017.01.018.
[4] P. Fitzpatrick Ibhadon, Heterogeneous photocatalysis: recent advances and applications, Catalysts 3 (1) (2013) 189–218, https://doi.org/10.3390/catal3010189.
[5] R. Daghrir, P. Drogui, D. Robert, Modified TiO_2 for environmental photocatalytic applications: a review, Ind. Eng. Chem. Res. 52 (10) (2013) 3581–3599, https://doi.org/10.1021/ie303468t.
[6] N. Bao, G. Wu, J. Niu, Q. Zhang, S. He, J. Wang, Wide spectral response and enhanced photocatalytic activity of TiO_2 continuous fibers modified with aminosilane coupling agents, J. Alloys Compd. 599 (2014) 40–48, https://doi.org/10.1016/j.jallcom.2014.02.072.
[7] Z.-h. Yuan, J.-h. Jia, L.-d. Zhang, Influence of co-doping of Zn(II)+Fe(III) on the photocatalytic activity of TiO_2 for phenol degradation, Mater. Chem. Phys. 73 (2002) 323–326, https://doi.org/10.1016/S0254-0584(01)00373-X.
[8] U. Hashim, Sh. Nadzirah, N. Azizah, M. Safwan Azmi, K. Bala, Silanization using APTES in different solvents on titanium dioxide nanoparticles, in: 2015 2nd International Conference on Biomedical Engineering, Penang, 2015, pp. 1–4, https://doi.org/10.1109/ICoBE.2015.7235907.
[9] D. Meroni, L. Lo Presti, G. Di Liberto, M. Ceotto, R.G. Acres, K.C. Prince, R. Bellani, G. Soliveri, S. Ardizzone, A close look at the structure of the TiO_2-APTES interface in hybrid nanomaterials and its degradation pathway: an experimental and theoretical study, J. Phys. Chem. C 121 (2017) 430–440, https://doi.org/10.1021/acs.jpcc.6b10720.
[10] L. Wang, X. Jiang, Ch. Wang, Y. Huang, Y. Meng, J. Shao, Titanium dioxide grafted with silane coupling agents and its use in blue light curing ink, Color Technol. 136 (2020) 15–22, https://doi.org/10.1111/cote.12434.
[11] V. Purcar, V. Rădiţoiu, A. Dumitru, C.-A. Nicolae, A.N. Frone, M. Anastasescu, A. Rădiţoiu, M.F. Raduly, R.A. Gabor, Simona Căprărescu, Antireflective coating

based on TiO_2 nanoparticles modified with coupling agents via acid-catalyzed sol-gel method, Appl. Surf. Sci. 487 (2019) 819–824, https://doi.org/10.1016/j.apsusc.2019.02.256.
[12] R. Klaysri, T. Tubchareon, P. Praserthdam, One-step synthesis of amine-functionalized TiO_2 surface for photocatalytic decolorization under visible light irradiation, J. Ind. Eng. Chem. 45 (2017) 229–236, https://doi.org/10.1016/j.jiec.2016.09.027.
[13] A.R.M. Dalod, L. Henriksen, T. Grande, M.-A. Einarsrud, Functionalized TiO_2 nanoparticles by single-step hydrothermal synthesis: the role of the silane coupling agents, Beilstein J. Nanotechnol. 8 (2017) 304–312, https://doi.org/10.3762/bjnano.8.33.
[14] E. Kusiak-Nejman, A. Wanag, J. Kapica-Kozar, A.W. Morawski, Preparation and characterisation of TiO_2 thermally modified with cyclohexane vapours, Int. J. Mater. Prod. Technol. 52 (2016) 286–297, https://doi.org/10.1504/IJMPT.2016.075501.
[15] D. Chen, L. Zou, S. Li, F. Zheng, Nanospherical like reduced graphene oxide decorated TiO_2 nanoparticles: an advanced catalyst for the hydrogen evolution reaction, Sci. Rep. 6 (2016), 20335, https://doi.org/10.1038/srep20335.
[16] F. Wu, W. Liu, J. Qiu, J. Li, W. Zhou, Y. Fang, Sh. Zhang, X. Li, Enhanced photocatalytic degradation and adsorption of methylene blue via TiO_2 nanocrystals supported on graphene-like bamboo charcoal, Appl. Surf. Sci. 358 (2015) 425–435, https://doi.org/10.1016/j.apsusc.2015.08.161.
[17] Ch. Sahoo, A.K. Gupta, I.M. Sasidharan Pillai, Photocatalytic degradation of methylene blue dye from aqueous solution using silver ion-doped TiO_2 and its application to the degradation of real textile wastewater, J. Environ. Sci. Health A 47 (2012) 1428–1438, https://doi.org/10.1080/10934529.2012.672387.
[18] Saepurahman, M.A. Abdullah, F.K. Chong, Dual-effects of adsorption and photodegradation of methylene blue by tungsten-loaded titanium dioxide, Chem. Eng. J. 158 (2010) 418–425, https://doi.org/10.1016/j.cej.2010.01.010.
[19] F. Khan, R. Wahab, M. Hagar, R. Alnoman, Lutfullah, M. Rashid, Nanotransition materials (NTMs): photocatalysis, validated high effective sorbent models study for organic dye degradation and precise mathematical data's at standardized level, Nanomaterials 8 (2018) 134, https://doi.org/10.3390/nano8030134.
[20] M. Winter, D. Hamal, X. Yang, H. Kwen, D. Jones, Sh. Rajagopalan, K.J. Klabunde, Defining reactivity of solid sorbents: what is the most appropriate metric? Chem. Mater. 21 (2009) 2367–2374, https://doi.org/10.1021/cm8032884.
[21] P. Rokicka-Konieczna, A. Markowska-Szczupak, E. Kusiak-Nejman, A. W. Morawski, Photocatalytic water disinfection under the artificial solar light by fructose modified TiO_2, Chem. Eng. J. 372 (2019) 203–215, https://doi.org/10.1016/j.cej.2019.04.113.
[22] P. Górska, A. Zaleska, E. Kowalska, T. Klimczuk, J.W. Sobczak, E. Skwarek, W. Janusz, J. Hupka, TiO_2 photoactivity in vis and UV light: the influence of calcination temperature and surface properties, Appl. Catal. B-Environ. 84 (2008) 440–447, https://doi.org/10.1016/j.apcatb.2008.04.028.
[23] Y. Kuroda, T. Mori, K. Yagi, N. Makihata, Y. Kawahara, M. Nagao, Sh. Kittaka, Preparation of visible-light-responsive TiO_2-xNx photocatalyst by a sol-gel method: analysis of the active center on TiO_2 that reacts with NH3, Langmuir 21 (2005) 8026–8034, https://doi.org/10.1021/la0508792.
[24] M. Janus, B. Tryba, M. Inagaki, A.W. Morawski, New preparation of a carbon-TiO_2 photocatalyst by carbonization of n-hexane deposited on TiO_2, Appl. Catal. B-Environ. 52 (2004) 61–67, https://doi.org/10.1016/j.apcatb.2004.03.011.
[25] A. Pramanik, K. Bhattacharjee, M.K. Mitra, G.C. Das, B. Duari, A mechanistic study of the initial stage of the sintering of sol-gel derived silica nanoparticles, Int. J. Mod. Eng. Res. Technol. 3 (2) (2013) 1066–1070.
[26] P.A. Saliba, A.A.P. Mansur, H.S. Mansur, Advanced nanocomposite coatings of fusion bonded epoxy reinforced with amino-functionalized nanoparticles for applications in underwater oil pipelines, J. Nanomater. 2016 (3) (2016) 1–16, https://doi.org/10.1155/2016/7281726.
[27] A. Razmjou, A. Resosudarmo, R.L. Holmes, H. Li, J. Mansouri, V. Chen, The effect of modified TiO_2 nanoparticles on the polyethersulfone ultrafiltration hollow fiber membranes, Desalination 287 (2012) 271–280, https://doi.org/10.1016/j.desal.2011.11.025.
[28] E. Ukaji, T. Furusawa, M. Sato, M. Suzuki, The effect of surface modification with silane coupling agent on suppressing the photo-catalytic activity of fine TiO_2 particles as inorganic UV filter, Appl. Surf. Sci. 254 (2007) 563–569, https://doi.org/10.1016/j.apsusc.2007.06.061.
[29] Z. Youssef, V. Jouan-Hureaux, L. Colombeau, P. Arnoux, A. Moussaron, F. Baros, J. Toufaily, T. Harmieh, T. Roques-Carmes, C. Frochot, Titania and silica nanoparticles coupled to Chlorin e6 for anti-cancer photodynamic therapy, Photodiagnosis Photodyn. Ther. 22 (2018) 115–126, https://doi.org/10.1016/j.pdpdt.2018.03.005.
[30] T. Oh, Ch.K. Choi, Comparison between SiOC thin films fabricated by using plasma enhance chemical vapor deposition and SiO_2 thin films by using fourier transform infrared spectroscopy, J. Korean Phys. Soc. 56 (4) (2010) 1150–1155, https://doi.org/10.3938/jkps.56.1150.
[31] C. Byrne, R. Fagan, S. Hinder, D.E. McCormack, S.C. Pillai, New approach of modifying the anatase to rutile transition temperature in TiO_2 photocatalysts, RSC Adv. 6 (2016) 95232–95238, https://doi.org/10.1039/C6RA19759K.
[32] D.M. Tobaldi, A. Tucci, A.S. Škapin, L. Esposito, Effects of SiO_2 addition on TiO_2 crystal structure and photocatalytic activity, J. Eur. Ceram. Soc. 30 (2010) 2481–2490, https://doi.org/10.1016/j.jeurceramsoc.2010.05.014.
[33] Z. Lu, X. Jiang, B. Zhou, X. Wu, L. Lu, Study of effect annealing temperature on the structure, morphology and photocatalytic activity of Si doped TiO_2 thin films deposited by electron beam evaporation, Appl. Surf. Sci. 257 (2011) 10715–10720, https://doi.org/10.1016/j.apsusc.2011.07.085.
[34] G. Xu, Z. Zheng, Y. Wu, N. Feng, Effect of silica on the microstructure and photocatalytic properties of titania, Ceram. Int. 35 (2009) 1–5, https://doi.org/10.1016/j.ceramint.2007.09.008.
[35] K.S.W. Sing, Reporting physisorption data for gas/solid systems with special reference to the determination of surface area and porosity, Pure Appl. Chem. 54 (1982) 2201–2218, https://doi.org/10.1351/pac198557040603.
[36] K.S.W. Sing, R.T. William, Physisorption hysteresis loops and the characterization of nanoporous materials, Adsorp. Sci. Technol. 22 (10) (2004) 773–782, https://doi.org/10.1260/0263617053499032.
[37] V.V. Kutarov, Y.I. Tarasevich, E.V. Aksenenko, Z.G. Ivanova, Adsorption hysteresis for a slit-like pore model, Russ. J. Phys. Chem. 85 (7) (2011) 1222–1227, https://doi.org/10.1134/S0036024411070193.
[38] Q. Sun, X. Hu, Sh. Zheng, Z. Sun, Sh. Liu, H. Li, Influence of calcination temperature on the structural, adsorption and photocatalytic properties of TiO_2 nanoparticles supported on natural zeolite, Powder Technol. 274 (2015) 88–97, https://doi.org/10.1016/j.powtec.2014.12.052.
[39] N.R.C. Fernandes Machado, V.S. Santana, Influence of thermal treatment on the structure and photocatalytic activity of TiO_2 P25, Catal. Today 107–108 (2005) 595–601, https://doi.org/10.1016/j.cattod.2005.07.022.
[40] K. Siwińska-Stefańska, F. Ciesielczyk, M. Nowacka, T. Jesionowski, Influence of selected alkoxysilanes on dispersive properties and surface chemistry of titanium dioxide and TiO_2-SiO_2 composite material, J. Nanomater. 2012 (2012) 1–19, https://doi.org/10.1155/2012/316173.
[41] W. Zhuang, Y. Zhang, L. He, R. An, B. Li, H. Ying, J. Wu, Y. Chen, J. Zhou, X. Lu, Facile synthesis of amino-functionalized mesoporous TiO_2 microparticles for adenosine deaminase immobilization, Microporous Mesoporous Mater. 239 (2017) 158–166, https://doi.org/10.1016/j.micromeso.2016.09.006.
[42] H.-F. Yu, Photocatalytic abilities of gel-derived P-doped TiO_2, J. Phys. Chem. Solids 68 (2007) 600–607, https://doi.org/10.1016/j.jpcs.2007.01.050.
[43] A.M. Luís, M.C. Neves, M.H. Mendonça, O.C. Monteiro, Influence of calcination parameters on the TiO_2 photocatalytic properties, Mater. Chem. Phys. 125 (2011) 20–25, https://doi.org/10.1016/j.matchemphys.2010.08.019.
[44] M. Hussaina, N. Russoa, G. Saracco, Photocatalytic abatement of VOCs by novel optimized TiO_2 nanoparticles, Chem. Eng. J. 166 (2011) 138–149, https://doi.org/10.1016/j.cej.2010.10.040.
[45] W. Zhanga, H. Guoa, H. Suna, R.-C. Zenga, Hydrothermal synthesis and photoelectrochemical performance enhancement of TiO_2 graphene composite in photo-generated cathodic protection, Appl. Surf. Sci. 382 (2016) 128–134, https://doi.org/10.1016/j.apsusc.2016.04.124.
[46] S.K.S. Kothaplamoottil Sivan Saranya, V.V.T. Padil, C. Senan, R. Pilankatta, S. K. Kunjumon Saranya, B. George, S. Wacławek, M. Cerńík, Green synthesis of high temperature stable anatase titanium dioxide nanoparticles using gum kondagogu: characterization and solar driven photocatalytic degradation of organic dye, Nanomaterials 8 (2018) 1002, https://doi.org/10.3390/nano8121002.
[47] E. Kusiak-Nejman, M. Janus, B. Grzmil, A.W. Morawski, Methylene blue decomposition under visible light irradiation in the presence of carbon-modified TiO_2 photocatalysts, J. Photochem. Photobiol. A Chem. 226 (1) (2011) 68–72, https://doi.org/10.1016/j.jphotochem.2011.10.018.
[48] P. Rokicka-Konieczna, A. Wanag, A. Sienkiewicz, E. Kusiak-Nejman, A. W. Morawski, Antibacterial effect of TiO_2 nanoparticles modified with APTES, Catal. Commun. 134 (2020), 105862, https://doi.org/10.1016/j.catcom.2019.105862.
[49] E.P. Ferreira-Neto, S. Ullah, M.B. Simões, A.P. Perissinotto, F.S. de Vicente, P.-L. M. Noeske, S.J.L. Ribeiro, U.P. Rodrigues-Filho, Solvent-controlled deposition of titania on silica spheres for the preparation of SiO_2@TiO_2 core@shell nanoparticles with enhanced photocatalytic activity, Colloids Surf. A 570 (2019) 293–305, https://doi.org/10.1016/j.colsurfa.2019.03.036.
[50] Ch.-H. Huang, H. Bai1, S.-L. Liu, Y.-L. Huang, Y.-H. Tseng, Synthesis of neutral SiO_2/TiO_2 hydrosol and its photocatalytic degradation of nitric oxide gas, Micro Nano Lett. 6 (8) (2011) 646–649, https://doi.org/10.1049/mnl.2011.0331.
[51] Sh. Wang, Z.H. Zhu, A. Coomes, F. Haghseresht, G.Q. Lu, The physical and surface chemical characteristics of activated carbons and the adsorption of methylene blue from wastewater, J. Colloid Interface Sci. 284 (2005) 440–446, https://doi.org/10.1016/j.jcis.2004.10.050.
[52] E. Blanco, H. Shen, M. Ferrari, Principles of nanoparticle design for overcoming biological barriers to drug delivery, Nat. Biotechnol. 33 (9) (2015) 941–951.
[53] F.G.L. Medeiros Borsagli, A green 3D scaffolds based on chitosan with thiol group as a model for adsorption of hazardous organic dye pollutants, Desalin. Water Treat. 169 (2019) 395–411.
[54] M.Sh. Beegam, S.G. Ullattil, P. Periyat, Selective solar photocatalysis by high temperature stable anatase TiO_2, Sol. Energy 160 (2018) 10–17, https://doi.org/10.1016/j.solener.2017.11.065.
[55] K. Bubacz, B. Tryba, A.W. Morawski, The role of adsorption in decomposition of dyes on TiO_2 and N-modified TiO_2 photocatalysts under UV and visible light irradiations, Mater. Res. Bull. 47 (2012) 3697–3703, https://doi.org/10.1016/j.materresbull.2012.06.038.
[56] A. Wanag, A. Sienkiewicz, P. Rokicka-Konieczna, E. Kusiak-Nejman, A. W. Morawski, Influence of modification of titanium dioxide by silane coupling agents on the photocatalytic activity and stability, J. Environ. Chem. Eng. 8 (2020), 103917, https://doi.org/10.1016/j.jece.2020.103917.
[57] Y. Su, J. Wu, X. Quan, Sh. Chen, Electrochemically assisted photocatalytic degradation of phenol using silicon-doped TiO_2 nanofilm electrode, Desalination 252 (2010) 143–148, https://doi.org/10.1016/j.desal.2009.10.011.
[58] R.-B. Zhang, Photodegradation of toluene using silica-embedded titania, J. Non-Cryst. Solids 351 (2005) 2129–2132, https://doi.org/10.1016/j.jnoncrysol.2005.04.048.

[59] Y. Cheng, F. Luo, Y. Jiang, F. Li, C. Wei, The effect of calcination temperature on the structure and activity of TiO_2/SiO_2 composite catalysts derived from titanium sulfate and fly ash acid sludge, Colloids Surf. A 554 (2018) 81–85, https://doi.org/10.1016/j.colsurfa.2018.06.032.

[60] Q. Wang, Ch. Chen, D. Zhao, W. Ma, J. Zhao, Change of adsorption modes of dyes on fluorinated TiO_2 and its effect on photocatalytic degradation of dyes under visible irradiation, Langmuir 24 (2008) 7338–7345, https://doi.org/10.1021/la800313s.

[61] M. Alvaro, C. Aprile, M. Benitez, E. Carbonell, H. García, Photocatalytic activity of structured mesoporous TiO_2 materials, J. Phys. Chem. B 110 (2006) 6661–6665, https://doi.org/10.1021/jp0573240.

[62] M. Abbas, B. Parvatheeswara Rao, V. Reddy, Ch. Kim, Fe_3O_4/TiO_2 core/shell nanocubes: single-batch surfactant less synthesis, characterization and efficient catalysts for methylene blue degradation, Ceram. Int. 40 (2014) 11177–11186, https://doi.org/10.1016/j.ceramint.2014.03.148.

[63] H. Wang, Y. Huang, Prussian-blue-modified iron oxide magnetic nanoparticles as effective peroxidase-like catalysts to degrade methylene blue with H_2O_2, J. Hazard. Mater. 191 (2011) 163–169, https://doi.org/10.1016/j.jhazmat.2011.04.057.

[64] Y. Su, J. Wu, X. Quan, S. Chen, Electrochemically assisted photocatalytic degradation of phenol using silicon-doped TiO_2 nanofilm electrod, Desalination 252 (2010) 143–148, https://doi.org/10.1016/j.desal.2009.10.011.

molecules

MDPI

Article

Artificial Solar Light-Driven APTES/TiO_2 Photocatalysts for Methylene Blue Removal from Water

Agnieszka Sienkiewicz, Paulina Rokicka-Konieczna *, Agnieszka Wanag, Ewelina Kusiak-Nejman and Antoni W. Morawski

Department of Inorganic Chemical Technology and Environment Engineering, Faculty of Chemical Technology and Engineering, West Pomeranian University of Technology in Szczecin, Pułaskiego 10, 70-322 Szczecin, Poland; agnieszka.sienkiewicz@zut.edu.pl (A.S.); agnieszka.wanag@zut.edu.pl (A.W.); ewelina.kusiak@zut.edu.pl (E.K.-N.); antoni.morawski@zut.edu.pl (A.W.M.)
* Correspondence: paulina.rokicka@zut.edu.pl

Abstract: A visible-light photocatalytic performance of 3-aminopropyltriethoxysilane (APTES)-modified TiO_2 nanomaterials obtained by solvothermal modification under elevated pressure, followed by calcination in an argon atmosphere at 800–1000 °C, is presented for the first time. The presence of silicon and carbon in the APTES/TiO_2 photocatalysts contributed to the effective delay of the anatase-to-rutile phase transformation and the growth of the crystallites size of both polymorphous forms of TiO_2 during heating. Thus, the calcined APTES-modified TiO_2 exhibited higher pore volume and specific surface area compared with the reference materials. The change of TiO_2 surface charge from positive to negative after the heat treatment increased the adsorption of the methylene blue compound. Consequently, due to the blocking of active sites on the TiO_2 surface, the adsorption process negatively affected the photocatalytic properties. All calcined photocatalysts obtained after modification via APTES showed a higher dye decomposition degree than the reference samples. For all 3 modifier concentrations tested, the best photoactivity was noted for nanomaterials calcined at 900 °C due to a higher specific surface area than materials calcined at 1000 °C, and a larger number of active sites available on the TiO_2 surface compared with samples annealed at 800 °C. It was found that the optimum concentration for TiO_2 modification, at which the highest dye decomposition degree was noted, was 500 mM.

Keywords: photocatalytic water treatment; titanium dioxide; APTES; artificial solar light; methylene blue decomposition

Citation: Sienkiewicz, A.; Rokicka-Konieczna, P.; Wanag, A.; Kusiak-Nejman, E.; Morawski, A.W. Artificial Solar Light-Driven APTES/TiO_2 Photocatalysts for Methylene Blue Removal from Water. *Molecules* **2022**, *27*, 947. https://doi.org/10.3390/molecules27030947

Academic Editor: Giuseppina Pinuccia Cerrato

Received: 18 January 2022
Accepted: 27 January 2022
Published: 30 January 2022

1. Introduction

In the past decades, photocatalysis has been proven to be an effective approach for degrading organic compounds. Due to its advantages, such as good chemical stability and low cost, TiO_2 as a photocatalyst is widely and successfully used in different fields, such as water and wastewater treatment, air cleaning, automotive, buildings materials, agriculture, and antiseptics production [1,2]. Nevertheless, it requires the use of relatively high photon energy for its activation (3.23 eV for the most photoactive anatase phase). For this reason, many methods have been proposed to reduce the band gap energy of TiO_2 [3–5]. Among them, doping TiO_2 with non-metals, such as nitrogen or carbon, is frequently described as one of the most effective ways to enhance its photoactivity under visible light [6,7]. In addition, TiO_2 doping with non-metals results in changes in the electronic band structure, lowering the band gap energy [8].

Additionally, the beneficial effects of single-, co-, and tri-doping on characteristics, photocatalytic activity, and the possible applications of the doped TiO_2 have been discussed in various publications over the years [8–11]. One promising solution for the modification of TiO_2 with tri-doping is an application of C, N, and Si [12]. Incorporating silicon into the

titanium dioxide surface would increase the specific surface area, reduce the particle size, and hinder the anatase-to-rutile phase transition [13,14], while modification with C and N would commonly improve the photocatalysts' efficiency in sunlight [15,16]. The most recent method involves using organosilane coupling agents to modify the surface of TiO_2 [17,18]. One of them is 3-aminopropyltriethoxysilane (APTES), which contains one aminopropyl and three ethoxy functional groups attached to the central Si atom [12,19]. APTES/TiO_2 nanomaterials can be successfully applied in many different fields. Shakeri et al. [20] investigated the self-cleaning ability of ceramic tile surfaces coated with APTES-modified TiO_2. They noted that the resulting coating was stable, and the surface could effectively photodegrade the pink food dye selected as an organic pollutant. Nadzirah et al. [21] obtained an APTES/TiO_2 nanoparticle biosensor-based transducer successfully applied as a sensing platform for *E. coli*. Andrzejewska et al. [22] reported the results of TiO_2 modification with various aminosilanes that was carried out to obtain pigments via adsorption of organic dyes on modified TiO_2 surface. Lee et al. [23] successfully prepared APTES-modified TiO_2 materials by simultaneous amination of TiO_2 nanoparticles in the gas phase synthesis for possible biomedical applications. Bao et al. [24] also proposed a production method of aminosilane-functionalized TiO_2 nanomaterials. They reported that prepared samples were capable of photocatalytic decolorization of brilliant red X-3B under UV and visible-light irradiation. López-Zamora et al. [25] presented a new method of TiO_2 modification with organosilane coupling agents to improve the dispersion of the particles in aqueous systems. They observed that APTES/TiO_2 samples showed better colloidal stability in water than untreated TiO_2.

The novelty of the present research was in investigating the photocatalytic activity of APTES-modified TiO_2 nanomaterials under artificial solar radiation. For the first time, photocatalysts were synthesized by solvothermal modification of TiO_2 in a pressure autoclave at 180 °C followed by calcination in an argon atmosphere in the temperature range from 800 to 1000 °C. A cationic dye methylene blue was chosen as a model organic pollutant of water.

2. Results and Discussion

2.1. Characterization of the APTES-Modified TiO_2

2.1.1. XRD Analysis

According to Figure 1A–D, in the presented X-ray diffraction patterns, all examined photocatalysts except TiO_2-Ar-900 °C and TiO_2-Ar-1000 °C showed reflections characteristic for the anatase (04-002-8296 PDF4+ card) and certain reflections characteristic for the rutile phase [26]. Only materials obtained by calcination of the starting TiO_2 at 900 °C and 1000 °C were characterized exclusively by reflections characteristic for the rutile (04-005-5923 PDF4+ card) [27,28]. The rutile presence in the starting TiO_2 was due to the addition of rutile nuclei during the raw TiO_2 pulp production process by the sulphate method [26]. The anatase-to-rutile phase transition starts generally above 600 °C [29]. Therefore, all reference materials consisted of the rutile phase.

Following the data listed in Table 1, the amount of anatase in all non-calcined APTES/TiO_2 materials was constant at about 96%. Furthermore, it should be noted that, after heating at 900 °C, the APTES-modified TiO_2 samples still had a very high amount of anatase phase (87–94%). Moreover, even nanomaterials calcined at 1000 °C did not consist exclusively of the rutile phase, as they contained 6–16% anatase phase. The silicon and carbon derived from APTES contributed to the successful delay of the anatase-to-rutile phase transformation during heating [14,30–32], so that the higher the concentration of the used modifier, the better effect of phase transformation inhibition. The crystallite size of both polymorphous forms of TiO_2 grew with increasing calcination temperature (see Table 1); although, when comparing the crystallites size of nanomaterials heated at the same temperature with and without the modifier, the crystallites of both rutile and anatase were smaller for the APTES/TiO_2 materials with respect to calcined reference samples.

For instance, the crystallite size of anatase for TiO_2-Ar-800 °C was >100 nm, while for TiO_2-4 h-180 °C-1000 mM-Ar-800 °C equalled merely 19 nm.

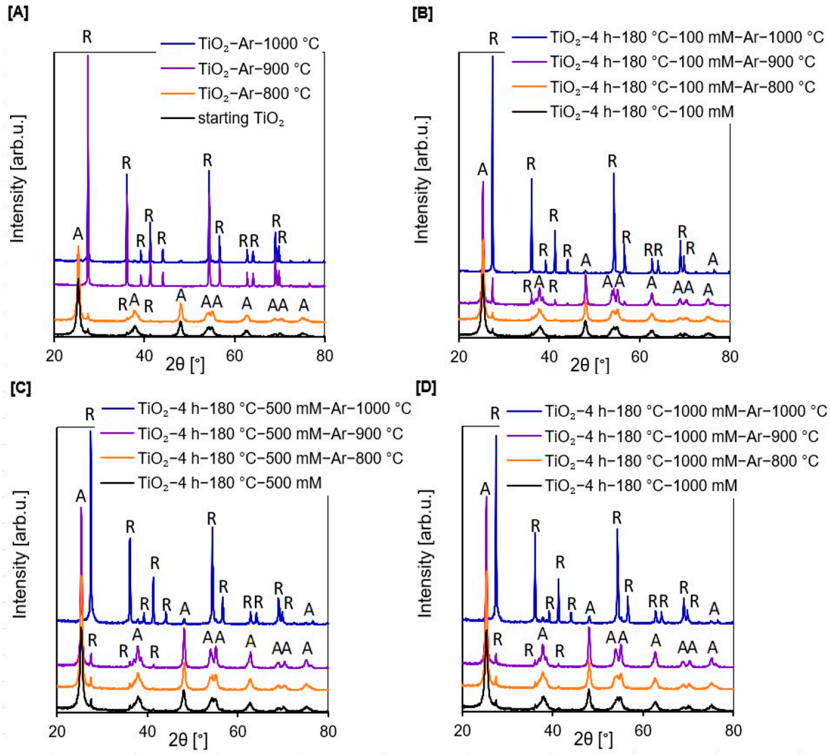

Figure 1. X-ray diffraction patterns of starting TiO_2, reference photocatalysts (**A**), and APTES/TiO_2 nanomaterials (**B**–**D**).

Table 1. Physicochemical properties of starting TiO_2, reference samples and APTES-modified TiO_2 nanomaterials.

Sample Name	S_{BET} [m^2/g]	V_{total} [cm^3/g]	V_{micro} [cm^3/g]	V_{meso} [cm^3/g]	Anatase in Crystallite Phase [%]	Anatase Crystallite Size [nm]	Rutile in Crystallite Phase [%]	Rutile Crystallite Size [nm]
starting TiO_2	207	0.370	0.070	0.300	95	14	5	21
TiO_2-Ar-800 °C	6	0.020	0.002	0.018	1	>100	99	>100
TiO_2-Ar-900 °C	3	0.008	0.002	0.006	-	-	100	>100
TiO_2-Ar-1000 °C	4	0.009	0.001	0.008	-	-	100	>100
TiO_2-4 h-180 °C-100 mM	169	0.226	0.065	0.161	96	15	4	51
TiO_2-4 h-180 °C-100 mM-Ar-800 °C	70	0.201	0.026	0.175	96	23	4	62
TiO_2-4 h-180 °C-100 mM-Ar-900 °C	35	0.113	0.041	0.072	87	34	13	>100
TiO_2-4 h-180 °C-100 mM-Ar-1000 °C	8	0.044	0.003	0.041	6	48	94	>100
TiO_2-4 h-180 °C-500 mM	124	0.162	0.048	0.114	96	15	4	48
TiO_2-4 h-180 °C-500 mM-Ar-800 °C	95	0.221	0.038	0.183	96	20	4	58
TiO_2-4 h-180 °C-500 mM-Ar-900 °C	46	0.192	0.017	0.175	94	30	6	55
TiO_2-4 h-180 °C-500 mM-Ar-1000 °C	16	0.069	0.006	0.063	12	47	88	>100
TiO_2-4 h-180 °C-1000 mM	121	0.174	0.049	0.125	96	15	4	51
TiO_2-4 h-180 °C-1000 mM-Ar-800 °C	104	0.215	0.039	0.176	96	19	4	67
TiO_2-4 h-180 °C-1000 mM-Ar-900 °C	55	0.166	0.021	0.145	94	30	6	54
TiO_2-4 h-180 °C-1000 mM-Ar-1000 °C	12	0.046	0.005	0.041	16	45	84	>100

The results reported by Xu et al. [13], Okada et al. [30], and Cheng et al. [33] were consistent with ours, and showed that, with the addition of Si to TiO_2 causes, during thermal modification, the increase in crystallite size of both polymorphous forms of TiO_2 was effectively inhibited. According to Wu et al. [34], replacement of surface hydroxyl groups prior to calcination stage with another functional group that does not condense

like –OH, such as methyl siloxyl surface group, and can produce small secondary phase particles, results in inhibition of grain boundary broadening at elevated temperatures.

The FT-IR/DRS measurements (see Figure 2A–D) confirmed the presence of silicon groups on the surface of APTES/TiO_2 nanomaterials after annealing, which could suppress the increase in crystallite size compared with the reference samples without silicon groups.

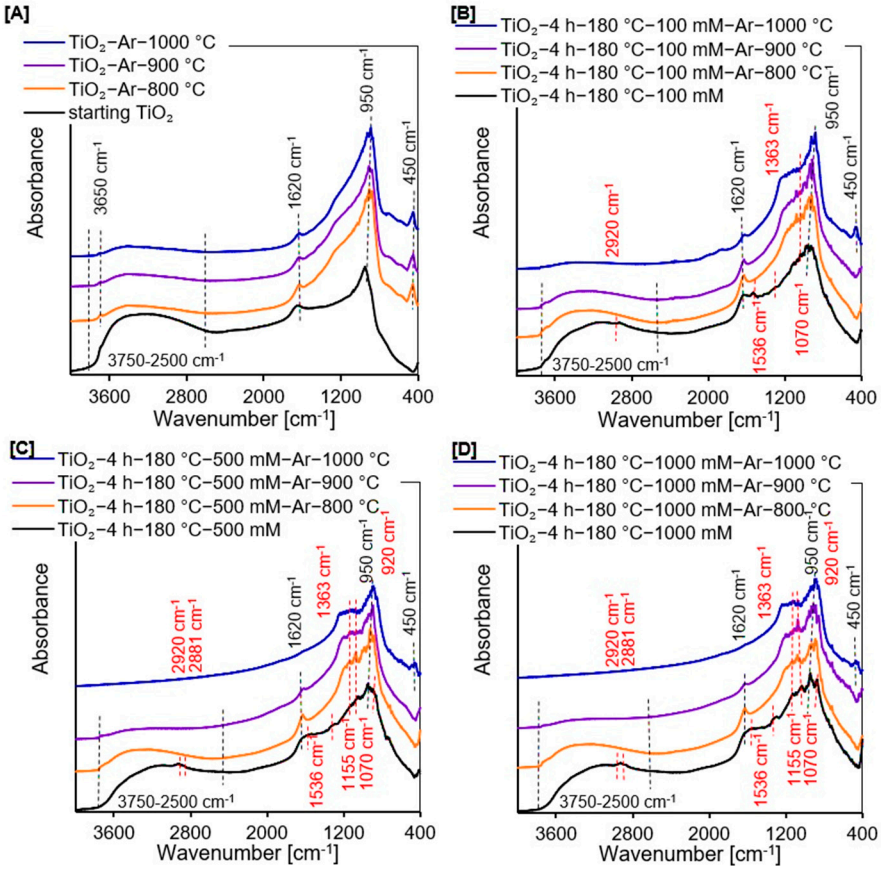

Figure 2. Diffuse reflectance Fourier transform infrared spectra of starting TiO2, reference photocatalysts (**A**), and APTES/TiO2 nanomaterials (**B**–**D**).

2.1.2. DRIFTS Measurements

The FT-IR/DRS measurements were used to identify the surface characteristics of all prepared samples. All spectra shown in Figure 2A–D exhibited certain peaks characteristic of TiO_2-based photocatalysts. A strong band located at 950 cm^{-1} is ascribed to the self-absorption of titania [35]. The narrow band at around 1620 cm^{-1} and a wide band from 3750 cm^{-1} to 2500 cm^{-1} attributed to the molecular water bending modes and stretching vibrations of surface –OH groups [14,35,36], respectively, which were observed for starting TiO_2, all non-calcined APTES-modified TiO_2, as well as for the reference materials and APTES/TiO_2 photocatalysts heated below 1000 °C. All reference samples also exhibited the low intensity band at 3650 cm^{-1}, ascribed to the stretching mode of various free –OH groups. This implies that the elimination of adsorbed water molecules followed by the removal of bridged –OH groups result in the formation of free –OH groups [37,38]. Moreover, enhancement of the annealing temperature caused a reduction in the intensity of these three aforementioned bands because of alterations in the amount of surface hydroxyl groups [39,40]. Additionally, for all reference materials and APTES-modified TiO_2 calcined at 1000 °C, a band located around 450 cm^{-1} attributed to the rutile phase was observed [41,42]. Several new characteristic bands from APTES were noted in the spectra presented in Figure 2C,D, indicating that the synthesis of new nanomaterials utilizing the solvothermal method was carried out successfully. The low-intensity bands at around

2881 cm^{-1} and 2920 cm^{-1} belong to the asymmetric and symmetric stretching vibration of alkyl groups [19,20,36,43]. The asymmetric $–NH_3^+$ deformation modes were noticed at 1552 cm^{-1} [19,39,44]. The next low-intensity band located at 1363 cm^{-1} falls in the characteristic region of C−N bonds [19,45]. In addition, the bands at about 1155 cm^{-1} and 1070 cm^{-1} correspond to the Si−O−Si stretching vibrations and Si–O–C stretching mode, respectively [19,46,47]. Furthermore, the bands located between 960 cm^{-1} and 910 cm^{-1} are characteristic for the stretching vibrations of Ti–O–Si bonds. However, the band recorded at around 920 cm^{-1} suggests that the condensation reaction occurred between silanol and surface –OH groups [36,48]. For all APTES/TiO_2 photocatalysts, bands characteristic for APTES assigned to alkyl groups, $–NH_3^+$ and C–N bonds did not occur after calcination. These groups were not permanently bonded to the TiO_2 surface. Therefore, annealing at high temperature contributed to the destruction of these bonds.

2.1.3. BET Measurements

In Figure 3A–D, the adsorption–desorption isotherms of all the prepared materials are presented. Based on the IUPAC classification, all reference samples and APTES/TiO_2 nanomaterials calcined at 1000 °C showed a type II isotherm typical for non-porous samples [49]. The other prepared photocatalysts exhibited a type IV isotherm specific for mesoporous materials, and they also showed the H3 type of hysteresis loops [49,50]. The isotherms revealing type H3 do not show limiting adsorption at high p/p_0 value and have specific desorption shoulders and lower closure points [49–51].

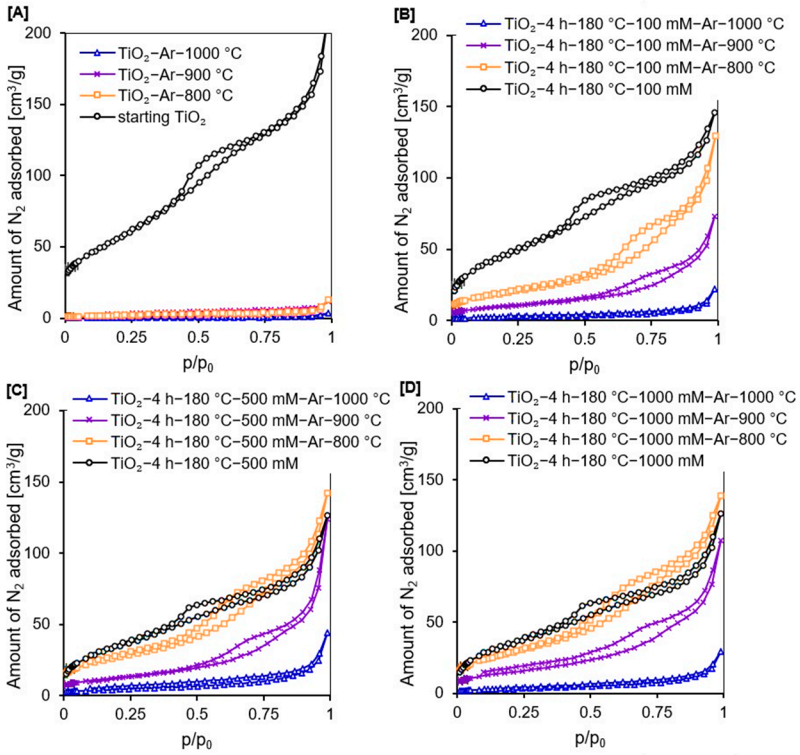

Figure 3. Adsorption–desorption isotherms of starting TiO_2, reference photocatalysts (**A**), and APTES/TiO_2 nanomaterials (**B**–**D**).

Confirmation of the observations that all calcined reference materials and APTES-modified TiO_2 heated at 1000 °C were non-porous materials, while all other photocatalysts were mesoporous materials with a small proportion of micropores, as shown by the data presented in Table 1. After modification with APTES, a significant decrease in the total pore volume and specific surface area was observed. Moreover, the higher the concentration of the organosilane modifier, the greater the reduction in the S_{BET} and V_{total}. For example, in comparison to the starting TiO_2, the S_{BET} of TiO_2-4 h-180 °C-1000 mM decreased by

86 m^2/g and V_{total} by 0.196 cm^3/g. Cheng et al. [52] noted that the specific surface area of APTES-modified TiO_2 was smaller than that of the unmodified photocatalyst due to the coating of modifier on the surface of P25 TiO_2 nanoparticles. Zhuang et al. [53] reported that the S_{BET} and the pore volume were smaller for APTES/TiO_2 materials than for untreated TiO_2 because APTES molecules could penetrate the pores of TiO_2, leading to a reduction in both S_{BET} and V_{total}. Additionally, Hou et al. [54] observed that as the concentration of APTES increases (over 2 wt.%), both the specific surface area and pore volume drastically decrease, due to the formation of a thick coating layer on the TiO_2 surface, thus, blocking the access of adsorption gas to pores.

After calcination, a significant decrease in S_{BET} and V_{total} was reported for all photocatalysts (see Table 1) due to the increase in crystallites size of the rutile and anatase phase and sintering of nanomaterials particles [55]. However, for the samples modified with APTES, the observed decrease was significantly lower than for the calcined reference materials prepared at the same temperature due to the effective inhibition of the anatase-to-rutile phase transition and the growth of the crystallites size of both TiO_2 polymorphous forms [13]. For example, for the TiO_2-Ar-900 °C, the S_{BET} was 3 m^2/g and V_{total} equalled 0.008 cm^3/g, while for the TiO_2-4 h-180 °C-1000 mM-Ar-900 °C the S_{BET} and V_{total} were 55 m^2/g and 0.166 cm^3/g, respectively. Moreover, the higher concentration of APTES used for modification, the better the inhibition of the crystallite size growth and, thus, the larger the specific surface area of the obtained nanomaterials [14]. So, for TiO_2-4 h-180 °C-100 mM-Ar-800 °C the S_{BET} was 70 m^2/g, for TiO_2-4 h-180 °C-500 mM-Ar-800 °C it was 95 m^2/g, while for TiO_2-4 h-180 °C-1000 mM-Ar-800 °C it equalled 104 m^2/g.

2.1.4. UV-Vis Diffuse Absorbance Spectroscopy

From the UV-Vis/DR spectra of all tested photocatalysts, presented in Figure 4A–D, it was noted that starting TiO_2, reference materials, and all non-calcined APTES/TiO_2 samples showed the typical absorption in the UV region because of the intrinsic band gap absorption of titanium [56]. However, after calcination, the reflectance of all examined nanomaterials decreased with the increase in the heating temperature due to the color change of photocatalysts from white (non-calcined samples), through to grey (materials calcined at 800 °C), to dark grey (semiconductors modified above 800 °C) [57,58]. The change of color was related to the presence of carbon in the studied samples. Additionally, the spectra of all reference samples and APTES-modified TiO_2 calcined at 1000 °C showed the absorption peak from 200 to 400 nm with the maximum at 226 and 305 nm. The absorption band at around 305 nm is associated with the charge transfer from O^{2-} to Ti^{4+}, related to the excitation from the valence to the conduction band [59–61]. After calcination, there was a red shift of the absorption edge towards visible light. The increased absorption was most likely due to the presence of rutile phase, which has an intrinsically smaller band gap energy compared with the pure anatase phase [62,63]. Moreover, the intensity of these bands decreased with increasing concentration of modifier due to the delay of the anatase-to-rutile phase transformation.

According to the band gap energy values of all the studied samples shown in Table 2, it was noted that after calcination in an inert atmosphere, the E_g of starting TiO_2 of 3.29 eV decreased to 3.03 eV for TiO_2-Ar-800 °C and TiO_2-Ar-900 °C samples and 3.01 eV for TiO_2-Ar-1000 °C. While for APTES/TiO_2 nanomaterials significant changes in E_g were reported only for photocatalysts calcined at 1000 °C. This was mainly attributed to the anatase-to-rutile phase transformation [64,65].

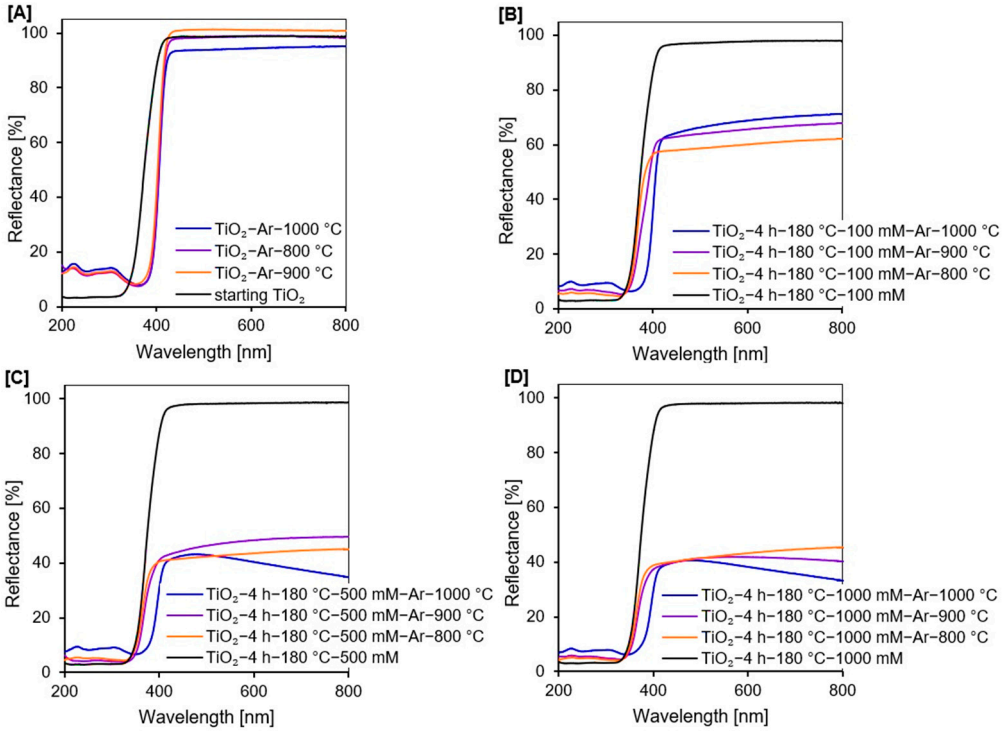

Figure 4. UV-Vis diffuse reflectance spectra of starting TiO_2, reference photocatalysts (**A**), and APTES/TiO_2 nanomaterials (**B**–**D**).

Table 2. The zeta potential values, carbon and nitrogen contents, and band gap energy (E_g) of starting TiO_2, reference samples, and APTES-modified TiO_2 nanomaterials.

Sample Name	Zeta Potential δ [mV]	Carbon Content [wt.%]	Nitrogen Content [wt.%]	E_g [eV]
starting TiO_2	+12.8	-	0.18	3.29
TiO_2-Ar-800 °C	−35.9	-	-	3.03
TiO_2-Ar-900 °C	−36.7	-	-	3.03
TiO_2-Ar-1000 °C	−41.3	-	-	3.01
TiO_2-4 h-180 °C-100 mM	+13.6	2.10	0.79	3.27
TiO_2-4 h-180 °C-100 mM-Ar-800 °C	−38.5	0.17	0.08	3.27
TiO_2-4 h-180 °C-100 mM-Ar-900 °C	−45.8	0.08	-	3.21
TiO_2-4 h-180 °C-100 mM-Ar-1000 °C	−49.1	0.03	-	3.02
TiO_2-4 h-180 °C-500 mM	+22.8	3.82	1.41	3.27
TiO_2-4 h-180 °C-500 mM-Ar-800 °C	−47.4	0.26	0.08	3.24
TiO_2-4 h-180 °C-500 mM-Ar-900 °C	−51.0	0.22	-	3.24
TiO_2-4 h-180 °C-500 mM-Ar-1000 °C	−41.3	0.11	-	2.97
TiO_2-4 h-180 °C-1000 mM	+12.1	4.10	1.47	3.27
TiO_2-4 h-180 °C-1000 mM-Ar-800 °C	−51.6	0.27	0.11	3.23
TiO_2-4 h-180 °C-1000 mM-Ar-900 °C	−60.0	0.22	-	3.22
TiO_2-4 h-180 °C-1000 mM-Ar-1000 °C	−54.4	0.08	-	2.95

2.1.5. SEM and EDX Mapping Analysis

From the SEM image shown in Figure 5A, it was noted that the starting TiO_2 morphology was relatively homogenous, but the particles formed aggregates. For TiO_2-4 h-180 °C-500 mM-Ar-900 °C sample (see Figure 5B), it was observed that functionalization contributed to the increase in aggregates size. The results of EDX mapping analysis, presented in Figure 5C,D, confirmed the presence of Ti and O, as well as Si and C expected after modification, and exhibited that all studied elements were uniformly dispersed on the TiO_2 surface. The results of EDX mapping analysis are the average of measurements

taken at 5 different points. As expected, it was noted that the silicon content increased with an increasing amount of APTES. Thus, the TiO_2-4 h-180 °C-100 mM-Ar-900 °C sample contained 1.25 wt.% Si, while TiO_2-4 h-180 °C-500 mM-Ar-900 °C and TiO_2-4 h-180 °C-1000 mM-Ar-900 °C had 2.13 and 2.26 wt.% Si, respectively.

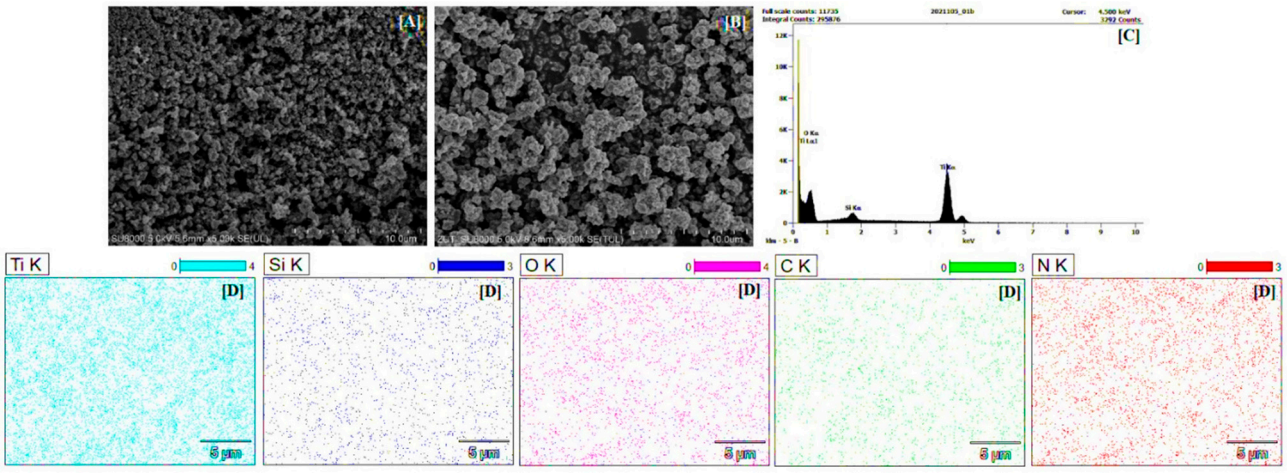

Figure 5. The SEM images of starting TiO_2 (**A**), TiO_2-4 h-180 °C-500 mM-Ar-900 °C (**B**), EDX spectrum (**C**), and EDX mappings of TiO_2-4 h-180 °C-500 mM-Ar-900 °C (**D**).

2.1.6. Carbon and Nitrogen Content Analysis

Based on the carbon and nitrogen content analysis (see Table 2), the existence of C and N in the non-calcined APTES/TiO_2 materials confirmed the APTES presence in the samples received after functionalization of starting TiO_2. As expected, it was also observed that the higher the amount of modifier, the higher the content of the analyzed elements [12,66]. Moreover, it was noted that the quantity of carbon and nitrogen reduced drastically after calcination and kept decreasing with increasing temperature of modification because of the N- and C-containing functional groups decomposition and removal them from the photocatalysts surface [35,67]. Unfortunately, the N content in the APTES/TiO_2 nanomaterials annealed above 800 °C was below the detection level of the device. The results derived from the C and N content analysis agreed with the data obtained from FT-IR/DR spectra (see Figure 2B–D), which demonstrated a significant decrease in the amount of both analyzed elements in APTES-modified TiO_2 after the calcination. The presence of 0.18 wt.% of nitrogen could be explained by the preparation procedure of the starting TiO_2 involving pretreatment with ammonia water, used to remove residual sulfuric acid from the crude TiO_2 slurry produced by the sulfate method [68].

2.1.7. Zeta Potential Measurements

The zeta potential measurements confirmed the change of surface character from positively to negatively charged after APTES modification (see Table 2). For the reference materials, the change in the TiO_2 surface charge was most likely related to the anatase-to-rutile phase transformation and total transition to rutile phase. Our observations were consistent with Haider et al. [69], Pinheiro Pinton et al. [70], and Chellappah et al. [71], who reported that the pure rutile exhibits negative zeta potential values. In the case of organosilane/TiO_2 nanomaterials, Talavera-Pech et al. [72] and Goscianska et al. [73] observed that the cationic amino groups from aminosilane readily link the TiO_2 surface groups resulting in the positively charged surface. However, the FT-IR/DR spectra shown in Figure 2B–D, and the reduction in nitrogen content (see Table 2), indicated that amino groups were not present on the TiO_2 surface after calcination. The silicon groups were mainly found on the calcined APTES/TiO_2 surface. Li et al. [74], Ferreira-Neto et al. [75], and Worathanakul et al. [76] noted that silica-modified titanium dioxide materials were characterized by a negative value of zeta potential.

2.2. Adsorption and Photocatalytic Studies

Before studying the photocatalytic activity of the prepared samples, tests were conducted to establish the adsorption–desorption equilibrium at the photocatalyst–dye interface. The results are presented in Figure 6A–D. For all examined nanomaterials, equilibrium was reached after 60 min. It was also observed that calcination enhanced the adsorption abilities of the obtained materials. From the zeta potential values (see Table 2), it can be concluded that transformation of TiO_2 surface charge from positive to negative after annealing increased the adsorption abilities of the tested samples. The negatively charged semiconductor surface has a higher potential of contact with the positively charged methylene blue molecules, due to the attractive electrostatic interactions [77–79]. Calcined APTES/TiO_2 nanomaterials showed clearly dissimilar adsorption degrees of the methylene blue compound; although, they demonstrated similar zeta potential values (i.e., 19% for TiO_2-4 h-180 °C-500 mM-Ar-1000 °C but 75% of adsorbed dye for TiO_2-4 h-180 °C-500 mM-Ar-800 °C). It is generally agreed that adsorption properties are ascribed to larger specific surface area values. In this case, among all calcined APTES/TiO_2 samples, nanomaterials heated at 800 °C were characterized by the highest S_{BET} area value, i.e., for TiO_2-4 h-180 °C-1000 mM-Ar-800 °C the value reached 104 m^2/g, while for TiO_2-4 h-180 °C-1000 mM-Ar-1000 °C it was only 12 m^2/g.

Photodegradation of methylene blue in the presence of APTES/TiO_2 photocatalysts was investigated under artificial solar light. The results are presented in Figure 7A–D as a plot of C_t/C_0 versus irradiation time, where C_0 is the initial concentration of dye and C_t is the concentration at time t.

Methylene blue decomposition in the absence of photocatalyst (photolysis test) was negligible (about 2%). Therefore, the effect of photosensitization can be neglected. After thermal modification of starting TiO_2 no significant changes were observed regarding the improvement of the dye decomposition by the reference materials (see Figure 7A). For the TiO_2-Ar-900 °C sample, only about 6% methylene blue decomposition degree was achieved (see Figure 8) after 360 min of irradiation.

For APTES-modified TiO_2 samples obtained after calcination, a marked improvement in photocatalytic activity was noted. The presence of silicon and carbon in the nanomaterials effectively delays the anatase-to-rutile phase transformation, as well as inhibit the growth of the crystallites size of both TiO_2 polymorphous forms during calcination [14,30,31]. Thus, compared with the reference samples heated at the same temperature, calcined APTES/TiO_2 photocatalysts exhibited higher values of specific surface area and pore volume, as well as a larger content of a more active anatase phase, which contributed to a higher methylene blue decomposition degree [12,80]. For all three modifier concentrations used for preparation (100 mM, 500 mM, and 1000 mM), the best methylene blue decomposition degree was received for samples annealed at 900 °C. To explain the highest activity of this nanomaterials, the FT-IR/DR spectra of selected materials were determined after the adsorption process (see Figure 9).

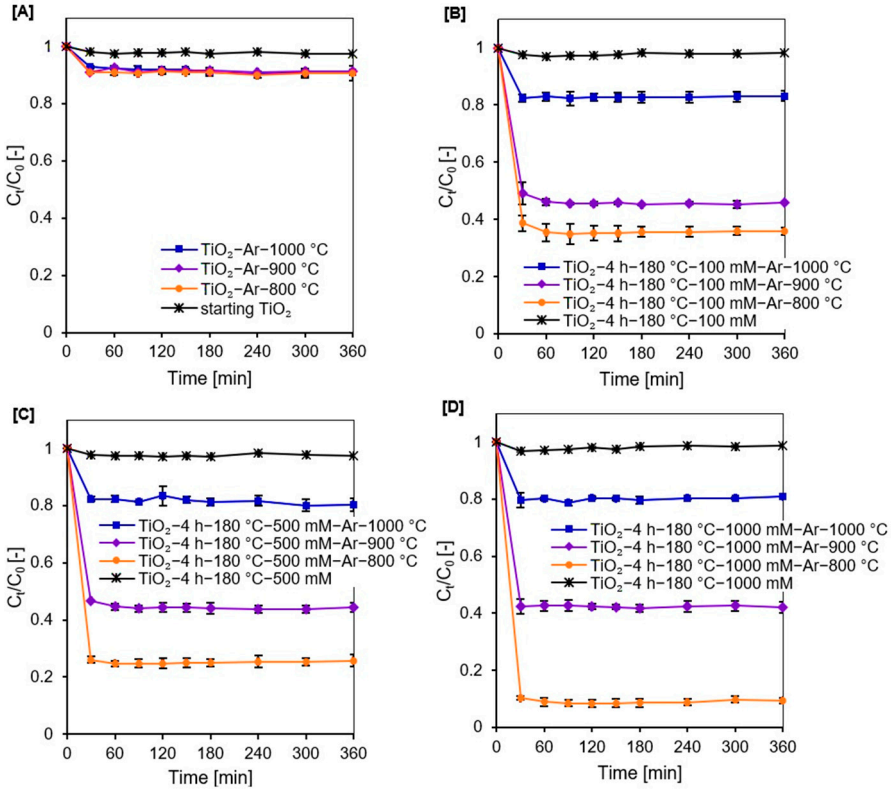

Figure 6. Methylene blue adsorption degree on the surface of starting TiO_2, reference nanomaterials (**A**), and APTES/TiO_2 photocatalysts before and after calcination (**B**–**D**).

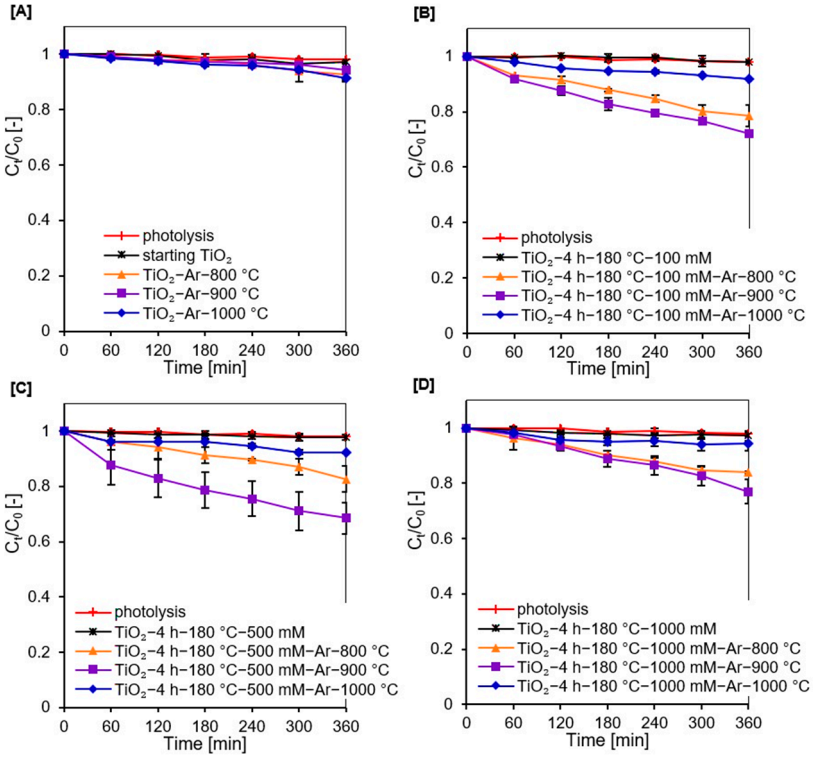

Figure 7. Methylene blue decomposition under artificial solar light irradiation for starting TiO_2, reference nanomaterials (**A**), and APTES/TiO_2 photocatalysts before and after calcination (**B**–**D**).

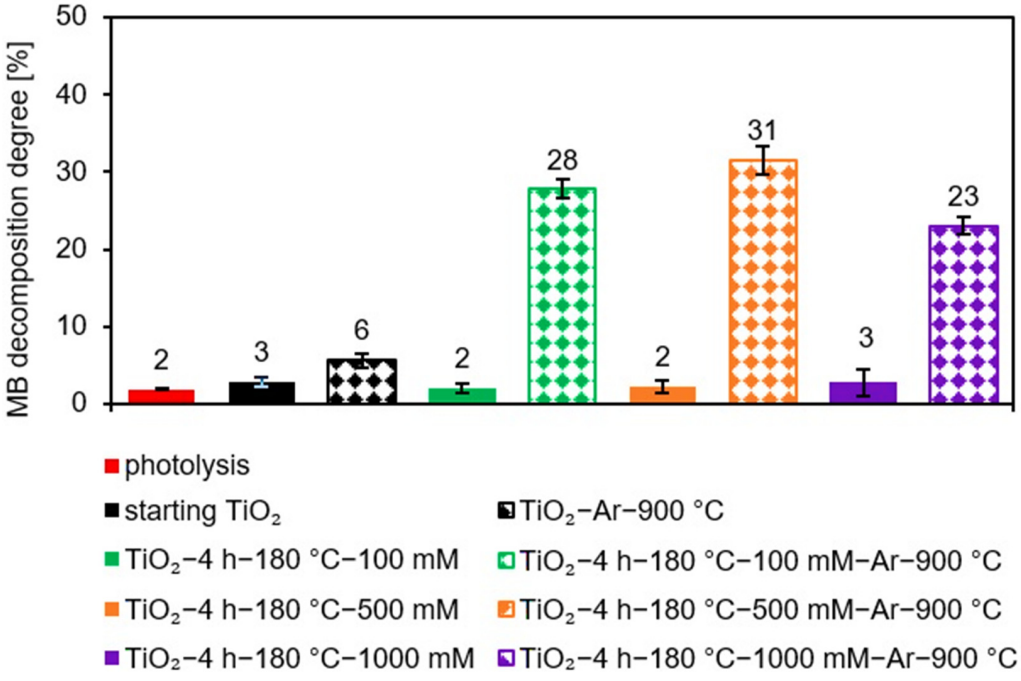

Figure 8. Methylene blue decomposition degree after 360 min of artificial solar light radiation for starting TiO_2, reference nanomaterial (TiO_2-Ar-900 °C), and APTES/TiO_2 samples modified with different amounts of organosilane before and after calcination at 900 °C.

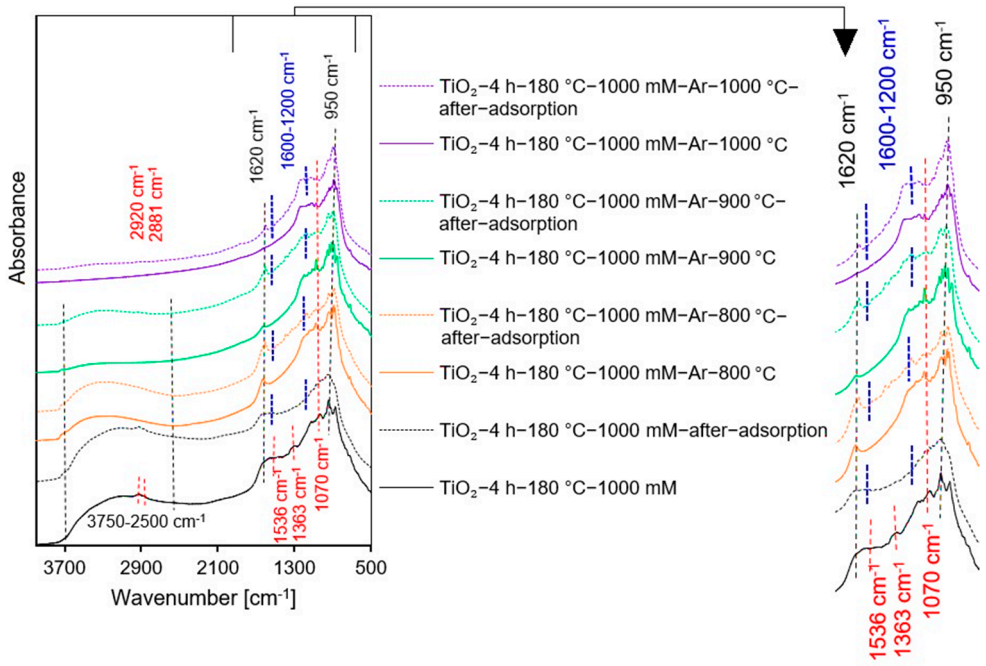

Figure 9. FT-IR/DR spectra of the selected samples before and after adsorption of methylene blue.

The noticeable enhancement in the intensity of the band localized at 1200–1600 cm^{-1} suggested that carbon deposits from methylene blue appeared on the photocatalyst surface after adsorption, which strongly limited the photocatalytic efficiency [81,82]. Although APTES-modified TiO_2 photocatalysts calcined at 800 °C showed the highest specific surface area and pore volume, they also showed the highest dye adsorption. As a result, the highest number of active sites on the TiO_2 surface was blocked by methylene blue molecules. Since presumably at high dye concentrations, the generation of hydroxyl radicals on the photocatalyst surface is limited due to the active sites being covered by dye ions, leading

to a decrease in activity [83]. Photocatalysts heated at 1000 °C were characterized by very small specific surface area and pore volume. They also contained a higher amount of rutile than the anatase phase resulting the low photoactivity [84]. Therefore, TiO_2 modified with APTES calcined at 900 °C showed the highest methylene blue decomposition degree. Furthermore, at a constant annealing temperature of 900 °C, after 360 min of artificial solar light radiation, the methylene blue degradation degree was 23%, 28%, and 31% for nanomaterials modified with 1000 mM, 100 mM, and 500 mM, respectively. Although the TiO_2-4 h-180 °C-1000 mM-Ar-900 °C photocatalyst exhibited a larger specific surface area than the TiO_2-4 h-180 °C-500 mM-Ar-900 °C and TiO_2-4 h-180 °C-100 mM-Ar-900 °C samples, it showed the highest dye adsorption degree. For the TiO_2 modified with 1000 mM of APTES, the methylene blue adsorption degree was 59%, while for 500 mM was 55%, and for 100 mM it equaled 53%. Therefore, most of active sites were blocked by adsorbed dye molecules on the surface of the TiO_2-4 h-180 °C-1000 mM-Ar-900 °C sample, resulting in a decrease in photocatalytic activity. Besides the confirmed influence of physicochemical properties on photocatalytic efficiency of the prepared semiconductors, the crucial role of adsorption process was also proved. Considering the highest photoactivity and economic aspects according to which the less modifier the better, TiO_2-4 h-180 °C-500 mM-Ar-900 °C was selected as the most prospective material.

3. Experimental

3.1. Materials and Reagents

All photocatalysts were obtained based on the crude TiO_2 slurry, delivered from the chemical plant Grupa Azoty Zakłady Chemiczne "Police" S.A. (Police, Poland). Before modification, raw TiO_2 pulp was pre-treated to reach a pH of 6.8. This step was described in detail in our previous article [26]. The received sample was denoted as starting TiO_2. The modifier of the starting TiO_2 was 3-aminopropyltriethoxysilane (APTES, ≥98%) from Merck KGaA (Darmstadt, Germany). Ethanol from P.P.H. "STANLAB" Sp.J., (96%, Poland) was utilized as a solvent of APTES. For photocatalytic activity tests, the methylene blue (Firma Chempur®, Piekary Śląskie, Poland) was used as a model organic water pollutant.

3.2. Preparation Procedure of APTES/TiO_2 Nanomaterials

The APTES-modified TiO_2 nanomaterials were prepared via the solvothermal method and calcination process. To modify the TiO_2 surface, various amounts of modifier were used and the concentrations of APTES in the solvent were 100, 500, and 1000 mM. In the first step, 5 g of starting TiO_2 was mixed with 25 mL solution of APTES and modified in a pressure autoclave at 180 °C for 4 h, providing continuous stirring at 500 rpm. Next, the obtained suspension was rinsed with ethanol and distilled water to remove all remaining chemicals. Then, the material was dried in a lab dryer for 24 h at 105 °C. The obtained samples were denoted as TiO_2-4 h-180 °C-XmM, where X is the concentration of modifier in a solvent. In the second stage, the photocatalyst was annealed in an argon atmosphere (purity 5.0, Messer Polska Sp. z o.o., Poland). The calcination process was carried out in a range of temperatures from 800 to 1000 °C, where Δt = 100 °C. The quartz crucible with the resulting material was inserted into a quartz tube in the central section of the GHC 12/900 horizontal furnace (Carbolite Gero, Ltd., UK). Before heating, Ar was run through a tube for 30 min to eliminate residual air. Afterwards, the furnace was heated to the desired temperature at an Ar flow rate of 180 mL/min, with a calcination time of 4 h. Next, the furnace cooled gradually to room temperature. Samples received after annealing of starting TiO_2 in the inert gas atmosphere were named reference materials, denoted as TiO_2-4 h-Ar-Y °C, while APTES-modified TiO_2 received after calcination were denoted as TiO_2-4 h-180 °C-XmM-Ar-Y °C, where Y is the temperature of annealing.

3.3. Characterization of Photocatalysts

The X-ray powder diffraction analysis (Malvern PANalytical B.V., Almelo, the Netherlands, utilizing Cu Kα radiation (λ = 1.54056 Å), applied to determine the crystalline

structure of the prepared samples. The PDF-4+ 2014 International Centre for Diffraction Data database was used to specify the phase composition (for rutile: 04-005-5923 PDF4+ card; for anatase: 04-002-8296 PDF4+ card) and to calculate the mean crystallites size the Scherrer's equation was used. The spectrometer FT-IR-4200 (JASCO International Co. Ltd., Tokyo, Japan), fitted with DiffuseIR accessory (PIKE Technologies, USA), was used to detect the functional groups on the surface of the tested nanomaterials. A CN628 elemental analyzer (LECO Corporation, St. Joseph, MI, USA) was selected to measure total carbon and nitrogen in photocatalysts' samples. For non-calcined APTES/TiO_2 nanomaterials, the certified ethylenediaminetetraacetic acid (EDTA) standard (Elemental Microanalysis Ltd., Okehampton, UK) containing 41.04 $\pm$ 0.15 wt.% of carbon and 9.56 $\pm$ 0.11 wt.% of nitrogen was utilized to prepare the calibration curves. While for calcined APTES-modified TiO_2, a certified soil standard (Elemental Microanalysis Ltd., Okehampton, UK) containing 0.043 wt.% $\pm$ 0.01 of nitrogen and 0.46 wt.% $\pm$ 0.15 of carbon, was used. The zeta potential values were measured using a ZetaSizer NanoSeries ZS (Malvern PANalytical Ltd., Malvern, UK) instrument. In order to calculate the Brunauer–Emmett–Teller (BET) specific surface area and pore volume, the low-temperature nitrogen adsorption–desorption measurements at 77 K were performed on the QUADRASORB evoTM Gas Sorption analyzer (Anton Paar GmbH, Graz, Austria). All materials were degassed for 12 h at 100 °C under a high vacuum prior to measurements to eliminate all remaining contaminants on the tested samples' surface. The total pore volume (V_{total}) was derived from the single-point value from the nitrogen adsorption isotherms at relative pressure p/p_0 = 0.99, while micropore volume (V_{micro}) was calculated using the Dubinin–Radushkevich method, and the mesopore volume (V_{meso}) was derived from the difference between V_{total} and V_{micro}. The Hitachi SU8020 Ultra-High Resolution Field Emission Scanning Electron Microscope (Hitachi Ltd., Tokyo, Japan) was used to characterize the surface morphology of synthesized photocatalysts. The spectrophotometer UV-Vis V-650 (JASCO International Co., Tokyo, Japan), fitted with a PIV-756 integrating sphere accessory, allowing measurement of DR spectra (JASCO International Co., Tokyo, Japan), was utilized to investigate the light reflectance abilities of the prepared samples. Spectralon® Diffuse Reflectance Material (Labsphere, New Hampshire, NE, USA) was selected as the reference material. The Tauc transformation was used to calculate the band gap energy (E_g) [85].

3.4. Photocatalytic Activity Measurements

The methylene blue decomposition process under artificial solar light irradiation (radiation intensity of 837 W/m^2 for 300–2800 nm and 0.3 W/m^2 for the 280–400 nm regions) was carried out to determine the photocatalytic properties of all the prepared samples. All experiments were conducted in a glass beaker using 0.5 L of dye solution with the initial concentration of 5 mg/L and 0.5 g/L of the appropriate semiconductor. Before irradiation, the suspension was magnetically stirred in light-free conditions for 60 min to establish the adsorption–desorption equilibrium at the photocatalyst–methylene blue interface. Then, the mixture was subjected to artificial solar light radiation, and the total exposure time was 360 min. The absorbance value of methylene blue, from which the dye concentration was calculated, was measured every 60 min using a spectrometer UV-Vis V-630 (Jasco International Co., Tokyo, Japan), at the maximum wavelength of 663 nm. Prior to each measurement, 10 mL of the collected suspension was centrifuged to eliminate the suspended TiO_2 nanoparticles. The methylene blue decomposition degree was calculated according to the following equation:

$$D = \frac{C_0 - C_t}{C_0} \times 100\% \quad (1)$$

where D is dye decomposition degree (%), C_0 is the initial concentration of the methylene blue solution after the adsorption process (mg/L), and C_t is the concentration of the dye after illumination for t min (mg/L).

4. Conclusions

The effect of solvothermal modification of TiO_2 via APTES, combined with the heat treatment at 800–1000 °C, on the photocatalytic activity of APTES/TiO_2 nanomaterials under artificial solar light irradiation, was a novelty of the presented study. The presence of APTES on the surface of TiO_2 was proved via FT-IR/DRS measurements, nitrogen and carbon analyses, and the EDX mapping. It was noted that the presence of Si and C in the APTES-modified TiO_2 contributed to the effective inhibition of the anatase-to-rutile phase transformation and the growth of the crystallites size of both polymorphous forms of TiO_2 during calcination at high temperature. Thus, the calcined APTES/TiO_2 photocatalysts exhibited higher values of S_{BET} and pore volume compared with unmodified reference samples. Changing the surface charge of modified TiO_2 from positive to negative after calcination increased the methylene blue adsorption degree. However, due to blocking of active sites on the semiconductor surface by APTES molecules, the adsorption process negatively affected the photocatalytic properties. The calcination process increased the artificial solar light-driven photoactivity of all APTES/TiO_2 materials. For all three tested APTES concentrations, the best dye decomposition degree was received for nanomaterials calcined at 900 °C due to higher S_{BET} values than materials calcined at 1000 °C and larger number of active sites available on the TiO_2 surface in comparison with samples heated at 800 °C. Considering the highest photocatalytic activity and economic aspects, TiO_2-4 h-180 °C-500 mM-Ar-900 °C was found to be the most promising photocatalyst.

Author Contributions: Conceptualization, A.S., A.W. and E.K.-N.; data curation, E.K.-N. and A.W.M.; formal analysis, A.S. and E.K.-N.; funding acquisition, A.W.M.; investigation, A.S. and A.W.; methodology, A.S. and A.W.; project administration, A.W.M.; visualization, P.R.-K.; writing—original draft preparation, A.S.; writing—review and editing, P.R.-K., A.W. and E.K.-N. All authors have read and agreed to the published version of the manuscript.

Funding: This work was supported by grant 2017/27/B/ST8/02007 from the National Science Centre, Poland.

Institutional Review Board Statement: Not applicable.

Informed Consent Statement: Not applicable.

Data Availability Statement: The data presented in this study are available on request from the corresponding author.

Conflicts of Interest: The authors declare no conflict of interest.

References

1. Piątkowska, A.; Janus, M.; Szymański, K.; Mozia, S. C-,N- and S-doped TiO_2 photocatalysts: A review. *Catalysts* **2021**, *11*, 144. [CrossRef]
2. Zhao, C.; Wang, Z.; Li, X.; Yi, X.; Chu, H.; Chen, X.; Wang, C.-C. Facile fabrication of BUC-21/$Bi_{24}O_{31}Br_{10}$ composites for enhanced photocatalytic Cr(VI) reduction under white light. *Chem. Eng. J.* **2020**, *389*, 123431. [CrossRef]
3. Reghunath, S.; Pinheiro, D.; Devi, K.R.S. A review of hierarchical nanostructures of TiO_2: Advances and applications. *Appl. Surf. Sci. Adv.* **2021**, *3*, 100063. [CrossRef]
4. Koe, W.S.; Lee, J.W.; Chong, W.C.; Pang, Y.L.; Sim, L.C. An overview of photocatalytic degradation: Photocatalysts, mechanisms, and development of photocatalytic membrane. *Environ. Sci. Pollut. Res.* **2020**, *27*, 2522–2565. [CrossRef] [PubMed]
5. Li, H.; Li, W.; Liu, X.; Ren, C.; Miao, X.; Li, X. Engineering of Gd/Er/Lu-triple-doped Bi_2MoO_6 to synergistically boost the photocatalytic performance in three different aspects: Oxidizability, light absorption and charge separation. *Appl. Surf. Sci.* **2019**, *463*, 556–565. [CrossRef]
6. Nasirian, M.; Lin, Y.P.; Bustillo-Lecompte, C.F.; Mehrvar, M. Enhancement of photocatalytic activity of titanium dioxide using non-metal doping methods under visible light: A review. *Int. J. Environ. Sci. Technol.* **2017**, *15*, 2009–2032. [CrossRef]
7. Mittal, A.; Mari, B.; Sharma, S.; Kumari, V.; Maken, S.; Kumari, K.; Kumar, N. Non-metal modified TiO_2: A step towards visible light photocatalysis. *J. Mater. Sci. Mater. Electron.* **2019**, *30*, 3186–3207. [CrossRef]
8. Ramandi, S.; Entezari, M.H.; Ghows, N. Sono-synthesis of solar light responsive S-N-C-tri doped TiO_2 photo-catalyst under optimized conditions for degradation and mineralization of diclofenac. *Ultrason. Sonochem.* **2017**, *38*, 234–245. [CrossRef]
9. Sushma, C.; Kumar, S.G. C–N–S tridoping into TiO_2 matrix for photocatalytic applications: Observations, speculations and contradictions in the codoping process. *Inorg. Chem. Front.* **2017**, *4*, 1250–1267. [CrossRef]

10. Dong, F.; Zhao, W.; Wu, Z. Characterization and photocatalytic activities of C, N and S co-doped TiO_2 with 1D nanostructure prepared by the nano-confinement effect. *Nanotechnology* **2008**, *19*, 365607. [CrossRef]
11. Lei, X.F.; Xue, X.X.; Yang, H.; Chen, C.; Li, X.; Niu, M.C.; Gao, X.Y.; Yang, Y.T. Effect of calcination temperature on the structure and visible-light photocatalytic activities of (N, S and C) co-doped TiO_2 nano-materials. *Appl. Surf. Sci.* **2015**, *332*, 172–180. [CrossRef]
12. Klaysri, R.; Tubchareon, T.; Praserthdam, P. One-step synthesis of amine-functionalized TiO_2 surface for photocatalytic decolorization under visible light irradiation. *J. Ind. Eng. Chem.* **2017**, *45*, 229–236. [CrossRef]
13. Xu, G.Q.; Zheng, Z.X.; Wu, Y.C.; Feng, N. Effect of silica on the microstructure and photocatalytic properties of titania. *Ceram. Int.* **2009**, *35*, 1–5. [CrossRef]
14. Tobaldi, D.M.; Tucci, A.; Skapin, A.S.; Esposito, L. Effects of SiO_2 addition on TiO_2 crystal structure and photocatalytic activity. *J. Eur. Ceram. Soc.* **2010**, *30*, 2481–2490. [CrossRef]
15. Abdullah, A.M.; Al-Thani, N.J.; Tawbi, K.; Al-Kandari, H. Carbon/nitrogen-doped TiO_2: New synthesis route, characterization and application for phenol degradation. *Arab. J. Chem.* **2016**, *9*, 229–237. [CrossRef]
16. Liu, S.; Yang, L.; Xu, S.; Luo, S.; Cai, Q. Photocatalytic activities of C–N-doped TiO_2 nanotube array/carbon nanorod composite. *Electrochem. Commun.* **2009**, *11*, 1748–1751. [CrossRef]
17. Martinez-Oviedo, A.; Kshetri, Y.K.; Joshi, B.; Wohn Lee, S. Surface modification of blue TiO_2 with silane coupling agent for NOx abatement. *Prog. Nat. Sci. Mater.* **2021**, *31*, 230–238. [CrossRef]
18. Nguyen, T.C.; Nguyen, T.D.; Vu, D.T.; Dinh, D.P.; Nguyen, A.H.; Ly, T.N.L.; Dao, P.H.; Nguyen, T.L.; Bach, L.G.; Thai, H. Modification of titanium dioxide nanoparticles with 3-(trimethoxysilyl)propyl methacrylate silane coupling agent. *J. Chem.* **2020**, 1381407. [CrossRef]
19. Meroni, D.; Lo Presti, L.; Di Liberto, G.; Ceotto, M.; Acres, R.G.; Prince, K.C.; Bellani, R.; Soliveri, G.; Ardizzone, S. A close look at the structure of the TiO_2 APTES interface in hybrid nanomaterials and degradation pathway: An experimental and theoretical study. *J. Phys. Chem. C* **2017**, *121*, 430–440. [CrossRef]
20. Shakeri, A.; Yip, D.; Badv, M.; Imani, S.M.; Sanjari, M.; Didar, T.F. Self-cleaning ceramic tiles produced via stable coating of TiO_2 nanoparticles. *Materials* **2018**, *11*, 1003. [CrossRef]
21. Nadzirah, S.; Zainudin, N.; Hashim, U.; Derman, M.N.B.; Chong, K.F.; Rahim Ruslinda, A. Rapid and sensitive *E. coli* DNA detection by titanium dioxide nanoparticles. In Proceedings of the 2014 IEEE Conference on Biomedical Engineering and Sciences, Miri, Malaysia, 8–10 December 2014.
22. Andrzejewska, A.; Krysztafkiewicz, A.; Jesionowski, T. Adsorption of organic dyes on the aminosilane modified TiO_2 surface. *Dyes Pigments* **2004**, *62*, 121–130. [CrossRef]
23. Lee, K.N.; Kim, Y.; Lee, C.W.; Lee, J.S. Simultaneous amination of TiO_2 nanoparticles in the gas phase synthesis for bio-medical applications. *IOP Conf. Ser. Mater. Sci. Eng.* **2011**, *18*, 082021. [CrossRef]
24. Bao, N.; Wu, G.; Niu, J.; Zhang, Q.; He, S.; Wang, J. Wide spectral response and enhanced photocatalytic activity of TiO_2 continuous fibers modified with aminosilane coupling agents. *J. Alloys Compd.* **2014**, *599*, 40–48. [CrossRef]
25. López-Zamora, L.; Martínez-Martínez, H.N.; González-Calderón, J.A. Improvement of the colloidal stability of titanium dioxide particles in water through silicon based coupling agent. *Mater. Chem. Phys.* **2018**, *217*, 285–290. [CrossRef]
26. Kusiak-Nejman, E.; Wanag, A.; Kapica-Kozar, J.; Kowalczyk, Ł.; Zgrzebnicki, M.; Tryba, B.; Przepiórski, J.; Morawski, A.W. Methylene blue decomposition on TiO_2/reduced graphene oxide hybrid photocatalysts obtained by a two-step hydrothermal and calcination synthesis. *Catal. Today* **2020**, *357*, 630–637. [CrossRef]
27. Sienkiewicz, A.; Wanag, A.; Kusiak-Nejman, E.; Ekiert, E.; Rokicka-Konieczna, P.; Morawski, A.W. Effect of calcination on the photocatalytic activity and stability of TiO_2 photocatalysts modified with APTES. *J. Environ. Chem. Eng.* **2021**, *9*, 104794. [CrossRef]
28. Haider, A.J.; Jameel, Z.N.; Taha, S.Y. Synthesis and characterization of TiO_2 nanoparticles via sol-gel method by pulse laser ablation. *Eng. Technol. J.* **2015**, *33*, 761–771.
29. Byrne, C.; Fagan, R.; Hinder, S.; McCormack, D.E.; Pillai, S.C. New approach of modifying the anatase to rutile transition temperature in TiO_2 photocatalysts. *RSC Adv.* **2016**, *6*, 95232–95238. [CrossRef]
30. Okada, K.; Yamamoto, N.; Kameshima, Y.; Yasumori, A.; MacKenzie, K.J.D. Effect of silica additive on the anatase-to-rutile phase transition. *Ceram. Soc.* **2001**, *84*, 1591–1596. [CrossRef]
31. Morawski, A.W.; Janus, M.; Tryba, B.; Toyoda, M.; Tsumura, T.; Inagaki, M. Carbon modified TiO_2 photocatalysts for water purification. *Pol. J. Chem. Technol.* **2009**, *11*, 46–50. [CrossRef]
32. Fu, G.; Zhou, P.; Zhao, M.; Zhu, W.; Yan, S.; Yu, T.; Zou, T. Carbon coating stabilized Ti_3^+-doped TiO_2 for photocatalytic hydrogen generation under visible light irradiation. *Dalton Trans.* **2015**, *44*, 12812–12817. [CrossRef] [PubMed]
33. Cheng, P.; Zheng, M.; Jin, Y.; Huang, Q.; Gu, M. Preparation and characterization of silica-doped titania photocatalyst through sol–gel method. *Mater. Lett.* **2003**, *57*, 2989–2994. [CrossRef]
34. Wu, N.L.; Wang, S.Y.; Rusakova, A. Inhibition of crystallite growth in the sol-gel synthesis of nanocrystalline metal oxides. *Science* **1999**, *285*, 1375–1377. [CrossRef] [PubMed]
35. Kusiak-Nejman, E.; Wanag, A.; Kapica-Kozar, J.; Morawski, A.W. Preparation and characterisation of TiO_2 thermally modified with cyclohexane vapours. *Int. J. Mater. Prod. Technol.* **2016**, *52*, 286–297. [CrossRef]

36. Zanchetta, E.; Della Giustina, G.; Brusatin, G. One-step patterning of double tone high contrast and high refractive index inorganic spin-on resist. *J. Appl. Phys.* **2014**, *116*, 103504. [CrossRef]
37. Pramanik, A.; Bhattacharjee, K.; Mitra, M.K.; Das, G.C.; Duari, B. A mechanistic study of the initial stage of the sintering of sol–gel derived silica nanoparticles. *Int. J. Mod. Eng. Res.* **2013**, *3*, 1066–1070.
38. Martra, G. Lewis acid and base sites at the surface of microcrystalline TiO_2 anatase: Relationships between surface morphology and chemical behaviour. *Appl. Catal. A Gen.* **2000**, *200*, 275–285. [CrossRef]
39. Kuroda, Y.; Mori, T.; Yagi, K.; Makihata, N.; Kawahara, Y.; Nagao, M.; Kittaka, S. Preparation of visible-light-responsive TiO_2-xNx photocatalyst by a sol−gel method: analysis of the active center on TiO_2 that reacts with NH_3. *Langmuir* **2005**, *21*, 8026–8034. [CrossRef]
40. Haque, F.Z.; Nandanwar, R.; Singh, P. Evaluating photodegradation properties of anatase and rutile TiO_2 nanoparticles for organic compounds. *Optik* **2017**, *128*, 191–200. [CrossRef]
41. San Andrés, E.; Toledano-Luque, M.; Del Prado, A.; Navacerrada, M.; Mártil, I.; González-Díaz, G. Physical properties of high pressure reactively sputtered TiO_2. *J. Vac. Sci. Technol. A* **2005**, *23*, 1523–1530. [CrossRef]
42. Gracia, F.; Holgado, J.P.; Contreras, L.; Girardeau, T.; González-Elipe, A.R. Optical and crystallisation behaviour of TiO_2 and V/TiO_2 thin films prepared by plasma and ion beam assisted methods. *Thin Solid Films* **2003**, *429*, 84–90. [CrossRef]
43. Pambudi, A.B.; Kurniawati, R.; Iryani, A.; Hartanto, D. Effect of calcination temperature in the synthesis of carbon doped TiO_2 without external carbon source. In Proceedings of the 3rd International Seminar on Chemistry, AIP Conference Proceedings, Surabaya, Indonesia, 18–19 July 2018; Volume 2049, p. 020074.
44. Razmjou, A.; Mansouri, J.; Chena, V. The effects of mechanical and chemical modification of TiO_2 nanoparticles on the surface chemistry, structure and fouling performance of PES ultrafiltration membranes. *J. Membr. Sci.* **2011**, *378*, 73–84. [CrossRef]
45. Cao, Y.; Li, Q.; Wang, W. Construction of a crossed-layer-structure $MoS_2/g\text{-}C_3N_4$ heterojunction with enhanced photocatalytic performance. *RSC Adv.* **2017**, *7*, 6131–6139. [CrossRef]
46. Grill, A.; Neumayer, D.A. Structure of low dielectric constant to extreme low dielectric constant SiCOH films: Fourier transform infrared spectroscopy characterization. *J. Appl. Phys.* **2003**, *94*, 6697–6707. [CrossRef]
47. Schramm, C. High temperature ATR-FTIR characterization of the interaction of polycarboxylic acids and organotrialkoxysilanes with cellulosic material. *Spectrochim. Acta A Mol. Biomol. Spectrosc.* **2020**, *243*, 118815. [CrossRef] [PubMed]
48. Ukaji, E.; Furusawa, T.; Sato, M.; Suzuki, M. The effect of surface modification with silane coupling agent on suppressing the photo-catalytic activity of fine TiO_2 particles as inorganic UV filter. *Appl. Surf. Sci.* **2007**, *254*, 563–569. [CrossRef]
49. Sing, K.S.W. Reporting physisorption data for gas/solid systems with special reference to the determination of surface area and porosity. *Pure Appl. Chem.* **1982**, *54*, 2201–2218. [CrossRef]
50. ALOthman, Z.A. A review: Fundamental aspects of silicate mesoporous materials. *Materials* **2012**, *5*, 2874–2902. [CrossRef]
51. Kutarov, V.V.; Tarasevich, Y.I.; Aksenenko, E.V.; Ivanova, Z.G. Adsorption hysteresis for a slit-like pore model. *Russ. J. Phys. Chem.* **2011**, *85*, 1222–1227. [CrossRef]
52. Cheng, F.; Sajedin, S.M.; Kelly, S.M.; Lee, A.F.; Kornherr, A. UV-stable paper coated with APTES-modified P25 TiO_2 nanoparticles. *Carbohydr. Polym.* **2014**, *114*, 246–252. [CrossRef]
53. Zhuang, W.; Zhang, Y.; He, L.; An, R.; Li, B.; Ying, H.; Wu, J.; Chen, Y.; Zhou, J.; Lu, X. Facile synthesis of amino-functionalized mesoporous TiO_2 microparticles for adenosine deaminase immobilization. *Microporous Mesoporous Mater.* **2017**, *239*, 158–166. [CrossRef]
54. Hou, J.; Dong, G.; Luu, B.; Sengpiel, R.G.; Ye, Y.; Wessling, M.; Chen, V. Hybrid membrane with TiO_2 based bio-catalytic nanoparticle suspension system for the degradation of bisphenol-A. *Bioresour. Technol.* **2014**, *169*, 475–483. [CrossRef] [PubMed]
55. Luís, A.M.; Neves, M.C.; Mendonça, M.H.; Monteiro, O.C. Influence of calcination parameters on the TiO_2 photocatalytic properties. *Mater. Chem. Phys.* **2011**, *125*, 20–25. [CrossRef]
56. Chen, Y.; Wang, Y.; Li, W.; Yang, Q.; Hou, Q.; Wei, L.; Liu, L.; Huang, F.; Ju, M. Enhancement of photocatalytic performance with the use of noble-metal-decorated TiO_2 nanocrystals as highly active catalysts for aerobic oxidation under visible-light irradiation. *Appl. Catal. B Environ.* **2017**, *210*, 352–367. [CrossRef]
57. Wawrzyniak, B.; Morawski, A.W. Solar-light-induced photocatalytic decomposition of two azo dyes on new TiO_2 photocatalyst containing nitrogen. *Appl. Catal. B Environ.* **2006**, *62*, 150–158. [CrossRef]
58. Beranek, R.; Kisch, H. Tuning the optical and photoelectrochemical properties of surface-modified TiO_2. *Photochem. Photobiol. Sci.* **2008**, *7*, 40–48. [CrossRef] [PubMed]
59. Riaz, N.; Chong, F.K.; Dutta, B.L.; Man, Z.B.; Saqib Khan, M.; Nurlaela, E. Photodegradation of Orange II under visible light using $Cu–Ni/TiO_2$: Effect of calcination temperature. *Chem. Eng. J.* **2012**, *185–186*, 108–119. [CrossRef]
60. Ponaryadov, A.; Kotova, O. Leucoxene photocatalysts for water purification. *IOP Conf. Ser. Mater. Sci. Eng.* **2013**, *47*, 012039. [CrossRef]
61. Nurlaela, E.; Chong, F.K.; Dutta, B.K.; Riaz, N. Bimetallic $Cu\text{-}Ni/TiO_2$ as photocatalyst for hydrogen production from water. In Proceedings of the International Conference on Fundamental and Applied Sciences (ICFAS2010), Kuala Lumpur, Malaysia, 15–17 June 2010.
62. Mohammad Jafri, N.N.; Jaafar, J.; Alias, N.H.; Samitsu, S.; Aziz, F.; Wan Salleh, W.N.; Mohd Yusop, M.Z.; Othman, M.H.D.; Rahman, M.A.; Ismail, A.F.; et al. Synthesis and characterization of titanium dioxide hollow nanofiber for photocatalytic degradation of methylene blue dye. *Membranes* **2021**, *11*, 581. [CrossRef] [PubMed]

63. Paul, S.; Choudhury, A. Investigation of the optical property and photocatalytic activity of mixed phase nanocrystalline titania. *Appl. Nanosci.* **2014**, *4*, 839–847. [CrossRef]
64. Phromma, S.; Wutikhun, T.; Kasamechonchung, P.; Eksangsri, T.; Sapcharoenkun, C. Effect of calcination temperature on photocatalytic activity of synthesized TiO_2 nanoparticles via wet ball milling sol-gel method. *Appl. Sci.* **2020**, *10*, 993. [CrossRef]
65. Saranya, K.S.; Vellora Thekkae Padil, V.; Senan, C.; Pilankatta, R.; Saranya, K.; George, B.; Wacławek, S.; Černík, M. Green synthesis of high temperature stable anatase titanium dioxide nanoparticles using gum kondagogu: Characterization and solar driven photocatalytic degradation of organic dye. *Nanomaterials* **2018**, *8*, 1002. [CrossRef] [PubMed]
66. Siwińska-Stefańska, K.; Ciesielczyk, F.; Nowacka, M.; Jesionowski, T. Influence of selected alkoxysilanes on dispersive properties and surface chemistry of titanium dioxide and TiO_2-SiO_2 composite material. *J. Nanomater.* **2012**, 1–19. [CrossRef]
67. Boscaro, P.; Cacciaguerra, T.; Cot, D.; Fajula, F.; Hulea, V.; Galarneau, A. C,N-doped TiO_2 monoliths with hierarchical macro-/mesoporosity for water treatment under visible light. *Microporous Mesoporous Mater.* **2019**, *280*, 37–45. [CrossRef]
68. Janus, M.; Bubacz, K.; Zatorska, J.; Kusiak-Nejman, E.; Czyżewski, A.; Morawski, A.W. Preliminary studies of photocatalytic activity of gypsum plasters containing TiO_2 co-modified with nitrogen and carbon. *Pol. J. Chem. Technol.* **2015**, *17*, 96–102. [CrossRef]
69. Haider, A.; Al-Anbari, R.; Kadhim, G.; Jameel, Z. Synthesis and photocatalytic activity for TiO_2 nanoparticles as air purification. In Proceedings of the 3rd International Conference on Buildings, Construction and Environmental Engineering (BCEE3-2017), 23–25 October 2017, Sharm el-Shiekh, Egypt. *MATEC Web Conf.* **2018**, *162*, 05006. [CrossRef]
70. Pinheiro Pinton, A.; De, S.; Bulhões, L.O. Synthesis, characterization, and photostability of manganese-doped titanium dioxide nanoparticles and the effect of manganese content. *Mater. Res. Express* **2019**, *6*, 125015. [CrossRef]
71. Chellappah, K.; Tarleton, E.S.; Wakeman, R.J. Filtration and sedimentation behaviour of fibre/particle binary suspensions. *Filtration* **2009**, *9*, 286–294.
72. Talavera-Pech, W.A.; Esparza-Ruiz, A.; Quintana-Owen, P.; Vilchis-Nestor, A.F.; Carrera-Figueiras, C.; Ávila-Ortega, A. Effects of different amounts of APTES on physicochemical and structural properties of amino-functionalized MCM-41-MSNs. *J. Sol-Gel Sci. Technol.* **2016**, *80*, 697–708. [CrossRef]
73. Goscianska, J.; Olejnik, A.; Nowak, I. APTES-functionalized mesoporous silica as a vehicle for antipyrine-adsorption and release studies. *Colloids Surf. A* **2017**, *533*, 187–196. [CrossRef]
74. Li, Q.Y.; Chen, Y.F.; Zeng, D.D.; Gao, W.M.; Wu, Z.J. Photocatalytic characterization of silica coated titania nanoparticles with tunable coatings. *J. Nanopart. Res.* **2005**, *7*, 295–299. [CrossRef]
75. Ferreira-Neto, E.P.; Ullah, S.; Simões, M.B.; Perissinotto, A.P.; Vicente, F.S.; Noeske, P.L.M.; Ribeiro, S.J.L.; Rodrigues-Filho, U.P. Solvent-controlled deposition of titania on silica spheres for the preparation of SiO_2@TiO_2 core@shell nanoparticles with enhanced photocatalytic activity. *Colloids Surf. A* **2019**, *570*, 293–305. [CrossRef]
76. Worathanakul, P.; Jiang, J.; Biswas, P.; Kongkachuichay, P. Quench-ring assisted flame synthesis of SiO_2-TiO_2 nanostructured composite. *J. Nanosci. Nanotechnol.* **2008**, *8*, 6253–6259. [CrossRef] [PubMed]
77. Wang, S.; Zhu, Z.H.; Coomes, A.; Haghseresht, F.; Lu, G.Q. The physical and surface chemical characteristics of activated carbons and the adsorption of methylene blue from wastewater. *J. Colloid Interface Sci.* **2005**, *284*, 440–446. [CrossRef]
78. Zhang, C.; Uchikoshi, T.; Liu, L.; Kikuchi, M.; Ichinose, I. Effect of surface modification with TiO_2 coating on improving filtration efficiency of whisker-hydroxyapatite (HAp) membrane. *Coatings* **2020**, *10*, 670. [CrossRef]
79. Barberi, J.; Spriano, S. Titanium and protein adsorption: An overview of mechanisms and effects of surface features. *Materials* **2021**, *14*, 1590. [CrossRef]
80. Li, Z.; Hou, B.; Xu, Y.; Wu, D.; Sun, Y. Hydrothermal synthesis, characterization, and photocatalytic performance of silica-modified titanium dioxide nanoparticles. *J. Colloid Interface Sci.* **2005**, *288*, 149–154. [CrossRef]
81. Bartošová, A.; Blinová, L.; Sirotiak, M.; Michalíková, M. Usage of FTIR-ATR as non-destructive analysis of selected toxic dyes. *Res. Pap. Fac. Mater. Sci. Technol. Slovak. Univ. Technol.* **2017**, *25*, 103–111. [CrossRef]
82. Ovchinnikov, O.V.; Evtukhova, A.V.; Kondratenko, T.S.; Smirnov, M.S.; Khokhlov, V.Y.; Erina, O.V. Manifestation of intermolecular interactions in FTIR spectra of methylene blue molecules. *Vib. Spectrosc.* **2016**, *86*, 181–189. [CrossRef]
83. Konstantinou, I.K.; Albanis, T.A. TiO_2-assisted photocatalytic degradation of azo dyes in aqueous solution: Kinetic and mechanistic investigations A review. *Appl. Catal. B Environ.* **2004**, *49*, 1–14. [CrossRef]
84. Cai, J.; Xin, W.; Liu, G.; Lin, D.; Zhu, D. Effect of calcination temperature on structural properties and photocatalytic activity of Mn-C-codoped TiO_2. *Mater. Res.* **2016**, *19*, 401–407. [CrossRef]
85. George, P.; Chowdhury, P. Complex dielectric transformation of UV-vis diffuse reflectance spectra for estimating optical band-gap energies and materials classification. *Analyst* **2019**, *144*, 3005–3012. [CrossRef] [PubMed]

Desalination and Water Treatment
www.deswater.com
doi: 10.5004/dwt.2022.28368

256 (2022) 35–50
April

Optimization of APTES/TiO_2 nanomaterials modification conditions for antibacterial properties and photocatalytic activity

Agnieszka Sienkiewicz, Paulina Rokicka-Konieczna*, Agnieszka Wanag, Ewelina Kusiak-Nejman, Antoni W. Morawski

Department of Inorganic Chemical Technology and Environment Engineering, Faculty of Chemical Technology and Engineering, West Pomeranian University of Technology in Szczecin, Pułaskiego 10, 70-322 Szczecin, Poland, emails: Paulina.Rokicka@zut.edu.pl (P. Rokicka-Konieczna), Agnieszka.Sienkiewicz@zut.edu.pl (A. Sienkiewicz), Agnieszka.Wanag@zut.edu.pl (A. Wanag), Ewelina.Kusiak@zut.edu.pl (E. Kusiak-Nejman), Antoni.Morawski@zut.edu.pl (A.W. Morawski)

Received 7 September 2021; Accepted 8 March 2022

ABSTRACT

In this work, the influence of the modifier concentration and the temperature of modification on the antibacterial and photocatalytic properties of titanium dioxide (TiO_2) functionalized with 3-aminopropyltriethoxysilane (APTES) was investigated. The new APTES/TiO_2 nanomaterials were obtained by the solvothermal method. The studies confirmed the presence of N, C and Si in the TiO_2 structure, indicating that the modification was performed successfully. Furthermore, the antibacterial properties of the samples were investigated based on *Escherichia coli* inactivation in saline solution. The decomposition of methylene blue determined the photocatalytic activity under UV irradiation. For the *E. coli* inactivation process, the best concentration of the photocatalyst was 0.1 g/L, while for dye degradation tests, the optimum semiconductor dose was 0.5 g/L. The best antibacterial properties presented photocatalysts obtained by modification with 250 mM of APTES solution. In the case of methylene blue decomposition, the photoactivity increased with the increase of APTES concentration, while the modification temperature from 120°C to 180°C had no significant impact on the activity of the tested samples.

Keywords: Photocatalysis; Titanium dioxide; 3-aminopropyltriethoxysilane; Methylene blue; *Escherichia coli*

1. Introduction

The world is facing a major challenge: providing safe and clean drinking water. Therefore, water security is considered the overarching goal of water management [1]. However, numerous places in the world are still struggling to solve problems of water contaminated by biological and chemical compounds. For example, pathogenic bacteria like *Escherichia coli* are responsible for many diseases (e.g., diarrhoea, urethritis or bladder infection) and even human death [2,3]. In addition, many water bodies are contaminated with chemical pollutants, including organic dyes, which are one of the primary contaminants of industrial wastewater [4,5]. Therefore, the important challenge is to develop alternative methods of water purification and disinfection that are effective against a wide range of contaminants (both microbial and chemical).

According to Ismail et al. [4], a method based on nanotechnology (e.g., photocatalysis) is an excellent alternative to conventional water treatment techniques. In the available literature, there are many reports which confirm the high disinfectant effect of various photocatalysts (like WO_3, ZnO, SnO_2, $BiVO_4$, TiO_2) against bacteria [6–9]. Bekkali et al. [7], for example, obtained ZnO/hydroxyapatite nanomaterials

* Corresponding author.

which presented good antibacterial properties against *E. coli*, *Pseudomonas aeruginosa*, *Staphylococcus aureus* and *Enterococcus faecalis*. Gnanamoorthy et al. [8] synthesized SnO_2 nanorods, which showed good antibacterial activity against *Staphylococcus aureus*, *E. coli* and *Pseudomonas aeruginosa*. In turn, Sharma et al. [9] observed satisfactory biocidal properties of monoclinic bismuth vanadate (m-$BiVO_4$) nanostructures toward *E. coli*. Numerous studies have also confirmed excellent antibacterial properties of TiO_2 based nanomaterials [10,11]. TiO_2 is considered the most widely applied oxide in photocatalysis, and its biocidal properties have been demonstrated on a wide range of bacteria [12–14]. Unfortunately, TiO_2 presents also some limitations like rapid recombination of photogenerated electron–hole pairs. Consequently, one of the widely investigated subjects in photocatalysis is a modification of pure TiO_2 to overcome the mentioned problem. To improve the photocatalytic process efficiency, many different ways of TiO_2 modification are applied (e.g., surface modification or co-modification, dye sensitization, combining TiO_2 with other semiconductors) [15,16]. One method involves using organosilanes such as 3-aminopropyltriethoxysilane (APTES) for TiO_2 surface modification [17]. Silica modification can improve TiO_2 photocatalytic activity, among others, by decreasing particles size, enhancing the specific surface area, or repressing the phase transformation from anatase to rutile [18,19]. Our previous study also confirmed that APTES modification enhanced adsorption properties and photocatalytic activity of obtained TiO_2 nanomaterials [20].

In our previous reports, the impact of APTES/TiO_2 nanomaterials obtained by utilizing different concentrations of APTES on antibacterial properties [21] or methylene blue decomposition were examined [22]. In the present work, modification of TiO_2 with APTES was also performed. The research idea was to determine an optimal dose of modifier (APTES) related to photocatalytic activity. However, the simultaneous effect of the two parameters: APTES concentration and modification temperature on the photocatalytic inactivation of bacteria *E. coli* and methylene blue degradation was investigated for the first time. In addition, in this paper, optimization towards the appropriate dose of APTES/TiO_2 photocatalyst, necessary to determine both antibacterial properties and yield of dye decomposition, was presented for the first time. Moreover, it was decided to evaluate the effect of low-temperature modification in the range of 120°C–180°C on the photoefficiency of the prepared nanomaterials.

2. Experimental

2.1. Materials and reagents

Crude TiO_2 slurry prepared by sulfate technology, supplied from the chemical plant Grupa Azoty Zakłady Chemiczne "Police" S.A. (Poland), was selected as a TiO_2 source. Before modification, the raw TiO_2 was rinsed with an aqueous solution of NH_4OH (purity 25%, Firma Chempur®, Poland) to remove sulphuric compounds' residues forming ammonium sulfate that is easily soluble in water [22]. In the next step, the suspension was rinsed with distilled water until pH equalled 6.8. The prepared material was named starting-TiO_2. 3-aminopropyltriethoxysilane (APTES, purity ≥98%) purchased from Merck KGaA (Germany) was utilized as a modifier of TiO_2. Ethyl alcohol (purity 96%) from P.P.H. "STANLAB" Sp.J., (Poland) was selected as a solvent of APTES. *E. coli* K12 (ATCC 29425, LGC Ltd., USA) was selected as model microbial contamination of water. Methylene blue (purity ≥82%, Firma Chempur®, Poland) was chosen as a model organic water pollutant.

2.2. APTES/TiO_2 nanomaterials preparation technique

The APTES-modified TiO_2 photocatalysts were prepared by the solvothermal method. The modifier concentrations in ethanol were 50, 250, 450, and 650 mM. At first, 5 g of starting-TiO_2 was dispersed in 25 mL of APTES solution. Next, a sample was modified in a pressure autoclave for 4 h at 120°C, 140°C, 160°C and 180°C with provided continuous stirring at 500 rpm. Afterwards, the obtained suspension was rinsed with ethanol and distilled water to remove any residual chemicals. Finally, the prepared material was dried for 24 h at 105°C in a lab dryer. The gained photocatalysts were denoted as TiO_2-4h-X°C-YmM, where *X* is the modification temperature, and *Y* is the concentration of APTES in ethanol.

2.3. Characterization

The X-ray powder diffraction analysis (Melvern PANalytical B.V., Netherlands) using Cu Kα radiation (λ = 1.54056 Å) was used to identify the crystalline structure of the examined samples. To calculate the mean crystallites size, Scherrer's equation was used. The PDF-4+ 2014 International Centre for Diffraction Data database (04-005-5923 PDF4+ card for rutile and 04-002-8296 PDF4+ card for anatase) was applied to identify the phase composition. In order to calculate the Brunauer–Emmett–Teller (BET) specific surface area and pore volume, the low-temperature N_2 adsorption–desorption measurements, carried out at 77 K, were performed with the QUADRASORB evoTM Gas Sorption analyzer (Anton Paar GmbH, Austria). Before each measurement, all materials were degassed under a high vacuum for 12 h at 100°C to eliminate any remaining impurities on the examined samples' surface. The total pore volume (V_{total}) was determined by the single point from the nitrogen adsorption isotherms at relative pressure p/p_0 = 0.99. The Dubinin–Radushkevich method was used to estimate the volume of micropores (V_{micro}), while the volume of mesopores (V_{meso}) was calculated as the difference between V_{total} and V_{micro}. The Fourier-transform infrared spectroscopy (FT-IR) 4200 spectrometer (JASCO International Co. Ltd., Japan) supplied with DiffuseIR accessory (PIKE Technologies, USA) was applied to identify the surface functional groups of APTES/TiO_2 nanomaterials. The ZetaSizer NanoSeries ZS (Malvern PANalytical Ltd., UK) was used to measure the zeta potential values. A CN628 elemental analyzer (LECO Corporation, USA) was used to determine total carbon and nitrogen content in tested samples. To prepare the calibration curve, a certified ethylenediaminetetraacetic acid (EDTA) standard (Elemental Microanalysis Ltd., UK), containing 41.04 ± 0.15 wt.% carbon and 9.56 ± 0.11 wt.% nitrogen was utilized. The surface morphology of the APTES/TiO_2 photocatalysts was observed via scanning electron microscopy (SEM) using a Hitachi SU8020 ultra-high resolution field emission

scanning electron microscope (Hitachi Ltd., Japan). The energy-dispersive X-ray spectroscopy (EDX) from Thermo Fisher Scientific Inc. (USA) was used to perform EDX mapping analysis of the tested samples.

The analysis of hydroxyl radical formation on photocatalysts surface was determined by fluorescence technique using terephthalic acid (Acros Organics B.V.B.A, Belgium). The fluorescence product of terephthalic acid hydroxylation, 2-hydroxyterephthalic acid (2-HTA), was detected as an emission peak at the maximum wavelength of 420 nm, with the 314 nm excitation wavelength and analysed on a Hitachi F-2500 fluorescence spectrophotometer (Hitachi Ltd., Japan).

2.4. Light source

Both antibacterial tests and photocatalytic activity studies were conducted under UV-Vis light with the radiation intensity of 65 W/m^2 for 300–2800 nm and 36 W/m^2 for the 280–400 nm region, provided by 6 lamps of 20 W each (Philips, Amsterdam, Netherlands). The radiation source used was called UV light due to the low intensity of visible radiation.

2.5. Antibacterial tests

The antibacterial properties of photocatalysts were determined using the standard plate count method toward the gram-negative *E. coli* K12 (ATCC 29425, LGC Ltd, USA). Before the experiments, bacteria were inoculated into Enriched Broth (BioMaxima S.A., Poland) and cultured at 37°C for 24 h. Next, bacteria were harvested through centrifugation (4,000 rpm, 10 min) and then re-suspended in sterile saline solution (0.9% NaCl, Firma Chempur®, Poland). The concentration of the bacteria was adjusted to approx. 1.5×10^7 CFU/mL by optical density measurement at a wavelength of 600 nm.

The antibacterial experiments were carried out in a sterilized 150 ml glass beaker containing 90 mL of saline solution, 10 mL of the bacterial suspension (1.5×10^7 CFU/mL) and appropriate photocatalyst (in a concentration of 0.05, 0.1, 0.25, 0.5 or 0.75 g/L). The suspension was continuously stirred to ensure homogeneity and irradiated with UV light for 90 min at room temperature. The distance between the reactor and the light source was fixed at approx. 35 cm. At given time intervals, 1 ml of bacterial suspension was collected and diluted by decimal dilution method in saline solution. Next, suspensions were spread on the Petri dish containing Plate Count Agar (BioMaxima S.A., Poland) and incubated at 37°C for 24 h. After incubation, the number of viable colonies was counted and depicted as log CFU/mL. Control experiments (under the dark conditions and for the saline solution) were also conducted. All measurements were performed in triplicates. The standard error of the measurements amounted less than 10%.

2.6. Photocatalytic activity studies

Before the photocatalytic activity studies, adsorption measurements were performed. A 0.6 L glass beaker containing 0.5 L of methylene blue solution with an initial concentration of 15 mg/L and 0.05, 0.1, 0.25, 0.5 or 0.75 g/L of the appropriate photocatalyst was placed in a thermostatic chamber at 20°C (Pol-Eko-Aparatura sp.j., Poland) in light-free conditions and stirred for 60 min to provide the adsorption–desorption equilibrium between dye molecules and the surface of the tested sample. After that, the solution was irradiated with UV light. The methylene blue concentration was analyzed every 60 min during photoactivity tests by the V-630 UV-Vis spectrometer (JASCO International Co., Japan). Before each measurement, 10 mL of the taken suspension was centrifuged to eliminate all suspended nanoparticles. Methylene blue decomposition degree was calculated based on the equation:

$$R\left[\%\right] = \frac{C_0 - C_t}{C_t} \times 100\% \quad (1)$$

where R is methylene blue decomposition degree (%), C_0 is the initial concentration of methylene blue measured after adsorption (mg/L), and C_t is the methylene blue concentration at the time t (mg/L).

3. Results and discussion

3.1. Characterization of the nanomaterials

3.1.1. X-ray powder diffraction analysis

X-ray diffraction (XRD) patterns of starting-TiO_2 and APTES-modified TiO_2 photocatalysts are shown in Fig. 1A–D. All nanomaterials exhibited reflections characteristic for anatase phase located at 25.3°, 37.8°, 48.1°, 53.9°, 55.1°, 62.7°, 68.9°, 70.3° and 75.1°, and some reflections characteristic for rutile phase: located at 27.4°, 36.0° and 41.2° [20]. The presence of rutile in the starting-TiO_2 is due to the addition of rutile nuclei during the manufacturing process of crude TiO_2 pulp via the sulfate method. According to the data presented in Table 1, all photocatalysts consist mainly of the anatase phase (94%–96%) with a small amount of a rutile phase (4–6%). Moreover, modification in the temperature range from 120°C to 180°C did not cause the anatase-to-rutile phase transformation, which is typical because anatase transforms into a rutile phase above 600°C [23]. Additionally, no significant changes in the crystalline structure of the tested samples were noted, which was consistent with the results obtained by Klaysri et al. [17]. They observed that the surface functionalization with APTES in the concentration range of 0.1–100 mM did not influence the phase structure and the crystalline size of titanium dioxide, which were about 17–19 nm, where in our case the crystallite size of anatase was in the range of 14 to 16 nm and rutile from 21 to 62 nm. Due to the low content of the rutile phase (4%–6%), the noted changes in the rutile crystallites size may have resulted from the conversion error of the method.

3.1.2. FT-IR/DRS (differential reflectance spectroscopy) measurements

All FT-IR/differential reflectance spectroscopy (DRS) (Fig. 2A–D) were characterized by a narrow band at around 1,628 cm^{-1} and a wide band from 3,750 to 2,500 cm^{-1}, ascribed to the molecular water and stretching mode of surface –OH groups, respectively [24,25]. On the spectra of the modified photocatalysts, characteristic bands originating

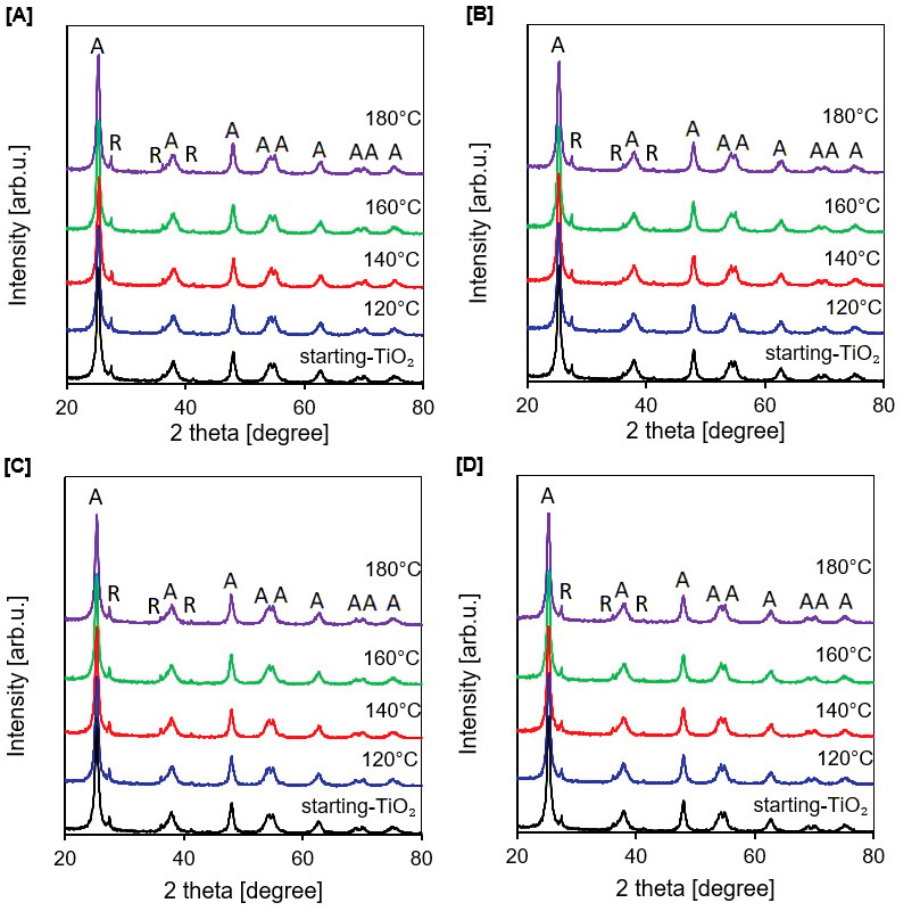

Fig. 1. X-ray diffraction (XRD) patterns of starting-TiO_2 and TiO_2 nanomaterials modified with APTES concentration of 50 mM (A), 250 mM (B), 450 mM (C), and 650 mM (D), where A-anatase, R-rutile.

Table 1
Physico-chemical properties of starting-TiO_2 and APTES-modified TiO_2 nanomaterials

Sample name	S_{BET} (m^2/g)	V_{total} (cm^3/g)	V_{micro} (cm^3/g)	V_{meso} (cm^3/g)	Anatase in crystallite phase (%)	Anatase crystallite size (nm)	Rutile in crystallite phase (%)	Rutile crystallite size (nm)
Starting-TiO_2	207	0.370	0.070	0.300	95	14	5	21
TiO_2-4h-120°C-50mM	185	0.280	0.070	0.210	95	15	5	40
TiO_2-4h-140°C-50mM	194	0.380	0.068	0.312	95	15	5	54
TiO_2-4h-160°C-50mM	189	0.386	0.066	0.320	94	15	6	27
TiO_2-4h-180°C-50mM	188	0.358	0.060	0.298	96	16	4	48
TiO_2-4h-120°C-250mM	148	0.290	0.060	0.230	95	15	5	56
TiO_2-4h-140°C-250mM	144	0.298	0.052	0.246	95	15	5	48
TiO_2-4h-160°C-250mM	150	0.304	0.054	0.249	95	15	5	48
TiO_2-4h-180°C-250mM	135	0.223	0.051	0.172	96	15	4	37
TiO_2-4h-120°C-450mM	133	0.195	0.051	0.140	95	15	5	31
TiO_2-4h-140°C-450mM	137	0.232	0.052	0.180	95	15	5	36
TiO_2-4h-160°C-450mM	137	0.226	0.052	0.174	96	15	4	48
TiO_2-4h-180°C-450mM	133	0.216	0.050	0.166	95	14	5	62
TiO_2-4h-120°C-650mM	128	0.199	0.050	0.149	96	15	4	39
TiO_2-4h-140°C-650mM	125	0.279	0.047	0.232	96	15	4	36
TiO_2-4h-160°C-650mM	131	0.218	0.049	0.159	96	15	4	45
TiO_2-4h-180°C-650mM	135	0.281	0.049	0.232	96	15	4	41

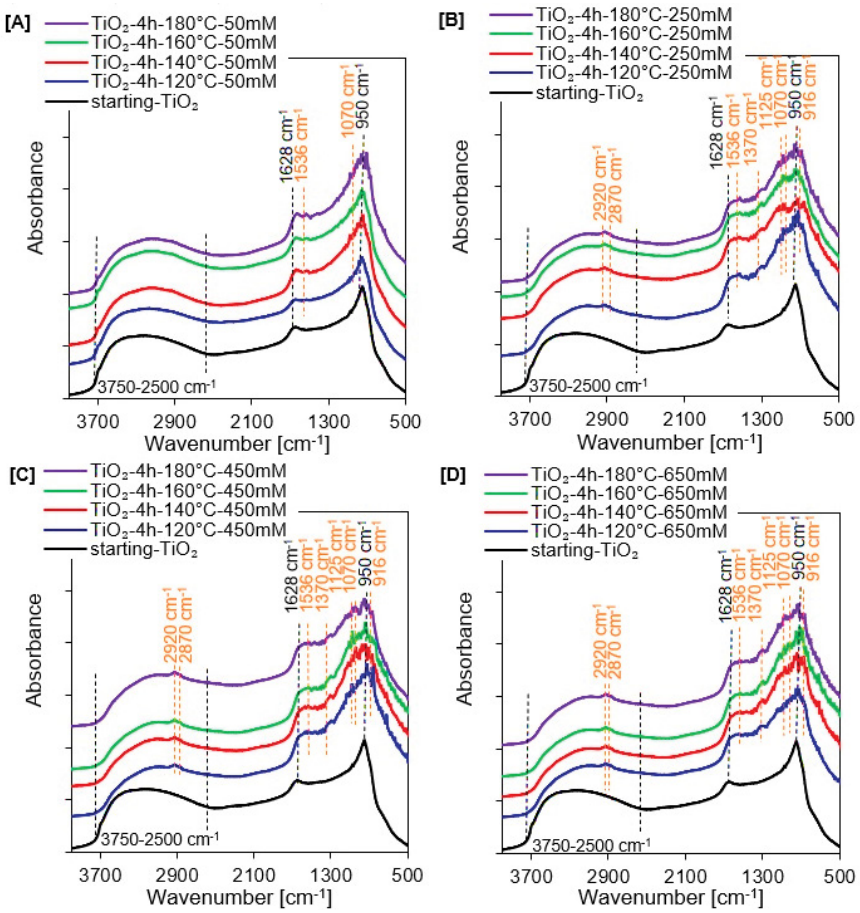

Fig. 2. FT-IR/DR spectra of starting-TiO_2 and TiO_2 nanomaterials modified with APTES concentration of 50 mM (A), 250 mM (B), 450 mM (C), and 650 mM (D).

from APTES were observed, which indicates that APTES/TiO_2 nanomaterials were prepared successfully. As the modification temperature increased, there were no significant changes in the surface characteristics of the tested materials. However, the amount and intensity of bands characteristic for APTES increased with increasing modifier concentration. In Fig. 2A, showing spectra of samples functionalized with 50 mM of APTES, the scissor vibrations of primary amine groups at around 1,536 cm^{-1} and Si–O–C groups at around 1,070 cm^{-1} were noted [26,27]. In Fig. 2B–D, additional bands typical for APTES were also noted – the bending and stretching modes of the alkyl groups detected at 2,929 and 2,879 cm^{-1} [27,28]. Bands at 1,370 and 1,125 cm^{-1} correspond to the symmetric C–H bending modes and asymmetric stretching vibrations of Si–O–Si, respectively [27,29–31]. Bands observed in the range from 960 to 910 cm^{-1} are attributed to the stretching vibrations of Ti–O–Si bonds. Moreover, the bond at around 916 cm^{-1} indicates that the condensation between surface hydroxyl groups and silanol groups occurred [32,33].

3.1.3. BET specific surface area and pore volume analysis

According to Fig. S1A–D, the adsorption–desorption isotherms of all tested photocatalysts based on the IUPAC classification, showed a type IV nitrogen isotherm. Typical features of this type of isotherm are its hysteresis loop, associated with capillary condensation occurring in mesopores, and the limitation of uptake in the range of high p/p_0 values [34]. Moreover, these nanomaterials presented the same H_3 type of hysteresis loop which is marked by slit-shaped pores and often continue into the low-pressure region [35,36]. It is worth mentioning that the size of the hysteresis loops presented in Fig. S1A–D decreased with increasing APTES concentration related to the decreasing amount of mesopores in the materials (Table 1) [37]. However, there was no significant effect of the modification temperature between 120°C and 180°C on the change in the size of the hysteresis loops. Thus no significant effect on the change of the specific surface area and total pore volume of the tested samples was noted. The specific surface area for starting-TiO_2 was 207 m^2/g, while APTES/TiO_2 nanomaterials ranged from 194 to 125 m^2/g. Furthermore, based on the data listed in Table 1, it was found that the decrease not only of S_{BET} but also of V_{total}, V_{meso} and a slight decrease of V_{micro} with increasing APTES concentration suggests that modifier molecules are not only placed on the TiO_2 outer surface but also captured in the pores. A similar effect was observed by Dalod et al. [28], Ukaji et al. [32], Zhuang et al. [38] and Pontón et al. [39].

Table 2
The zeta potential values and carbon and nitrogen content of starting-TiO_2 and APTES-modified TiO_2 nanomaterials

Sample name	Zeta potential δ (mV)	Carbon content (wt.%)	Nitrogen content (wt.%)
Starting-TiO_2	+12.80	–	0.18
TiO_2-4h-120°C-50mM	+15.75	1.16	0.43
TiO_2-4h-140°C-50mM	+13.83	1.14	0.44
TiO_2-4h-160°C-50mM	+15.02	1.17	0.43
TiO_2-4h-180°C-50mM	+15.70	1.25	0.44
TiO_2-4h-120°C-250mM	+17.89	3.22	1.13
TiO_2-4h-140°C-250mM	+20.26	3.49	1.24
TiO_2-4h-160°C-250mM	+21.96	3.53	1.25
TiO_2-4h-180°C-250mM	+22.34	3.64	1.27
TiO_2-4h-120°C-450mM	+23.12	3.76	1.32
TiO_2-4h-140°C-450mM	+25.53	3.70	1.28
TiO_2-4h-160°C-450mM	+26.18	3.72	1.31
TiO_2-4h-180°C-450mM	+26.73	3.87	1.35
TiO_2-4h-120°C-650mM	+26.18	3.34	1.30
TiO_2-4h-140°C-650mM	+24.90	4.10	1.39
TiO_2-4h-160°C-650mM	+27.11	3.98	1.31
TiO_2-4h-180°C-650mM	+26.95	4.15	1.76

3.1.4. Zeta potential analysis

Based on the data presented in Table 2, all photocatalysts were characterized by positive surface charge, and the zeta potential values changed from +12.80 mV for starting-TiO_2 to +27.11 mV for TiO_2-4h-160°C-650 mM sample. According to Talavera-Pech et al. [40], Youssef et al. [41], and Zhao et al. [42], APTES has cationic amino groups, which can easily bond to the semiconductor surface. Thus, the zeta potential values of the amino-functionalized TiO_2 nanomaterials enhanced with increasing concentration of APTES used for the modification, which was due to the higher presence of $–NH_2$ groups on the surface of the obtained samples. The presence of the positively charged amino groups on the TiO_2 surface was confirmed by FT-IR/DRS measurements and the nitrogen content analysis shown in Fig. 2A–D and Table 2, respectively.

3.1.5. Carbon and nitrogen content analysis

According to the results presented in Table 2, carbon and nitrogen content in the tested materials grew with the increasing concentration of APTES modifier, and the largest amount of the analyzed elements was found for photocatalysts modified with the 650 mM of APTES. However, the highest growth was observed when the concentration increased from 50 to 250 mM. Further increase contributed to slight growth in the amount of the tested elements. Moreover, the data derived from the FT-IR/DR spectra (Fig. 2A–D) agreed with the carbon and nitrogen elemental analysis, which showed a continued increase of C and N in APTES/TiO_2 nanomaterials as the amount of modifier increases. Additionally, at constant APTES concentration, no significant effect of the modification temperature in the range of 120°C to 180°C on carbon and nitrogen contents in the tested materials was found. The presence of 0.18 wt.% nitrogen in the starting-TiO_2 can be explained by the preparation procedure, involving preliminary rinsing with ammonia water, applied to remove residual sulfuric acid from the raw TiO_2 slurry prepared by sulfate technology.

3.1.6. SEM images and EDX mapping

Following the SEM images of the starting-TiO_2 and TiO_2-4h-180°C-650mM sample exhibited in Fig. 3A and B, respectively, it was observed that on the surface of the starting-TiO_2, the grains formed small uniformly distributed aggregates. After TiO_2 functionalization with APTES (Fig. 3B), it was noted that modification increased the size of the aggregates. However, the nanomaterial particles were still characterized by irregular and unspecified shapes. Based on the results of EDX mapping analysis, along with the element stratification and the distribution diagram of an appropriate examined element shown in Fig. 3C and D, it was found that the tested nanomaterials contained Ti, O, C, N and Si elements. Furthermore, it was noted that all elements were homogeneously dispersed over the entire surface of the photocatalyst. The data presented in Table 3 shows that the Si content tends to increase with increasing concentration of the used modifier. Hence, the highest Si content was observed for photocatalyst modified with the APTES concentration of 650 mM.

3.2. Optimization of antibacterial studies

In the first stage of the study, the optimum concentration of photocatalyst for bacteria inactivation in water was determined. Optimization of photocatalyst concentration

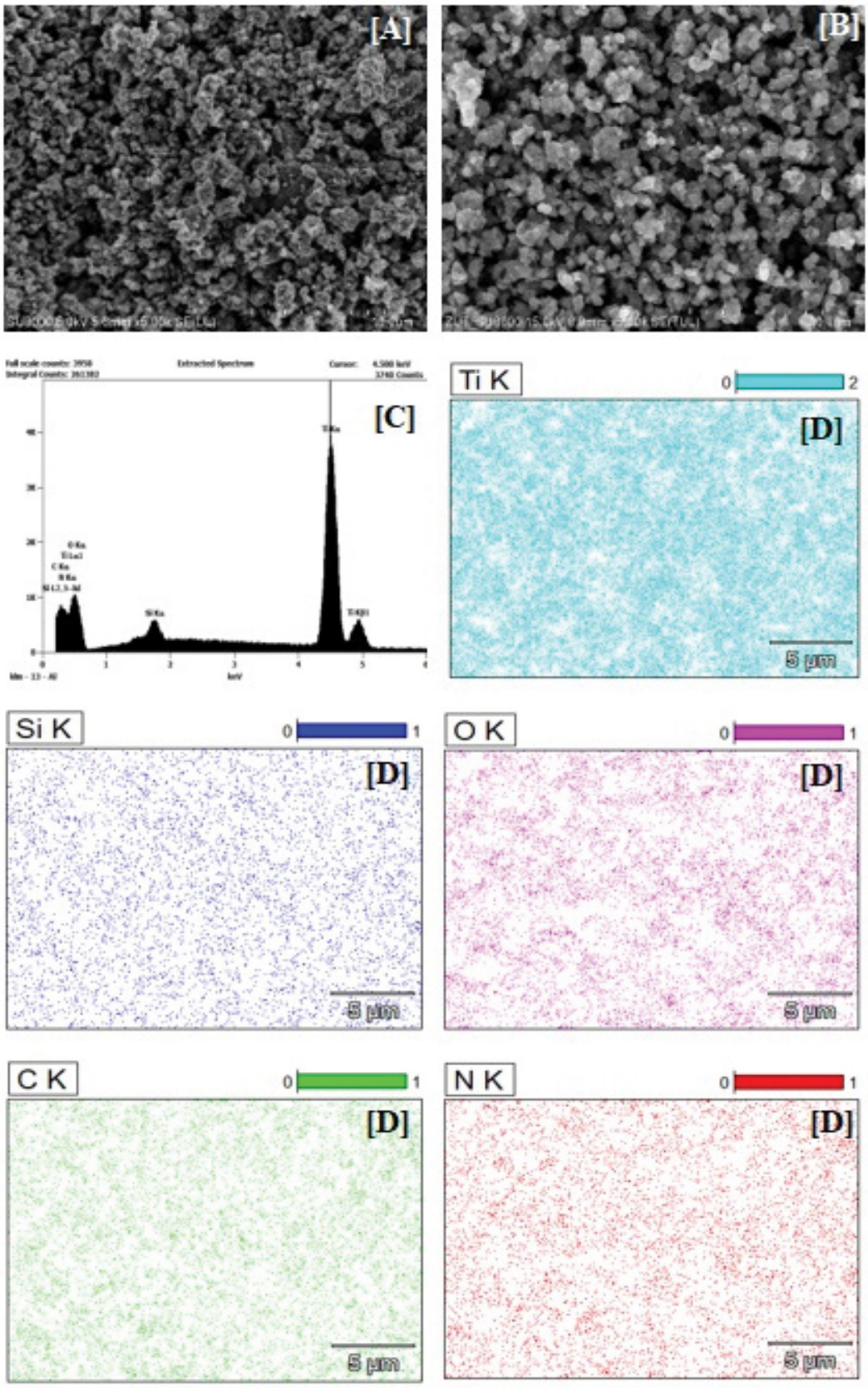

Fig. 3. Example SEM images of starting-TiO_2 (A), and TiO_2-4h-180°C-650mM (B), EDX spectrum (C) and EDX mappings of TiO_2-4h-180°C-650mM (D).

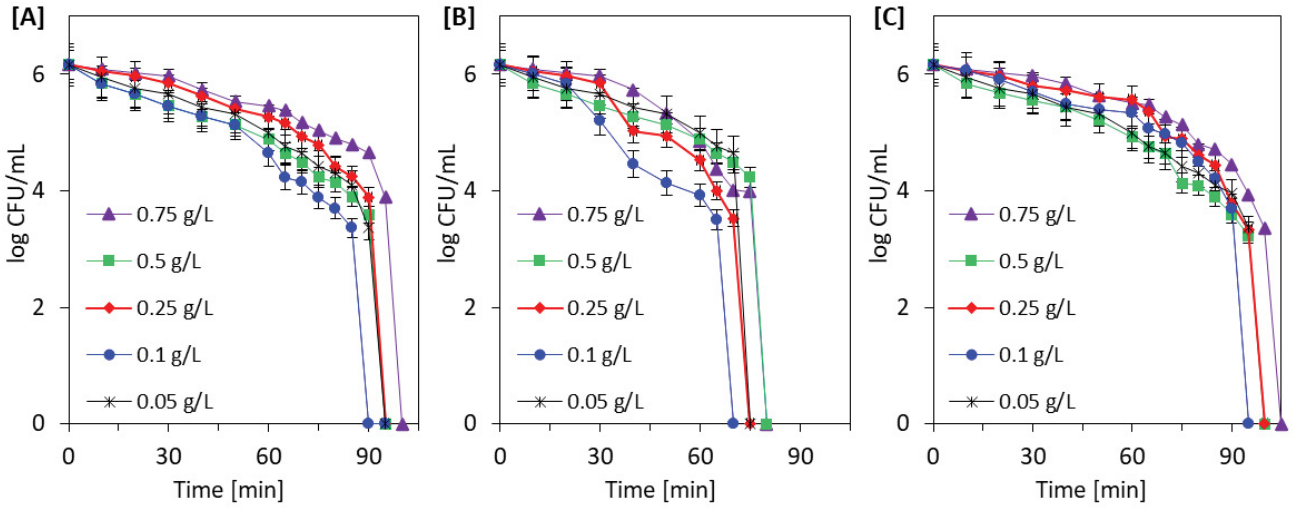

Fig. 4. Inactivation of *E. coli* in the presence of various concentrations of starting-TiO_2 (A), TiO_2-4h-120°C-250mM (B) and TiO_2-4h-160°C-650mM (C) under UV irradiation.

was performed using 3 randomly selected photocatalysts (starting-TiO_2, TiO_2-4h-120°C-250mM and TiO_2-4h-160°C-650 mM) in five concentration (0.05, 0.1, 0.25, 0.5 or 0.75 g/L). In turn, the initial *E. coli* concentration in the reaction mixture amounted approx. 1.5 × 10^6 CFU/mL, according to our previous studies [21,43], was an optimal concentration of bacteria. The fastest bacteria inactivation was observed for all examined samples for a photocatalyst dose of 0.1 g/L (Fig. 4A–C). Therefore, a concentration of 0.1 g/L has been selected as the optimal dose for photocatalytic antibacterial tests. It was also observed that both an increase and a decrease in photocatalysts dose caused extension of time needed for total bacteria inactivation. The dose of 0.05 g/L could be insufficient. In turn, at higher photocatalyst concentration, the activation of TiO_2 particles may be hindered. The increased turbidity of the suspension caused a screening effect and impeded radiation access [44].

A control experiment in the darkness showed that the bacterial number remained unchanged after 90 min of incubation (Fig. S2A–D). Thus, this indicated no toxic effect of the APTES/TiO_2 samples to *E. coli*. Furthermore, the influence of the photolysis on bacterial cells under UV irradiation was also not found (results for NaCl solution presented in Fig. 5A–D).

The bacteria inactivation was observed only in experiments conducted in the presence of APTES/TiO_2 under UV irradiation. As was presented in Fig. 5A–D, APTES/TiO_2 presented better antibacterial properties than starting-TiO_2. The better antibacterial activity was presented for photocatalysts obtained by modification with a 250 mM modifier solution. For this group of photocatalysts, 100% of bacteria were inactivated after 65 min UV irradiation.

Studies have shown that the antibacterial properties strongly depended on the amount of APTES in a solution used for modification and the amount of silica (confirmed by EDX analysis see Table 3), carbon and nitrogen in samples. This, in turn, contributes to changes in the zeta potential of APTES/TiO_2 samples. As shown in Table 2, the zeta potential value increased with increasing carbon and nitrogen content from +12.80 mV for starting-TiO_2 to +27.11 mV for TiO_2-4h-160°C-650 mM, respectively. Therefore, the positively charged surface of APTES/TiO_2 presented a higher potential of contact with the negatively charged *E. coli* cells (−44.2 mV), which led to faster bacteria inactivation. However, the group of samples presented the better antimicrobial properties (TiO_2-4h-120°C-250 mM – TiO_2-4h-180°C-250 mM) were characterized by the less positive zeta potential (from +17.89 to +22.34 mV) in comparison to samples modified by 450 (from +23.12 to +26.73 mV) or 650 mM (from +24.90 to +27.11 mV) of modifier. A similar observation was presented in our previous works [21,43], where this phenomenon was explained by the amount of photogenerated hydroxyl radicals (•OH) produced on nanomaterials surface during the photocatalytic process. It is recognized that •OH radicals play a crucial role in the photocatalytic inactivation of microorganisms, especially bacteria [13,45,46]. In this case, the amount of •OH produced on photocatalysts surface during UV radiation was also examined and obtained results were presented in Fig. 6A–D. The hydroxyl radicals' formation analysis showed that the highest amounts of •OH radicals were observed for a group of samples modified by 250 mM of APTES solution (Fig. 6B). Therefore, a large number of hydroxyl radicals generated during the photocatalytic process led to faster inactivation of *E. coli* in water. Additionally, a two-step mechanism of bacteria destruction in the presence of APTES-modified photocatalyst was observed, which was in accordance with results presented by Desai and Kowshik [47]. As shown from Figs. 4 and 5, the bacteria inactivation proceeded in two phases. In the first phase, the number of live *E. coli* bacteria after the first 80 min of the photocatalytic process was relatively high. Bacteria could trigger some self-repair and self-defence mechanisms [43,47]. In the second stage of the photocatalytic process, many highly reactive radicals led to disturbances and damages in bacteria cells. The cell membranes and walls

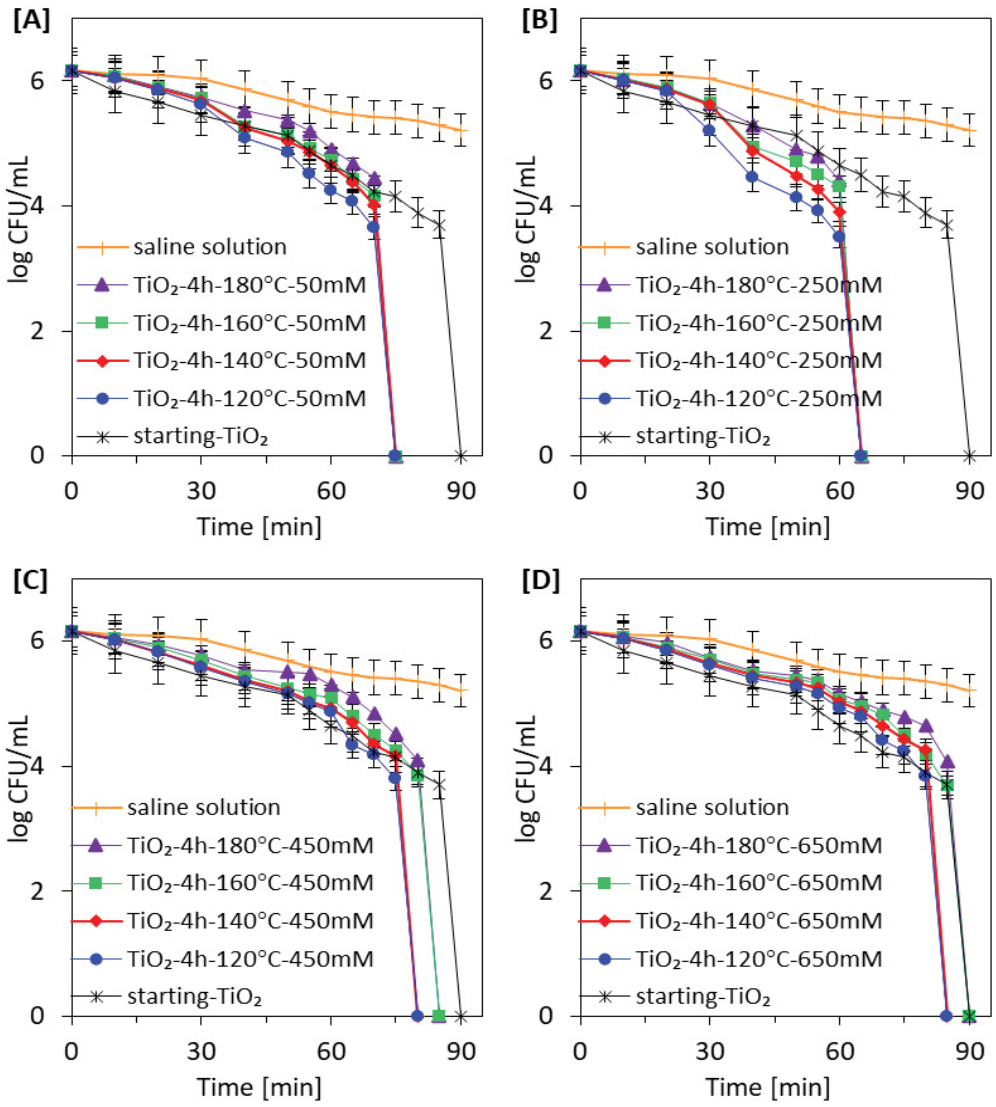

Fig. 5. Inactivation of *E. coli* in the presence of starting-TiO_2 and TiO_2 nanomaterials modified with various APTES concentration: 50 mM (A), 250 mM (B), 450 mM (C), and 650 mM (D) under UV irradiation.

Table 3
Silicon EDX mapping results for APTES/TiO_2 nanomaterials

Element \ Sample name	TiO_2-4h-180°C-50mM	TiO_2-4h-180°C-250mM	TiO_2-4h-180°C-450mM	TiO_2-4h-180°C-650mM
Si (at.%)	0.33	0.74	1.15	1.35

became permeable, and intracellular cytoplasmic components began to leak from the cells. As a consequence, a rapid bacteria inactivation was observed.

It should also be mentioned that increasing the modification temperature from 120°C to 180°C had no significant effect on the antibacterial properties of samples. The temperature did not affect the antimicrobial properties in samples modified with 50 and 250 mM of the modifier solution. In turn, in the case samples modified with 450 and 650 mM of APTES solution at 160°C and 180°C, the time needed to total bacteria inactivation slightly increased (by 5 min) in comparison to lower temperatures of modification.

3.3. Optimization of photocatalytic activity studies

Prior to the photocatalytic activity studies, tests were conducted to investigate the adsorption–desorption equilibrium at the semiconductor-methylene blue

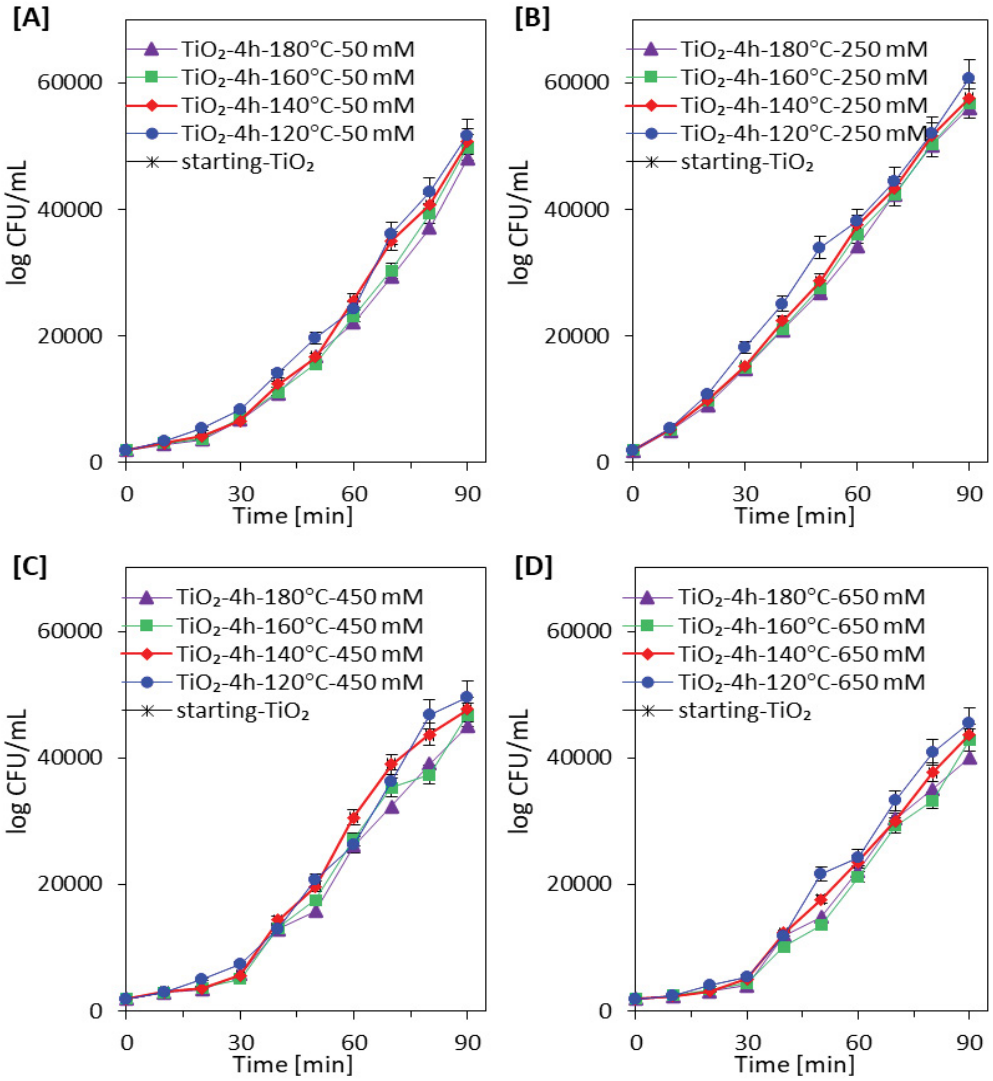

Fig. 6. The amount of generated 2-hydroxyterephthalic acid expressed as the peak area of the fluorescent product during UV irradiation.

interface. Based on the results shown in Figs. S3A–C and S4A–D, it was observed that the dye adsorption degree under light-free conditions was not dependent on either the dose of photocatalyst or the modification temperature or the APTES concentration. For all tested samples, the adsorption–desorption equilibrium was established after 60 min. According to the zeta potential values presented in Table 2, starting-TiO_2 and all APTES-modified TiO_2 nanomaterials exhibited positively charged surfaces. Moreover, it is well known that the positively charged semiconductor surface has a low potential of contact with methylene blue molecules, which is a positively charged cationic dye. Therefore, the adsorption of the dye was negligible, with a maximum of 4% [48–51].

The photocatalytic activity of the starting-TiO_2 and APTES/TiO_2 nanomaterials was evaluated by the methylene blue decomposition under exposure to UV light. To determine the appropriate dose of photocatalyst, three random samples were selected from the entire series of prepared materials and tested for five different concentrations: 0.05, 0.1, 0.25, 0.5 and 0.75 g/L. From the results shown in Fig. 7A–C, it was found that, in general, the photocatalytic activity increased with the increase of the photocatalyst concentration. Although the highest degree of dye decomposition for most samples was observed for 0.75 g/L, a concentration of 0.2 g/L lower, that is, 0.5 g/L, was suitable for further photocatalytic activity tests. For all the materials tested, the difference in the efficiency achieved for the two highest dosages after 360 min of UV irradiation was minor and ranged from 4% to 9%. Considering the slight difference in yield and economic considerations, the less nanomaterial needed, the better, 0.5 g/L was an appropriate sample dosage. Therefore, the photocatalytic activity of all remaining nanomaterials was determined only for the best semiconductor concentration of 0.5 g/L.

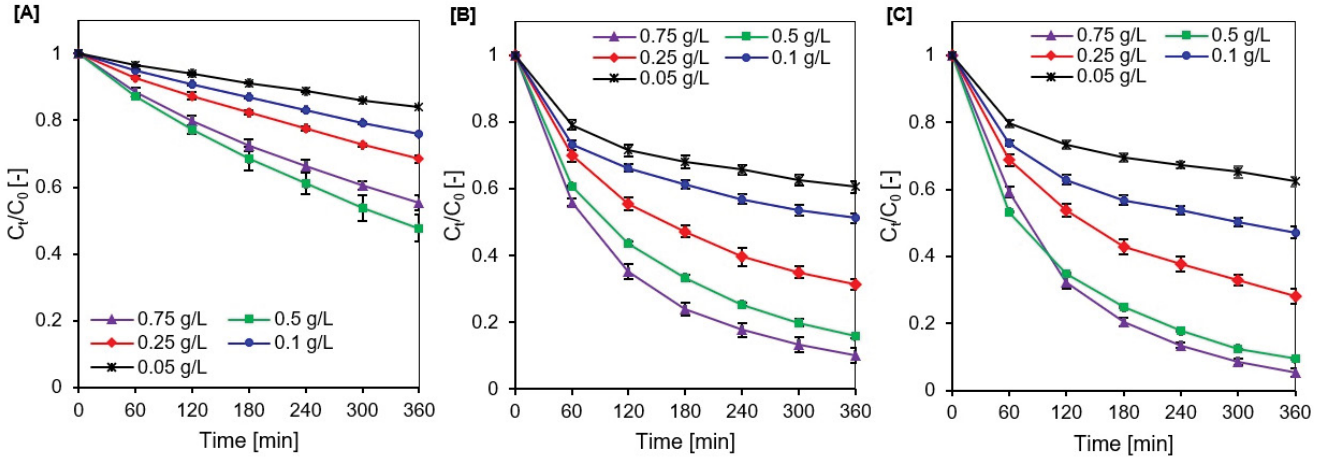

Fig. 7. Methylene blue decomposition under UV irradiation for selected photocatalysts: starting-TiO_2 (A), TiO_2-4h-120°C-250mM (B) and TiO_2-4h-160°C-650mM (C).

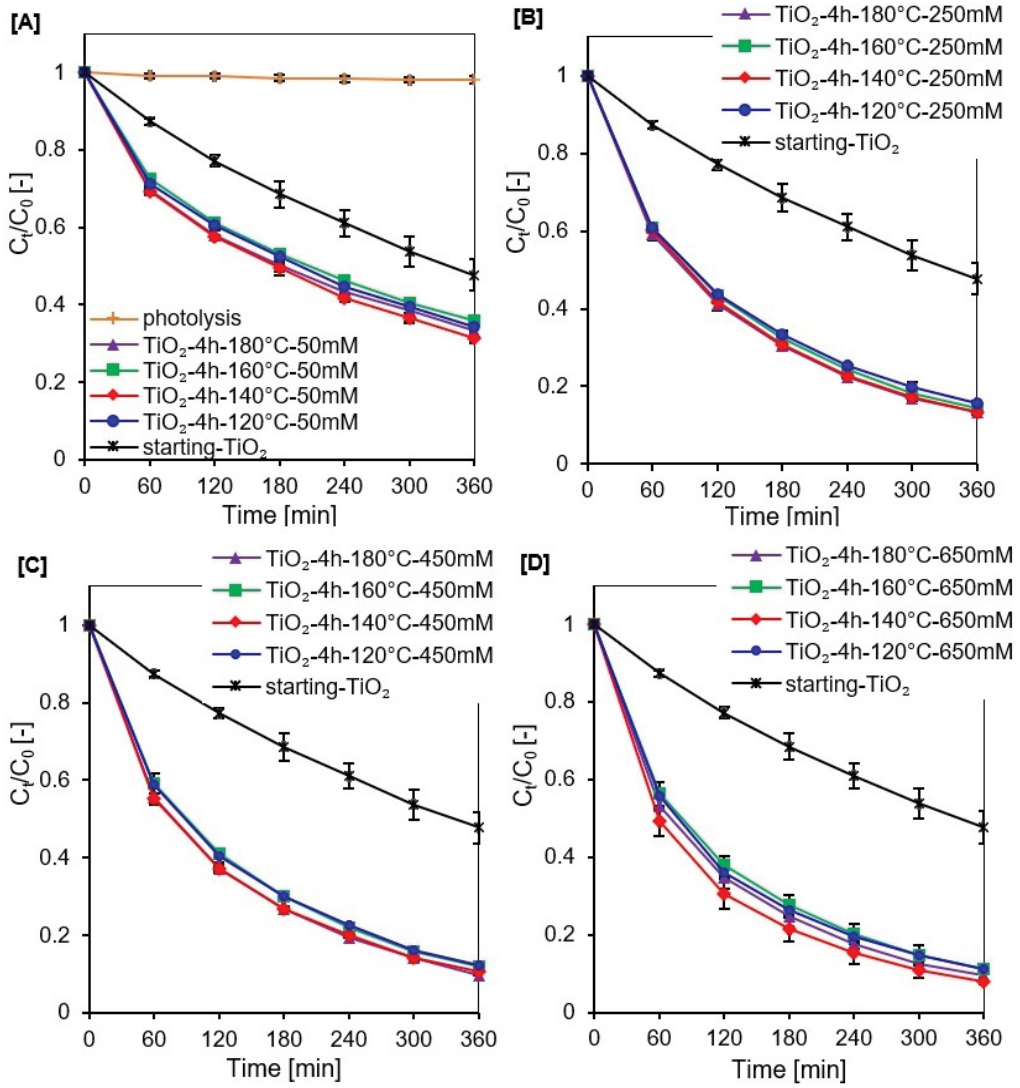

Fig. 8. Methylene blue decomposition under UV irradiation for starting-TiO_2 and APTES/TiO_2 photocatalysts (concentration of semiconductor 0.5 g/L).

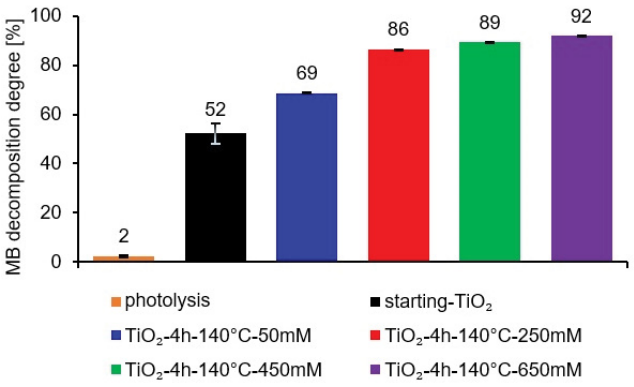

Fig. 9. Methylene blue decomposition degree after 360 min of UV light irradiation for starting-TiO_2 and APTES/TiO_2 photocatalysts (concentration of semiconductor 0.5 g/L).

According to Fig. 8A, tests performed without photocatalyst demonstrated that dye degradation by photolysis was marginal compared to the photocatalysis processes, resulting in about 2% methylene blue degradation after 360 min of exposure same conditions as in the photoactivity measurements. It was noted that all prepared APTES-functionalized TiO_2 samples exhibited a higher dye decomposition degree than starting-TiO_2. Furthermore, the amount of utilized modifier influenced the photocatalytic performance significantly. It was observed that the photoactivity increased with the increasing concentration of APTES used for modification. The highest decomposition degree of about 92% was noted for materials modified with 650 mM modifier solution, while it was only 52% for starting-TiO_2 (Fig. 9). Our observations were consistent with the results obtained by Kassir et al. [52], who also noted that the higher the amount of organosilane used for modification, the better the efficiency of the pollutants decomposition process. Based on the silicon EDX mapping results for APTES/TiO_2 samples (Table 3) and the carbon and nitrogen content analysis (Table 2), it can be concluded that the enhancement of photoactivity with the increase of APTES concentration can be related to the increase of Si, N and C content in the prepared nanomaterials. According to Bui et al. [53], the effect of Si modification on the photoactivity can be attributed to the easy transfer and separation of photogenerated holes and electrons. Also, Viet et al. [54] observed that the performance of silicon-modified TiO_2 was enhanced by adding increasing numbers of Si atoms in the crystal structure. In contrast, Zamiri et al. [55] observed that an increase in the amount of C and N in the modified TiO_2 particles will enhance the number of absorbed photons, resulting in improved degradation efficiency of pollutants. Moreover, it was also noted that increasing the modification temperature from 120°C to 180°C had no significant influence on the activity of the tested samples (Fig. 8A–D).

Summarizing, it was generally concluded that the temperature of modification in the range from 120°C to 180°C was too low to significantly affect the photocatalytic inactivation of bacteria *E. coli* and the efficiency of the methylene decomposition. In contrast, the APTES concentration used for a modification had a key influence on the efficiency of the obtained nanomaterials.

4. Conclusions

The APTES-modified TiO_2 nanomaterials were obtained via solvothermal process at 120°C, 140°C, 160°C and 180°C with the concentrations of APTES equal 50, 250, 450, or 650 mM. The studies confirmed the presence of C, N and Si in the TiO_2 structure, indicating that the modification was carried out successfully. It was noted that APTES inserts into both the external surface of the semiconductor and the pores, resulting in reduced S_{BET} values and pore volumes. It was found that for photocatalytic inactivation of bacteria *E. coli* studies, the best concentration of the photocatalyst was 0.1 g/L, while for methylene blue degradation tests, the best dose of the sample was 0.5 g/L. It was generally observed that all APTES/TiO_2 nanomaterials exhibited higher activity than starting-TiO_2. The best antibacterial properties were observed for a group of samples modified by 250 mM of APTES, attributed to the highest amount of $^{\bullet}OH$ radicals generated from the surface and positive zeta potential (from +17.89 to +22.34 mV). In the case of methylene blue decomposition, the photoactivity increased with increasing concentration of APTES used for modification which can be related to the growth of Si, N and C content in the nanomaterials. After 360 min of UV irradiation, the highest methylene blue decomposition degree was noted for samples modified with 650 mM of APTES. The temperature of modification in the range from 120°C to 180°C had no significant effect on antibacterial properties and the efficiency of the dye decomposition.

Acknowledgement

This work was supported by grant 2017/27/B/ST8/02007 from the National Science Centre, Poland.

Conflicts of interest

The corresponding author states no conflict of interest on behalf of all authors.

References

[1] A.Y. Hoekstra, J. Buurman, K.C.H. van Ginkel, Urban water security: a review, Environ. Res. Lett., 13 (2018) 053002, doi: 10.1088/1748-9326/aaba52.
[2] N. Allocati, M. Masulli, M.F. Alexeyev, C. Di Ilio, *Escherichia coli* in Europe: an overview, Int. J. Environ. Res. Public Health, 10 (2013) 6235–6254.
[3] S. Zhang, M. Abbas, M.U. Rehman, Y. Huang, R. Zhou, S. Gong, H. Yang, S. Chen, M. Wang, A. Cheng, Dissemination of antimicrobial resistance genes (ARGs) via integrons in *Escherichia coli*: a risk to human health, Environ. Pollut., 266 (2020) 115260, doi: 10.1016/j.envpol.2020.115260.
[4] M. Ismail, K. Akhtar, M.I. Khan, T. Kamal, M.A. Khan, A. Asiri, J. Seo, S.B. Khan, Pollution, toxicity and carcinogenicity of organic dyes and their catalytic bio-remediation, Curr. Pharm. Des., 25 (2019) 3645–3663.
[5] A. Tkaczyk, K. Mitrowska, A. Posyniak, Synthetic organic dyes as contaminants of the aquatic environment and their implications for ecosystems: a review, Sci. Total Environ., 717 (2020) 137222, doi: 10.1016/j.scitotenv.2020.137222.

[6] R.A. Capeli, T. Belmonte, J. Caierão, C.J. Dalmaschio, S.R. Teixeira, V.R. Mastelaro, A.J. Chiquito, M.D. Teodoro, J.F.M. Domenegueti, E. Longo, L.G. Trindade, F.M. Pontes, Effect of hydrothermal temperature on the antibacterial and photocatalytic activity of WO_3 decorated with silver nanoparticles. J. Sol-Gel Sci. Technol., 97 (2021) 228–244.
[7] C. El Bekkali, J. Labrag, A. Oulguidoum, I. Chamkhi, A. Laghzizil, J.-M. Nunzi, D. Robert, J. Aurag, Porous ZnO/hydroxyapatite nanomaterials with effective photocatalytic and antibacterial activities for the degradation of antibiotics, Nanotechnol. Environ. Eng., 7 (2022) 1–9, doi: 10.1007/s41204-021-00172-7.
[8] G. Gnanamoorthy, V.K. Yadav, K.K. Yadav, K. Ramar, J. Alam, A.K. Shukla, F.A. Ahmed Ali, M. Alhoshan, Fabrication of different SnO_2 nanorods for enhanced photocatalytic degradation and antibacterial activity, Environ. Sci. Pollut. Res., (2021) 1–11, doi: 10.1007/s11356-021-13627-w.
[9] R. Sharma, Uma, S. Singh, A. Verma, M. Khanuja, Visible light induced bactericidal and photocatalytic activity of hydrothermally synthesized $BiVO_4$ nano-octahedrals, J. Photochem. Photobiol., B, 162 (2016) 266–272.
[10] H.A. Foster, I.B. Ditta, S. Varghese, A. Steele, Photocatalytic disinfection using titanium dioxide: spectrum and mechanism of antimicrobial activity, Appl. Microbiol. Biotechnol., 90 (2011) 1847–1868.
[11] C.S. Uyguner Demirel, N.C. Birben, M. Bekbolet, A comprehensive review on the use of second generation TiO_2 photocatalysts: microorganism inactivation, Chemosphere, 211 (2018) 420–448.
[12] A.O. Ibhadon, P. Fitzpatrick, Heterogeneous photocatalysis: recent advances and applications, Catalysts, 3 (2013) 189–218.
[13] P. Venkata Laxma Reddy, B. Kavitha, P.A.K. Reddy, K.-H. Kim, TiO_2-based photocatalytic disinfection of microbes in aqueous media: a review, Environ. Res., 154 (2017) 296–303.
[14] H.M. Yadav, J.-S. Kim, S.H. Pawar, Developments in photocatalytic antibacterial activity of nano TiO_2: a review, Korean J. Chem. Eng., 33 (2016) 1989–1998.
[15] M.R. Al-Mamun, S. Kader, M.S. Islam, M.Z.H. Khan, Photocatalytic activity improvement and application of UV-TiO_2 photocatalysis in textile wastewater treatment: a review, J. Environ. Chem. Eng., 7 (2019) 103248, doi: 10.1016/j.jece.2019.103248.
[16] R. Li, T. Li, Q. Zhou, Impact of titanium dioxide (TiO_2) modification on its application to pollution treatment—a review, Catalysts, 10 (2020) 804, doi: 10.3390/catal10070804.
[17] R. Klaysri, T. Tubchareon, P. Praserthdam, One-step synthesis of amine-functionalized TiO_2 surface for photocatalytic decolorization under visible light irradiation, J. Ind. Eng. Chem., 45 (2017) 229–236.
[18] G. Xu, Z. Zheng, Y. Wu, N. Feng, Effect of silica on the microstructure and photocatalytic properties of titania, Ceram. Int., 35 (2009) 1–5.
[19] D.M. Tobaldi, A. Tucci, A.S. Škapin, L. Esposito, Effects of SiO_2 addition on TiO_2 crystal structure and photocatalytic activity, J. Eur. Ceram., 30 (2010) 2481–2490.
[20] A. Sienkiewicz, A. Wanag, E. Kusiak-Nejman, E. Ekiert, P. Rokicka-Konieczna, A.W. Morawski, Effect of calcination on the photocatalytic activity and stability of TiO_2 photocatalysts modified with APTES, J. Environ. Chem. Eng., 9 (2021) 104794, doi: 10.1016/j.jece.2020.104794.
[21] P. Rokicka-Konieczna, A. Wanag, A. Sienkiewicz, E. Kusiak-Nejman, A.W. Morawski, Antibacterial effect of TiO_2 nanoparticles modified with APTES, Catal. Commun., 134 (2020) 105862, doi: 10.1016/j.catcom.2019.105862.
[22] A. Wanag, A. Sienkiewicz, P. Rokicka-Konieczna, E. Kusiak-Nejman, A.W. Morawski, Influence of modification of titanium dioxide by silane coupling agents on the photocatalytic activity and stability, J. Environ. Chem. Eng., 8 (2020) 103917, doi: 10.1016/j.jece.2020.103917.
[23] C. Byrne, R. Fagan, S. Hinder, D.E. McCormack, S.C. Pillai, New approach of modifying the anatase to rutile transition temperature in TiO_2 photocatalysts, RSC Adv., 6 (2016) 95232, doi: 10.1039/C6RA19759K.
[24] P. Praveen, G. Viruthagiri, S. Mugundan, N. Shanmugam, Structural, optical and morphological analyses of pristine titanium di-oxide nanoparticles – synthesized via sol-gel route, Spectrochim. Acta, Part A, 117 (2014) 622–629.
[25] M. Ghosh, M. Mondal, S. Mandal, A. Roy, S. Chakrabarty, G. Chakrabarti, S.K. Pradhan, Enhanced photocatalytic and antibacterial activities of mechanosynthesized TiO_2–Ag nanocomposite in wastewater treatment, J. Mol. Struct., 1211 (2020) 1280762, doi: 10.1016/j.molstruc.2020.128076.
[26] A. Razmjou, J. Mansouri, V. Chen, The effects of mechanical and chemical modification of TiO_2 nanoparticles on the surface chemistry, structure and fouling performance of PES ultrafiltration membranes, J. Membr. Sci., 378 (2011) 73–84.
[27] D. Meroni, L. Lo Presti, G. Di Liberto, M. Ceotto, R.G. Acres, K.C. Prince, R. Bellani, G. Soliveri, S. Ardizzone, A close look at the structure of the TiO_2 APTES interface in hybrid nanomaterials and its degradation pathway: an experimental and theoretical study, J. Phys. Chem. C, 121 (2017) 430–440.
[28] A.R.M. Dalod, L. Henriksen, T. Grande, M.-A. Einarsrud, Functionalized TiO_2 nanoparticles by single-step hydrothermal synthesis: the role of the silane coupling agents, Beilstein J. Nanotechnol., 8 (2017) 304–312.
[29] V.A. Zeitler, C.A. Brown, The infrared spectra of some Ti–O–Si, Ti–O–Ti and Si–O–Si compounds, J. Phys. Chem., 61 (1957) 1174–1177.
[30] Q. Chen, N.L. Yakovlev, Adsorption and interaction of organosilanes on TiO_2 nanoparticles, Appl. Surf. Sci., 257 (2010) 1395–1400.
[31] F. Cheng, S.M. Sajedin, S.M. Kelly, A.F. Lee, A. Kornherr, UV-stable paper coated with APTES-modified P25 TiO_2 nanoparticles, Carbohydr. Polym., 114 (2016) 246–252.
[32] E. Ukaji, T. Furusawa, M. Sato, N. Suzuki, The effect of surface modification with silane coupling agent on suppressing the photo-catalytic activity of fine TiO_2 particles as inorganic UV filter, Appl. Surf. Sci., 254 (2007) 563–569.
[33] A.N. Murashkevich, A.S. Lavitskaya, T.I. Barannikova, I.M. Zharskii, Infrared absorption spectra and structure of TiO_2-SiO_2 composites, J. Appl. Spectrosc., 75 (2008) 730, doi: 10.1007/s10812-008-9097-3.
[34] M. Muttakin, S. Mitra, K. Thu, K. Ito, B.B. Saha, Theoretical framework to evaluate minimum desorption temperature for IUPAC classified adsorption isotherms, Int. J. Heat Mass Transfer, 122 (2018) 795–805.
[35] V.V. Kutarov, E. Robens, Yu. I. Tarasevich, E.V. Aksenenko, Adsorption hysteresis at low relative pressures, Theor. Exp. Chem., 47 (2011) 163–168.
[36] Z. Al-Othman, A review: fundamental aspects of silicate mesoporous materials, Materials, 5 (2012) 2874–2902.
[37] N.R.C. Fernandes Machado, V.S. Santana, Influence of thermal treatment on the structure and photocatalytic activity of TiO_2 P25, Catal. Today, 107–108 (2005) 595–601.
[38] W. Zhuang, Y. Zhang, L. He, R. An, B. Li, H. Ying, J. Wu, Y. Chen, J. Zhou, X. Lu, Facile synthesis of amino-functionalized mesoporous TiO_2 microparticles for adenosine deaminase immobilization, Microporous Mesoporous Mater., 239 (2017) 158–166.
[39] P.I. Pontón, J.R.M. d'Almeida, B.A. Marinkovic, S.M. Savić, L. Mancic, N.A. Rey, E. Morgado, F.C. Rizzo, The effects of the chemical composition of titanate nanotubes and solvent type on 3-aminopropyltriethoxysilane grafting efficiency, Appl. Surf. Sci., 301 (2014) 315–322.
[40] W.A. Talavera-Pech, A. Esparza-Ruiz, P. Quintana-Owen, A.F. Vilchis-Nestor, C. Carrera-Figueiras, A. Ávila-Ortega, Effects of different amounts of APTES on physicochemical and structural properties of amino-functionalized MCM-41-MSNs, J. Sol-Gel Sci. Technol., 80 (2016) 697–708.
[41] Z. Youssef, V. Jouan-Hureaux, L. Colombeau, P. Arnoux, A. Moussaron, F. Baros, J. Toufaily, T. Harmieh, T. Roques-Carmes, C. Frochot, Titania and silica nanoparticles coupled to Chlorin e6 for anti-cancer photodynamic therapy, Photodiagn. Photodyn. Ther., 22 (2018) 115–126.
[42] J. Zhao, M. Milanova, M.M.C.G. Warmoeskerken, V. Dutschk, Surface modification of TiO_2 nanoparticles with silane coupling agents, Colloids Surf., A, 413 (2012) 273–279.

[43] P. Rokicka-Konieczna, A. Wanag, A. Sienkiewicz, E. Kusiak-Nejman, A.W. Morawski, Effect of APTES modified TiO_2 on antioxidant enzymes activity secreted by *Escherichia coli* and *Staphylococcus epidermidis*, Biochem. Biophys. Res. Commun., 534 (2021) 1064–1068.
[44] A.K. Benabbou, Z. Derriche, C. Felix, P. Lejeune, P. Guillard, Photocatalytic inactivation of *Escherischia coli*: effect of concentration of TiO_2 and microorganism, nature, and intensity of UV irradiation, Appl. Catal., B, 76 (2007) 257–263
[45] M. Cho, H. Chung, W. Choi, J. Yoon, Linear correlation between inactivation of *E. coli* and OH radical concentration in TiO_2 photocatalytic disinfection, Water Res., 38 (2004) 1069–1077.
[46] O.K. Dalrymple, E. Stefanakos, M.A. Trotz, D.Y. Goswami, A review of the mechanisms and modeling of photocatalytic disinfection, Appl. Catal., B, 98 (2010) 27–38.
[47] V.S. Desai, M. Kowshik, Antimicrobial activity of titanium dioxide nanoparticles synthesized by sol-gel technique, Res. J. Microbiol., 4 (2009) 97–103.
[48] K. Bubacz, B. Tryba, A.W. Morawski, The role of adsorption in decomposition of dyes on TiO_2 and N-modified TiO_2 photocatalysts under UV and visible light irradiations, Mater. Res. Bull., 47 (2012) 3697–3703.
[49] M.A. Al-Ghouti, R.S. Al-Absi, Mechanistic understanding of the adsorption and thermodynamic aspects of cationic methylene blue dye onto cellulosic olive stones biomass from wastewater, Sci. Rep., 10 (2020) 15928, doi: 10.1038/s41598-020-72996-3.
[50] V. Saxena, D.K. Aswal, Surface modifications of photoanodes in dye sensitized solar cells: enhanced light harvesting and reduced recombination, Semicond. Sci. Technol., 30 (2015) 064005, doi: 10.1088/0268-1242/30/6/064005.
[51] M.R. Shenoy, S. Ayyasamy, M.V.V. Reddy, G. Kadarkarai, J. Suryakanth, S. Tamilarasan, S. Thangavelu, A.Ch. Jeyaramane, The effect of morphology-dependent surface charges of iron oxide on the visible light photocatalytic degradation of methylene blue dye, J. Mater. Sci.: Mater. Electron., 31 (2020) 17703–17717.
[52] M. Kassir, T. Roques-Carmes, K. Assaker, T. Hamieh, A. Razafitianamaharavo, J. Toufaily, F. Villiéras. Enhanced photocatalytic degradation of salicylic acid in water-ethanol mixtures from titanium dioxide grafted with hexadecyltrichlorosilane, Phys. Procedia, 55 (2014) 403–408.
[53] D.-N. Bui, S.-Z. Kang, X. Li, J. Mu, Effect of Si doping on the photocatalytic activity and photoelectrochemical property of TiO_2 nanoparticles, Catal. Commun., 13 (2011) 14–17.
[54] P. Van Viet, T.H. Huy, S.J. You, L.V. Hieu, C.M. Thi, Hydrothermal synthesis, characterization, and photocatalytic activity of silicon doped TiO_2 nanotubes, Superlattices Microstruct., 123 (2018) 447–455.
[55] M. Zamiri, M. Giahi, Photochemical degradation of an anionic surfactant by TiO_2 nanoparticle doped with C, N in aqueous solution, Russ. J. Phys. Chem., 90 (2016) 2668–2674.

Supplementary information

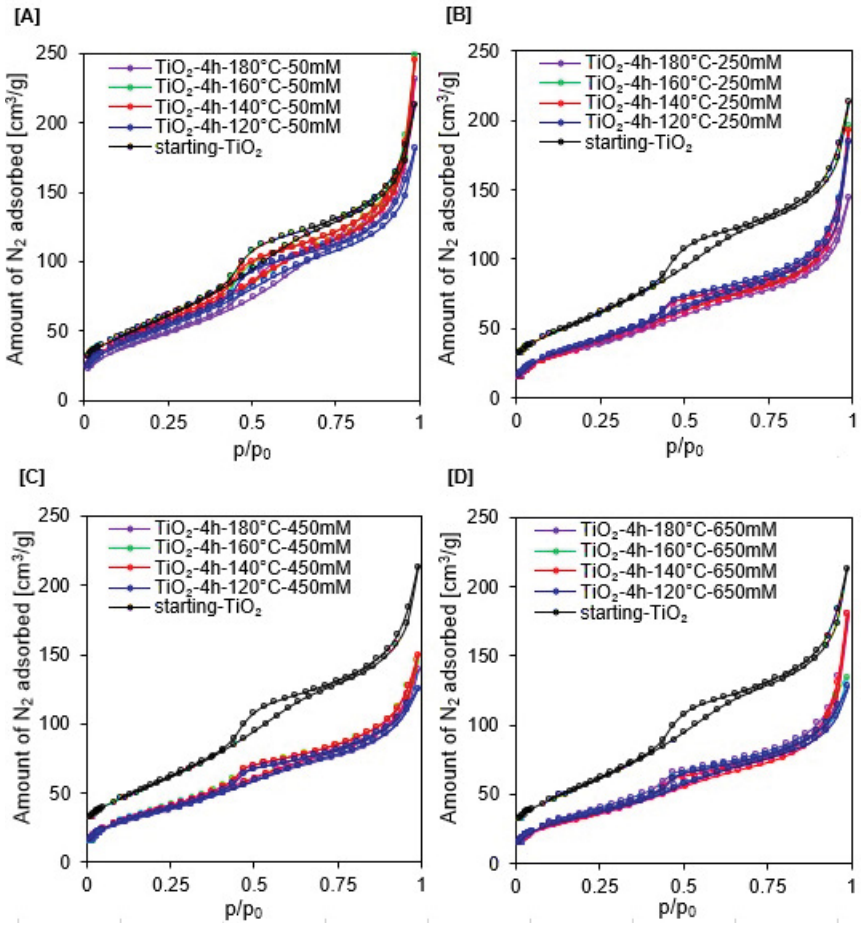

Fig. S1. Adsorption–desorption isotherms of starting-TiO_2 and TiO_2 nanomaterials modified with APTES concentration of 50 mM (A), 250 mM (B), 450 mM (C), and 650 mM (D).

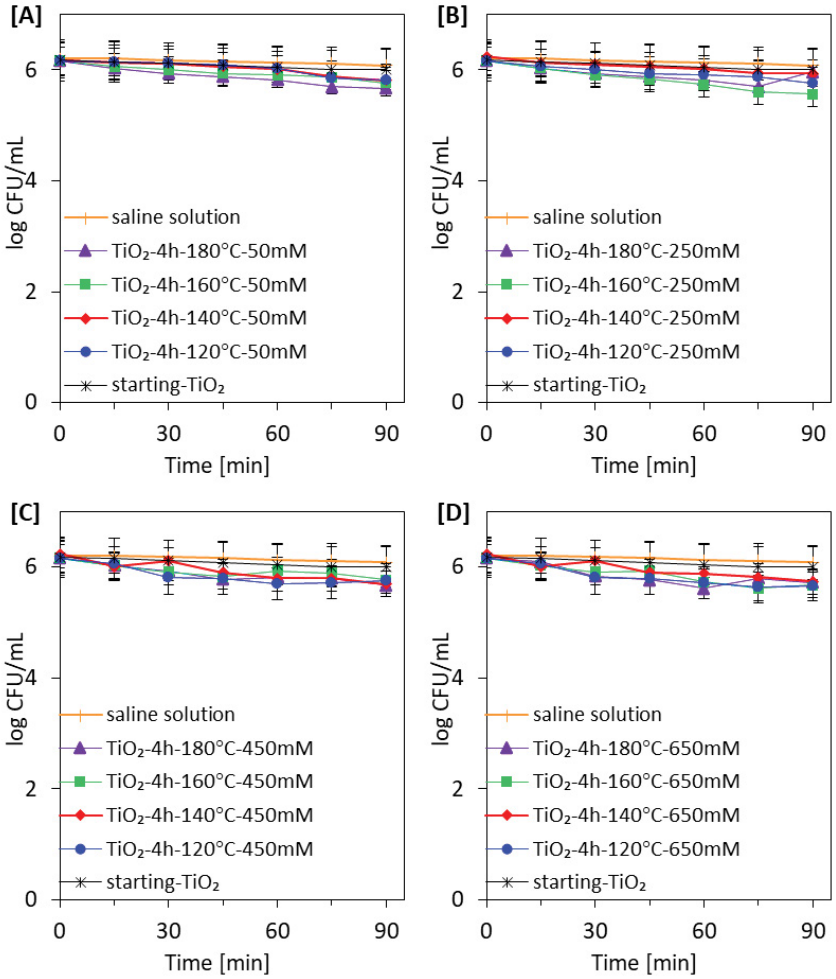

Fig. S2. Inactivation of *E. coli* in the presence of starting-TiO_2 and TiO_2 nanomaterials modified with APTES concentration of 50 mM (A), 250 mM (B), 450 mM (C) and 650 mM (D) under dark conditions.

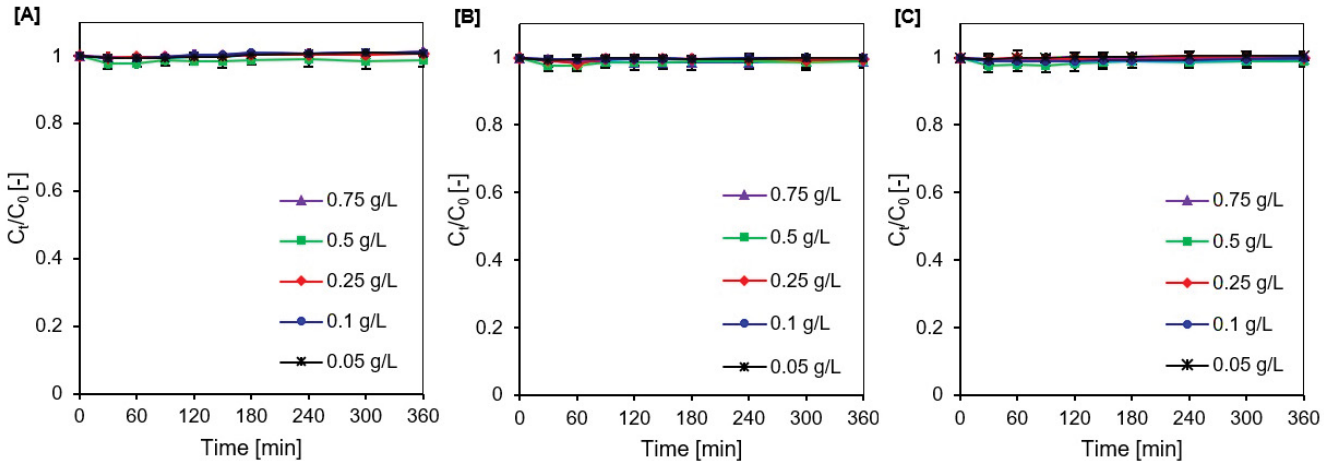

Fig. S3. Methylene blue adsorption degree on the surface of selected photocatalysts: starting-TiO_2 (A), TiO_2-4h-120°C-250mM (B) and TiO_2-4h-160°C-650mM (C).

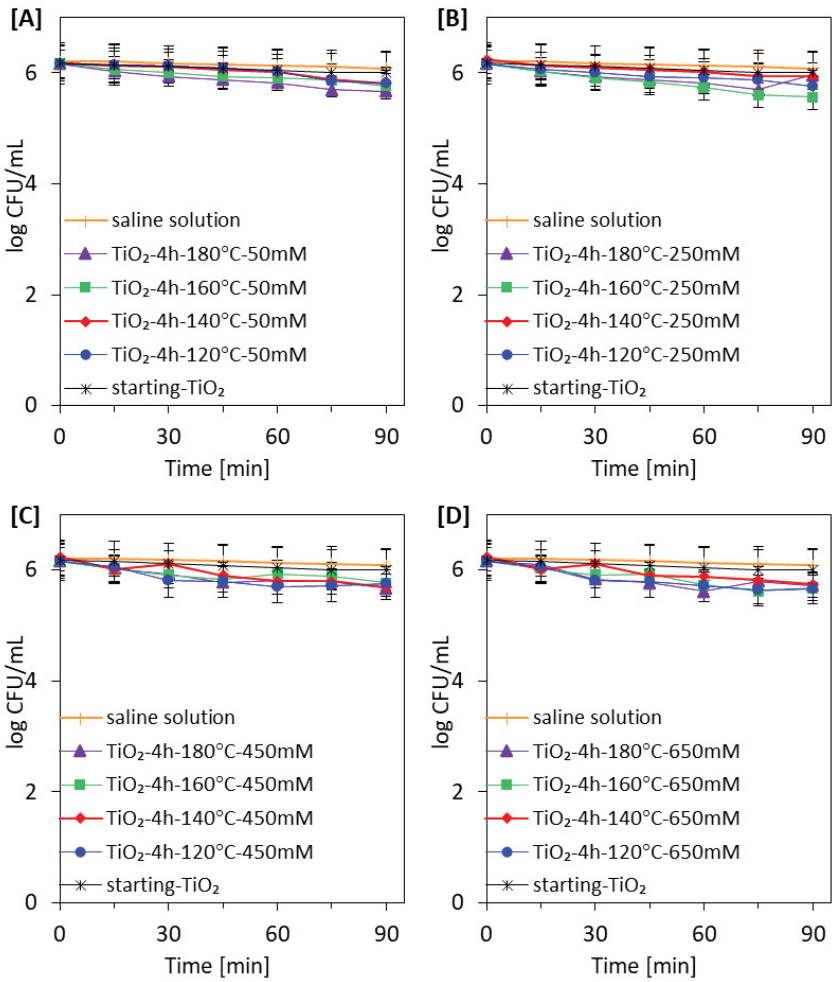

Fig. S4. Methylene blue adsorption degree on the surface of starting-TiO_2 and APTES/TiO_2 photocatalysts (concentration of semiconductor 0.5 g/L)